

Development of a Direct Drive Synchronous Reluctance Motor with Finite Element Analysis and Surrogate- Assisted Optimisation

Syed Abid Ali Shah Bukhari

Aston University

Doctor of Philosophy

June 2019

Syed Abid Ali Shah Bukhari asserts his moral right to be identified as the author of this thesis. This copy of the thesis has been supplied on condition that anyone who consults it is understood to recognize that its copyright belongs to its author and that no quotation from the thesis and no information derived from it may be published without appropriate permission or acknowledgment.

Abstract

This thesis is concerned about the development and evaluation of reluctance machines used for variable speed Raymond Pulveriser and centrifugal pump applications. The research is carried out through analytical and numerical analysis of two types of reluctance machines Synchronous Reluctance and Switched Reluctance machines, followed by experimental validation on prototype motors.

In the synchronous reluctance machine, the rotor is a crucial part in terms of magnetic flux configuration and is a specific focus of this research is on the design, evaluation, and manufacturing of the rotor to improve the motor drive performance. An analytical procedure is firstly proposed for the rotor design. The rotor elements including the ribs and the bridges that maintain the mechanical strength of the rotor as well as the Q-axis insulation ratio (air-to-steel ratio) are studied. A FEM simulation with surrogate optimisation method is adopted, the main parameters of rotor geometry such as flux barrier and flux carrier are designed thoroughly investigated on the square and round shapes. Then, final designs are optimised, prototyped and tested on a test bench.

The first machine is 75kW, 105rpm switched reluctance machine designed and prototyped for the direct-drive the application of Raymond Pulveriser. FEM modelling is carried out for 72/48 Switched reluctance motor in Motor Solver Software.

The second machine is a 10kW synchronous reluctance motor for the application of Raymond Pulveriser used for mining applications. In order to improve the overall machine performance, a Surrogate assisted optimisation technique is applied with a particle swarm optimisation (PSO) method. FEM models are established by electromagnetic design software (*Magnet*) for both the stator and rotor. The Surrogate-based optimisation is tested on 24 and 36 stator slots while considering both the square and round shapes. 5 stator variables to generate Latin Hypercube samples are airgap, slot depth, tooth width, number of turns and slot openings. The rotor optimisation variables are flux barrier width, flux carrier width, and edge angle. Three and four flux barriers are tested with square and round shapes. Additionally, design of 10kW Switched reluctance motor for the same application of Raymond Pulveriser is carried out. FEM models are established on Motor Solver machine design software. The SBO is tested on 12/8 SRM on both stator and rotor. The following variables are considered: stator pole arc, stator yoke thickness, air gap, rotor pole arc, number of turns, shaft diameter, and rotor yoke thickness and then the comparison is made between SynRM and SRM. These designs are initially for the machines operating in both directions. However, the applications only require uni-directional rotation of the machine. It is necessary to consider an optimised design for the uni-directional operation. Additionally, the study on the asymmetrical rotor design is also conducted to analyse the machine performance and its merits and drawbacks.

Thirdly, a 24-kW synchronous reluctance motor is designed for the centrifugal pump applications. The stator structure is similar to the induction motor but has 36 slots and 4 poles. The research mainly is

focused on reducing the power losses and torque ripple, and a new rotor design of motor with different optimisation arrangements of flux barrier shapes have been studied and tested through the FEM. The rotor optimisation is carried out by varying the flux carrier width, flux barrier width, shaft diameter, and barrier edge angle. The simulation carried on different designs and shapes. Finally, a rotor design with 3 V-shaped flux barriers is chosen and is prototyped for testing. Experimental results show the effectiveness of the optimal rotor designs which can provide a required torque profile with low torque ripples and low power losses. The main advantage of the proposed designs is the good thermal performance of the machine which increases motor efficiency. The study shows the benefits of utilizing a reluctance machine.

Keywords:

Direct-drive applications, Field lines shape, Harmonics. Particle Swarm Optimisation, Speed Range, Saliency Ratio. Switched Reluctance Motor, Synchronous Reluctance Machine (SynRM), Torque, Torque Ripple, Surrogate-based Optimisation, Variable Speed Drive (VSD).

Dedication

I dedicate this work to my dear parents for the lifelong and boundless love that I received from them as well as their unwavering support, also dedicated to my wife and my children for their unfaltering encouragement throughout my study. Without their support, reaching this point would not have been possible.

Acknowledgments

First of all I am thankful to Almighty Allah for giving me the opportunity to pursue the doctoral program and the strength and patience to successfully complete it, and then foremost, I would like to thank my supervisors, Prof. Wenping Cao, and Dr. Zhengyu Lin for their patience and confidence and imparted a lot of knowledge and critical thinking in the field of electrical machine design.

The work would not have been possible without technical support and realization of the prototype of the rotor from Prof. Guofeng Li and Dr. Zheng Liu. I would also like to thank Esmail Elhomdy, Yin Sheng, Yu Yan, Ming Zhang, Guo Guang Li, and Hong-Jun Xiao, who gave me much help and advice.

I would like to acknowledge Dr. Nan Yang for the times we spent together trying to solve problems. Many friends and colleagues made my life in the Aston University enjoyable and motivated, these friends, to name but a few are Debjani Goswami, Nasir, Vallery, Marrie, Yang Liu, Du, Paulami, My special thanks go to my wife and children, for supporting and encouraging me all the time.

Finally, I could never have completed a doctorate without the ongoing support of my parents, who are the most understanding, supportive and loving persons in my life. Words are not profound enough to express my love and respect to both of them, and they have encouraged me to become a responsible and strong person.

This work has generated 17 publications which are published at peer-reviewed journals, book chapters, and conference proceedings.

A List of Publications

- 1) **Syed Abid Ali Shah Bukhari**, Wenping Cao, Zheng Liu, Zhengyu Lin, Guofeng Li, and Esmail Elhomdy, "Development of a direct drive, low-cost synchronous reluctance motor with a surrogate-assisted Optimisation technique", IEEE Transaction for Energy Conversion. Submitted.
- 2) Esmail. Elhomdy, Zheng Liu, Guofeng Li, **Syed Abid Ali Shah Bukhari**, Nan Yang "Multi-objective optimisation based on surrogate model of a 72/48 switched reluctance motor for low-speed direct-drive mining applications. Electric Power components and systems. Submitted.
- 3) **Syed Abid Ali Shah Bukhari**, WenPing Cao, Lassi Aarniovuori "Review of electrical motor drives for electric vehicle applications" Mehran University of Research Journal of Engineering & Technology. Vol. 38, No. 3, 525-540 July 2019.
- 4) Lan Li, Hao Wang, Wenping Cao, Xiangping Chen, **Syed Abid Ali Shah Bukhari**, Lun Chai, Bing Li, "High Efficient Solar Power Generation with improved discontinuous pulse width modulation (SPWM) overmodulation algorithms" *Energies*, vol.12, p. 1765, 2019.
- 5) Fayyaz Jandan, Suhail Khokhar, **Syed Abid Ali Shah Bukhari**, and Farhan Abbasi, "Recognition and classification of power quality disturbances by DWT-MRA and SVM classifier", International Journal of Advanced Computer Science and Applications(IJACSA), 10(3), 2019. <http://dx.doi.org/10.14569/IJACSA.2019.0100348>.
- 6) Fayaz Ali Jandan, Suhail Khokhar, Zubair Memon, **Syed Abid Ali Shah Bukhari**, "Wavelet-based simulation and analysis of single and multiple power quality disturbances", Engineering Technology & Applied Science Research, vol. 9, No. 2, 3909-3914, 2019.
- 7) Esmail Elhomdy, Guofeng Li, Zheng Liu, **Syed Abid Ali Shah Bukhari**, and WenPing Cao, "Design and experimental verification of a 72/48 switched reluctance motor for low-speed direct-drive mining applications," *Energies*, vol. 11, p. 192, 2018.
- 8) **Syed Abid Ali Shah Bukhari**, Wenping Cao, Kamran Ahmed Samo, Zheng Liu, and Shahzeb Ansari, "Electrical motor drive technologies for a green electric vehicle: A review," *Engineering Science and Technology International Research Journal*, vol. 1, pp. 1-10, 2017.
- 9) Kamran Ahmed Samo, Andrew Ragai Henry Rigit, Imran Ahmed Samo, and **Syed Abid Ali Shah Bukhari**, Suitable Powerhouse Design for Kuching Barrage Tidal Power Scheme". "International Journal of Engineering Science & Research Technology, vol. 6, p. 154-172, September, 2017.
- 10) **Syed Abid Ali Shah Bukhari**, WenPing Cao, Tiejiang Yuan, and Kamran Ahmed Samo, "Design and comparative investigation of a 12/8 and A 6/4 switched reluctance machines for electric vehicles," International Journal of Engineering Science & Research Technology, vol. 6, p. 13- 25, August, 2017.
- 11) Shahzeb Ansari, Imtiaz Leghari, Syed Qurban, Fayyaz Jandan, **Syed Abid Ali Shah Bukhari**, "Dynamic performance analysis of ac voltage regulator feeding RLC load," *Engineering Science and Technology International Research Journal*, vol. 1, No.4, pp. 21-26, December 2017.
- 12) **Syed Abid Ali Shah Bukhari**, WenPing Cao, Xiangping Chen "Hybrid electric energy storage and its dynamic performance". Book Chapter in the book, *Cases on Green Energy and Sustainable Development*, in the book IGI Global. In press.

- 13) **Syed Abid Ali Shah Bukhari**, Wenping Cao, Toufique Ahmed Soomro and D. Guanhao, "Future of microgrids with distributed generation and electric vehicles," Book chapter 3, in the book *Development and Integration of Microgrids*, W.-P. Cao and J. Yang, InTech, 2017.
- 14) **Syed Abid Ali Shah Bukhari**, Wenping Cao, Guofeng Li, Shady Gadoue and Ayman Abdel-Khalik, " Development of a direct-drive synchronous reluctance motor with a surrogate-assisted Optimisation technique", The IEEE Conference on *Power Electronics and Renewable Energy (CPERE)* on Electrical Machines, Aswan, Egypt. October, 2019.
- 15) Izhar Ahmed Sohu, Asif Ahmed Rahimoon, Asadullah Shaikh, **Syed Abid Ali Shah Bukhari**, Arslan Ahmed Sohu, "Implementation of solar tracking design using FPGA tool," The International Conference in *Computing, Mathematics and Engineering Technologies (iCoMET)*, Sukkur-Sindh, Pakistan. January, 2019, pp. 1-5.
- 16) **Syed Abid Ali Shah Bukhari**, Belema Prince.Alahbo, Wenping Cao, Zhengyu lin, Shahid Hussain Shaikh, Toufique Ahmed Soomro, Shahzeb Ansari, Fayyaz Ali Jandan," Switched reluctance motor design for electric vehicle based on harmonics and back amf analysis," The IET Journal of Engineering, 2019, in press.
- 17) **Syed Abid Ali Shah Bukhari**, Wenping Cao, Safdar Ali, Shahid Hussain Shaikh, Toufique Ahmed Soomro and Zhengyu Lin, "Design of a high speed 18/12 switched reluctance motor drive with an asymmetrical bridge converter for electric vehicles," The International Conference in *Computing, Mathematics and Engineering Technologies (iCoMET)*, Sukkur-Sindh, Pakistan. March, 2018, pp. 1-6.

List of Abbreviations

AC	Alternating Current
AFPM	Axial Flux Permanent Magnet Motor
AFD	Adjustable Frequency Drive
ASD	Adjustable Speed Drive
CCD	Central composite design
CO ₂	Carbon Dioxide
CPSR	Constant Power Speed Range
DC	Direct Current
DOE	Department of Energy (United States)
DoE	Design of Experiments
EMDO	Electrical machine design and optimisation
EMF	Electromotive force
EU	European Union
FE	Finite element
FEM	Finite element method
GA	Genetic algorithm
GHG	Green House Gas
HVAC	Heat Ventilation and Air Condition
IEC	International Electrotechnical Commission
IM	Induction motor
IPCC	Intergovernmental Panel on Climate Change
L&H	Linton and Hirst
LHS	Latin Hypercube Samples
LSDD	Low speed direct drive
MTOE	Million Tons of Oil Equivalent
NdFeB	Neodymium Iron Boron
OAD	Orthogonal array design
PM	Permanent Magnet
PMG	Permanent magnet generator
PR	Polynomial regression
PSO	Particle swarm optimisation

RM	Reluctance machine
SBO	Surrogate-Based Optimisation
SEMs	Stochastic evolutionary methods
SmCo	Samarium cobalt
SRM	Switched Reluctance Motor
SynRM	Synchronous Reluctance Motor
VFD	Variable Frequency Drive
VSD	Variable Speed Drive
2D	Two dimensional
3D	Three dimensional

List of Symbols

Item	Expression
Bs	Stator pole arc in degree
Br	Rotor pole arc in degree
Ts	Stator teeth width in mm
Tr	Rotor teeth width in mm
Do	Outer diameter in mm
Bry	Rotor yoke thickness in mm
Bsy	Stator yoke thickness in mm
B	air gap flux density in tesla
D	air gap diameter in mm
Dsh	shaft diameter in mm
Np	Number of turns
l...	machine length in mm
P _{mag...}	iron loss in watts
P _{el...}	copper losses in watts
T _{em...}	Torque in Nm
φ	Flux...
Ψ...	magnetic flux linkage
V _{ph}	Rated phase voltage
I _{ph}	Rated phase current in amps
N _{ph}	Number of turns per phase
Φ	Main Flux
K _w	Winding factor
B _{av} /B _p	Average air-gap/pole flux density
D	The outer diameter of the rotor in mm
L	The axial length of the rotor in mm
p	Pole number
τ	Pole pitch
w _p	Width of pole in mm

A_p	The surface area of the pole mm ²
L_p/l_{core}	Length of stator pole/stator core in mm
A_f	Excitation MMF
K_{teeth}/K_{core}	The empirical coefficient of iron loss in rotor teeth/stator core
α_p	Pole-arc ratio
p_{bm}	Rotor iron loss coefficient
$R_a(x)$	Stator copper resistance based on insulation level
$R_{f(x)}$	Rotor copper resistance based on insulation level
v	The rated voltage of the machine

Table of Contents

Abstract	2
Dedication	4
Acknowledgments	5
A List of Publications	6
List of Abbreviations	8
List of Symbols	10
Table of Contents	12
List of Tables	17
List of Figures	21
Chapter 1 Introduction	27
1.1 Background.....	27
1.2 Motivation and objectives.....	31
1.3 Methodology.....	32
1.4 Thesis Overview.....	32
1.5 Contribution to knowledge	33
Chapter 2 Literature Review	35
2.1 Introduction.....	35
2.2 Motor Drives System and Energy Savings.	35
2.3 Variable Speed Drive	36
2.4 Method of speed control	37
2.5 Mechanical variable speed drives.....	37
2.6 Electric variable speed drive.....	38
2.7 Hydraulic VSDs	38
2.8 Importance of Direct Drive.....	38
2.8.1 Direct Drive Systems.....	39
2.8.2 Advantages of direct-drive.....	39

2.9 Permanent Magnet Direct Drive	40
2.10 Current state-of-the-art SR Motor Drives for Raymond Pulveriser	41
2.11 Synchronous Reluctance Motors.....	43
2.11.1 Comparison RMs with IMs.....	45
2.11.2 SynchRM Working Principle and Operation	45
2.11.3 Rotor Geometry	46
2.12 Switched Reluctance Motor	47
2.12.1 Working Principle of Switched Reluctance Motors	47
2.12.2 Modeling of SRM.....	49
2.13 Types of Power Losses in Electric Motor.....	51
2.13.1 Fixed and variable losses.	51
2.13.2 Stray Losses	51
2.13.3 Copper losses	51
2.13.4 Iron or core losses.....	52
2.13.5 Windage and friction losses	52
2.13.6 Ways to reduce power losses	52
2.14 Applications of Electrical Machines.....	53
2.14.1 Types of electric motors and drives.....	54
2.14.2 DC Motors	55
2.14.3 Induction Motors	56
2.14.4 Permanent magnet motors.....	57
2.14.5 Reluctance Motors.....	58
2.15 The trend of Electric Motors for Electric vehicle.....	60
2.15.1 Flux configuration	60
2.15.2 Hybridization of different machine features	61
2.16 Summary.....	63
Chapter 3 Surrogate-based Optimisation of Reluctance Machines.....	64
3.1 Introduction.....	64

3.2 Design Optimisation	66
3.3 Problem Definition	66
3.4 Design of Experiment	67
3.5 Construction of Surrogate Model.	68
3.5.1 Error Analysis.	68
3.5.2 Heuristic Search Method.....	68
3.5.3 Model Validation.....	69
3.5.4 Performance Analysis	69
3.6 Design process based on optimisation	70
3.7 Arrangements of Rotor and Stator Optimisation parameters for SynRM design	74
3.8 Three round shaped flux barriers and 4 flux carriers	78
3.9 Four round shape flux barriers and 5 round flux carriers	79
3.10 3 square shape flux barriers and 4 flux carriers.....	83
3.11 Optimisation with round stator slots with round flux barrier shape	85
3.11.1 Round shape with 4 flux barriers and 5 flux carriers.....	85
3.12 24 Square Shape Stator Slots Design.....	88
3.13 24 Round Shape Stator Slots Design	90
3.14 Final Optimisation with 4 flux barriers with square shaped	92
3.15 12/8 SRM Design process based on Surrogate-Based Optimisation	95
3.16 12/8 SRM optimisation through constant speed and constant power	98
3.17 Constant speed analysis at 170mm and 105rpm.....	98
3.17.1 Efficiency at a constant Power	99
3.18 Summary.....	99

Chapter 4 Numerical design and simulation of Synchronous Reluctance Stator and Rotor ..101

4.1 FEM Simulation	101
4.2 Synchronous Reluctance Rotor Design	101
4.3 Standard Design and Simulations of the SynRM	105
4.4 The final design of the proposed SynRM rotor	108
4.5 Design of 10kW SynRM for Direct- Drive Applications	113

4.6 Asymmetrical Rotor Geometry design	121
4.7 12/8 SRM FEM Simulation	126
4.8 72/48 SRM Design and Simulation	136
4.8.1 Step 1 Initial design	136
4.8.2 Step 2 Optimisation of major parameters	137
4.8.3 Characteristics of 72/48 SRM design.	141
4.9 Summary.....	143
Chapter 5 Experimental Validation	144
5.1.1 Rotor Fabrication.....	148
5.2 Specifications of the Original Machine	149
5.3 Test proceedings.....	149
5.3.1 Voltage.....	150
5.3.2 Frequency.....	150
5.3.3 Resistance	150
5.4 Direct measurement.....	150
5.4.1 Winding resistance and inductance measurements.....	150
5.4.2 Torque measurement	151
5.4.3 Speed measurement	153
5.4.4 Megger Testing. (Winding short circuit test).	153
5.5 Indirect Measurement	154
5.5.1 No-Load test.....	154
5.5.2 No Load Test while coupling the shaft with 55kW load motor	156
5.5.3 LOW-Speed test	160
5.5.4 Steps of parameter settings of Siemens Micromaster 440	161
5.6 Steps of parameter settings of ABB Drive ACC800	162
5.6.1 Low-speed test operation	166
5.6.2 Over speed test	166
5.6.3 Retardation Test	169

5.6.4 Analysis of Experiment Results	170
5.6.5 Electromagnetic Comparison Between FEM and Experimental Results.....	171
5.7 Experimental verification of 72/48 Switched reluctance motor	175
5.7.1 Electromagnetic Comparison of 72/48 SRM	179
5.8 Summary.....	182
Chapter 6 Conclusion and Future Work.....	183
6.1 Conclusions.....	183
6.2 Future Work	187
REFERENCES	189
Appendices	202
6.2.1 PSO optimised parameters by Surrogate	203
6.2.2 PSO optimised values No 1*	206
6.2.3 PSO optimised values No 2*	207
6.2.4 PSO optimised values No 3*	207
6.2.5 PSO optimised values for 4 flux barriers and 5 carriers and.....	209
6.2.6 PSO Optimisation for 4 square shape flux barriers	210
6.2.7 PSO Optimisation for square shape 3 flux barrier and 4 flux carrier design.....	211
6.2.8 PSO generated optimised variables for 24 square stator slots.....	214
6.2.9 PSO generated optimised variables for 24 round stator slots.....	216
6.2.10 1st PSO optimisation variable for 12/8 SRM design with 100 samples	221
6.2.11 2nd PSO Optimisation from 60 samples while varying inner rotor.....	227
6.3 Constant power analysis at 170mm and 10kW	229
6.4 Constant speed analysis at 200mm and 105rpm	230
6.5 Constant speed analysis at 200mm and 10kW	231

List of Tables

Table 2-1 The features of conventional IM drive in Raymond Pulveriser [43].....	42
Table 2-2 The drive mechanism of a Raymond Pulveriser [43].....	43
Table 2-3 Specifications of Induction motor used for closed coupled centrifugal pump.....	43
Table 2-4 Comparison between SynRM and SRM machines [176].....	45
Table 2-5 Light-weight passenger Electric Car specifications [119].....	53
Table 3-1 stator parameters for the Latin Hypercube samples	67
Table 3-2 PSO Optimisation for efficiency, torque, and power in kW. for the first Optimisation.....	69
Table 3-3 variable range selection for Latin Hypercube Samples for 36 stator slots.....	70
Table 3-4 Initial 40 Latin Hypercube Samples with square slot shape for SynRM design.....	73
Table 3-5 PSO parameters for square and round stator slots.....	74
Table 3-6 PSO more parameters for square and round stator slots.....	74
Table 3-7 range of design parameter for the 2nd optimisation process	75
Table 3-8 Optimised parameters achieved from PSO method with the 1st optimisation process	75
Table 3-9 Optimised parameters achieved from PSO method with the 2nd optimisation process	77
Table 3-10 Optimised parameters achieved from PSO method with the 3rd optimisation process.....	78
Table 3-11 Optimised parameters achieved from PSO method only with stable torque.....	79
Table 3-12 Optimised parameters achieved from PSO method with 4 flux barriers and 5 flux carriers	80
Table 3-13 Optimised parameters at 1500ms simulation time	81
Table 3-14 Optimised parameters of square shape flux barriers	83
Table 3-15 Optimised parameters of 3 square shape flux barriers and 4 flux carriers.....	83
Table 3-16 Optimised with round stator slots parameters of 4 round shape flux barriers and 5 flux carriers	86
Table 3-17 variable range selection for Latin Hypercube Samples for 24 stator slots.....	89
Table 3-18 Optimised parameter by PSO for 24 square slots.....	89
Table 3-19 Optimised more parameter by PSO for 24 square slots.....	90
Table 3-20 Optimised parameter by PSO for 24 round stator slots	90
Table 3-21 Optimised more parameter by PSO for 24 round stator slots	90

Table 3-22 Optimised parameter by PSO for 4 square shaped flux barriers	93
Table 3-23 3-Phase Winding specifications	94
Table 3-24 initial parameters for 12/8 SRM design at 170mm length.....	97
Table 4-1 Latin Hypercube samples for SynRM rotor design.	102
Table 4-2 SynRM rotor flux barrier optimisation steps with and without ribs.....	103
Table 4-3 design specifications of the 8.58kW motor for direct drive application.....	114
Table 4-4 performance of SynRM motor by different optimisations.....	119
Table 4-5 performance of asymmetrical rotor when 3 rd flux barrier end near the outer boundary	123
Table 4-6 specifications for final model of SRM	134
Table 4-7 The initial design parameters of the 72/48 SRM	137
Table 4-8 The final dimensions of the design	140
Table 5-1 Specification of Cummins stator PI-144F	149
Table 5-2 Resistance and Inductance measurement results.....	150
Table 5-3 specifications of 55kW load motor	157
Table 5-4 Siemens micro master drive parameters selected for Synchronous Reluctance Machine settings	162
Table 5-5 ABB Drive parameters selected for couples machine ACC800 start-up settings	163
Table 5-6 Low-speed Test Temperature readings of the test machine from 0-50 frequency and 0 to 1500RPM rated speed.	163
Table 5-7 low speed test current, voltage, power and power factor.....	164
Table 5-8 Harmonics produces by the SynRM and parameter settings of load motor.....	165
Table 5-9 Torque applied by load machine ABB drive penal	166
Table 5-10 Overspeed test results while varying frequency 50 to 55Hz.....	167
Table 5-11 Overspeed Test Temperature readings of the test machine from 0-50 frequency and 0 to 1500RPM rated speed.	167
Table 5-12 over speed test results data at 55hz	169
Table 5-13 retardation test results	170
Table 5-14 Experimental results for loading test [43].....	178
Table 5-15 comparisons with the cost proposed the design of SRM and IM (2SIE 280 S4) for mining application	178

Table 6-1 Initial 40 Latin Hypercube Samples with round slot shape for SynRM design	202
Table 6-2 rotor optimisation and turns with 3 flux barriers.....	204
Table 6-3 shows the 3 flux barriers and 4 flux carriers while considering only stable torque	208
Table 6-4 shows the data of 4 flux barriers and 5 flux carriers	208
Table 6-5 square shape flux barrier design with stable torque data	209
Table 6-6 shows 3 square shape flux carrier and 4 flux carriers data	211
Table 6-7 shows round stator slots shape with 4 round flux carrier and 5 flux carriers data	212
Table 6-8 square slot design with 24 slots LHS samplings points at 100 turns.....	212
Table 6-9 square slot design with 24 slots LHS samplings points at 50 turns.....	213
Table 6-10 round slots design with 24 slots LHS samplings points	215
Table 6-11 12/8 Switched Reluctance Motor (10Kw; 105 rpm) achieved parameters of 12/8 SRM	217
Table 6-12 variable range selection for Latin Hypercube Samples for 12/8 SRM.....	218
Table 6-13 12/8 SRM parameters for the 100 Latin Hypercube samples	218
Table 6-14 12/8 SRM parameters for the 60 Latin Hypercube samples	222
Table 6-15 7 Variables Global Optimisation Latin Hypercube Sampling Points of 12/8 SRM.....	224
Table 6-16 More variables Global Optimisation Latin Hypercube Sampling Points of 12/8 SRM	225
Table 6-17 (New) 6 Variables Global Optimisation Latin Hypercube Sampling Points of 12/8 SRM. ...	225
Table 6-18 Global optimisation sample for 170mm at constant speed 105rpm	228
Table 6-19 Global optimisation sample for 170mm at constant power 10kW	229
Table 6-20 Global optimisation sample for 200mm at constant speed 105rpm	230
Table 6-21 Global optimisation sample for 200mm at constant power 10kW	231
Table 6-22 Design Specifications of the 24kW SynRM.	232
Table 6-23 Design Specifications of the SynRM rotor	233
Table 6-24 Design specifications.....	233
Table 6-25 rotor dimensions.....	234
Table 6-26 stator dimensions of 8.58kW direct drive SynRM	234
Table 6-27 rotor dimensions of the 8.85kW motor for direct drive.....	234
Table 6-28 3-phase Winding specifications of 8.85kW rotor design.....	234
Table 6-29 asymmetrical rotor design parameters when length decreased (from the right side) and angle increased.....	235

Table 6-30 parameters when length decreased and angle length remain the same.....	235
Table 6-31 The equipment used in the experiment.....	236
Table 6-32 Results of No-load test	241
Table 6-33 No-load test data while coupling the shaft with 55kW load motor or No-load experimental data of temperature, speed, current, voltage, power, power factor, harmonics and vibration from 0-50Hz frequency.....	241
Table 6-34 low slip test data while connecting 55kW motor as a load.....	242
Table 6-35 List of Equipment used in the experimental setup	243
Table 6-36 Magnetic Flux density of 3 flux barrier synchronous reluctance motor.....	244

List of Figures

Fig. 1.1 The global electricity demand by different countries [9]	28
Fig. 1.2 Electricity consumption by European Union motors are responsible for total electricity consumption [15]	29
Fig. 1.3 Life cycle assessment and material which are commonly used in electrical machines [23].	30
Fig. 2.1 Motor energy usage in the industrial sector	36
Fig. 2.2 Mechanical variable speed drive system [33]	37
Fig. 2.3 Basic block diagram of VSD system.....	38
Fig. 2.4 The current system of gear drive used for Raymond Pulveriser [43].....	42
Fig. 2.5 shows the FEM model of SynchRM rotor geometry.....	46
Fig. 2.6 Three Alignments of SRM.....	47
Fig. 2.7 Basic SR motor stator, rotor, shaft and winding [23].....	48
Fig. 2.8 inductance vs torque profile.....	48
Fig. 2.9 Equivalent circuit of one phase of SRM [104]	50
Fig. 2.10 Power flow diagram in electrical motors	51
Fig. 2.11 electric vehicle motor drives characteristics	54
Fig. 2.12 Machine options for the EV propulsion applications.	55
Fig. 2.13 Electrical machines for EV propulsion drives.	55
Fig. 2.14 Axial flux PM motor for electric vehicles [192].....	60
Fig. 2.15 Model of liner transfer flux machine.....	61
Fig. 2.16 Synchronous reluctance machine based on hybrid technology.....	62
Fig. 2.17 SR motor based on hybrid technology	62
Fig. 3.1 Surrogate optimisation process [212].....	65
Fig. 3.2 Latin Hypercube samples for 1 st optimisation	68
Fig. 3.3 Flowchart of SynRM Machine design and optimisation	71
Fig. 3.4 Initial 40 Latin Hypercube Samples for SynRM design.....	72
Fig. 3.5 shows (a) 3 flux barriers and 4 flux carriers model with a round shape (b) torque waveform and (c) three-phase current waveform	77
Fig. 3.6 torque waveform while considering stable portion after 600ms	79

Fig. 3.7 round shape 4 flux barrier and 5 flux carrier SynchRM Numerical FEM Model	80
Fig. 3.8 shows the 1500ms time simulation (a) Torque waveform (b) 3-phase current waveform	82
Fig. 3.9 Square flux barrier design.....	83
Fig. 3.10 square shape 4 flux barrier and 5 flux carrier (a) SynchRM Numerical FEM Model (b) Torque waveform and 3-phase current waveform.....	85
Fig. 3.11 shows (a) round stator slot with round flux barrier FEM model (b) torque waveform	87
Fig. 3.12 Square slot design with 24 slots	88
Fig. 3.13 SynchRM with 24 slots (a) FEM Model (b) 3-phase voltage waveform (c) Torque wave form and (d) current waveform	92
Fig. 3.14 square shaped 4 flux barriers design (a) FEM model (b) torque waveform (c) current wave form (voltage wave form at 1500ms simulation time.....	93
Fig. 3.15 flux function view of (a) 4 square flux barrier design (b) flux function without exterior air	94
Fig. 3.16 square shape slot design and 4 flux barriers AutoCAD design used for SynRM.....	94
Fig. 3.17 Three-phase overall winding design arrangement of red, yellow and blue phase.....	95
Fig. 3.18 efficiency and torque graph os 60 samples with 3rd optimisation	97
Fig. 3.19 Efficiency and torque graph for final 60 samples	98
Fig. 3.20 efficiency at a constant speed	99
Fig. 3.21 Efficiency at constant power.....	99
Fig. 4.1 20 Latin Hypercube samples of flux barriers for rotor Optimisation	103
Fig. 4.2 Different rotor design steps for rotor optimisation. (a) Different flux barrier width with ribs (b) without ribs but equal flux barrier widths (c) different flux barrier width without ribs.....	104
Fig. 4.3 design of Rotor flux barrier No: 1 (a) starting away from rotor outer diameter (b) starting near to rotor diameter.	104
Fig. 4.4 different four flux barrier rotor designs for SynRM (a) 4 V-shaped flux barrier rotor (b) 4 square shaped rotor (c) 4 straight flux barriers with a slight angle at the edges.	106
Fig. 4.5 Three and four flux barrier rotor designs for SynRM (a) 4 square shaped flux barrier rotor (b) 3V-shaped rotor (c) 4 square shaped flux barriers with a slight angle at the end and (d) 3 square shaped flux barriers.	108
Fig. 4.6 (a) Flux barrier width and edge angle (b) flux barrier upper and lower length (c) full rotor dimensions.....	109
Fig. 4.7 Torque waveform of the proposed rotor.....	110

Fig. 4.8 2D SynRM model (a) side view only stator and rotor (b) side view with shaft (c) Mesh view..	111
Fig. 4.9 shows (a) the shaded plot view with 2.1 (Tesla) magnetic flux density (b) Flux linkage (c) shows the load force torque produced by the proposed machine	113
Fig. 4.10 4 poles 36 slots double layer stator	113
Fig. 4.11 Square shaped 4 flux barrier for Raymond Pulveriser	114
Fig. 4.12 Combined layoutwinding arrangement of all phases	115
Fig. 4.13 stator slots and teeth dimensions in millimeters.....	115
Fig. 4.14 8.58kW proposed SynRM (a) side view of motor thickness (c) side view of stator, rotor, and shaft	116
Fig. 4.15 shows 3.58kW SynRM design (a) current waveform (b) voltage waveform (c) Torque wave form	117
Fig. 4.16 shaded plot view of magnetic flux density 2.5T of 8.58kW motor	118
Fig. 4.17 shaded plot field arc graph.....	118
Fig. 4.18 shaded plot view of magnetic flux density 2.5T (b) Torque waveform of the 10.21kW motor	119
Fig. 4.19 shaded plot view of magnetic flux density 2.47T (b) Torque waveform of the 9.10kW motor	120
Fig. 4.20 Asymmetrical rotor design at 20mm length decreased final Model.....	121
Fig. 4.21 efficiency improvement profile.....	122
Fig. 4.22 torque improvement profile	122
Fig. 4.23 Torque profile of best machine when 2mm length decreased.....	123
Fig. 4.24 Rotor with increase 3rd flux barrier end near the outer boundary	123
Fig. 4.25 Asymmetrical rotor while cutting one left side angle.....	124
Fig. 4.26 asymmetrical rotor while cutting one right side angle.....	124
Fig. 4.27 Asymmetrical rotor with one side square one side round.....	125
Fig. 4.28 Asymmetrical rotor with length decreased from left and angle length remains the same	125
Fig. 4.29 Efficiency profile when length decreased and angle length remain the same.....	126
Fig. 4.30 12/8 switched reluctance model	127
Fig. 4.31 12/8 SRM simulation results of sample 15	127
Fig. 4.32 Three phase current, and voltage graph of sample 15	128
Fig. 4.33 12/8 SRM copper and core losses of sample 15.....	128
Fig. 4.34 12/8 SRM simulation results of sample 29	129

Fig. 4.35 Three phase current, and voltage graph of sample 29	130
Fig. 4.36 12/8 SRM copper and core losses of sample 29.....	130
Fig. 4.37 12/8 SRM simulation results of modified sample 15	131
Fig. 4.38 Three phase current, and voltage graph of modified sample 15	131
Fig. 4.39 12/8 SRM copper and core losses of modified sample 15	132
Fig. 4.40 12/8 SRM simulation results of modified sample 29	132
Fig. 4.41 Three phase current, speed and voltage graph of modified sample 29	133
Fig. 4.42 SRM copper and core losses of modified sample 29.....	133
Fig. 4.43 final 12/8 Switched Reluctance Motor Design	134
Fig. 4.44 final 12/8 SRM simulation results of flux density and torque	135
Fig. 4.45 average torque of final optimised design 12/8 SRM	135
Fig. 4.46 Current Vs rotor position of final 12/8 SRM	135
Fig. 4.47 3-Phase voltage of final 12/8 SRM	136
Fig. 4.48 Initial 72/48 SRM design (a) from view (b) side view	137
Fig. 4.49 variations of the torque and torque ripple as a function of major parameters (a) B_s (b) B_r (c) b_{sy} (d) b_{ry} (e) N_p (f) D_{sh} [43].....	138
Fig. 4.50 torque ripple and average torque profile while parameters variations instantaneously. (a) B_s and B_r (b) B_{sy} , B_{ry} and N_p (c) B_s and B_r (d) B_{sy} , B_{ry} and N_p	139
Fig. 4.51 Energy loop comparison in between flux linkage and current curves for initial and optimised design	140
Fig. 4.52 The diagram of the optimised design 72/48 SRM.....	141
Fig. 4.53 static torque versus rotor position of optimised SRM design at the variable current	141
Fig. 4.54 The flux density of the proposed machine.....	142
Fig. 4.55 Position of the rotor and developed Torque.....	142
Fig. 4.56 position of rotor against current supplied	143
Fig. 5.1 photographs during the manufacturing (a) initial rotor manufacturing stage laminations of the prototyped rotor (b) dimensions of rotor design settings on CNC machine (c) cutting of laminations as per the proposed shape of the rotor.....	145
Fig. 5.2 Cummins BCI-184F machine	145
Fig. 5.3 photograph of the manufactured rotor from the factory	146

Fig. 5.4 photograph of the PVC filling inside of the rotor flux barriers.....	146
Fig. 5.5 photograph of the PVC filling inside of the rotor with cover plate.....	146
Fig. 5.6 photograph is assembled rotor with shaft	147
Fig. 5.7 photograph of the assembled rotor after machining	147
Fig. 5.8 prototype development stages of the proposed rotor (a) early manufacturing from the factory (b) manufactured design rotor (c) flux barrier filling with magic (d) flux barrier insertion with magic and PVC filling with magic and PVC (e) assembled rotor with shaft (f) final assembled rotor after machining	148
Fig. 5.9 Experimental test rig	149
Fig. 5.10 Three-phase double layer winding terminals	151
Fig. 5.11 3 resistance taken from winding Photographs of (a) 3-phase terminals (b) winding 1 resistance (c) winding 2 resistance (d) winding 3 resistance	151
Fig. 5.12 Torque measuring instrument JN-338 series	152
Fig. 5.13 Torque transducer coupled with the shaft.....	152
Fig. 5.14 Torque signal	152
Fig. 5.15 photographs of (a) torque and (b) oscilloscope signals of speed measurement	153
Fig. 5.16 photograph of 3-phase stator winding megger testing.....	154
Fig. 5.17 Siemens Micromaster 440 of 22kW variable frequency drive.....	155
Fig. 5.18 No-load test results (a) RMS current and voltage and current value (b) voltage waveform (c) total harmonic distortion	155
Fig. 5.19 load machine of 55kW coupled with during no load.....	156
Fig. 5.20 Photographs of (a) thermocouples PT100 (b) Ohmic reading on multimeter (c) location of 5 thermocouples on the stator.....	157
Fig. 5.21 Temperature graph as different input frequency and speed	158
Fig. 5.22 frequency Vs speed chart and linearly trend line	158
Fig. 5.23 vibration measurement at variable frequency	159
Fig. 5.24 shows (a) 3-phase current and voltage reading (b) total harmonic distortion measurement at 50Hz	159
Fig. 5.25 equipment used and test results of over speed	168
Fig. 5.26 over speed test results up to 55hz maximum	168
Fig. 5.27 retardation test results.....	170

Fig. 5.28 V- Shape rotor of (a) numerically and (b) experimentally design.....	171
Fig. 5.29 Numerical and experiment speed results	172
Fig. 5.30 Magnetic flux density vs time graph	173
Fig. 5.31 Comparison of Numerical and experimental results of voltage vs speed.....	173
Fig. 5.32 Comparison of Numerical and experimental results of RMS current vs speed	174
Fig. 5.33 Combined current, voltage and RPM graph of experimental results.....	175
Fig. 5.34 Combined current, voltage and RPM graph of numerical results	175
Fig. 5.35 fabrication of SRM (a) The stator (b) The rotor.....	176
Fig. 5.36 The complete diagram of the experimental test test bench.....	176
Fig. 5.37 Pulse width modulation waveform.....	177
Fig. 5.38 Current waveform of a prototype of 72/48 SRM (a) No-load (b) Load	177
Fig. 5.39 The THD of the supply current [43].....	178
Fig. 5.40 Numerical and experimental results of the output current of 72/48 SRM	179
Fig. 5.41 Numerical and experimental results of the output torque of 72/48 SRM.....	180
Fig. 5.42 Numerical and experimental results of efficiency of 72/48 SRM.....	181
Fig. 5.43 Numerical and experimental results of power losses with respect to current of 72/48 SRM ...	181
Fig. 6.1 Latin Hypercube samples for 2nd optimisation	205
Fig. 6.2 Latin Hypercube Samples for 24 square shaped stator slots.....	215
Fig. 6.3 Initial 100 Latin Hypercube samples for 12/8 SRM design	217
Fig. 6.4 Initial 60 Latin Hypercube samples for 12/8 SRM design	222
Fig. 6.5 60 samples of LHS samples.....	228
Fig. 6.6 40 LHS samples for constant speed and constant power analysis	228
Fig. 6.7 Photographs of duplicate Cummins stator (PI-144F) (a-d).....	241

Chapter 1 Introduction

This doctoral thesis focuses on the novel design and optimisation of reluctance machines for the application of Raymond Pulveriser and Closed Couple centrifugal pumps. The aim of the optimisation is to reduce losses and torque ripples and to improve the output power and efficiency. This chapter gives a brief overview of the research background and goals while discussing the approaches used to achieve these objectives for this project. The thesis structure is also described in detail.

1.1 Background

Climate change is a matter of serious concern that belongs to the whole world in every country [1]. Presently, the world faces enormous challenges due to continuous urban and rural industrialisation. Due to population growth in the 21st century, have speed up the demand in the power generation, transportation and corresponding CO₂ emissions [2, 3]. The Intergovernmental panel on climate change (IPCC) 2014 projects that overall global temperature could increase 3.7°C to 4.8°C [4]. Therefore, it has been essential to debate at different international forums with legitimately binding agreements signed on different occasions. As an outcome, global CO₂ emission progression has declined from the last three years. In developed countries such as the United Kingdom, the lowest level of CO₂ emission has been recorded since the 19th century [5-7].

It has been estimated between 2014-2017, there had been three consecutive years of slight or no progression in carbon emissions from energy consumption. This actually became possible due to speeding up advantages in the energy efficiency development, energy demand and fast progress in renewable energy joined with a continuous decline in global coal consumption leading to enhancement in the fuel mix [8, 9]. The progress to some extent upturned during last year and the growth in energy demand again increased. Similarly, in the recent policies situation, the global energy requirements rise more than in the past but then again it expands by 30% between today and 2040 [10, 11]. The global electricity demand by different countries is shown in **Error! Reference source not found..**

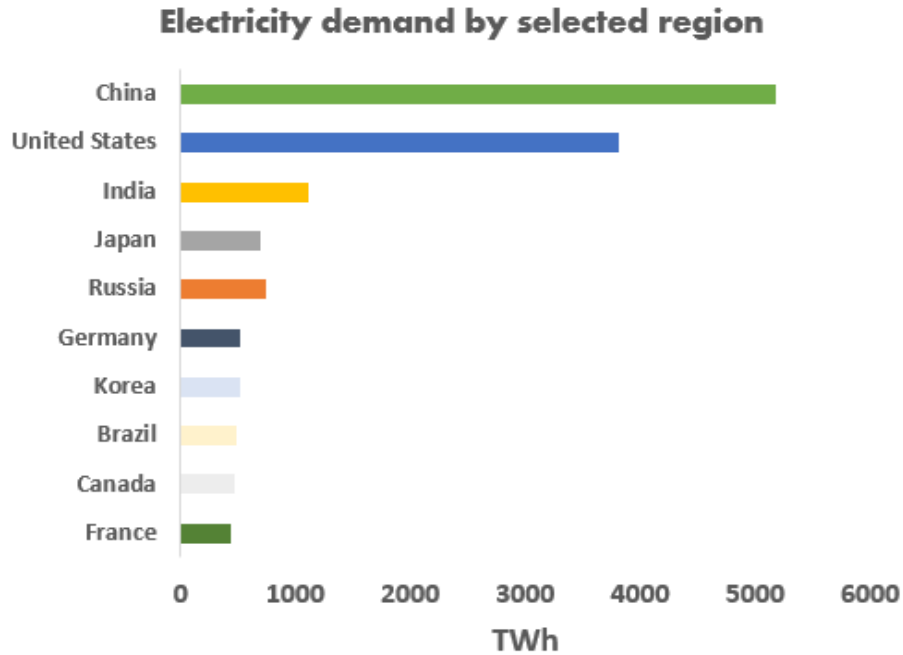
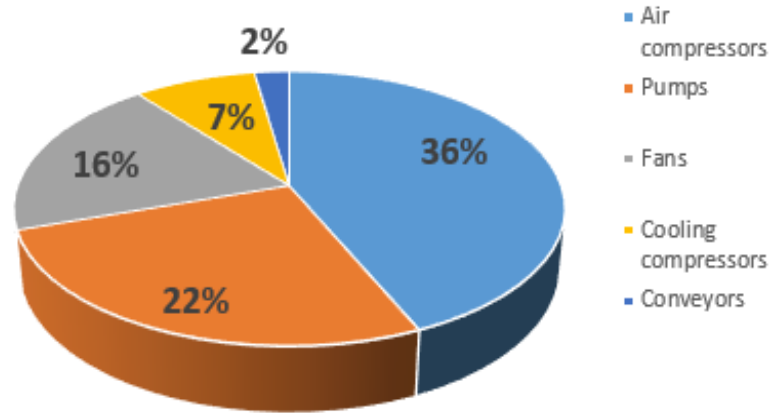
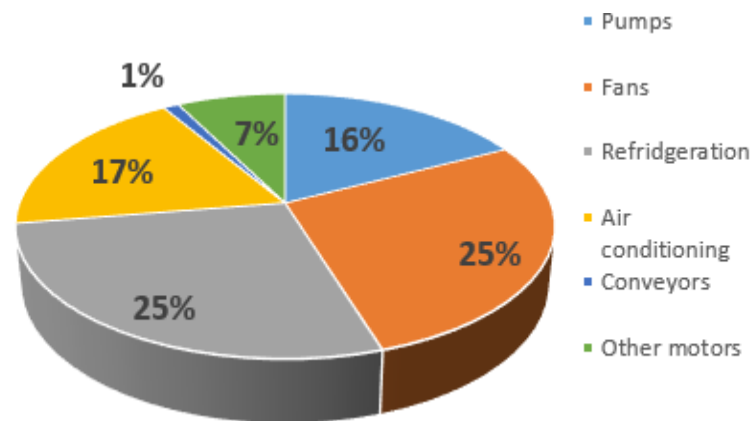


Fig. 1.1 The global electricity demand by different countries [9]

As per European Union eco-design, generally, the electric motors are subject to different design requirements. Almost 50% of the electricity is consumed by motors which are found for different applications like for industries as well as the service sector. If the motor is more efficient then a lot of money can be saved over the lifetime of the product and in terms of electricity saving and as per eco-design statistical data analysis 135TWh of the electricity can be saved by 2020 [12] and this would be equivalent to the annual electricity utilisation of Sweden. This reflects that more than 60 million tons of CO₂ will be stopped to liberate in the environment. In the EU, different products e.g. fans, compressors, washing machines and conveyors with cooking appliances carry energy consumption labels and are planned to design to run at minimum energy efficiency standards. The electricity consumption by EU motors for industrial as well as the service sector is shown in Fig. 1.2 (a) industrial sector and (b) service sector. The whole results of these labels and standards will be an annual energy saving of nearby 175 Mtoe (million tons of oil equivalent) up to 2020 emission target. It is approximately comparable to the yearly major energy consumption of Italy. For users, this means a regular savings of up to €500 in a year on the domestic energy bills, so that's why different regulations and directives have been driven to reduce the energy bills. In this thesis the major aim has been set to achieve the low losses, low torque ripples, energy efficient SynRM according to IEC standards [13, 14], Nowadays there is a trend towards green technology so that's why the demand for increasing machines which are highly efficient is increasing. The government systems like US energy Department [15], EU [16] declared guidelines for electrical machines.



(a)



(b)

Fig. 1.2 Electricity consumption by European Union motors are responsible for total electricity consumption [15]

The IPM is well-known in EV technology for its high efficiency and great power density, but because of the increasing demand of NdFeB has increased the price of permanent magnet machines and there are lots of environmental concerns due to waste products generated during the process of exploration and refinement of these materials [17, 18].

Mainly the common materials used in machines are NdFeB and SmCo Magnet, copper, aluminum, steel, and polyethylene as per available properties, these materials are used for purposes like for producing a magnetic field, as good conductor of electricity and for electric and heat insulation. Among this material, the NdFeB has serious environmental effects. Fig. 1.3 shows the chart of Life cycle assessment of the material which is commonly used in electrical machines, this actually shows the environment impact of NdFeB compared with copper, aluminum, steel, and polyethylene. Fig. 1.3(a) shows almost 30kg of CO₂ equivalent by NdFeB whereas other material such as copper, aluminum, steel and polyethylene has low CO₂

emission. Similarly there is higher photochemical ozone creation by NDFeB almost 0.018kg equivalent as depicted in Fig. 1.3(b). The acidification and eutrophication potential is also higher in the usage of NDFeB material as shown in figure 1.3 (c-d). Because of this reason, the reluctance machines have become the strong candidate for applications of EV and HEV and various other usages because of non-existence of magnetic material, cheap in cost, simple in construction, very robust, absence of demagnetisation issues and can be operated smoothly at excessively high temperature [19-22].

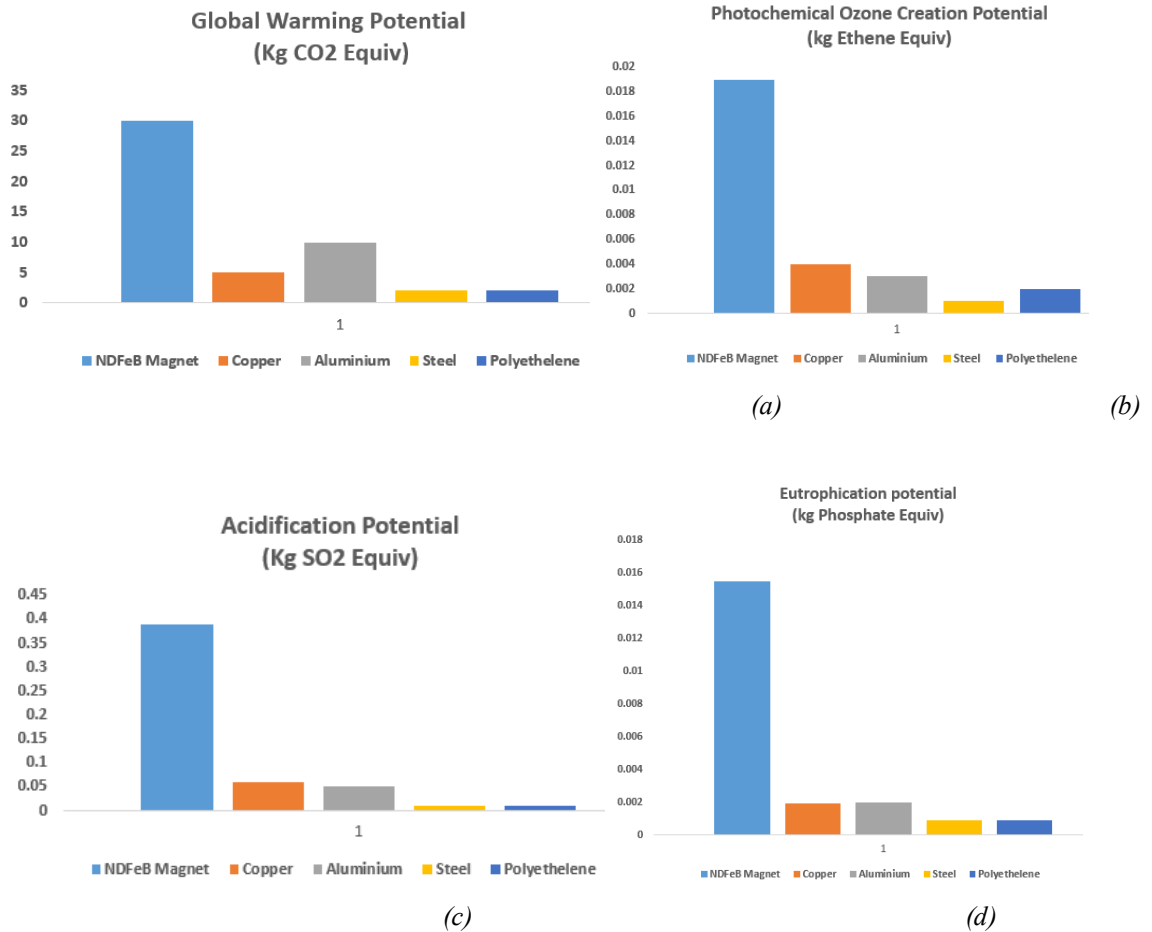


Fig. 1.3 Life cycle assessment and material which are commonly used in electrical machines [23].

Thus, the worldwide investigation for reducing the practice of conventional fossil fuel and magnet-free machines has been greater than before. Therefore, despite induction motors (IMs) have been the most prominent choice for marketable industrialised applications, new technologies, and applications, such as industrial equipment, closed coupled centrifugal pumps, Raymond pulveriser, hybrid and electric vehicles are attracting more attention.

The synchronous reluctance motors (SynRM) has been great attention owing to numerous benefits (i) fault tolerant capability (ii) great torque density (iii) wide flux weakening capability (iv) good efficiency (v) robust structure [24, 25]. The other properties of Synchronous Reluctance motor are as under:

- Stator is similar to IM
- No winding in the rotor
- Low power factor
- Cheap
- Simple and rugged construction
- Higher efficiency also with partial loads
- Higher reliability due to lower winding and bearing temperatures.

Additionally, the nonexistence of permanent magnets (PMs) which actually reduces the cost of material and due to the high-temperature environment, restrict the demagnetisation problems in the PMs. Generally, reluctance machines (RM) have been examining in various applications at multiple speed ranges [26-29]. But, there are few disadvantages (i) low power factor (ii) torque ripple is high [30, 31]. The above disadvantages can be effectively mitigated through the proper FEM design and optimisation and through accurate analysis with proper choices of flux barriers and flux carriers and their edge angles. Though several parameters and other quantities should be considered into account.

1.2 Motivation and objectives

If engineering industry is offered a chance to make choice between two alternatives of electrical machines, which have the identical performance such as efficiency, but one machine can be built at lower cost of manufacturing, with better thermal stability, it is understandable that the later design with cheaper cost will be chosen and preferred for the large-scale development. It is the manufacturing interest of the industry to construct highly reliable machines at a low cost. The limiting factors are the mechanical properties, efficiency, and cooling of the machine. To create a reliable comparison, a sufficient volume of different machine designs should be considered. In this thesis, a comparison between synchronous reluctance and the switched reluctance machine is given.

The main focus of the design is to obtained high efficiency, output power, and low torque ripples. The motivation for the research work is to attain the following objectives:

- (1) To design and simulate a synchronous reluctance and switched reluctance motor while optimising both stator and rotor to simplify the manufacturing process for mining applications.
- (2) To provide a detailed analysis of the influence of round and square shaped stator slots and rotor flux barriers through simulation on the SynRM performance.

- (3) To compare the performance of SynRM with Switched Reluctance motor with simulation results.
- (4) To design a synchronous reluctance motor while optimising rotor only to simplify the manufacturing process for closed couple centrifugal pump with simulation and hardware results.
- (5) To validate the FEM simulation results using the experimental test rig.

Accomplishing the above objectives involves a reduction in the power loss and ripple with low losses of SynRM rotor with novel geometry. An appropriate method of optimisation and an equivalent set of rules are established and applied through surrogate-based optimisation (SBO).

1.3 Methodology

The thesis is basically on the 24kW Synchronous Reluctance rotor design and optimisation in a double layer 36 slots stator commercially made by Cummins to achieve energy efficiency and thermally stable performance with low ripples. Two applications for the machine design have been considered which are: (1) Direct-Drive Centrifugal pump (2) Raymond Pulveriser for mining application. The following methods have been utilised for machine design simulation and to validate the results:

- First of all, the design of the 3 phase induction motor stator and switched reluctance motor is carried out through *MOTOR SOLVE* machine design software. This software has the capability to generate a magnet and *AutoCAD* file.
- The files are imported into Infolytica *MAGNET* machine design software and converted into solid material.
- The SynRM rotor geometry is designed using *AutoCAD*.
- The synchronous reluctance motor performance with switched reluctance motor is analysed by means of FEM analysis *MAGNET software*.
- The proposed machines and the novel rotor design parameters are optimised by surrogate optimisation process by generating different Latin Hypercube samples of various geometry constraints. The analogous information is managed in *MATLAB*.
- To validate the results, the novel designed rotor is prototyped and experimentally verified.

1.4 Thesis Overview

This thesis presents the design and optimisation of Synchronous Reluctance motor having 3V-shaped flux barriers and 4 flux carriers on the rotor. Six chapters are included in the thesis which is summarised as under.

Chapter 1 describes the background of the research in the introduction and with a detailed methodology of the research. The main objective of the research and motivation are also discussed in this chapter.

Chapter 2 reviews the types of different machines for mining application, electrical vehicles (EV) and for other industrial usages. The development of machines which work on the basis of reluctance torque such as synchronous and switched reluctance machines is presented with different designs. All the design shapes and topologies are also covered in the chapter with advanced design and methodologies used in the existing research. The process of flux barriers and carrier in SynRM selection and shape designing have also been reviewed in this chapter. Additionally, the design of SRM and its working principle has been described in this chapter.

Chapter 3 analyses the surrogate optimisation process with square and round shape of the stator design for SynRM. In this chapter, the detailed Latin Hypercube Sampling generation along with algorithm used has been described. The Optimisation process and data results of 3 and 4 flux barriers are also described. Additionally, the FEM design of three-phase 8kW 12/8 SRM configuration has been carried out along with most influencing parameters to improve the torque and efficiency. At the end novel rotor design of SynRM optimised through surrogate-based optimisation method is selected for the prototype and testing.

Chapter 4. Focuses on 3 synchronous reluctance machines for the application of Raymond Pulveriser and Centrifugal pump, the machines are design and simulated. The design of SynRM and SRM through simulation (FEM results) based on optimisation are analysed with a different arrangement of stator and rotor shapes (square and round) and for SRM parameters (stator and rotor pole arcs and yoke thicknesses, airgap thickness, shaft diameter, rotor inner diameter). Then based on the design experiment, SynRM design is further simulated for the application of the direct-drive closed couple centrifugal pump. The SynRM final design is proposed for prototype development. The asymmetrical rotor geometry is also analysed by decreasing the length from both sides and their effects on efficiency, and torque is analysed. Additionally, the simulation and design specification 72/48 SRM for Raymond Pulveriser which is the initial machine to replace the existing induction motor has been presented.

Chapter 5. The rotor manufacturing steps and the arrangement of the experimental test rig are presented. In this chapter, the final validation through different test is performed on the optimised 3V shaped rotor design. In addition to this, the experimental testing of 72/48 SRM has been presented. Finally, the electromagnetic aspects of the design with simulation and experimental results are analysed, which verifies the FEM models and the proposed design.

Chapter 6 overall conclusion and the research findings are presented, along with suggestions regarding future work has been described.

1.5 Contribution to knowledge

The following contribution has been made in this research work.

- Design and optimisation of both stator and rotor of synchronous reluctance and switched reluctance motor by using surrogate based optimisation technique.
- Efficiency and torque comparison through finite element method result of synchronous reluctance and switched reluctance motors for the application of Raymond pulveriser.
- 4 square shaped flux barriers for rotor have been optimised by using SBO with 24 and 36 square stator slots and compared with 12/8 SRM while keeping the same stator and rotor dimensions. The simulation analysis carried out on *Infolytica Magnet* software for SynRM and *Motor solve* software for SRM. The analysis carried out in terms of power rating, current, voltage, efficiency and torque improvement of both machines and the advantages and disadvantages have been conducted under design applicable constraints.
- This work also provides the new SynRM rotor scheme with the SBO process. The arrangement of FEM with the surrogate optimisation is capable to minimise the time cost of the random or outdated process of optimisation and address the rotor design complexities.
- Introduced novel rotor design strategy (Symmetrical and Asymmetrical rotors) with 3V-shaped flux barriers and four flux carriers for the SynRMs for a centrifugal pump.

Infolytica Magnet software is used for electromagnetic performance analyses then validated the effectiveness after prototyping and testing on the experimental test rig. The rotor performance is analysed while using 36 slots structured stator made by Cummins as same as IM's stator. For the rotor design, flux barrier, flux carrier, edge angle, and shaft diameter are optimised through surrogate based technique and particle swarm optimisation (PSO) method is used to achieve the best design.

The work truly proves that a new rotor design can enhance thermal performance and with reduced torque ripple. The rotor manufacturing process improved mechanical integrity, reduces the vibration and increase efficiency.

Chapter 2 Literature Review

This chapter introduces the reluctance machine (RM) history and evolution in the introduction. In addition, SynRM and SRM technology are presented, the main benefits and the challenges related to reluctance machine technology are reviewed. As the greatest influence in the performance of a synchronous reluctance motor relies on rotor architecture, therefore design pattern, the shape, and flux barriers and carriers width of rotor geometry are analysed. This thesis aims to present the work to lower torque ripple and to enhance energy efficiency with maximum power output. So, the survey will concentrate on introducing the synchronous reluctance construction and the state-of-the-art rotor design topologies. This study brings brief research on the advancement of reluctance machines, as well as design, application, specific topologies, investigation methods along with their merits and demerits. Furthermore, to this, the other applications such as electrical machines in the field of electric vehicles (EV) is presented with different types of machines, their merits and demerits have been described.

2.1 Introduction

In this literature review, the main data and information have been taken from MSc and Ph.D. thesis, books, reports, web materials, journal articles, and handbooks on electrical motor energy use, losses, efficiency, and energy savings strategies. In addition to this, the types of motor losses are identified which occur and the ways to efficiently mitigate them are explained.

In industrialised countries, electric motors account for the huge consumption of overall electric power. The literature indicates that mostly 2/3 of industrial power is consumed by motors in each country, which is overall 60 to 70% consumption of power. Because, the application of electric motors is found distinctively in different areas such as industry, household electrical appliances, municipal and commercial services, and other applications to power a variety of equipments comprising machine apparatuses, compressors, pumps, and wind blowers [32, 33].

2.2 Motor Drives System and Energy Savings.

From the last few decades, due to rapid economic growth and development towards industrialization from agriculture, there is a huge number of efficiencies declining in electrical machines. At the same time, there is great potential for energy improvement. Currently, to reduce greenhouse gas emissions, the government and other research organisations are actively involving to enhance the energy efficiency in machines.

The operational speed and torque of electrical motors are controlled by the use of drives. Corresponding to the load requirement, motor drive technology is used to regulate the speed of the motor. Various types of

terminologies are used to define the drive. AFD, VSD, VFD, but all have the same meaning. In many applications, there have been significant savings through variable speed drives (VSDs) based system.

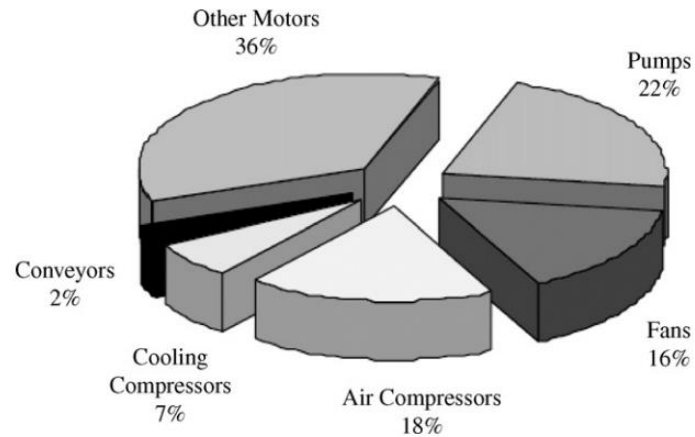


Fig. 2.1 Motor energy usage in the industrial sector

The motor energy used in the industrial sector is depicted in Fig. 2.1. It should be noted that in existing literature, there is no comprehensive literature about the comparison between Direct-Drive SynRM and SRM for Raymond Pulveriser and Close Coupled Centrifugal Pumps and their analysis. It is anticipated that this comprehensive literature will fill that gaps in terms of Ph.D. thesis.

Additionally, the study could provide significant strategies for machine design optimisation and visions for future development provisions and research work to reduce motors losses and efficient development of rotor fabrication process. Among industrial energy users, this will bring awareness to reduce environmental pollution and motor energy losses.

2.3 Variable Speed Drive

In the earlier year, the study shows that various control procedures have been adopted for the enhancement of flexibility and monitoring in manufacturing processes which are regulating the speed of the device [34]. In most of the cases, the electric motors are controlled through a valve that adjusts the flow of fuel or a blade which regulates the water or airflow. During this operation machine's speed remains unaltered. The methods like using semiconductor devices and controlling motors by switching it on and off are ineffective ways in which there is a wastage of energy. The most popular reasons that make electric drives efficient is, energy is saved by varying the speed of a motor and regulates the power which is fed towards the machine. Besides this, by means of motor drives cut the quantity of CO₂ radiations by millions of tons each year [33].

A VSD changes the speed, output torque and rotational force of the mechanical device. Few main applications of the mechanical devices in which variable speed drives are installed are centrifugal or

reciprocating pumps, blowers, compressors, and conveyors. In addition to this, many other types of mechanical equipment would benefit from the drives because they are running inadequately and inefficiently. Whereas, in order to reduce the losses of mechanical equipment and to improve the efficiency, the manufacturing companies are bringing together variable speed drives (VSD). As by the usage of VSDS technology efficiency is enhanced by allowing electric motors to operate at the precise speed as per load requirement. In most of the cases for different applications, the VSDs have decreased 30-60% of the motor's electricity consumption. Thus, the potential for saving of energy is huge because the motor system utilises more than 60% of the electrical energy in the industry [35-37]. Around the world, there are many motors with a wide variety of industrial applications such as centrifugal pumps, ski lifts, sawmills, paper mills, conveyors, heat ventilation and air-conditioning (HVAC) system, which can efficiently enhance the efficiency mainly where flow control is involved.

2.4 Method of speed control

Variable speed drives and variable frequency drives are the controllers which electronically control the speed of the motor and allows the wide range of speed variation. In the industry, there are three methods which are used to control the speed of the motor. Such as mechanical drives, electrical drives and hydraulic drives [38].

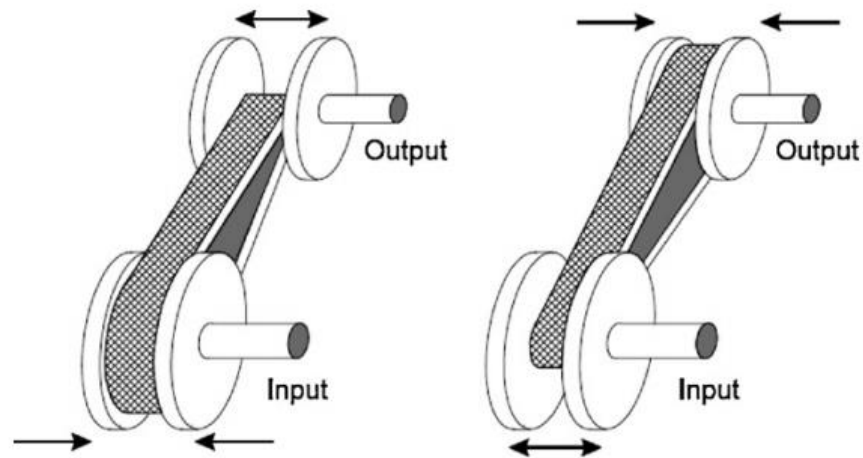


Fig. 2.2 Mechanical variable speed drive system [33]

2.5 Mechanical variable speed drives

The mechanical VSD is the choice of many engineers because it is very simple and low cost. The most common mechanically speed control methods are gear drive, chain drive, belt drive, idler wheel drives [39-41]. The mechanically controlled moving conical pulleys belt drive system is shown in Fig. 2.2. These techniques have comparable physical characteristics. The machine is operated at constant speed whereas

only the coupling ratio is altered, not the speed of the load. Thus increase the output load torque which actually increases the torque on the motor [38, 42].

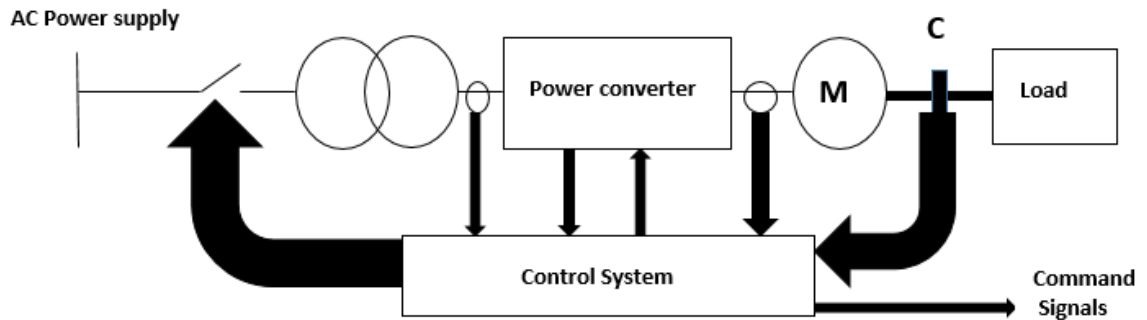


Fig. 2.3 Basic block diagram of VSD system

2.6 Electric variable speed drive

Typically, three main components of electric VSDs are motor, converter and the control unit. Usually, the motor is coupled with load or indirectly (with gears) towards the load. The power is controlled via a converter and power flow is regulated from alternating current (most of the time by transformer), appropriate semiconductor switches (BJT, IGBT, and MOSFET) are used in the controller. The basic block diagram and components of electric VSDs are depicted in Fig. 2.3.

2.7 Hydraulic VSDs

The main working principle of hydraulic coupling is based in turbines. By fluctuating the oil volume, the coupling will vary the speed difference in between the driving and driven shafts. The volume of the oil is precisely controlled by regulating valves and pumps [42].

2.8 Importance of Direct Drive

In today's modern world of technology, the importance of direct drive cannot be denied by many machine manufacturers. However, those who are familiar but might not wish to adopt this technology. Because they consider it too heavy and bulky as compare to the geared motor which is preferred for many years. Similarly, as the internet and smartphones have been evolved too much from the necessity to luxury, and on the other hand the lower end technology is still being used for example, still people buy flip phones as well as dial-up touch tones, ultimately the advantages of more developed technology become too challenging to ignore. Nowadays for an extremely efficient and competitive domain, the better someone knows the benefits of direct-drive systems, then they will have much-improved gains and superiority over the other. In order to understand the main benefits, it is essential to start with the basic concept of direct drive. Where the power of the motor is straight away applied to machinery without any in-between drive train such as the pulley, belt or gearbox.

The inheritance of extremely efficient electrical machines has been the strategy for as long as the motor familiarised. Industrially established and the well-developed induction motor is no doubt the least expensive, very rugged and enormously reliable motor as compared to available other AC machines in the market. These motors are being used in the wide variety of applications such as underwater or fully dry surroundings or for any other hazardous environment like coal mines, oil and gas industries. In spite of the above various application of such motors, advance development of such type of machines is technically challenging due to legacy obstacles such as winding on the rotor.

2.8.1 Direct Drive Systems

The applications of low speed, high torque direct-drive motor systems are greatly demanded their high efficiency, reliability, responsiveness and great maintainability [43, 44]. Usually, the Induction motors (IMs) drives performance is based on a driving force in the manufacturing industry which connects with load via a mechanism of mechanical systems of reduction, such as a belt, gear, or pulley. Mostly IMs does not work without reduction mechanism for low-speed and high torque application [45]. The commonly used applications of direct drive are: Home appliances such as washing machines which actually run at low speed with large torque, spinning which required high speed and low torque, and there are different methods used in washing machine for driving which are classified as gear drive, belt drive, pulley drive, and the most common drive system is belt drive. But the major disadvantage still exists which is heavy noise and vibration due to belt and gear. Conversely, the direct drive system has the advantage of low noise and vibration. However, the direct drive motors require to carry very large load compared to the gear of belt-drive. The usage of direct drives ranges from broad applications and originates in diverse systems but for this thesis, we are interested to limit our discussion in normally used gear motors.

2.8.2 Advantages of direct-drive

The main advantages of direct-drives (DDs) as compare to indirect drives, such as working mechanism is simple thus increases the reliability and robustness, additionally, friction losses are minimum, gaining higher rigidity, and improving the driving torque [46]. Therefore, it is frequently being used in the following applications [47, 48].

- (1) Manufacturing systems of semiconductor
- (2) Industrial robotics
- (3) Computerised numerically controlled (CNC)
- (4) Machine tool
- (5) Servo applications
- (6) Variety of applications in automated industries

2.9 Permanent Magnet Direct Drive

Another most widely used machine for high torque-low speed application is Permanent magnet synchronous machines (PMSM) operated by an electronic controller [45, 49]. The main advantage is that they have the capability of having high torque density, Therefore, IPM type brushless motors have both magnets as well as reluctance torque, are used so as to achieve the high efficiency. In addition, to reduce the copper losses, the concentrated winding is used in the stator core. But, as the cost of requiring large amounts of rare-earth permanent magnets, whose price indicates a great proportion of the total expense of the machine. Additionally, the rapid upsurge of the price of rare-earth magnets which happened at the start of the decade increased the cost of PMSMs significantly. Hence, the importance of other technologies has increased. Among them, reluctance technology arises as a good substitute. Several studies have presented that SynRMs offer many advantages compared to induction machines (IM), such as a higher torque density and efficiency, lesser rotor temperature and, the lower price [50-54].

The construction of transverse-laminated rotor structure of SynRM is having attention by the different users, because of its simple construction, cost, robustness, and manufacturing process [55, 56]. Typically, a pumping arrangement is mostly accompanied to couple 1500rpm induction motor with a centrifugal pump but, this system has a lot of disadvantages such as heavy and bulky motor drive system with low energy efficiency. In this regard, for high-torque applications, PMSMs are dominated, but the most important issue is the recycling of these rare-earth metal permanent magnets. Additionally, the cost of magnetic material collectively with demand and supply chain issues is preventing these machines from assuming its rightful place as a motor of choice near future. Due to the rare-earth magnet's increasing price, their market stability is declining [57]. Thus, a universal satisfactory solution has not been adopted for the application of closed coupled centrifugal pumps. After the advancement in electrical drives in the 20th century by reason of fast dynamic response and high efficiency of the drives, the reluctance motors represent a much possible alternative [58],[53].

In order to reduce the high torque ripple which is not desirable for many industrial applications, lots of studies have been conducted and to enhance the performance of the machine, like in [59],[60],[31],[24], the torque ripple is investigated and multiple solutions are tested. Further to enhance the torque density of the machine, the rotor design is investigated in [61],[57],[62] in which the saliency ratio is examined which denotes the ratio between the d-axis and q- axis.

Recent research investigations in the high-speed operation of SynRM are mainly dedicated to the type of rotor which is axially laminated anisotropy (ALA) [63-66]. Because of its higher saliency ratio [67-69] and a very rigid structure. However, the disadvantage of ALA structure is, it produces very high iron losses due to thicker rotor laminations as compare to TLA type rotor in addition as ALA has undesirable flux

oscillations. Hence, because of low iron losses, as well as simple construction using normal punching of lamination with skewing, moderate saliency ratio in most of the applications the TLA type rotor is preferred [29, 70-72]. Therefore, the TLA type rotor has been used in these studies for the SynRM simulation model design. The major aim has been set to select the number and shape of flux barriers to achieving low power losses along with low torque ripples.

2.10 Current state-of-the-art SR Motor Drives for Raymond Pulveriser

This section is based on our published journal paper which can be found at [43]. In recent times pulverised coal has emerged a most widely used fuel in the mining applications. However, in order to get the optimum output, it is important that the supply chain of coal is properly maintained [73, 74]. The coal typically used is characterised by high ash and low calorific content. This leads to premature cracks and failure of the refractory lining. Ash deposits require more heat to be added to the charge for maintaining the desired temperature thus increasing the burning losses [75]. Also, high ash contents lead to choking of the recuperated tubes. This necessitates frequent cleaning thus high maintenance cost and reduced the performance of heat exchangers [76]. The ideal size of the pulverised coal should be at least 75-80% of 75 microns. In the conventional systems fine coal ranges from 10-30% of 75 microns. Non-uniform coal particles undergo partial combustion and result in deposition in the furnace walls [77]. These cause particles escape from the furnace with flue gas in the form of un-burnt carbon or ash [78]. The energy efficiency alternative to use in pulverised coal as fuel starts with procurement of good quality coal. Coal with high calorific value and low ash content is ideally suited as pulverised coal. The next step is to process or pulverised coal into the desired finest consistently [79]. To do so certain modifications in the pulveriser are required. The critical components of a pulveriser are: (1) Hammer, (2) Mild steel liner (3) classifier and (4) In-built blower. For better and long-lasting quality of the pulveriser, the metallurgy of the hammer should be improved to increase its resistance to wear and tear. The performance and efficiency of Raymond Pulveriser is directly depending upon its prime mover. A unique 72/48 SRM design with 75kW motor for the direct-drive having low-speed used for mining application has been proposed in [43]. This gives the essential part of the study throughout the thesis. This is already mentioned that the IM drives in the industry, typically acts as a driving force and is connected with the mechanical load via a reduction gear mechanism, by means of belt or pulley. The Raymond Pulveriser is mostly worked at a very low speed of 105 rpm, This requires 7kN.m torque [80]. The existing gear system for Raymond Pulverizing is shown in Fig. 2.4. And the conventional IM drive features are given in Table 2-1.

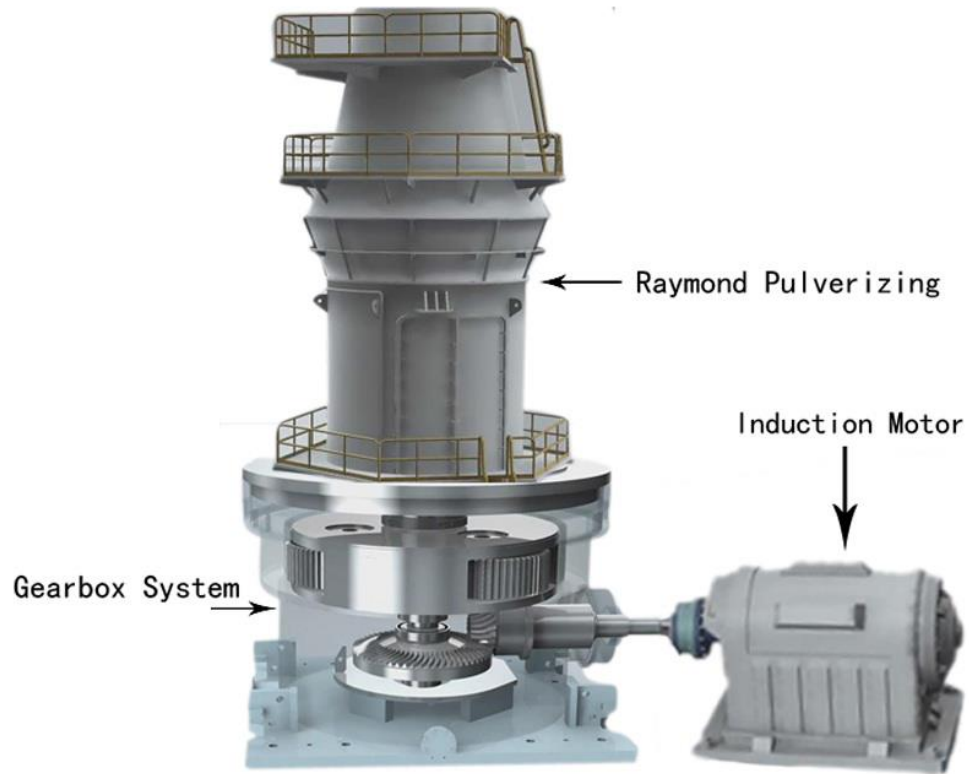


Fig. 2.4 The current system of gear drive used for Raymond Pulveriser [43]

Table 2-1 The features of conventional IM drive in Raymond Pulveriser [43].

Parameter	Value	Parameter	Value
Weight in Kg	678	Power in kW	75
Voltage in V	400	The gear system outer diameter in mm	1000
Power factor	0.9	The Efficiency of a gear system in %	62.98
Efficiency in %	94.2	The gear system stack length in mm	340
Rated torque in Nm	481	The total efficiency of a geared drive system in %	59.32
The output speed of a gear system in rpm	105	Frequency in Hz	50
The total weight of a gear drive system in kg	1050	Rate Speed in rpm	1488
Current in A	128		

There is widespread usage of the gear drive mechanism; the torque is transferred by the gear. But, there are some downsides e.g: noise, vibration and low efficiency, [81]. Contrariwise, it has a very good dynamic performance with reliability, [81-84]. Thus, the efficiency of the gear system is 62.98%, the conventional drive system has 59.32%, and the motor has 94.2% efficiency. The gear and direct-drive comparison are shown in Table 2-2 [85-87].

Table 2-2 The drive mechanism of a Raymond Pulveriser [43]

Construction	Direct drive system	Geared drive system
Reliability	high	moderate
Efficiency	high	low
Noise	low	high
Balance	good	poor
Gear Ratio	—	14.28: 1
Lubrication system	not significant	significant

A low-speed direct-drive for wet grinding has 36 applications by using External-Rotor Synchronous Reluctance Motor was presented [44]. For high performance of servo-applications, the Direct-drive motors are engaged. An electrical motors robot consists of a mechanical arm or directly coupled to the joints is described [88]. The features of SR motor, are the capability of very high torque at low speed, reliability cheapness as an alternative. As SRMs can be operated at high temperature so there is a huge potential to replace induction motors in Raymond Pulveriser applications, [89-93]. As there is an absence of permanent magnet in SRMs, therefore the cost of these motors is much lower [91, 92].

This thesis project is dedicated to environmentally hazardous mining applications to develop motor drive systems for high torque with the finite element method. The design investigation is done while using the surrogate-based optimisation technique. The second application of the machine design in which the main rotor has been optimised and tested is closed couple centrifugal pump. The specifications of the existing induction motor which is used for this application is shown in **Error! Reference source not found.3**, and the full machine design performance and optimisation are explained in chapter 3 and 4.

Table 2-3 Specifications of Induction motor used for closed coupled centrifugal pump

Number	Item	Value
01	Power	22kW
02	Current	40Amp
03	Horse Power	30
04	Speed	1450rpm

2.11 Synchronous Reluctance Motors

Nowadays, the trend of high efficiency and high torque electric machines are increasing research concern and mainly the machine which contains no permanent magnet is growing rapidly. Although there is lack of

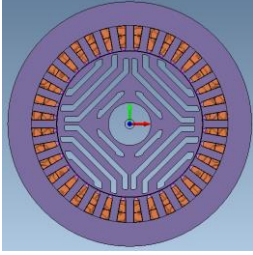
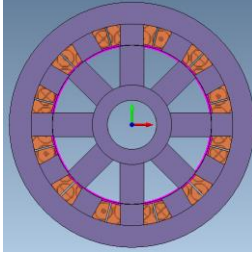
interest in this technology of synchronous reluctance during last 2 decades, the magnet free synchronous reluctance motors are reviving once again and emphasizing a research interest due to its construction without the usage of permanent magnet [94] and because of this, SynchRMs are being considered as key solution for industrial applications and energy conversion [95]. The focus on synchronous reluctance has become the potential future technology for the industries as well as the application of electric vehicle EVs. A SynRM is a singly salient motor which works on the basis of reluctance torque without using the PM material at synchronous speed. The SynRM has cylindrical stator same as that of an induction motor. The main advantage is the magnetically salient rotor structure which removes the copper and aluminum bars [96, 97].

The SynRM performances can be enhanced with the lowest possible financial cost. Because its rotor construction is passive, no permanent magnets neither windings are installed into it. So that's why it is the economical part that could be re-designed and easily replaced. The literature reveals that a lot of research work has been done on the synchronous reluctance for different applications. And due to the absence of slip losses and the simplicity in control, propose the opportunity of performance as well as with the advantages in the cost, the latest awareness in the synchronous reluctance motor has enhanced in the perspective of possible application in the field oriented Ac drive and more advantageous over induction motor [61].

Smoothly distributed poles with an iron core of open or semi-closed slots arrangements are laminated. the sinusoidal rotating magnetic field is created on the stator air gap side through the symmetrical 3-phase winding. The slots are placed at an even pitch angle. Due to the property of magnet field to adopt minimum reluctance path, a reluctance torque is developed because of the induced magnetic field in the rotor which has the tendency to cause the rotor to align with the stator field.

To improve the performance of SynRM, the d-q axis ratio (saliency ratio) should be as high as possible. The SynRM saliency ratio is the electromagnetic design of the rotor within a decoupled reference frame the d represents direct-axis which means the minimum reluctance path and the q represents quadrature-axis which means the maximum reluctance path. In other words, a high direct axis inductance and a low quadrature axis inductance; this ensures high production of torque and energy efficiency. This thesis work has attempted to achieve a 60-to-70% saliency ratio of SynRM rotor.

Table 2-4 Comparison between SynRM and SRM machines [176]

	Synchronous Reluctance Motor (SynRM) 	Switched Reluctance Motor (SRM) 
Rotor	Arrangement of internal flux barriers and carriers	Salient pole structure
Stator	Conventional AC machine similar to IM	Salient poles
Excitation	Balanced sinusoidal supply current	Pulsed DC and voltage input sequence
Machine saliency	Single Solid (Rotor)	Double Saliency (both stator and rotor)
Winding	Polyphase distributed winding	Single tooth concentrated winding
Converter	Conventional 3-Phase Inverter	Asymmetrical Half-Bridge Converter
Inductance waveform	Sinusoidal	Triangular/Trapezoidal

2.11.1 Comparison RMs with IMs

The comparison between SynRM and SRM is shown in **Error! Reference source not found.**4. The SynRM is like the AC induction motor but it does not have rotor bars, whereas due to salient construction in the SRM does not need AC rotating field. Pulsating DC source is required to produce torque in the SRM. As the main benefit is single tooth coils with short end windings but there is an essential requirement of the non-standard converter, the Asymmetric Half Bridge (AHB) – this converter is not easily available, therefore cannot be purchased from the market. It has to be built as per the design requirement. So, this is the main reason, the SRM is not being considered in most of the special applications. In addition to this, other issues include the number of current-carrying conductors required; the SRM necessitates 2 leads per phase [20], whereas a conventional AC machine needs only one conductor per phase. Also, the SR motor typically requires a separate current sensor per phase and the conventional AC machine does not [98].

2.11.2 SynchRM Working Principle and Operation

The torque is produced in the SynchRM by the variation of reluctance which is caused by the position of the rotor. The reluctance torque produced depends upon the saliency effect that is directly proportional to the difference of the magnetising inductance (L_d-L_q) of the d-q axis which influences the rotor reference frame coordinate system which is known as saliency ratio. In order to get the maximum output, the saliency ratio must be maximised.

2.11.3 Rotor Geometry

Six rotor geometries of low-speed direct-drive synchronous reluctance for domestic application have been presented in [44]. Actually, there are three main geometries of synchronous reluctance used in rotor. The simple salient pole, axially laminated anisotropy and transversally laminated anisotropy (TLA) rotors. As this is the essential factor for optimisation in the synchronous reluctance machine design.

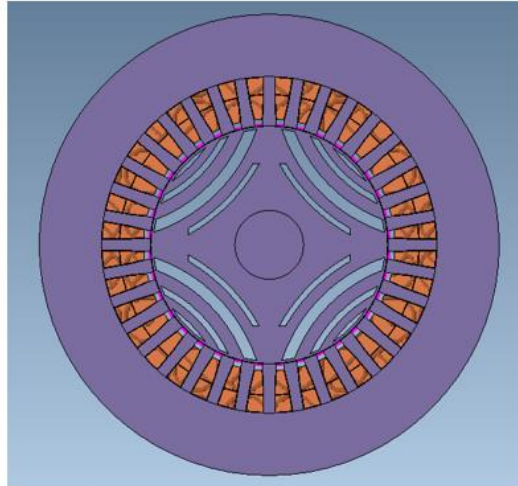


Fig. 2.5 shows the FEM model of SynchRM rotor geometry

The rotor geometry is very important to achieve high peak and average torque having a smaller amount torque ripples as shown in Fig. 2.5. The saliency ratio is affected due to rotor geometry which defines the number of flux barriers, pole numbers, edge effect its shape and dimensions. As the complete focus is on the flux barrier width of the rotor, thus the study of pole number and edge effect is not the subject of this report, therefore a rotor having 4 poles will be studied and has been considered for the SynchRM design. The shape of the flux barrier is already depicted in Fig. 2.5, so that is why their positioning and width (dimension) is the subject of this study.

The rotor design procedure in SynchRM concerns the profile and the flux barrier dimensions. The actual target is to get the high L_d/L_q in order to develop a high reluctance torque. The literature shows that the flux barriers can be calculated by conformal mapping theory [25, 99] or through the simple solution of the magnetostatic model via analytical approach [55, 100] which is beyond the scope of this study. However, the field line-shape of the flux barrier is considered as the most favourable method [101] and the author has considered this in the study. For the barrier endpoint, the best method is presented in [102], and the analytical optimisation method is presented in [103]. Whereas the barriers and endpoints are disseminated from the centre along the rotor circumference which has been used for this study and explained in detail in the section of results and discussion.

2.12 Switched Reluctance Motor

A switched reluctance motor (SRM) is considered as DC motors that that follows the behaviour of an alternating current (AC) motor by changing the switching sequence of the DC current in the stator winding. It should be noted that in order to control the switching procedure it is necessary to use a controller. The working principle of SRM is as follows.

2.12.1 Working Principle of Switched Reluctance Motors

The Switched Reluctance Machine is the category of the distinct electrical machine. A stepper motor is usually made for discrete rotational based on the sequential pulse than it will produce the discrete rotation. Here the identical construction but in switched reluctance machine we obtain a constant rotation. The construction is, it is a double salient machine, the opposite poles are attached together to form a phase. The windings are employed in a stator only, and there is no any rotor windings or magnet and it is simple material made of silicon steel stampings, so the inertia of the rotor is very less that is the major future of the SRM machine. It is required to energize the phase windings in a consecutive manner with the help of switching pattern, to achieve a reluctance torque. First of all, what is reluctance torque?

Why the name switched reluctance machine. Reluctance is the property of magnet that competes with magnetic flux as the resistance competes against electricity. The switching stroke will be managed through the power electronics converters, so through the switching actions, we energize the machine windings. The rotor poles start rotation, it continuously varies the inductance. The different alignment positions of the SRM are shown in **Error! Reference source not found.6**, and the basic SR motor is shown in **Error! Reference source not found.7**.

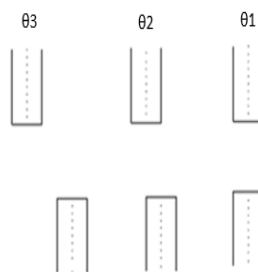


Fig. 2.6 Three Alignments of SRM

θ_3 =Unaligned Position

θ_2 =Intermediate Position

θ_1 =aligned Position

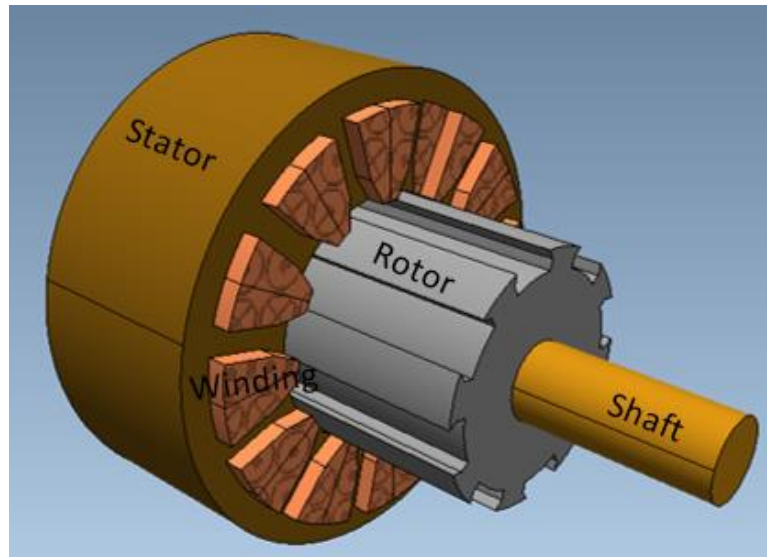


Fig. 2.7 Basic SR motor stator, rotor, shaft and winding [23]

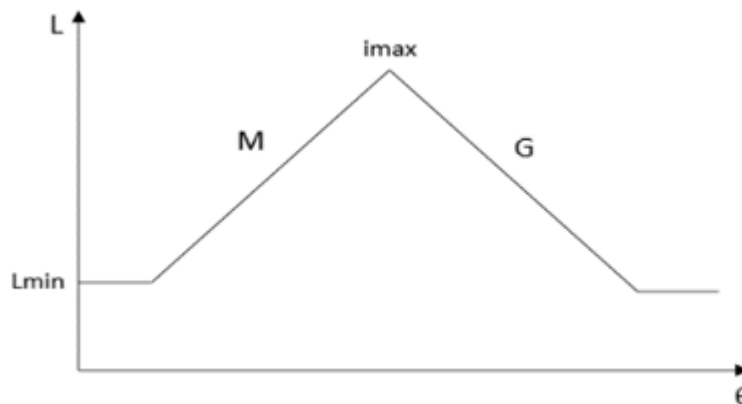


Fig. 2.8 inductance vs torque profile

In the aligned position, the rotor and stator poles air gap are minimum. As soon as the energisation will occur in the stator poles the rotor will attract the stator poles, so it starts the rotation and θ_2 denotes the rotor moment during intermediate state from unaligned to aligned position. The rotor will start the movement and that position will generate the torque. Based on the variation in the reluctance, the θ_1 position is called as an aligned position, in that position mutually stator and rotor are in aligned so the air gap will be least compare to θ_3 , so at all times rotor tries to appeal towards the minimum reluctance position that is the idea of switched reluctance machine. Once the inductance varied from L_{min} , that is lowest inductance value to highest inductance value we try to change in inductance with respect θ , so the torque depends upon two major factors, one is current and another one is changed in inductance. So machine designer decides the variable inductance with respect to (θ) movement and this (i^2) current will be deliberated by power electronic

converter circuit the magnitude of the current, so the torque proportional to half $i^2 \frac{dl}{d\theta}$. And torque is achieved through excitation the current and $\frac{dl}{d\theta}$. So when we apply generating action means, we have energized the machine in a falling inductance profile that means maximum inductance to minimum inductance $\frac{dl}{d\theta} (-ve)$ that is representing G, which means generating action whereas, M represents the motor action. The inductance versus torque profile is shown in Fig. 2.8. So, the prime mover we run the machine in the falling inductance profile we obtain as a generator. Consequently, this machine appropriate for both motoring as well as generating applications.

As wind turbine needs to start the prime mover, and SRM drives the wind turbine and in a car, it needs starter motor after that one the starting process has happened, later it will be converted as a generator action. So, this SRM is suitable for dual mode application because simply we converted this from motor to generator action. The working principle is through the power electronic converter, we obtain an excitation based on the position signal and torque is obtained, so ease of action, the mechanical design is very simple, and we have to switch in an appropriate period based on the position information. This machine is currently very useful in the research area to obtain the required outputs. The major drawbacks are Torque Ripple and Acoustic Noise.

The torque ripple can be removed from phase overlapping scheme and acoustic noise are removed by default as the torque ripple removal. So, the major drawbacks can be removed by good machine design approaches. As this machine replaces all the industrial requirements surely. It is a very attractive machine compare to all the conventional and special machines like BLDC and synchronous machines, those machines have permanent magnets and it has the problem of long term running and demagnetized issues and these are major problems. But SRM does not have any windings or permanent magnets in the rotor part and is energized in the stator part alone that is why this is a highly preferable machine in the future.

2.12.2 Modeling of SRM

The SRM model is shown in Fig. 2.9 [104].

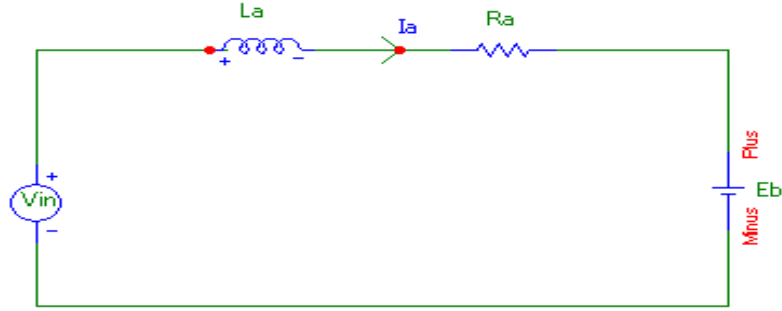


Fig. 2.9 Equivalent circuit of one phase of SRM [104]

$$V_{in} = R_a i_a + L_a \frac{di_a}{dt} + E_b \quad \text{Eq (2.1)}$$

Whereas the (Ψ) is the flux linkage, V is source voltage. So, the relationship between the rotor position angle (θ) are:

$$V_{in} = R_a I_a + L_a \frac{di}{dt} + \frac{d\psi_a}{dt} \times \frac{d\theta}{dt} \quad \text{Eq (2.2)}$$

Since, ' $\Psi_\phi = L_a i_a$,

$$V_{in} = R_a I_a + L_a \frac{di_a}{dt} + I_a \frac{dL}{d\theta} \times \frac{d\theta}{dt} \quad \text{Eq (2.3)}$$

The instantaneous electromagnetic torque (T_e) of the SRM produced by one phase:

$$T_a = \frac{1}{2} i^2 \frac{dL_a}{d\theta} \quad \text{Eq (2.4)}$$

And

$$T - T_L = J \frac{d\omega}{dt} + B\omega \quad \text{Eq (2.5)}$$

$$\omega = \frac{d\theta}{dt}$$

Where speed of the motor represented by ω , the torque produced by the load represented T_L , and electromagnetic torque of the motor represented T .

The illustrated equations (2.4) to (2.5) represent the SRM model.

2.13 Types of Power Losses in Electric Motor

One of the key factors in the designing method and optimisation of the electrical machines is the losses. By using the proper optimising technique in FEM design and simulation the losses can be reduced significantly reduced. However, it is very essential to be familiarised with the losses which are occurred in the machine.

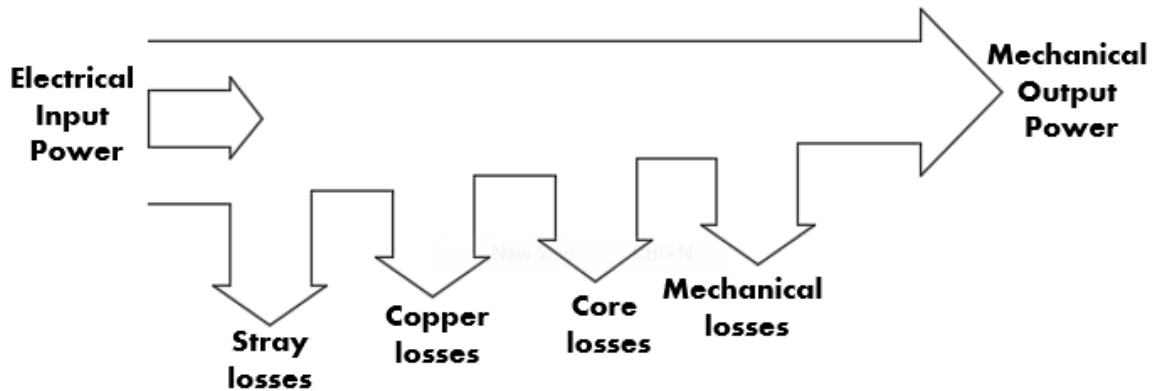


Fig. 2.10 Power flow diagram in electrical motors

2.13.1 Fixed and variable losses.

The power flow diagram in electrical motors is shown in Fig. 2.10. The main energy losses which occur inside of the motor are categorised into five types, each type of losses is influenced by design and constructions. This effect of losses improves the entire machine's performance significantly, therefore minimisation of losses reduces the cooling loads such as air conditioning system in the industrial sector. The types of power losses in the electrical motor are as follows.

2.13.2 Stray Losses

Stray losses account for 4–5% of the overall losses. The losses which are produced due to leakage fluxes are known as Stray losses. These types of losses appear only if the machine is in the operational condition during full load. The stray losses are produces, when the leakage current is induced inside of the machine due to leakage flux because of load current, [105, 106].

2.13.3 Copper losses

Copper losses are major losses and considered as 55–60% of entire losses. These losses are represented as an I^2R losses and appear as heating because of current flows through the winding. As the winding conductor

has resistance (R), and the square of the current, so that is why excessive heating is produced in the machine. If the resistivity of the winding material will be less then there will be low copper losses [107, 108].

2.13.4 Iron or core losses

There are mainly 2 types of core losses eddy current and Hysteresis losses. Core loss represents the energy required to magnetize the core material (hysteresis) and includes losses due to the creation of eddy currents that flow in the core. These losses are found in both stator and rotor steel material. Such losses are 20–25% of the total losses and are not dependent on the load. The eddy current losses are produced due to eddy current effect because of magnetization in the core material and circulating current is produced in lamination steel. Hysteresis losses are also produced due to the magnetisation effect and function of flux density in the core material. The hysteresis losses are a function of flux density. Eddy current losses are generated by circulating current within the core steel laminations [105, 109]. Additionally, the core losses are increased with operating frequency [110]. The primary conditions illustrate that, in the typical field of frequencies of the power electronics applications hysteresis losses are more dominant in a ferrite core. In frequency of 100 kHz range the eddy current losses are very small part of the overall core losses and the dielectric losses are negligible up to 1 MHz [111, 112].

2.13.5 Windage and friction losses

Windage losses and friction losses account for 8–12% of entire losses and do not depend upon the load on the motor. These losses occur due to friction between the moving parts such as bearing friction. These losses are also produced due to excessive air resistance. Usually, a small fan is used to reduce heat accumulation inside the machine and permits the motor to run smoothly [113, 114].

2.13.6 Ways to reduce power losses

Core losses can be reduced using higher permeability electromagnetic (silicon) steel and by lengthening the core to reduce magnetic flux densities. Thus, lower operating flux densities, iron losses are reduced. Additionally, the thinner gauge size should be used because core-steel decreases eddy current losses in the machine. Windage and friction losses are reduced using low loss fan design and size, which reduces losses due to improvement in air circulation. Use of bearing with lower friction also contributes to losses minimisation. The most important losses in the electrical machine are the winding copper losses. which contributes the major losses. Typically, I^2R losses can be reduced by using more copper and larger conductors with an increased cross-sectional area of the windings. Hence, this decreases the resistance as $R=\rho L/A$, whereas R is the resistance in Ω , ρ is the resistivity of conducting material in Ω/m and A is the cross-sectional area of a conductor in mm^2 . This increasing area lowers the winding resistance and reduces losses due to the current flowing through it. By adjusting the proper stator slot design, I^2R or copper losses

can be reduced or if the insulation thickness is reduced to allows more volume for copper wire in the stator. In the rotor, by using larger conductor bars increases the cross-section, by this means conductor resistance and losses are decreased due to current flow. Motor operation closer to synchronous speed will also reduce rotor I^2R losses.

It should be noted that, the above machine designing aspects can also be considered for other applications such as Electrical Vehicle (EV). Therefore, author has included some detailed machine design characteristics relevant to electrical vehicles in the literature review which are described as under.

2.14 Applications of Electrical Machines

In the past three decades, the production of gas and oil-based fuel has become a major factor in increasing greenhouse gases, consequently contributing to global warming. One of the attempt to decelerate change in climate has been the drive towards achieving emission-free transportation solutions. The market for emission-free vehicles has been growing rapidly and has become commercially competitive. There is a range of effective and reliable vehicles on the market, and these are electric vehicles (EVs), plug-in hybrid electric vehicles (PHEVs), hybrid electric vehicles (HEVs), all-electric vehicles (AEVs), and more electric vehicles (MEVs).

The passenger transportation system (Automobiles) are the main cause of environmental pollution in most populated urban areas, [115-117]. Thus, for meeting the increasing demand for electric vehicles, government investments, research institutes, industry, and people are participating in a lot of activities such as investment, production, and trading. There is a very wide range of specifications of EV, and each type of motor and its application has different demands, therefore several different technologies are appropriate. Without an uncertainty, EVs offering environmental, social and economic benefits which improves air quality and causes in the reduction of petroleum conservation. Thus, up to 10% of fuel consumption is potentially being reduced [118]. Typically required specifications of Light-Weight passenger car shown in Table 2-5.

Table 2-5 Light-weight passenger Electric Car specifications [119]

Parameter	Value
Total loaded weight	800 kg
load (40 kg with 3 persons)	250 kg
(0-50 Km/h) Swift Acceleration	9 seconds
Radius of Wheel	0.3 m

maximum speed covered in a straight road	120 km/hour
Coefficient of Aerodynamic Drag	0.35
The front windscreen area	1.5 m ²

The electrical vehicle's propulsion drives are summarised in terms of major requirements as follows [120-122]:

- It should have high power density
- Throughout the functioning of the vehicle, it should be robust and reliable
- Should have total lower cost
- Initially, torque should be high at low speed and capability of climbing during cruising
- High regenerative braking capacity and performance
- Very broad in terms of constant-power regions

2.14.1 Types of electric motors and drives

The characteristics of the motor drive of each type are described in detail in this section. The EV drive system need can be depicted in **Error! Reference source not found.** [9] and should be found in accordance with the drive of an electric motor. Generally, in terms of torque requirement and for cruising, the EV should be capable to produce 5-10 times higher [123-125]. In the figure, the fastest speed of continuous power region offers maximum-speed which can be 5 times high than the base speed. Gearbox costs show 10,000 rpm of the motor speed.

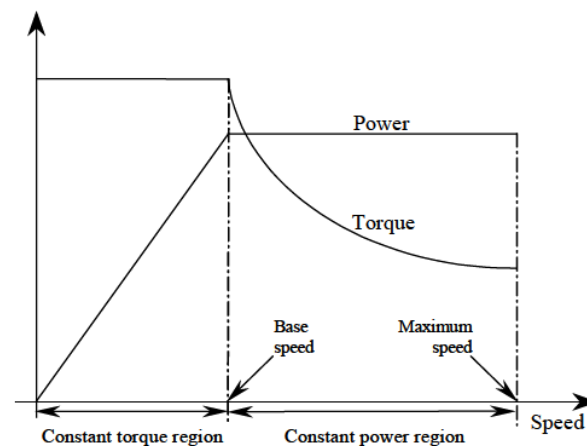


Fig. 2.11 electric vehicle motor drives characteristics

Generally, the drive system for electric vehicles uses four types of motors which are, direct current (DC) motors, induction motors (IMs) and permanent magnet (PM) motors. Particularly in the automotive market, nowadays reluctance technologies have started emerging. Most potential options for various electrical machines are described in **Error! Reference source not found.**, and are shown in **Error! Reference source not found.** compared to their cross-section [126].

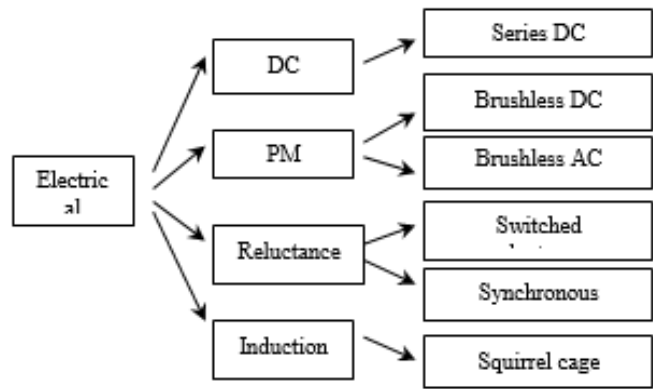


Fig. 2.12 Machine options for the EV propulsion applications.

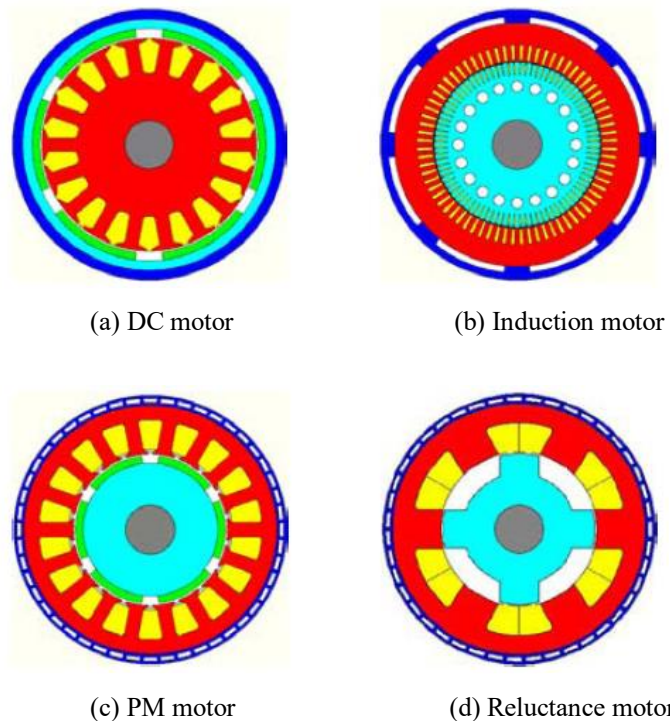


Fig. 2.13 Electrical machines for EV propulsion drives.

2.14.2 DC Motors

The magnetic field in DC motor is stationary and is formed by the permanent magnet or electromagnets and winding is placed on the armature which is rotary part as depicted in **Error! Reference source not found.**(a). For EV propulsion system its speed-torque features completely suited. Especially, the DC series motors are a very adopting and suitable option. The field and armature are attached and has the unique characteristics of speed and torque. DC series motor provides high torque at low speed. Additionally, its main advantage is, DC series motor does not require source from separate excitation. During the overloading condition, the field is firmly balanced by armature reaction. This characteristic makes the DC motors (series) important technology for electric vehicle applications up to 1980s [123]. Because of the availability of DC supply power from the battery, DC motors were commonly used for the application of EV in the past [127].

However, by the usage of advanced power electronics, their counterpart machine's performance is more effective. Therefore, DC motors are away in terms of the performance competition. Because the drive is mainly connected with commutators and carbon brushes this increases the repetition of maintenance and ultimately increases the cost. The other drawbacks from a construction point of view, dc motors are very bulky and have very poor efficiency. In addition, the regenerative braking capacity is very limited in these machines [123]. Nevertheless, modern electric drives can still find DC motors such as *Danavolt* of Peugeot Citroen [128].

2.14.3 Induction Motors

Induction motor is shown in **Error! Reference source not found.**(b). Generally, due to high maintenance requirements in machines, the commutators and brushes are not ideal. IMs can obtain equivalent performance as the DC motor drives. Such as using field weakening process, the extended range of speed can be beyond the base speed. About further performance, the high efficiency can be achieved with low torque range at high speed (because iron and I^2R losses will be reduced). Whereas, efficiency decreases during low speed due to greater rotor losses [129]. Therefore, squirrel-cage induction motors are considered in the following discussion. The three-phase AC (alternating current) is fed at the windings which are wound on the stator. The rotor has cast aluminum bars short-circuited with each other. Due to cheapness, uncomplicatedness, ruggedness, and reliability, IM (squirrel-cage type) are universally accepted and recognised for the industrial drives. Their overall low construction costs and enormous field-weakening capability mark them a reasonable and economical contestant for the application of EV motor drives. Currently from speed-torque characteristics, a review from the specialist's opinions [115] and complete evaluation of motor drives system for electric vehicle [126] all categorically explain that on the basis of their manufacturing, high reliability, low cost, and power converter technologies, for EV propulsion

applications, induction motor drives are most suitable. On the other hand, its main disadvantages are low power factor and efficiency [126, 130, 131], which essentially prevents its use for the electric vehicles.

Induction motor-driven electric vehicles are used by *Durango* of Daimler Chrysler *Silverado* of Chevrolet, *Kangoo* of Renault and *X5* of BMW [126].

2.14.4 Permanent magnet motors

In a high-performance permanent magnet motor, the Neodymium magnet (NdFeB) a kind of rare-earth is generally used. The 3-phase alternating current windings are installed on the stator and magnet is installed on the rotor as depicted in **Error! Reference source not found.**(c). When the alternating current (AC) is supplied to the machine and the shape is sinusoidal, that is known as brushless AC motors (BLAC). If the supply current is alternating, whereas the shape is a rectangular or trapezoidal wave, the machine is known as brushless DC motors or simply (BLDC). The two machines can be similar in terms of stator and rotor configurations, but only there is a difference in input supply waveform. The control strategy is modified through the software and additional details in terms of different design configuration are described in [132].

There are mainly two methods to mount the permanent magnets, which are either to mount on the rotor's surface or inner side of the rotor. In the surface-mounted schemes, NdFeB magnet is placed within the flux path as a result, the reluctance of the magnetic circuit is very high. Thus in extremely cold machines, the obtained force of armature to magnetomotive is high, and the reluctance is compensated. From the rotor dimensions point of view, the surface mount permanent magnet motors, have usually small rotor diameter with very low inertia. Therefore, it has very good dynamic performances. In the IPM, there is a high reactance and magnetic loadings due to flux concentrating modes. This leads to the saturation as armature current is applied, reducing much of its advantages. These types of motors are capable to provide higher field weakening capability [133].

It is essential to equalise the supply waveform along with back emf. So that it can be decided that, brushless ac motors have superior performances as compare to brushless ac motors for the application of EV drives and systems [132]. However, If the transformation of $d-q$ coordinate is replaced [134], brushless dc motors can be chosen as this will superior torque as compared to brushless ac motors [134, 135].

Generally, rare earth materials have very low reserves and it is very expensive. Therefore, it does not have very huge mass production due to supply chain and cost sensitive issues. In operation, the magnetic field is fixed in the machine due to the constant permanent magnet so that's why for constant power operation, there is a limitation in the high-speed range. The range can be extended with the process of field weakening, the increase can be 3-4 times higher as the base speed [126, 136-144]. Conversely, for the application of the electric vehicle, due to high power density, good controllability, torque to volume ratio and torque

requirements, the permanent magnet motors are best appropriate. The machine is also well-matched as direct-drive used for in-wheel motors [145-149].

Permanent magnet brushless motor drives systems are extensively found in electric vehicles made by Japan Toyota *Prius*, Honda and Nissan [126].

2.14.5 Reluctance Motors

The reluctance technology has already been discussed in section 2.7.6 to 2.7.12. Whereas the previous explanation is about for the application of Raymond Pulveriser. In this section, reluctance motor technology and its potential use for the application of electric vehicle has been described. Reluctance motors are operated on the basis of reluctance torque. The motor is unique in terms of specific rotor structure which is fixed from steel laminations. If the structure of stator is salient poles, the motor is known as switched reluctance (SR) motor, as shown in **Error! Reference source not found.**(d). If there is a round structure of the stator similar to the induction motor, and supplied by multi-phase alternating current, they are known as SynRM. The SynRMs are commonly operated by sinusoidally distributed windings, on the contrary, concentrated windings are used in switched reluctance machines which are wound on the stator poles.

The rotor usually runs at synchronous speed, therefore, no electromotive force (emf) is induced inside of the rotor (hence no joule loss) of SynRM. However, these types of machines have a low power factor and restricted saliency ratio [150]. Therefore, for the application of electric vehicles, SRM is considered as extensive research [23, 151-160]. As reluctance motors can offer high-speed potential, simplicity and high reliability [115]. Their torque vs high-speed range can be enhanced more than 7 times from the base speed [161], and particularly for transportation vehicles, this specialty is highly demanded.

As the working principle of SR motor is such that, the excitation current is only provided on the stator windings, therefore both torque and magnetizing current are produced from the stator. Therefore, the machine is almost fifty percent bigger than permanent magnet motors [152]. There is a drawback in switched reluctance motor. Apart from that, there is a need of complex supply waveform and accurate rotor position which requires costly power controllers and converters. Additional disadvantage is, they also yield acoustic noise and high torque ripples [162].

In recent years, the performance of the switched reluctance machine has been increased in terms of thermal capabilities by efficient FEM design so that is why the SRM is being preferred in special-purpose applications. For example, a 48/36 SRM for direct drive SR motor has been proposed in [163] for the rotary table. A direct drive actuator with switched reluctance motor has been used in [164] with plunger assembly. The kinetic energy storage system (KESS) as a primary power source for the bi-directional bus which

includes a flywheel and a switched reluctance motor is proposed in [165] for mining and traction application which can be used for the surface as well as an underground machine while incorporating SR technology.

Increasing needs for renewable sources have enhanced the increasing interest in electrified transportation.

The best qualifications for the above-mentioned electric machine (EM) can be summarised [166] as follows:

- High power and torque density;
- high fault tolerance capability;
- High efficiency
- quick active response;
- Extra continuous power speed range (CPSR);
- low- repairs and overhauling requirement;
- high power to accelerate cruising at high speeds;
- high torque at low speeds for starting, and mountain climbing;
- wide range of speed performance;
- capable of regenerative braking;
- low price.
- capable to work in extreme conditions such as in harsh environments such as hot temperatures, water, dust and cold;
- Can withstand the two times the rated power overload capability (for a short period of time);
- must be robust and strong;

The significant challenge and restraining aspect in the machine design stand thermal limitations because of windings [167]. After technology development in a semiconductor material, IPM is greatly being used by automotive [168]. As IM generates excessive flux saturation consequently, enormous eddy current losses are generated, and the losses in secondary winding are significantly high than normal values. Therefore, due to these reasons as stated in literature [157, 169-171] the conventional IM is not suitable to be used for EV applications. Nowadays to meet the demand, low cost switched reluctance motor drive system is getting more attention due to several advantages such as no winding on rotor, very cheap in cost, design simplicity, robust structure, and no demagnetization issues are the most appropriate for EV applications [23, 124, 157, 158, 172-174]. The literature tells that, major applications are electric vehicles, electric train, airplane engine starter [175]. The SRM agreements extraordinary reliability and mechanical integrity, which is desirable for EV application [176, 177]. Diverse comparison of switched reluctance motors has been made in [178] with the analysis of an improved taper angle and number of turns.

A 30kW Switched reluctance motor with the thermal performance and water cooling design has been analysed in [179]. To achieve high efficiency, speed, and torque density, 18/12 SRM has 18 poles on the stator 12 poles on the rotor is designed in [176, 180] having a diverse material structure. In [181, 182], For decreasing the vibration and acoustic noise, the novel current profile has been suggested to investigate the radial forces. Another 18/12 SRM has been proposed with In-wheel structure in [183] by means to provide attention on dimensional parameters. So SRM has pushed the boundaries for traction motor drives applications and high-temperature environment applications [172]. In addition to this, SRM has a very large field weakening area, which has been appealed up to 10 times. Basically, 2 layouts to drive the electric vehicle. (1) Single motor (2) multi motors free to propel separate individual wheel. A variable-reluctance motor or SRM, in which current pulses are produced related to rotor position which actually requires a shaft position transducer similar to the brushless dc motor. Unlike stepper motor, the SRM produces the continuous torque at any speed and rotor position. However, it suffers from inherent torque ripple [184].

2.15 The trend of Electric Motors for Electric vehicle

A lot of improvement has been made in the electric vehicle through different ways and significant R&D efforts have been done in developing EVs, but in order to achieve all-electric vehicles, still, it seems a long way. For upcoming years, the development to integrate different machine features and configuration re-arrangement in magnetic flux will be continued.

2.15.1 Flux configuration

In order to develop a novel machine topology, there is a good opportunity for the machine designer to use different designs and flux configuration. Mostly, the inner rotor is used for electric vehicle applications and their flux configuration is radial, as it is shown in Fig. 2.14. In addition to this, EV applications offer further approaches such as axial-flux [185-188] and transverse-flux [145, 189, 190] as an attempt to achieve good performances. In an axial flux machine, both stator and rotor disks are arranged in such a manner to have a sandwich structure [191]. The flux flows similar to the rotor direction. Such as axial flux permanent magnet (AFPM) motors are characterised with large diameter and high pole numbers [192].

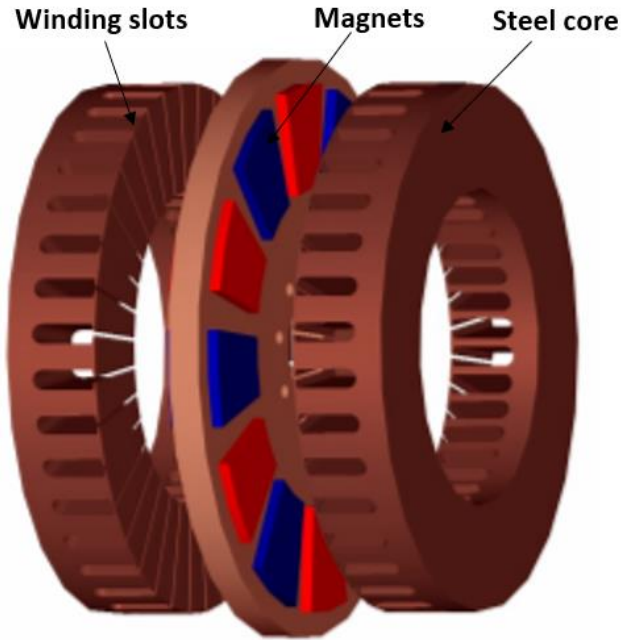


Fig. 2.14 Axial flux PM motor for electric vehicles [192]

Generally, for direct-drive in wheel mounting, transverse flux motors geometry is suitable [191], but they normally have low power factor [192], therefore power converter needs to have high power ratings [150]. In addition to this, in transverse flux motors, there are fewer magnets as compare to permanent magnet motors with similar torque output, due to this it has low cost and size is very compact. A model of linear transverse flux machine is shown in Fig. 2.15 Linear transverse flux machine [193].

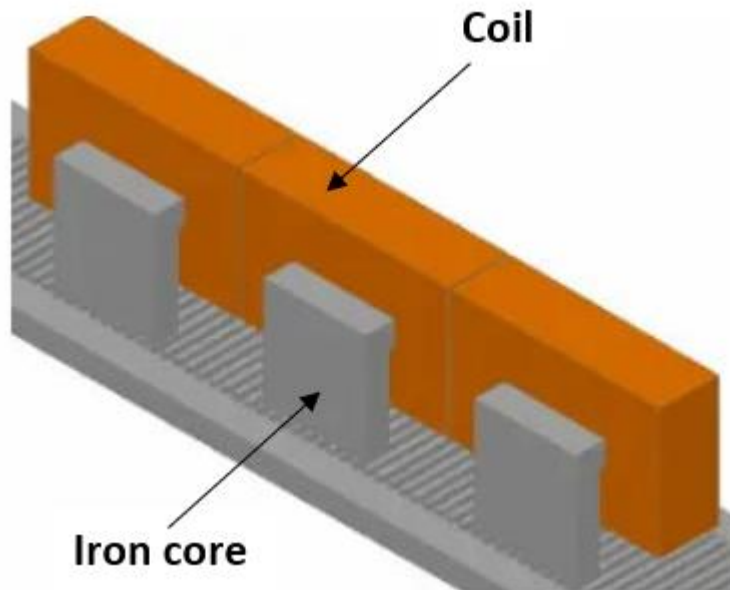


Fig. 2.15 Model of liner transfer flux machine

2.15.2 Hybridization of different machine features

Hybridization is the combination of permanent magnet and electromagnet machines. For taking the benefit of the induction motor as a self-starting feature in permanent magnet motors are well-defined in [150]. In order to control in permanent magnet motor, an electric excitation is provided in a stator to superimpose on the permanent magnet excitation. By doing this, high speed extended power range is achieved [194], this also reduces the risk of demagnetization in permanent magnet machines. A switched reluctance based hybrid machine with small permanent magnets is given in [195, 196] and its topology is shown in **Error! Reference source not found.**17. In [197] a SynRM with hybrid technology that contained small permanent magnet structures is given and its configuration is depicted in Fig. 2.16.

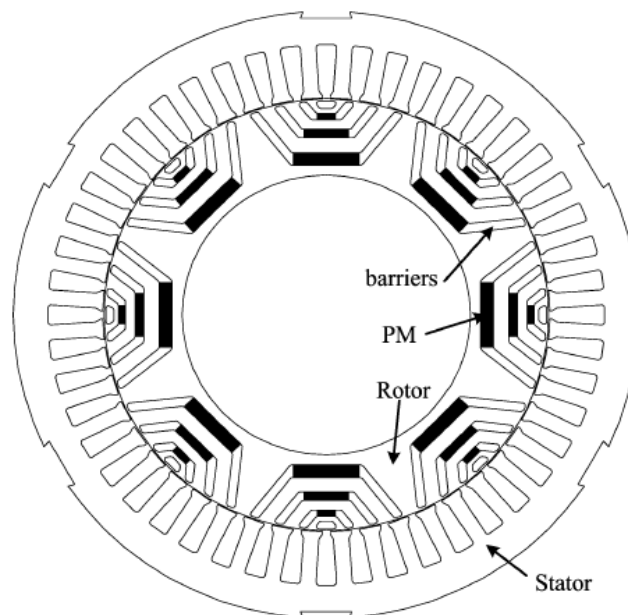


Fig. 2.16 Synchronous reluctance machine based on hybrid technology.

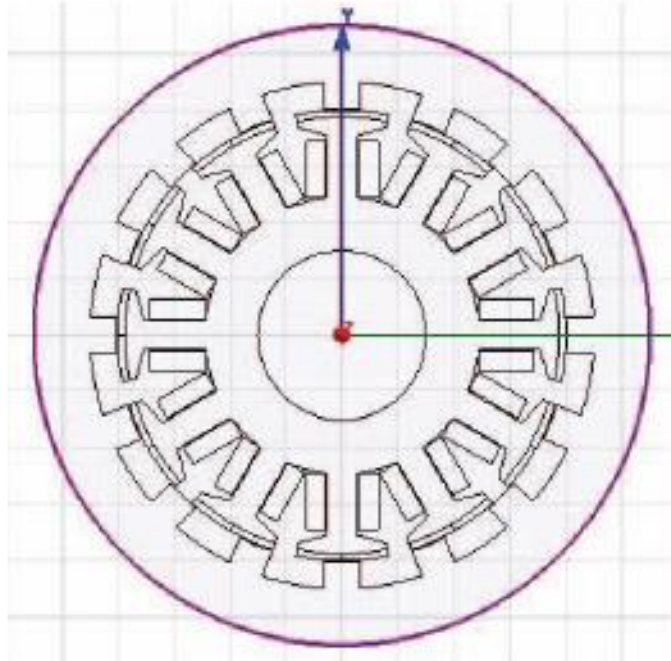


Fig. 2.17 SR motor based on hybrid technology

Table 2-6 Comparison of Motor Drive Technologies and their performance

Performance	SR	IM	DC	PM
Power density	medium	low	low	high
Torque ripple	high	low	low	medium
Acoustic noise	high	low	medium	low
Overload capacity	low	Medium	high	High
Controllability	low	high	high	medium
Max speed	very high	high	medium	low
Speed range	high	medium	medium	low
Size	large	medium	medium	small
Reliability	high	high	low	medium
Efficiency	medium	medium	low	high
Cost	medium	low	medium	high

2.16 Summary

In the current situation, the usage of electrical machine is increasing day by day. So, the advancement in machine designing, motor drive system and energy savings is essentially needed in various applications. In this chapter, the concept of variable speed drive, and its advancement has been thoroughly described. As the main targeted application is mining and for centrifugal pump, so and importance of direct drive system and their advantage and disadvantage are discussed.

By adopting a suitable drive system with proper geometry of Synchronous Reluctance and Switched Reluctance motors are described in detail. Additionally, both the machines are compared with different design perspectives. As it is essential to know the types of power losses occurred in the machine so, each type of machine losses and its stages are discussed with their methods of improvement. The above machine design technique can also be applied for the application of electric vehicle; therefore, a complete scenario of different types machines has been thoroughly described.

The advancement in machine design technique will significantly be helpful in various applications and for mass production in the market. Such as for mining applications, electric vehicles, centrifugal pumps which will improve the overall performance of the machine.

Chapter 3 Surrogate-based Optimisation of Reluctance Machines

The optimisation process is combined with FEA simulation for the electrical machines design optimisation (EMDO). This has higher calculation time, particularly for multi-objective (MO) optimisation issues. Overall a novel optimisation solution is required. The main aim of this Ph.D. work is to demonstrate how a novel method can be applied to the optimisation of synchronous reluctance rotor design for the application of Raymond Pulveriser and closed coupled centrifugal pump, to enhance the performance of the machine. A different number of places of sampling points used for simulation is determined as per Latin Hypercube sampling. Then the method of construction of surrogate is examined in detail. The first 72/48 SRM design is having 1000mm in diameter. The complete machine details are described in section (4.8.3). This machine design is very bulky. Therefore, 50% of the machine diameter is reduced of two machines (SynRM and SRM). Hence two machines are designed and optimised within 500mm overall diameter. The relationship between machine performance and different reluctance machine design parameters is investigated thoroughly for both stator and rotor design. For Synchronous reluctance motor, two shapes of rotor and stator designs (round and square) have been considered for optimisation. The surrogate-based optimisation (SBO) technique on 3 and 4 flux barriers for rotor design have been analysed. Then 12/8 SRM parameters are investigated by generating Latin hypercube samples (LHS). The SRM is characterised by simple structure, high robustness, and low manufacturing cost. Nevertheless, comparatively the main disadvantage of SRM is high torque ripple created by the pole structure of the doubly salient machine. Surrogate-based optimisation based on maximising the average torque and minimising the torque ripple has been considered in 12/8 SRM design.

3.1 Introduction

There are many techniques for conducting design optimisations. The most prominent methods comprise gradient-based methods [198, 199], adjoint methods [200-202], and the surrogate-based model optimisation (SBO) technique such as the response surface methodology (RSM) [203-206]. With the uninterrupted progress in computational simulations, the optimisation based on computational methods has been verified to be a worthwhile tool in minimising the design practice duration and expense. The gradient-based method depends on the searching through step by step for the best and optimal design while spending the method of the steepest lineage of the objective function as per the convergence criterion. An adjoint method needs the structure which essentially is combined into the computational model comprised of physical laws. For computationally expensive design or for a new design, the method of optimisation based on inexpensive

surrogate such as response surface method is a good choice for optimisation. As the SBO permits the best design of the optimisation, it instantly deals with inner understandings of the design. Recently, the SBO technique has been used in machine design [207, 208]. This technique of optimisation not only provides the benefits of low cost but also helpful in problem definition of the design task. Besides this, multiple design problems can be handled and evaluated simultaneously [209, 210]. Therefore, SBO technique has been recognized as very suitable for novel or empirical projects, designs on everyday work because it deals with the global assessment with the characteristics of design space, and it permits the investigator to refine and improve the design experiments. It also helps to amend the design spaces. Additionally, the sensitivity analysis can be problematic when it is conducted with two or more objective functions which are incompatible in nature [211].

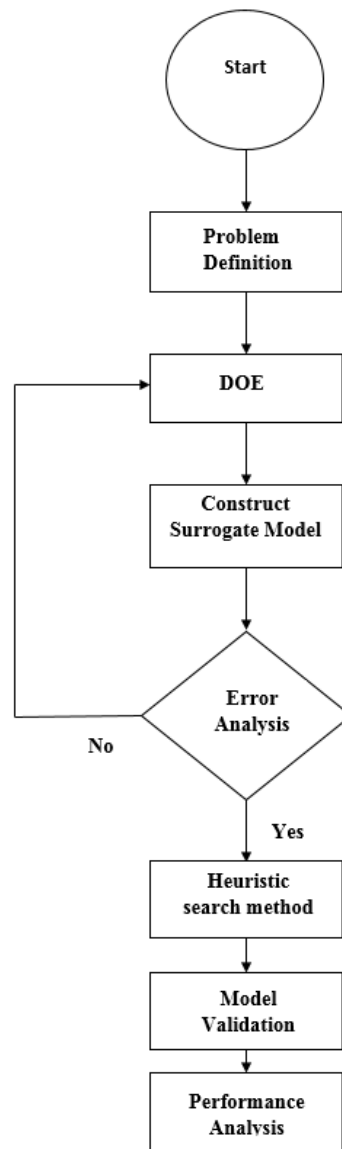


Fig. 3.1 Surrogate optimisation process [212]

In this work, a surrogate optimisation procedure is developed to improve the efficiency and torque of the synchronous reluctance motor. The particle swarm optimisation technique has been implemented to find out the optimum performance point through *Matlab*. Five initial design variables for SynchRM such as rotor diameter, shaft diameter, stator teeth length or depth, airgap and stator slot opening and 7 variables for SRM such as stator pole arc, stator yoke, stator inner diameter, air-gap, rotor yoke thickness, rotor pole arc and shaft diameter have been taken which essentially influence the torque and efficiency, the flow chart of the surrogate optimisation is shown in Fig. 3.1.

3.2 Design Optimisation

The investigation is planned into three different sections. Initially the stator of the synchronous reluctance motor needed to be optimised before the full rotor structure. Therefore, first, the brief investigation was done to optimise through a surrogate model which is shown as in Table 3-1. Secondly, the study of rotor design optimisation was carried out through different designs of flux barriers with and without ribs. Finally, the investigation on the results was analysed for further verification and the conclusion was made. However, the prototype design experiment overall has been experimentally tested.

The SBO analysis with flowchart is depicted in Fig. 3.1, which is an effective method for the design of computationally costly prototypes such as those found in mining, electrical vehicles as well as other industrial applications.

The following key steps in the surrogate optimisation modelling are described as follows.

3.3 Problem Definition

The problem definitions mean the number of input variables provided in the surrogate, initially different inputs and their ranges are given to generate the samples within the range. This should be noted that, it is the special feature in the surrogate optimisation method by which multiple numbers of problem definitions or input variables can be provided. The key influencing input variables which have been used for the design and optimisation for SynchRM are (Rotor diameter, shaft diameter, slot depth or stator teeth length, airgap, slot openings) as shown in Table 3-1, row 1, and column 2-6.

Table 3-1 stator parameters for the Latin Hypercube samples

No	Rotor dia in mm	Shaft dia in mm	Slot depth in mm	Airgap in mm	Slot openings in mm	Torque in Nm	Efficiency in %	Fill factor in %	Power kW
01	262.5	64.25	65	0.8875	8.875	747	84	55	9.76
02	212.5	53.75	69	0.9375	7.375	659	81.4	67	8.91
03	267.5	58.25	79	0.6375	9.025	736	78	78	9.741
04	287.5	71.75	63	0.6875	9.625	707	83.4	50	9.32
05	207.5	79.25	41	0.8375	7.225	338	79	40	4.70
06	202.5	55.25	43	0.9125	7.075	330	70.7	40	5.13
07	247.5	76.25	77	0.6625	8.425	689	82.1	47	9.23
08	297.5	62.75	51	0.8125	9.925	777	83.79	64	10.2
09	272.5	56.75	61	0.9625	9.175	694	83.16	57	9.18
10	242.5	68.75	49	0.8625	8.275	724	87	56	9.89
11	227.5	77.75	75	0.7875	7.825	619	82.1	54	9.25
12	257.5	74.75	53	0.5625	8.725	814	84.4	78	10.6
13	232.5	70.25	71	0.5375	7.975	726	82.8	58	9.64
14	237.5	61.25	45	0.7375	8.125	586	85	67	9.33
15	222.5	65.75	57	0.7125	7.675	635	83.09	68	8.41
16	282.5	67.25	47	0.6125	9.475	959	82.4	79	12.8
17	217.5	59.75	73	0.5875	7.525	676	79.7	60	9.32
18	292.5	73.25	55	0.9875	9.775	740	80	60	10.1
19	252.5	52.25	67	0.5125	8.575	757	80.6	57	10.3
20	277.5	50.75	59	0.7625	9.325	765	83.5	59	10

3.4 Design of Experiment

Through the design of experiment different range of parameters are achieved which gives the initial structure for the machine design. Additionally, it has tendency to analyse the machine performance at different stages at different variable ranges. There are two procedures utilised for electrical machine optimisation (1) is the surrogate models (SMs) based on the design of experiments (DoE) and (2) stochastic evolutionary methods (EMDO) [213]. The Latin Hypercube sampling (LHS) and central composite design (CCD) methods are the types of DoE. The elements samples are not dispersed at the centre and corner of the design space in the CCD, this disadvantage makes it complicated to accurately assemble the overall apparatus performance on extended design space. The LHS is a random sampling technique that has the advantage of the flexibility and an ideal space filling features [214]. The number of generation samples of the LHS can be controllable. The SBO method is a beneficial tool for the analysis and optimisation of computationally expensive models [215-217]. It provides a compromise between the high-precision low-speed calculations finite element analysis (FEA) and high-speed low-accuracy simplified analytical methods. The design of the experiment gives the sampling plan as per the design space. There is always unique value (in contrast to random values) on each sample point which can be modelled independently. It is used efficiently for fitting in a variety of models. The main question of this step is to evaluate the design approach considering the number of samples

through computational expense on each sample. As depicted in Table 3-1, initially 20 Latin hypercube samples have been generated for testing as shown in Fig. 3.2.

3.5 Construction of Surrogate Model.

In the construction of a surrogate model, parametric and non-parametric functions are used together. This results in the global function and the relationship between the response variable and the design variable are identified. The non-parametric used different types of samples with different regions and local models. In this thesis, only parametric kriging model is intended to be focused on research.

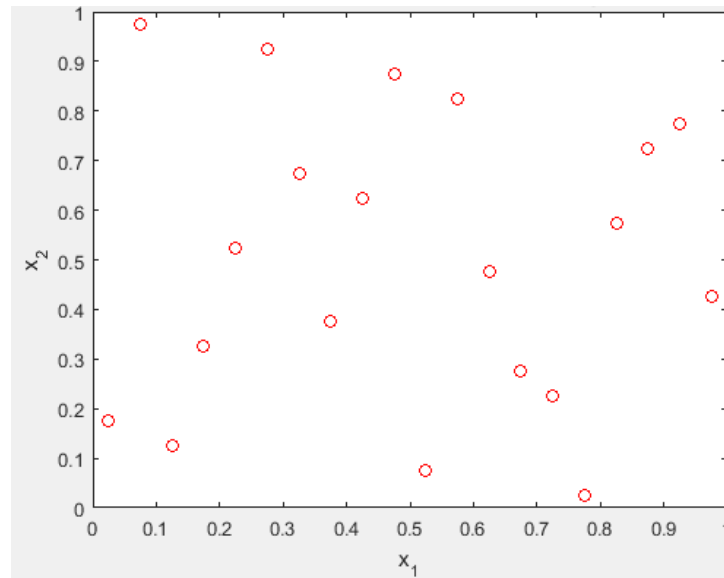


Fig. 3.2 Latin Hypercube samples for 1st optimisation

3.5.1 Error Analysis.

The surrogate models (SMs) are constructed by using the data obtained from FEA, and it gives a quick approximation of constraints and objectives at new design points so that optimisation studies are practicable [210]. The error analysis is used just to confirm the surrogate results with FEA analysis. Initially, a few points are tested to determine whether the model works properly. If the model does not give satisfactory results, the design process reverts to earlier stages so that further Latin hypercube samples can be generated. It is worthwhile to note that this process can be repeated several times until the satisfactory results are achieved.

3.5.2 Heuristic Search Method

The stochastic evolutionary methods (SEMs), which are particle swarm optimisation (PSO) and genetic algorithm (GA) are appropriate in electrical machine design optimisation (EMDO) [218]. Once all the desired output variables are achieved through FEA, then all the input variables of Latin hypercube samples

are inserted through Matlab coding as Xs, and the desired objective functions which need to be optimised are placed in Ys. All the limiting factors or constraints which need to be reduced are placed in Zs. This generates further optimised point by using Particle Swarm Optimisation process and final optimised variable points are achieved.

3.5.3 Model Validation

This step is used to check whether the model is correct and ready to use for analysis and optimisation studies for validation. In this step, we need to test the achieved points from PSO into FEA so that suitable objective can be achieved. The achieved from surrogate-based optimisation by following the above steps and generating the final points through PSO are shown in Table 3-2.

Table 3-2 PSO Optimisation for efficiency, torque, and power in kW. for the first Optimisation

No	Rotor dia in mm	Shaft dia in mm	Slot depth in mm	Airgap in mm	Slot opening in mm	Torque in Nm	Efficiency in %	Fill factor in %	Power in kW
01	248.51	73.634	61.64	0.5	8.47	788.6	83.9	65	10.32
PSO optimisation for Efficiency, Torque and fill factor (%)									
02	281.16	52.706	40.03	0.537	9.6144	683.88	81.7	52.9	9.206
PSO optimisation for Efficiency, Torque and fill factor (%)									
03	295.009	79.5788	64.35	0.5	9.9986	658.12	83.4	48.04	8.679
PSO optimisation for Efficiency, Torque and Power kW									
04	283.135	74.8259	62.85	0.502	9.508	733.31	83.9	52	9.612
PSO optimisation for Efficiency, Torque and Power kW									
05	299.789	60.0317	51.47	0.524	9.9990	786.59	84.39	63.3	10.25

3.5.4 Performance Analysis

This is the final step to analyse the model performance. In this thesis, the performance analysis has been done through Infolytica magnet and its performance results are explained in detail in the next section of the design process based on optimisation.

Table 3-3 variable range selection for Latin Hypercube Samples for 36 stator slots

Variable	Range in mm (Min to Max)
Airgap	0.5-1
Slot depth	50-60
Tooth Width	12-17
Shaft dia	50-150
Flux barrier width	22-43
Flux carrier width	11-17
Slot openings	6-8
Flux barrier edge angle	10-50°

3.6 Design process based on optimisation

The optimisation process is shown in Fig. 3.3. A first optimisation test is performed while selecting the variables range as depicted in Table 3-3, then the SBO generates the sampling points shown in Fig. 3.4. This is directly used on the surrogate models as input variables. It starts with the selection of an initial parameters range and sampling plan of 40 points and these 40 initial sampling points are then assessed by means of FEM model objective and the constraints function values are achieved. Afterward, for each objective and constraint function, a Kriging surrogate model is fixed over the initial sampling plan [212]. According to the optimisation results in their torque, efficiency, fill factor and power output values are compared. These are shown in Table 3-4. This approach clearly indicates the range of variables which can be considered into a surrogate to use all the available degree of freedom. So, in order to select the proper design variables and their ranges are selected as follows.

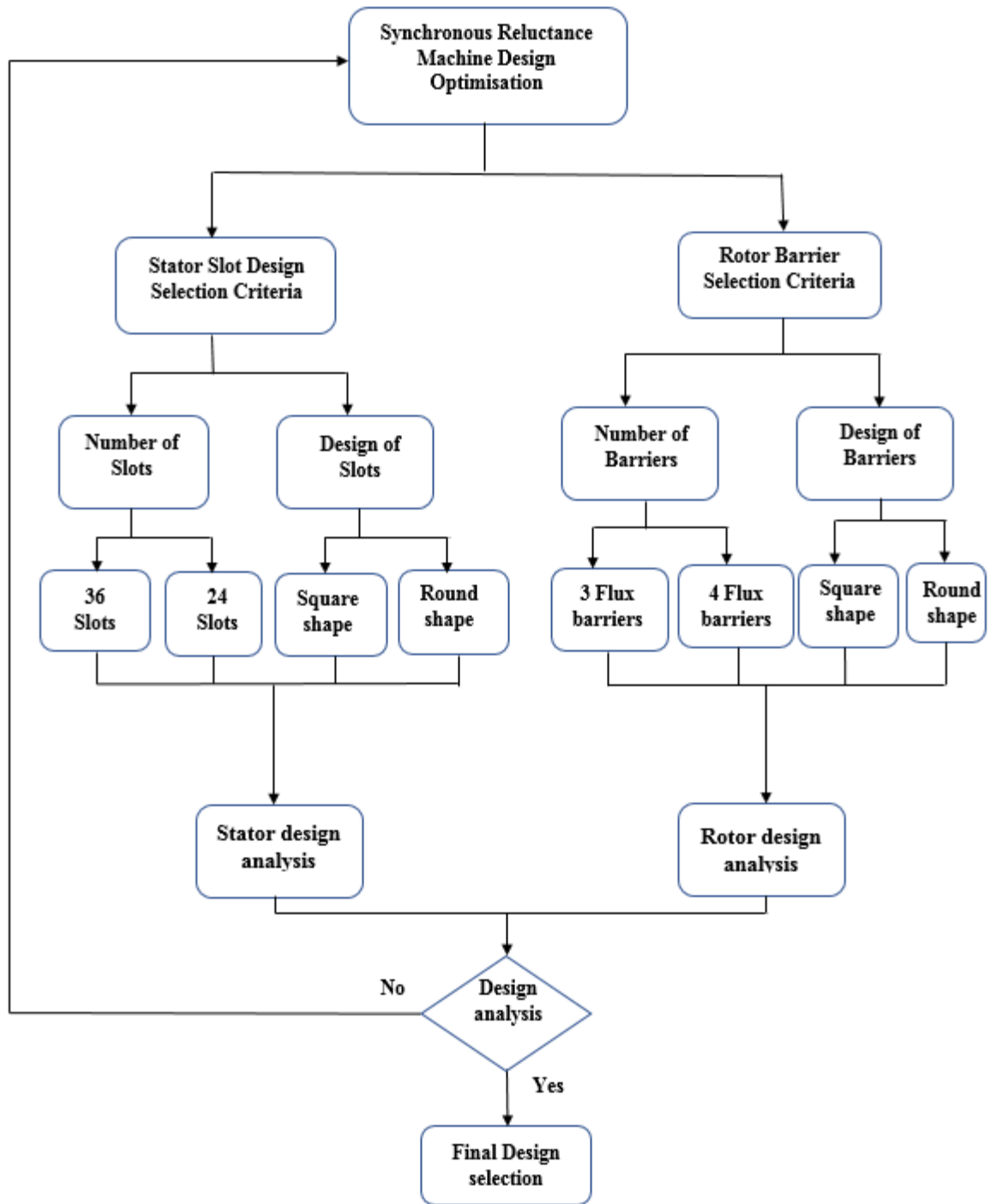


Fig. 3.3 Flowchart of SynRM Machine design and optimisation

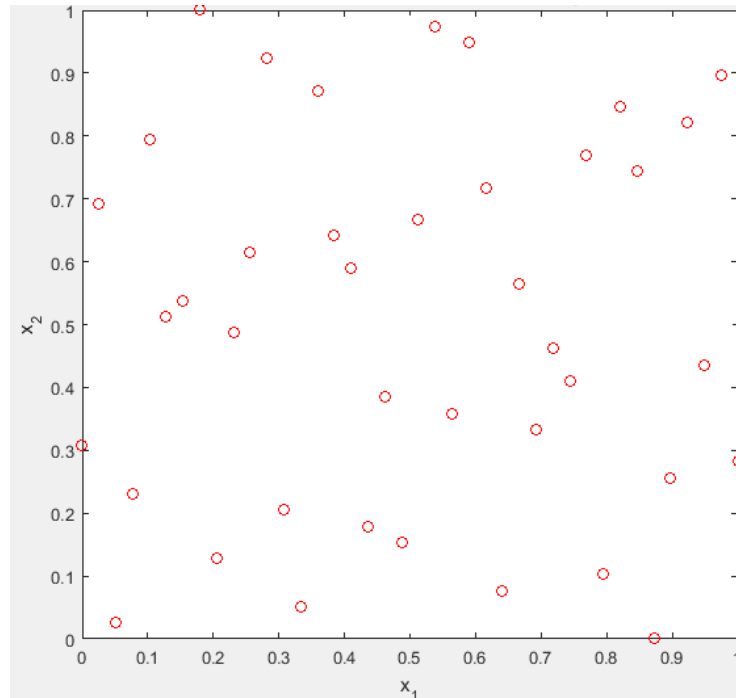


Fig. 3.4 Initial 40 Latin Hypercube Samples for SynRM design

from Table 3-5 and Table 6-1 (in the appendices), it can be analysed that:

- air gap between stator and rotor
- slot depth
- shaft diameter
- flux barrier width
- flux carrier width
- slot openings

are the most influencing parameters for the performance of SynRM. In order to validate the FEM model testing, the PSO parameters are further generated which are shown in section 6.2.1 (in the appendices) and their FEM values are shown are tested which are shown in Table 3-5 and 3-6 respectively. For the square slot shape, the PSO efficiency is around 89% which differs from the FEM efficiency calculated in Magnet that is 91%. However, the torque is higher 800Nm as compare to FEM which is 619Nm at 7.46kW power. Whereas the efficiency in a round shape of stator slots by PSO is 85% and 89% calculated by FEM and the torque is also lower 577Nm. This should be noted that for the square slot shape the filling factor used is 78% and 65% for the round shape.

Table 3-4 Initial 40 Latin Hypercube Samples with square slot shape for SynRM design

S, No	Airgap in mm	Slot depth in mm	Tooth width	Shaft dia in mm	Flux Barrier width in mm	Barrier edge angle in °	Flux carrier width mm	Slot openings mm	Torq: in Nm	Eff: in %	Power in kW	Fill factor in %
1	0.93	50.3	15.4	111	11.6	34.4	14.6	7.22	778.	86	9.62	75
2	0.65	55.5	12.3	121	12.3	38.4	15.2	7.42	768	86	9.72	50
3	0.78	52.5	13.3	127	12.7	40.8	15.6	7.54	809	86	9.87	58
4	0.58	50.7	14.1	63	8.24	15.2	11.7	6.26	644	89	7.88	64
5	0.72	51.7	16.6	77	9.21	20.8	12.6	6.54	723	90	8.77	73
6	0.70	53.3	12.7	119	12.16	37.6	15.1	7.38	726	87	9.09	55
7	0.80	56.9	16.3	101	10.90	30.4	14.0	7.02	681	89	8.41	62
8	0.73	55.3	13.9	110	14.26	49.6	16.9	7.98	784	87	9.88	56
9	0.77	58.9	13.8	120	13.56	45.6	16.3	7.78	749	86	9.48	51
10	0.84	58.3	13.6	79	9.36	21.6	12.7	6.58	611	87	7.73	52
11	0.63	54.5	15.8	71	8.80	18.4	12.2	6.42	727	90	7.83	64
12	0.91	51.1	12.1	69	8.66	17.6	12.1	6.38	611	87	7.71	56
13	0.82	58.7	15.3	145	13.98	48	16	7.9	749	87	9.46	56
14	0.56	59.5	13.0	117	12.02	36.8	15.0	7.34	712	86	9.00	48
15	0.51	55.9	15.6	123	12.44	39.2	15.3	7.46	784	88	9.80	61
16	0.57	50.9	13.7	97	13.82	28.8	13.8	6.94	716	88	8.87	62
17	0.90	55.1	13.5	95	13.7	28	13.7	6.9	664	88	8.23	55
18	0.55	57.7	16.0	73	8.94	19.2	12.3	6.46	630	90	7.65	60
19	0.53	59.9	16.4	57	7.82	12.8	11.4	6.14	556	90	6.75	58
20	0.85	53.5	12.9	99	10.76	29.6	13.9	6.98	684	87	8.57	55
21	0.54	52.7	16.8	51	7.40	10.4	11.0	6.02	572	91	6.90	72
22	0.96	56.7	14.8	129	12.83	41.6	15.7	7.58	754	88	9.4	57
23	0.52	57.3	14.9	53	7.54	11.2	11.1	6.06	545	89	6.68	57
24	0.89	54.9	15.9	85	9.78	24	13.1	6.7	654	90	7.96	64
25	0.74	58.1	12.4	125	13.14	43.2	15.9	7.66	749	86	9.56	48
26	0.67	51.3	15.7	87	9.92	24.8	13.2	6.74	690	90	8.39	69
27	0.92	57.1	15.0	89	10.06	25.6	13.3	6.78	642	89	7.86	57
28	0.69	51.9	16.7	125	13.42	44.8	16.2	7.74	813	87	10.1	73
29	0.60	53.9	16.2	103	11.04	31.2	14.1	7.06	723	89	8.91	67
30	0.94	59.7	13.2	120	13.84	47.2	16.5	7.86	732	86	9.30	48
31	0.97	54.1	14.4	107	11.28	32.8	14.4	7.14	719	87	8.99	55
32	0.86	54.3	14.0	122	13	42.4	15.8	7.62	732	88	9.11	57
33	0.61	51.5	12.8	67	8.52	16.8	12.0	6.34	566	88	7.07	58
34	0.59	53.7	12.2	81	9.50	22.4	12.8	6.62	628	87	7.94	53
35	0.50	54.7	12.0	115	11.88	36	14.9	7.3	737	86	9.40	51
36	0.98	50.5	14.5	55	7.68	12	11.3	6.1	589	90	7.19	65
37	0.71	57.5	13.4	93	10.34	27.2	13.5	6.86	644	88	8.00	52
38	0.95	52.1	13.1	109	11.46	33.6	14.5	7.18	744	87	9.32	58
39	0.66	56.3	15.1	113	11.74	35.2	14.7	7.26	738	88	9.20	59
40	0.79	53.1	12.5	65	8.38	16	11.9	6.3	602	87	7.55	55

Table 3-5 PSO parameters for square and round stator slots

	Airgap in mm	Slot depth in mm	Tooth width in mm	Shaft dia in mm	Flux Barrier width in mm	Barrier Edge angle in °
Square	0.5	50	17	111	22	50
Round	1	59	17	147	43	46

Table 3-6 PSO more parameters for square and round stator slots

	Flux Carrier width in mm	Slot opening in mm	Torque in Nm	Efficiency in %	Power in kW	Fill factor in %
Square	15.8	8	619	91	7.46	78
Round	17	6	577	89	7.11	65

3.7 Arrangements of Rotor and Stator Optimisation parameters for SynRM design

As per general criteria and design approach stated in [219] [220], the ratio of the flux barrier to flux carrier should be controlled within 0.6 to 0.7. In order to design the SynRM machine, the following parameters are needed to be calculated: As it has been already mentioned in the beginning of the chapter, in this application, the outer diameter of the stator is limited to 500mm and that of the rotor is 300mm. At this stage the shaft diameter is kept at 90mm and then remaining 105mm radius is available for the flux barrier and carriers and then these parameters are given by:

$$105 * 0.6 = 63 \text{ and } 105 - 63 = 42 \quad \text{Maximum Flux barrier width.}$$

$$105 * 0.7 = 73.5 \text{ and } 105 - 73.5 = 31.5 \quad \text{Minimum Flux barrier width.}$$

For the stator design the number of turns initially the stator slot area has been fixed to 653 mm² and from different fill factor ranges the number turns are calculated. 10kW machine power rating is estimated with 105RPM and 900Nm Torque. As per design 26Amp current is estimated with 400 supply voltage, and as a rough idea 4Amp current is passed through 1mm² in air cooled, so 7mm² conductor area is required to be passed around 26amps. This shows that if the filling factor is in between 40% to 75% then the range of a number of turns will be as follows.

$$\text{Slot Area} = 635$$

$$\text{Fill factor } 75\% = 635 * 0.75 = 476 \text{ then } 68 \text{ Turns}$$

$$40\% \text{ Filling Factor} = 635 * 0.40 = 254 = 36 \text{ Turns}$$

It should be noted that in the previous design the shaft diameter was also considered as a variable, so due to this reason the range of flux barriers are slightly change in Table 3-7.

Table 3-7 range of design parameter for the 2nd optimisation process

Variable	Range
Flux barrier width (mm)	22-40,
Flux carrier width (mm)	11-17
Flux barrier edge angle	10°,50°
Number of turns	36-68
Note: The above was previous range because we did not optimise the shaft, now as the shaft diameter is available 87mm so remaining area is also 105mm from 1 side	
Flux barrier width (mm)	31.5 to 42
Flux carrier width (mm)	63 to 73.5
Flux barrier edge angle in °	10°-50°
Number of turns	36-68

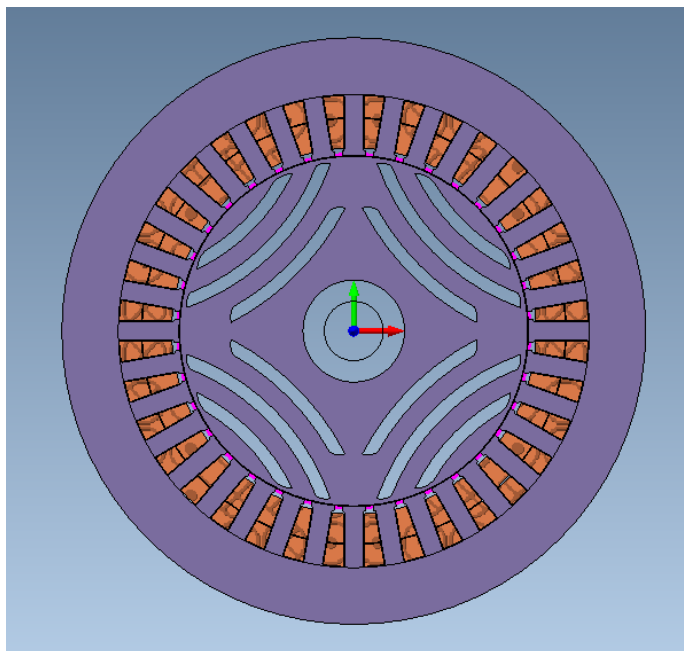
31.5 to 42 flux Barriers-Divided by 3 or 4

63 to 73.5 Flux Carriers- Divided by 4 of 5

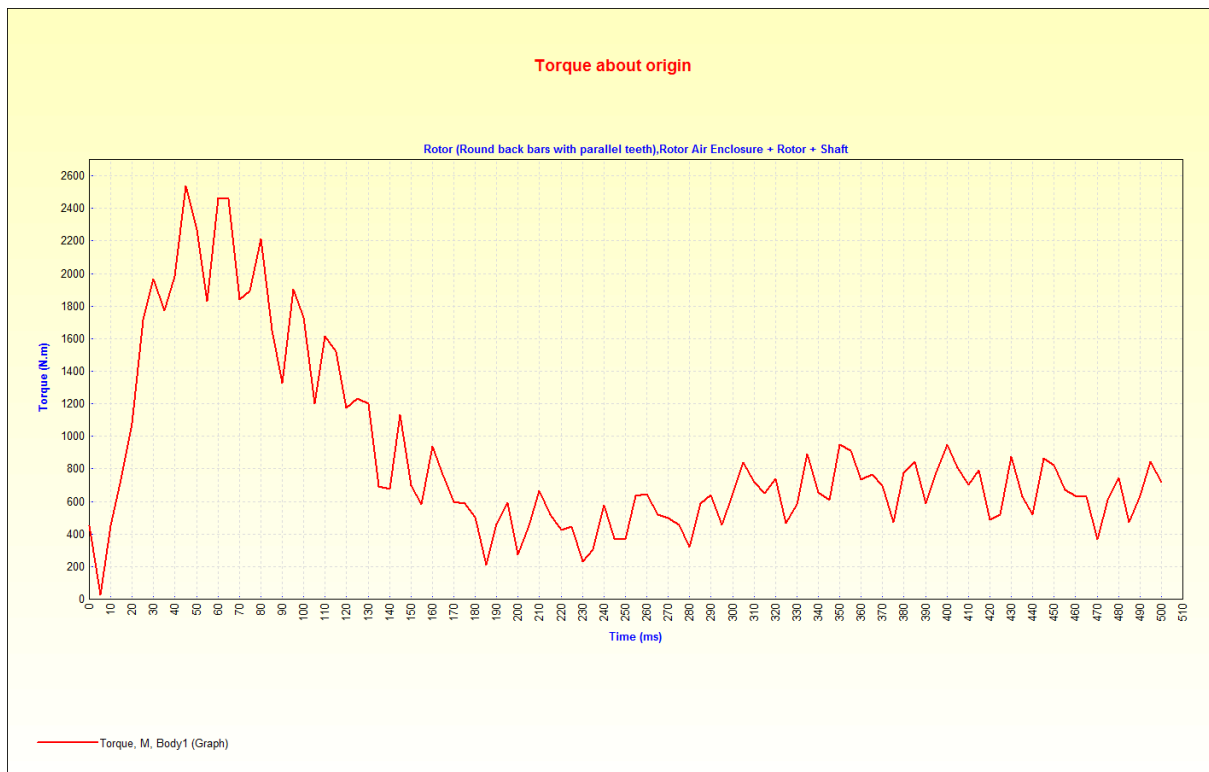
By considering the above variable ranges, the model accuracy can be increased by increasing sample data. As the objective criterion is satisfied, the optimisation process is stopped, and the final FEM result is validated by getting the optimum solution. The results are shown in Table 6-2 (in the appendices), the LHS sampling is shown in fig. 6.1. (in the appendices). The final solution with SBO algorithm while applying the particle swarm optimisation method is marked by the red star (see section 6.2.2 PSO optimised values No 1 in the appendices), which gives the solution of optimised values with the set of 20 points. From this process, the 877.86Nm torque is achieved with 93.6% efficiency at 10kW rated power. This should be noted that at 32.49 and 63.82 are the total width of flux barriers and carriers respectively, as the three-flux barriers and 4 flux carriers have been used in this rotor optimisation process, so each flux carriers are 10.83mm wide and flux carrier is 15.95mm wide. Additionally, from this process it has been identified that higher the flux barrier edge angle higher will be efficiency; hence this solution is found with all the available constraints shown in Table 3-8.

Table 3-8 Optimised parameters achieved from PSO method with the 1st optimisation process

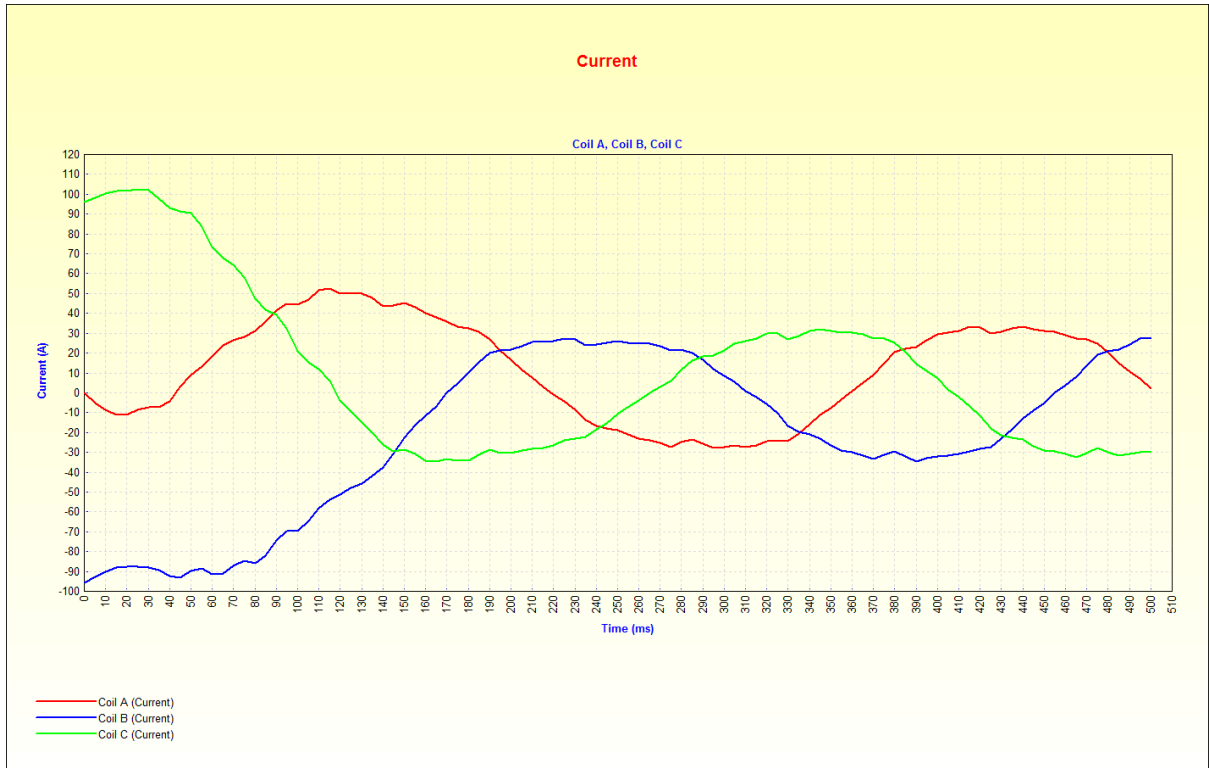
No	3 flux barriers width in mm	Flux carrier width in mm	Flux barrier edge angle in °	No: of turns	Torque in Nm	Efficiency in %	Power in kW
Optimisation 01	32.49	63.82	49.29	51	877.86	93.6	10



(a)



(b)



(c)

Fig. 3.5 shows (a) 3 flux barriers and 4 flux carriers model with a round shape (b) torque waveform and (c) three-phase current waveform

Fig. 3.5 shows the round flux barrier shape and 36 square shape stator slots. The machine has high starting torque up to 2400Nm and after 300ms the torque becomes good up to 877 Nm, whereas the current is also stable as expected 26A. A modification of objective function and constraint is then chosen and allows finding a solution through the FEM method and gives (91.95% efficiency and 811Nm torque with 9.7kW power) in 2nd optimisation process and (93.3% efficiency and 831.48Nm Torque with 9.8kW power). The solution with SBO algorithm while applying the particle swarm optimisation method is marked by the red star (see section 6.2.3 PSO optimised values No 3 in the appendices). In 3rd optimisation process marked by the red star (see section 6.2.4 PSO optimised values No 3 in the appendices), that verifies the constraints with acceptable tolerance with different flux barrier and flux carrier width, edge angle and number of turns as shown in Table 3-9 and Table 3-10.

Table 3-9 Optimised parameters achieved from PSO method with the 2nd optimisation process

No	3 flux barriers width in mm	Flux carrier width in mm	Flux barrier edge angle in °	No: of turns	Torque in Nm	Efficiency in %	Power in kW
Optimisation 02	37.60	73.49	49.99	58	811	91.95	9.7

Table 3-10 Optimised parameters achieved from PSO method with the 3rd optimisation process

No	3 flux barriers width in mm	Flux carrier width in mm	Flux barrier edge angle in °	No: of turns	Torque in Nm	Efficiency in %	Power in kW
Optimisation 03	33.22	66.38	50	53	831.48	93.3	9.8

3.8 Three round shaped flux barriers and 4 flux carriers

After adding 20 points around the initial optimal solution, a new optimisation with these 20 points is done. Now only good torque after 600 milliseconds has been considered. The torque waveform is shown in Fig. 3.6, and LHS values are shown in Table 6-3 (in the appendices). The numerical values which are depicted in column flux barriers and flux carrier are the total width obtained from LHS sampling. The values are further divided into 3 flux barriers and 4 flux carriers respectively. However, the values of edge angle and number of turns are exactly the same. The optimised PSO solution is shown in Table 3-11, this gives 7.58kW power rating and 91.1% efficiency with 672.58Nm torque. After the PSO optimisation solution, it gives 40.61m for flux barriers and 71.91mm width for flux carriers and the actual width of each flux barrier and carrier is 13.53 and 17.97 respectively. Hence, from the above results of efficiency torque and power values, the optimal solution couldn't be found with respected constraints.

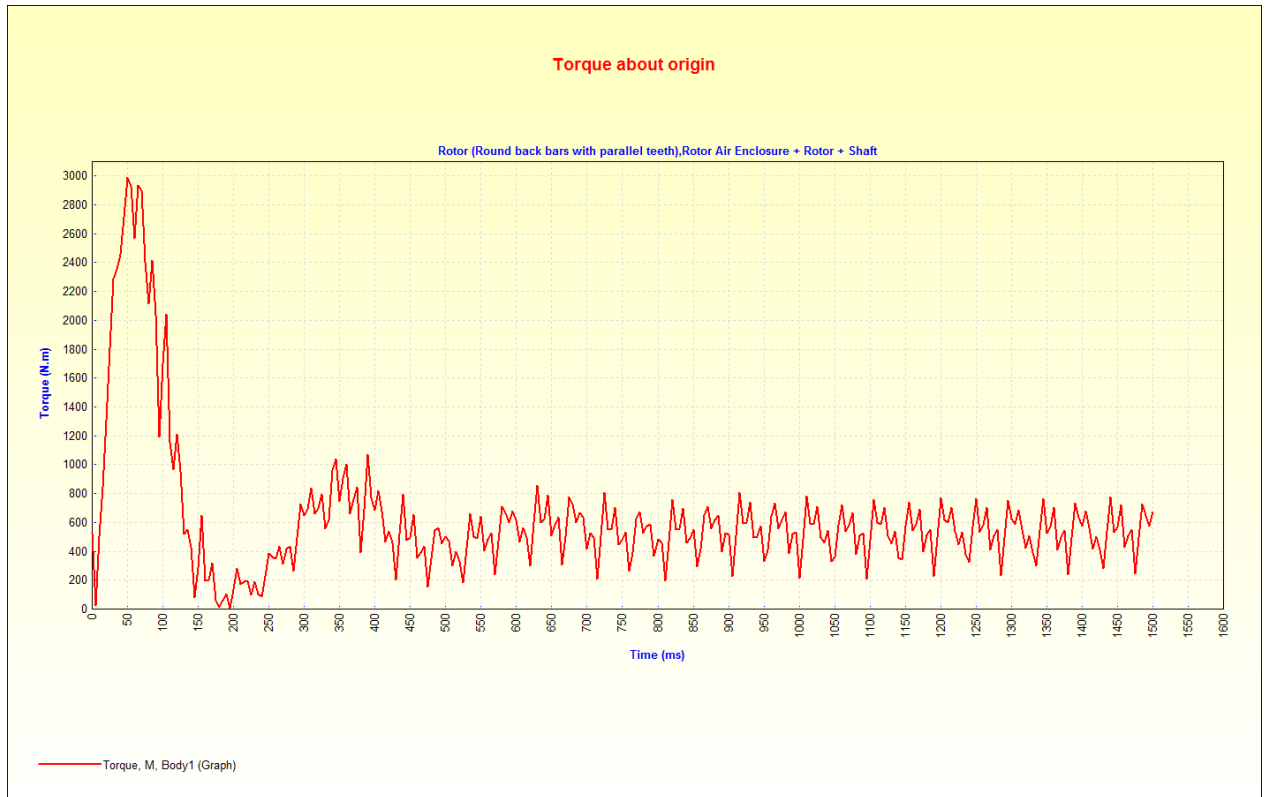


Fig. 3.6 torque waveform while considering stable portion after 600ms

Table 3-11 Optimised parameters achieved from PSO method only with stable torque

No	3 flux barriers width in mm	Flux carrier width in mm	Flux barrier edge angle in °	No: of turns	Torque in Nm	Efficiency in %	Power in kW
	40.61	71.91	49.99	60	672.58	91.1	7.58

3.9 Four round shape flux barriers and 5 round flux carriers

The new model for the objective and the constraints functions are simulated with the 20 points. The new model of four flux barrier is shown in Fig. 3.7. In this model, similar LHS samples are considered which have been considered for 3 flux barriers and carriers.

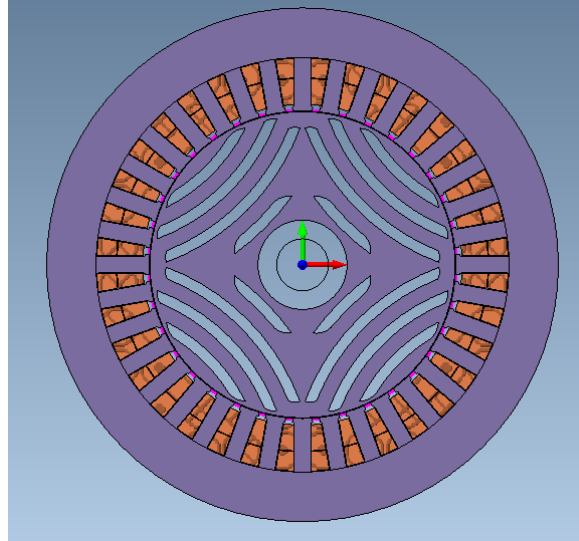


Fig. 3.7 round shape 4 flux barrier and 5 flux carrier SynchRM Numerical FEM Model

Table 6-4 (in the appendices) compares each optimal value found by the same Latin Hypercube Sampling generation with FEM model for a set of 20 points. The optimised values of efficiency, torque, and power through PSO optimisation are given at first and in second calculated values with FEM model.

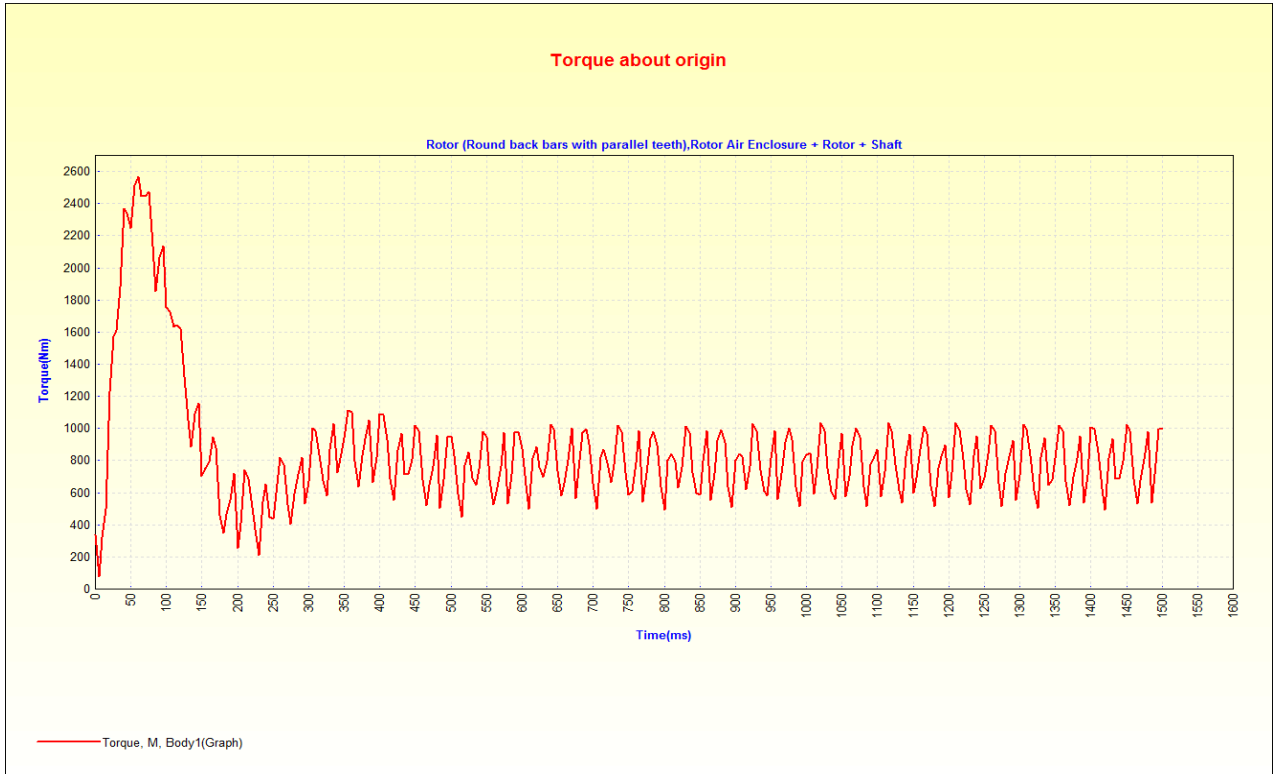
Table 3-12 Optimised parameters achieved from PSO method with 4 flux barriers and 5 flux carriers

No	4 flux barriers width in mm	Flux carrier width in mm	Flux barrier edge angle in °	No: of turns	Torque in Nm	Efficiency in %	Power in kW
	41.30	70.59	49	53	778	92.13	11.92

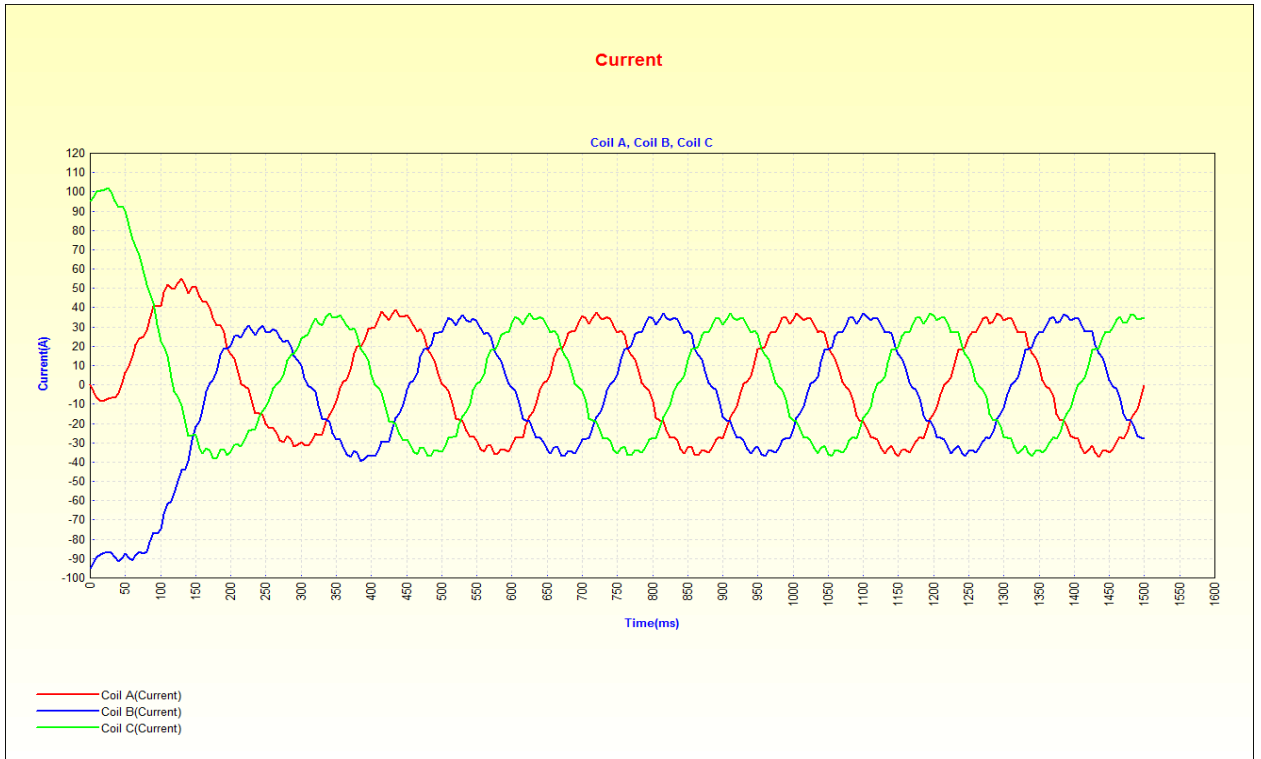
With the set of 20 points, it appears that the PSO optimisation leads to a slight error of 0.39% only for the efficiency (see section 6.2.5 PSO optimised valued for 4 flux barriers in the appendices). The power and torque lack behind 19.2%, 1.24% in the FEM model as shown in Table 3-12. The same set of 20 points are tested to verify the machine at higher speed 1500ms and compared the results with previous data. The relative data is used to compare with obtained results of PSO optimisation from FEM. The FEM results are taken as a reference. Table 3-13 shows the optimised parameters with 10.32mm flux barrier width and 14.11 flux carrier width having a 49-degree edge angle at 53 number of turns. The average torque from this is 851Nm and the stable torque after 300ms is calculated which is 786 Nm. The efficiency is slightly smaller 90.94% and the power ratings are also low 9.5kW. The torque and current waveform are shown in Fig. 3.8.

Table 3-13 Optimised parameters at 1500ms simulation time

No	4 flux barriers width in mm	Flux carrier width in mm	Flux barrier edge angle in °	No: of turns	Torque in Nm	Efficiency in %	Power in kW
	10.32	14.11	49	53	786	90.94	9.5



(a)



(b)

Fig. 3.8 shows the 1500ms time simulation (a) Torque waveform (b) 3-phase current waveform

It should be noted that above all the optimisation and their solution have been checked with the round shape optimisation and then the further author decided to check the similar variable into square shape design and to compare with round shape. The PSO optimised valued for 4 square flux barriers are shown in the appendices (see section 6.2.6). The square flux barrier design is shown in shown Fig. 3.9 and Table 6-4 and 6-5 (in the appendices) depicts the data with actual and stable torque. Here as it is observed that, power and efficiency are reasonable but, its stable torque is low 686Nm as depicted in Table 3-14. Note: (The stable torque means good torque when the torque become smooth after some initial high start-up transients).

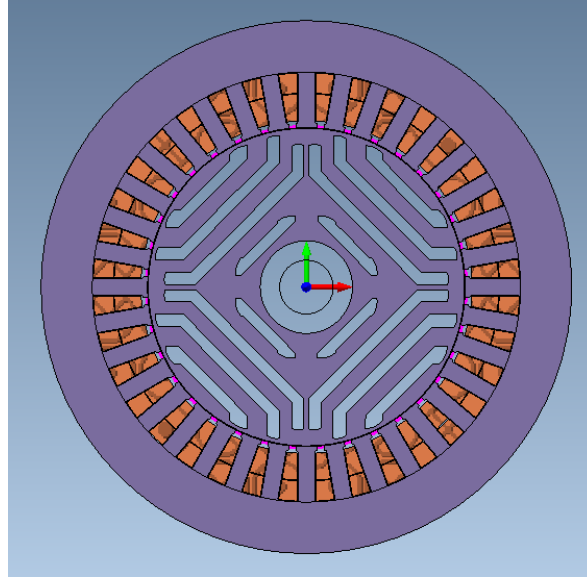


Fig. 3.9 Square flux barrier design

Table 3-14 Optimised parameters of square shape flux barriers

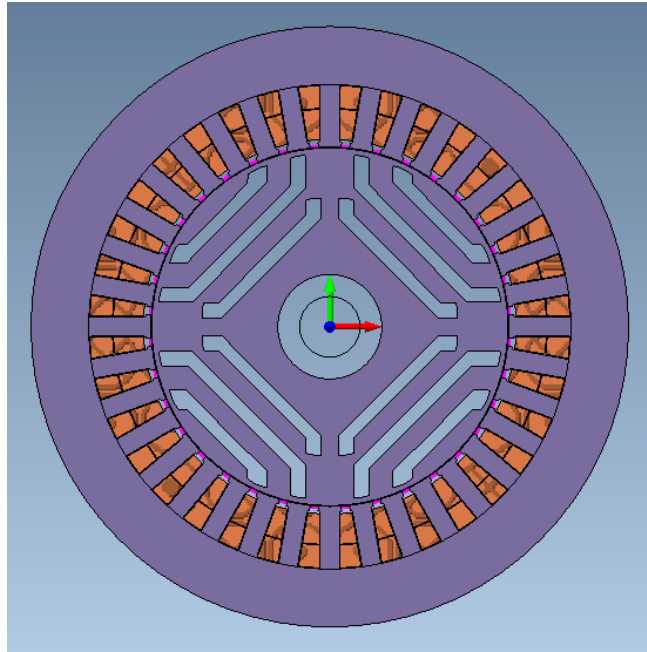
No	4 flux barriers width in mm	Flux carrier width in mm	Flux barrier edge angle in °	No: of turns	Torque in Nm	Efficiency in %	Power in kW
	31.5	63	50	55	686	91.2	8.26

3.10 3 square shape flux barriers and 4 flux carriers

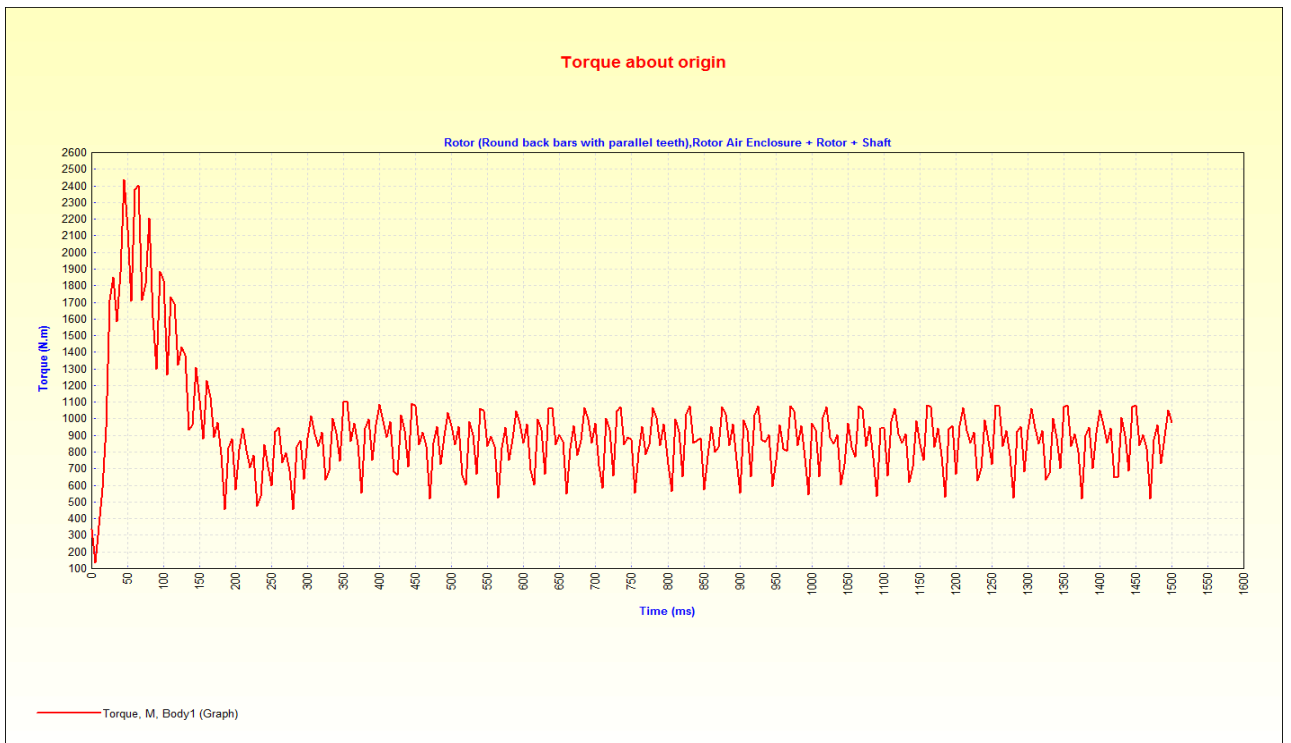
3 flux barriers and 4 flux carriers are tested to determine the efficiency, power, and torque from the available constraints, and to know the optimised PSO variable and their performance (see section 6.2.7 PSO optimised valued for 3 square shape flux barriers and 4 flux carriers in the appendices). In order to minimize the computational time, the same 20 LHS are taken. To get the width of the flux barrier and flux carrier, each sample is divided by 3 and 4 respectively. Table 6-6 (in the appendices) shows the efficiency, torque, power and fill factor at various width of the flux barrier and flux carrier. In the model of optimisation 91.01% efficiency is achieved at 10.02kW power rating with 830Nm torque as shown in Table 3-15. It should be noted that here the stable torque is considered after 300 milliseconds and the starting torque is not considered. The optimised variable from PSO are shown (in the appendix) and the FEM model of square shape 3 flux barrier and 4 flux carriers with torque and current waveform are shown in Fig. 3.10.

Table 3-15 Optimised parameters of 3 square shape flux barriers and 4 flux carriers

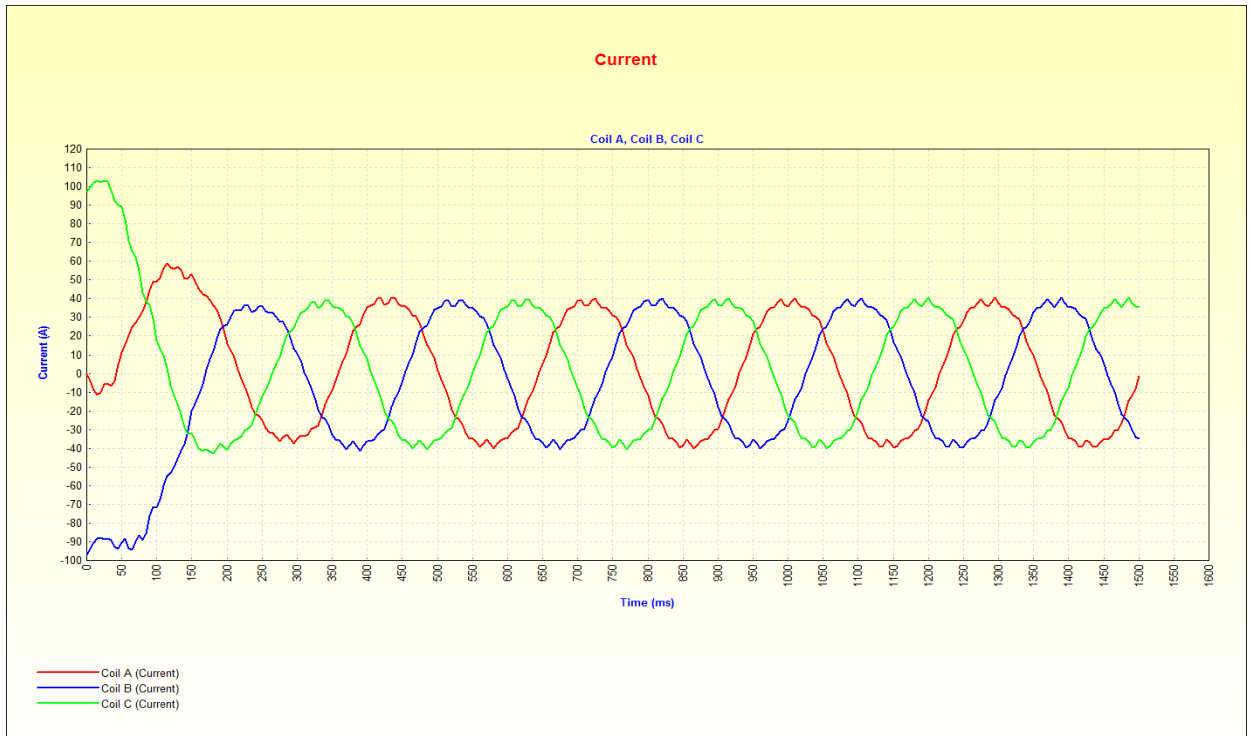
No	4 flux barriers width in mm	Flux carrier width in mm	Flux barrier edge angle in °	No: of turns	Torque in Nm	Efficiency in %	Power in kW
	10.5	16.13	28	48	830	91.08	10.02



(a)



(b)



(c)

Fig. 3.10 square shape 4 flux barrier and 5 flux carrier (a) SynchRM Numerical FEM Model (b) Torque waveform and 3-phase current waveform

3.11 Optimisation with round stator slots with round flux barrier shape

In order to investigate the flux barrier performance with round stator slots, the SBO optimisation carried out. The shape of the round stator slot is directly taken from the inbuilt *Motor Solve* software and for 2D FEM simulation is done on magnet while importing geometry of the flux barrier imported into *Magnet* from AutoCAD. The step by step process is shown as follows.

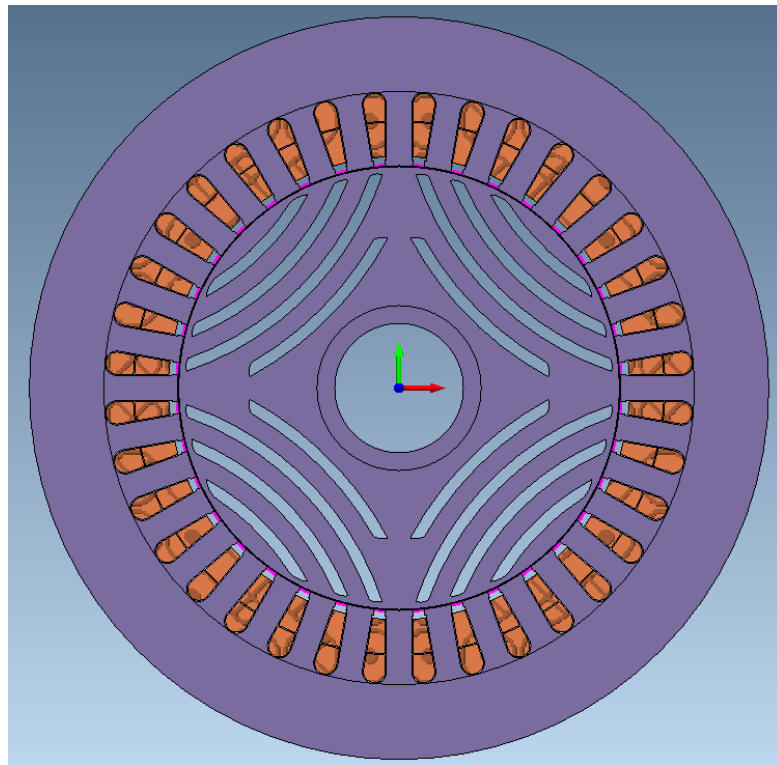
3.11.1 Round shape with 4 flux barriers and 5 flux carriers

Using the same optimisation process but, flux barriers and flux carriers are in a round shape and with round stator slot shape. The Latin Hypercube Samples are shown in Table 6-6 (in the appendices). The feasible solutions of torque, efficiency, and power are different. The analysis of the results of the optimisation process show that the torque produced is higher up to 905Nm and the efficiency is 91.61% at 10.86kW power as depicted in Table 3-16. The design FEM model and torque waveform are shown in Fig. 3.11. The starting torque is very high around 3400Nm which gradually decreased to average 900Nm. 4 flux barriers have been used with thickness of 7.875mm and 5 flux carriers with 12.6mm thickness. The number of turns is also optimised, and 50 turns are achieved as an optimised number of turns of the machine. Consequently,

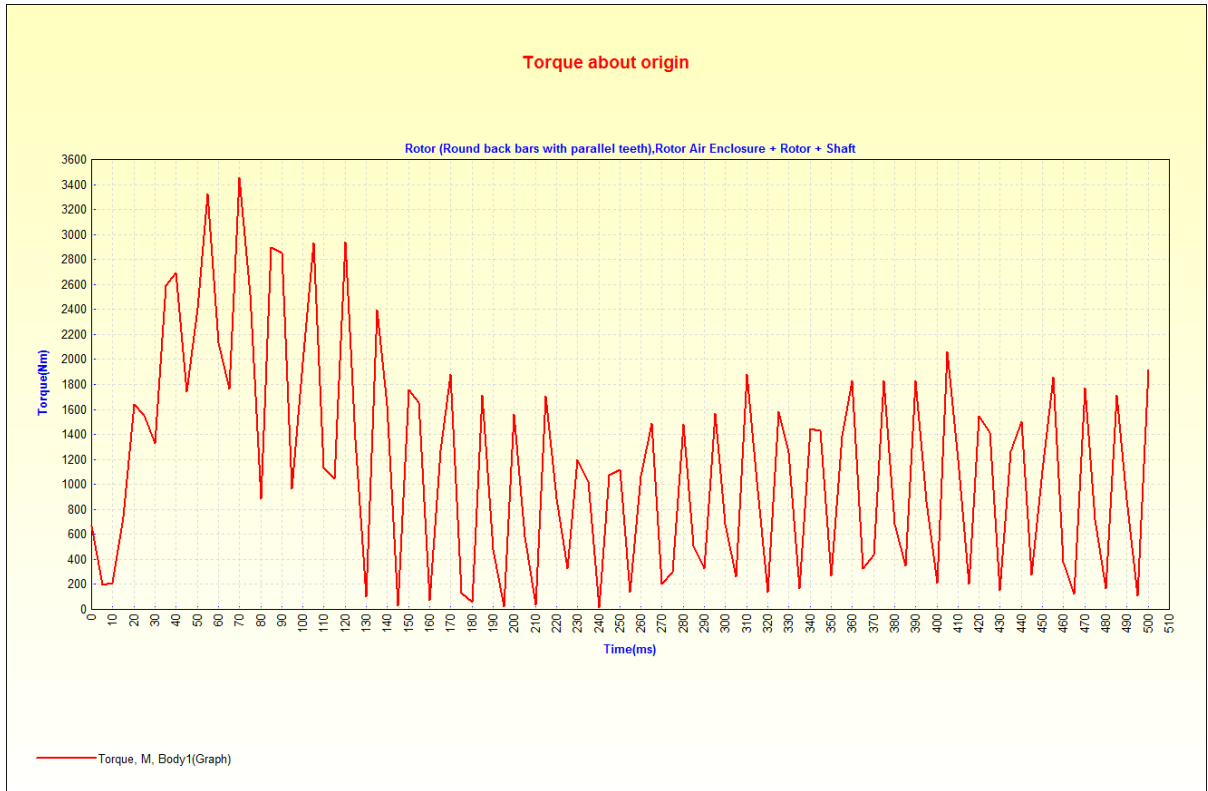
it has been necessary to further explore the impact of a number of slots on the machine performance i.e. efficiency and torque production, so the design of 24 stator slot is considered which is described as follows.

Table 3-16 Optimised with round stator slots parameters of 4 round shape flux barriers and 5 flux carriers

No	4 flux barriers width in mm	Flux carrier width in mm	Flux barrier edge angle in °	No: of turns	Torque in Nm	Efficiency in %	Power in kW
	7.87	12.6	50	50	905	91.61	10.86

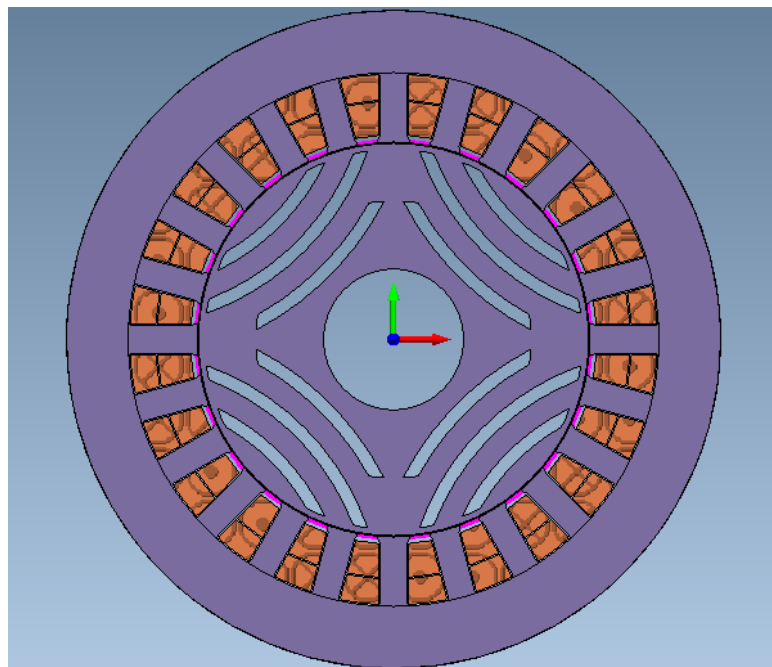


(a)

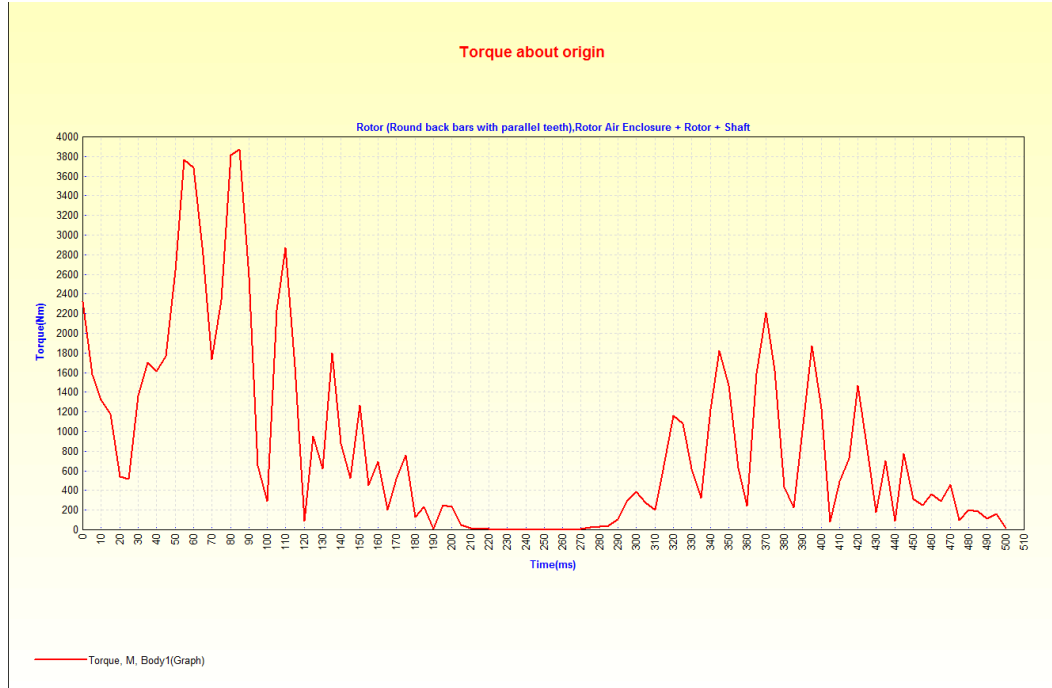


(b)

Fig. 3.11 shows (a) round stator slot with round flux barrier FEM model (b) torque waveform



(a)



(b)



(c)

Fig. 3.12 Square slot design with 24 slots

3.12 24 Square Shape Stator Slots Design

The torque and efficiency are the major figure of merit pertaining to the capability of the machine. These figures of merit give indication as the higher level of performance. Therefore, further simulation is tested

on 24-stator slot design with 3 round flux barriers as shown in Fig. 3.12. The simulation has been run upto 500 milli seconds. The measurement of torque vs speed and current vs speed is taken into account. In figure (a) 3 round flux barriers are tested with 24 slots. From the transient analysis it has been observed that the torque profile is not good as depicted in figure 3.12(b). The starting torque is good around 3800Nm. There is a zero current in between 210mm to 300mm, so that torque reaches almost negligible as depicted in figure 3.139(c). Thus, measurement of torque speed envelope is not desirable with 24 slots. After 300mm the current again increased to rated value at 38amps. As the previous testing was with 36 slots, so the author decided the check the SynRM performance at 24 stator slots. In the 24 slots stator, we have more margin to select the stator design variables, so the range of influencing parameters increased are shown in Table 3-17, and LHS generated samples are shown in Table 6-7 (in the appendices).

Table 3-17 variable range selection for Latin Hypercube Samples for 24 stator slots

Variable	Range in mm (Min to Max)
Airgap	0.5-1
Slot Depth	50-60
Tooth Width	17-26
Shaft Diameter	50-150
Flux Barrier Width	22-43
Flux Barrier Edge Angle	10-50°
Flux Carrier Width	17-26 in mm (same as tooth width)
Slot Openings	8-17

It should be noted that the torque which is low between, 400 to 600Nm, as for 24 slots stator design, we have more slot area as compare to 36 slots. Therefore, to check the results at higher number of turns the simulation has also been tested at 100 turns as depicted in Table 6-8 (in the appendices), but this increases the resistance and inductance by default in the software which reduces the current. Hence overall torque of the machine is low, actually as the stator has been designed on the motor solve software, by selecting 100 turns, The simulation with 50 turns in motor solve with low external resistance and inductance are shown in Table 6-9 (in the appendices) and their FEM results are shown Table 3-18 and Table 3-19 with PSO optimised variables are shown in section 6.2.8 (in the appendices) with 20 LHS sampling points in Fig. 6.2 (in the appendices).

Table 3-18 Optimised parameter by PSO for 24 square slots

No	Airgap in mm	Slot depth in mm	Tooth width in mm	Shaft dia in mm	Flux Barrier width in mm	Barrier Edge angle in °
01	0.57	51.4	26	50	27.92	59.99

Table 3-19 Optimised more parameter by PSO for 24 square slots

	Flux Carrier width in mm	Slot opening in mm	Torque in Nm	Efficiency in %	Power in kW	Fill factor in %
01	20	10.81	752	88	8.27	70

3.13 24 Round Shape Stator Slots Design

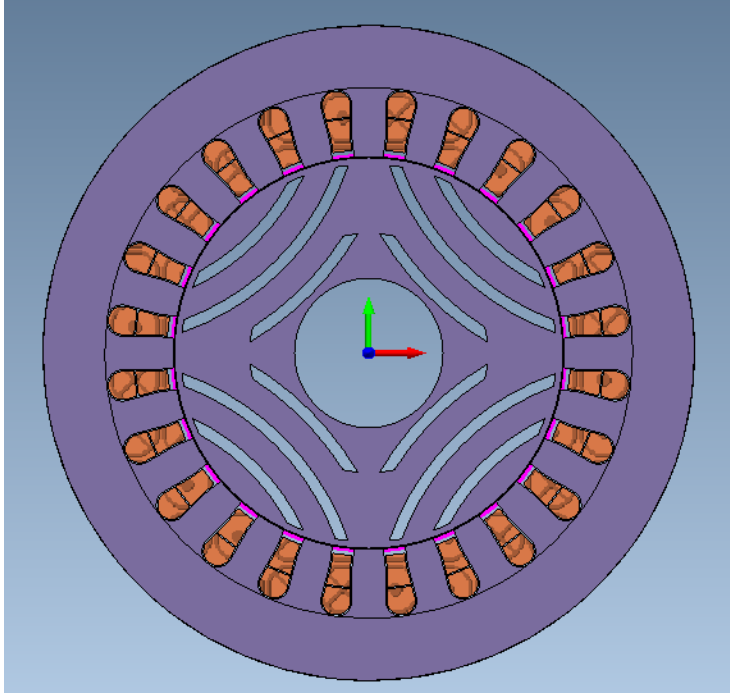
The 24 round stator slot design variables are shown in Table 6-10 (in the appendices). The previous testing was done at 24 round slots, in order to know the performance at 24 round stator slots, the same number of round slot design with 3 round flux barriers are shown in Fig. 3.13(a). (see section 6.2.9 PSO generated optimised variable for 24 round stator slots in the appendices). The measured curve runs to 500 milli seconds at 380 voltage with maximum 3800 Nm starting torque is presented in fig. 3.13 (b-c). The torque starts to drop off around 200 to 300 milli-seconds. Due to simulation time process the full torque speed graph upto 1500 milli-seconds is not taken. The stator design parameter's range remains the same as per previous LHS samples. In this design, the efficiency is almost the same and the torque production is higher as compared to a square shape, but the torque ripple is higher because the current reaches to zero as depicted in Fig. 3.13(d). The torque ripple can be minimized through separate rotor design optimisation. The FEM results are shown in Table 3-20 and 3.21 respectively. This shows that torque is increased up to 804Nm and efficiency is 92.4% with good power rating 9.56kW. The SBO design variables with FEM results are shown below Fig. 3.13, and PSO generated optimised variables are shown as follows.

Table 3-20 Optimised parameter by PSO for 24 round stator slots

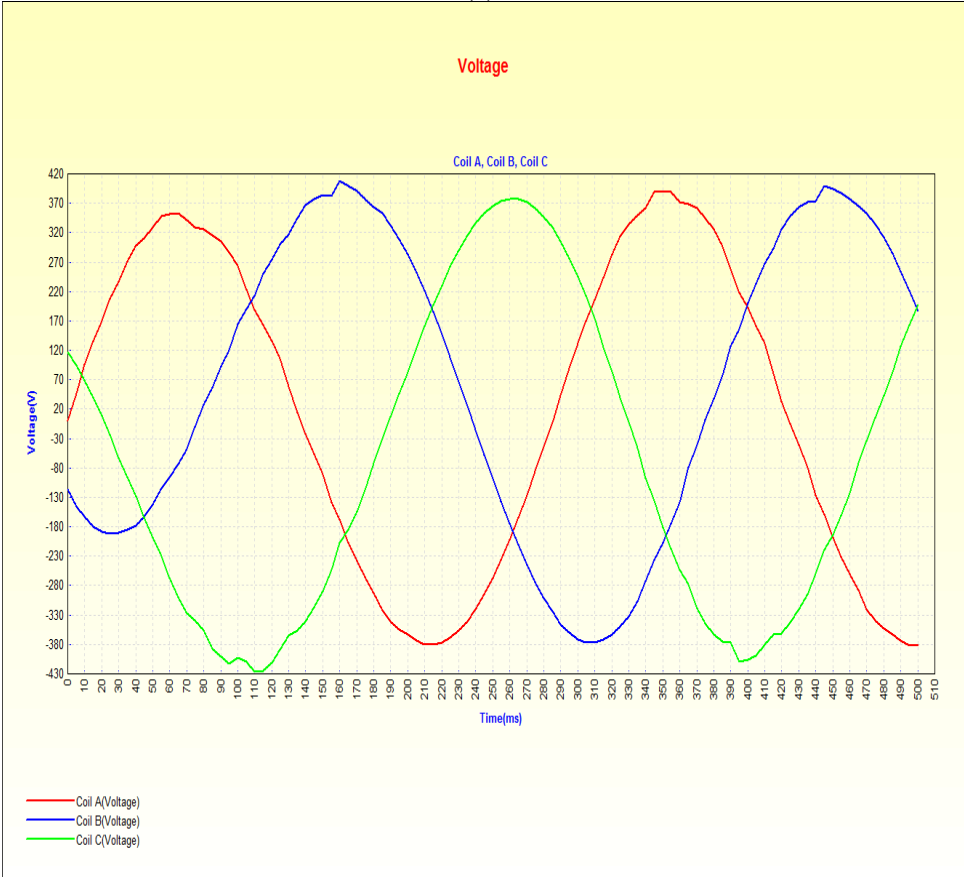
No	Airgap in mm	Slot depth in mm	Tooth width in mm	Shaft dia in mm	Flux Barrier width in mm	Barrier Edge angle in °
01	0.57	52.6	26	114	8.72	10

Table 3-21 Optimised more parameter by PSO for 24 round stator slots

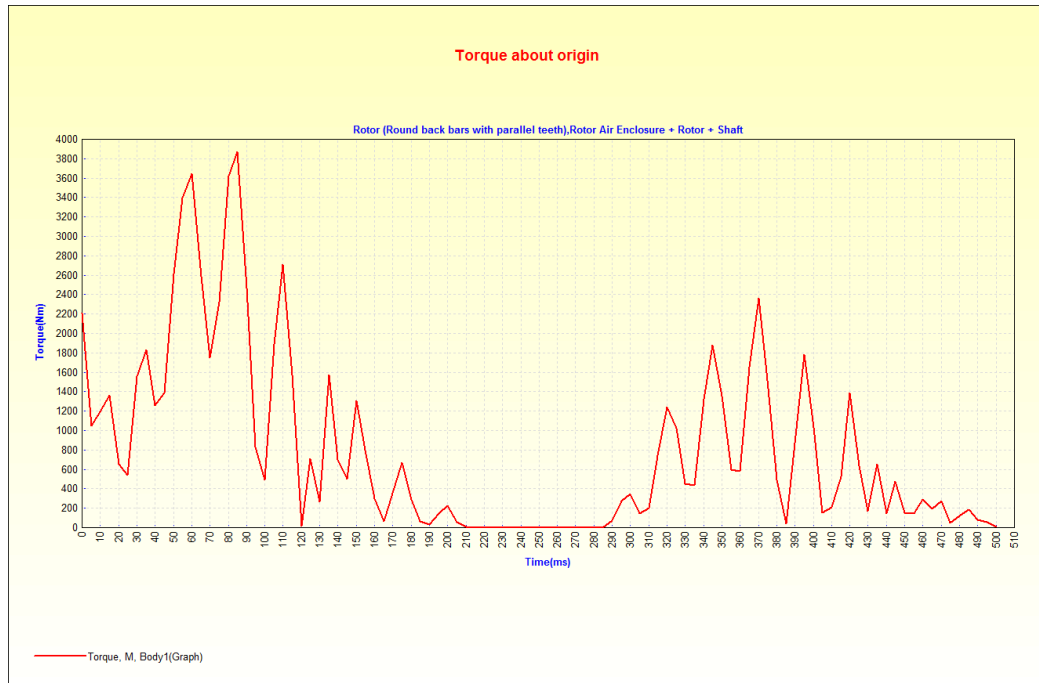
No	Flux Carrier width in mm	Slot opening in mm	Torque in Nm	Efficiency in %	Power in kW	Fill factor in %
01	20	10.81	804	92	9.56	71



(a)



(b)



(c)



(d)

Fig. 3.13 SynchRM with 24 slots (a) FEM Model (b) 3-phase voltage waveform (c) Torque wave form and (d) current waveform

3.14 Final Optimisation with 4 flux barriers with square shaped

After checking all design shapes of stator slots and rotor flux barriers, and keeping all the results in mind, the author decided to analyse the optimisation of round 4 flux barriers. Because, on the basis of considering the design and simulation experience, 4 flux barriers produce high average torque 905Nm with 91.61%

efficiency at 10.86kW power ratings as depicted in Table 3-22. The round flux barriers have been replaced with square-shaped flux barriers. The simulation results are tested at 1500ms which gives very good results from a performance point of view. Fig. 3.14 shows the FEM model and torque, current and voltage waveform of 4 square flux barriers shape with 36 square stator slots. Table 3-22 shows the PSO optimised parameters. It should be noted that the power is high 9.6kW with 91.01% efficiency.

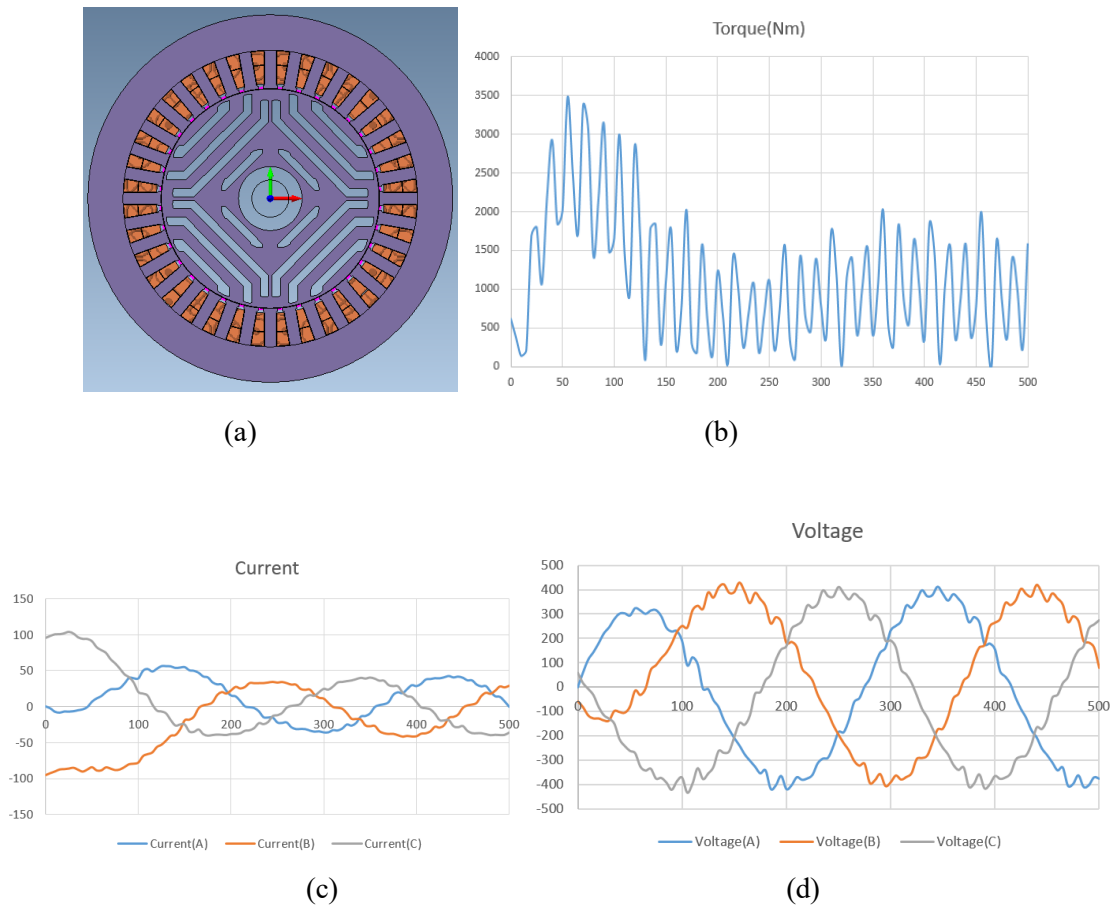


Fig. 3.14 square shaped 4 flux barriers design (a) FEM model (b) torque waveform (c) current wave form (voltage wave form at 1500ms simulation time

Table 3-22 Optimised parameter by PSO for 4 square shaped flux barriers

No	4 flux barriers width in mm	Flux carrier width in mm	Flux barrier edge angle in °	No: of turns	Torque in Nm	Efficiency in %	Power in kW
01	10.32	14.11	49	53	802	91.01	9.6

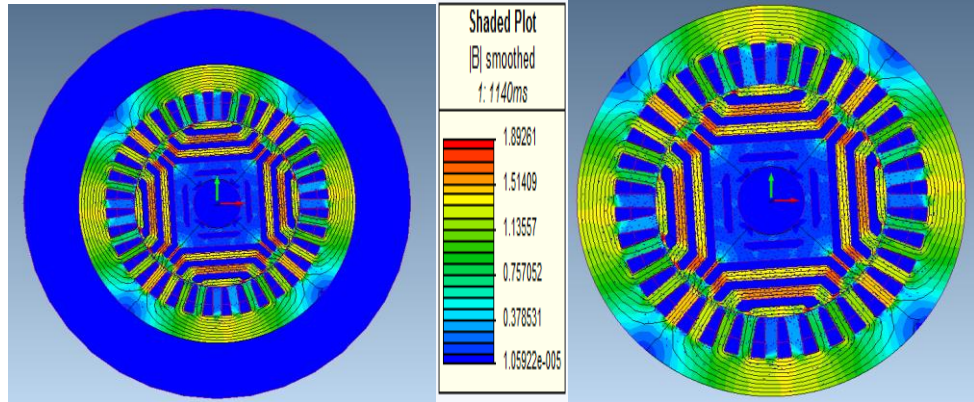


Fig. 3.15 flux function view of (a) 4 square flux barrier design (b) flux function without exterior air

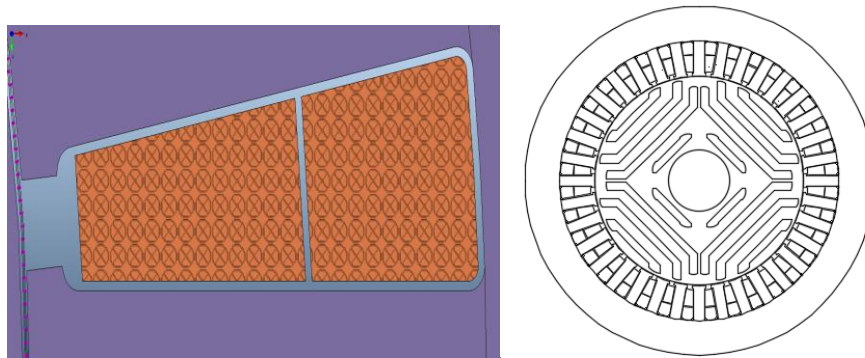


Fig. 3.16 square shape slot design and 4 flux barriers AutoCAD design used for SynRM

Table 3-23 3-Phase Winding specifications

Item	Specification
Insulating material	Epoxy resin
Hub material	Non-Magnetic
Ambient Temperature	20 degree C
Iron Core	M-19 29 Ga
Winding Material	100% IACS (Copper)
Shaft Material= CR10	Cold rolled 1010 steel

Usually, it is complicated to find accurate surrogate model due to increase number of design variables. 2 types of approaches exist to develop the accurate surrogate model such as (1) increase the sampling points and (2) use proper sample plan which is shown in Fig. 3.3. In our design strategy, 40 LHS sampling is chosen for 8-design variable problem. Total of 320 FEM models are evaluated during the SBO Optimisation technique. Fig. 3.15 presents the comparison results of flux function between a shaded plot with and without exterior air and the square shape stator slot. The 3-phase winding design and specifications are shown in

Fig. 3.16, and Table 3-23. The winding arrangements are shown in Fig. 3.17. The final design parameters are deliberated while SynRM rotor design with 4 variables in the simulation section.

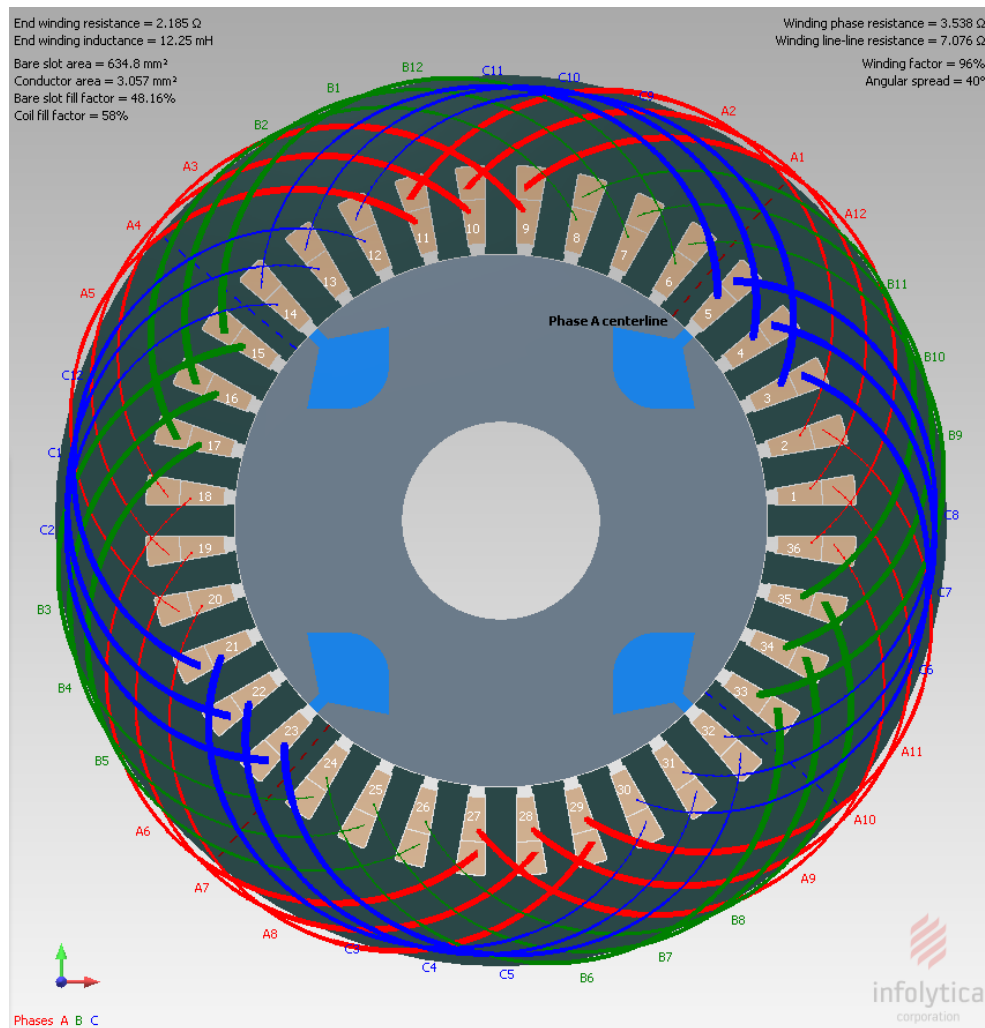


Fig. 3.17 Three-phase overall winding design arrangement of red, yellow and blue phase

3.15 12/8 SRM Design process based on Surrogate-Based Optimisation

The process of optimisation and algorithm is already depicted in Fig. 3.1. The first optimisation test is conducted by choosing random variables which are: stator pole arc, stator inner diameter, stator yoke thickness, rotor pole arc, rotor yoke thickness, shaft diameter and airgap range as shown in Table 3-24. In these variables, the stator inner diameter is taken 335mm as a fixed value at 170mm length. The sampling points of SBO are generated as depicted in section 6.2.10 (1st PSO optimisation variable for 12/8 SRM design with 100 samples in the appendices) and LHS samples are shown in Fig. 6.4 (in the appendices) and considered as a surrogate model input variable. In the following optimisation, the stator inner diameter is reduced up to 301.2mm and the machine length is increased to 200mm. The optimisation carried out from

the two different parameters settings as shown in Table 6-11 and 6-12 (in the appendices). The FEM results of efficiency, torque, speed, and slot filling factor are compared. It is started with the selection of an initial parameters range and sampling plan of 100 points and these 100 initial sampling points are then assessed by means of FEM model and the constraints function values are achieved. Afterward, for each objective and constraint function, a main surrogate model is fixed over the initial sampling plan. According to the optimisation results their torque and efficiency values are analysed as shown in Table 6-13 (in the appendices). This method clearly indicates the range of variables which can be considered into a surrogate to use all the available degree of freedom.

Further 60 Latin Hypercube samples are generated as shown in Fig. 6.4 (in the appendices). From the **Error! Reference source not found.**, it can be analysed that, stator pole arc, stator yoke, stator inner diameter, air gap, rotor yoke thickness, rotor pole arc, and shaft diameter are the most influencing parameters to enhance the performance of SRM. The efficiency of row number 15 in Table 6-14 (in the appendices) is around 90.26% and the torque is 671Nm. In row 29 sample the torque is lower 630Nm at 8kW power, and the efficiency is 90.66%. This should be noted that for the 12/8 SRM the filling factor used is 75.52% and 73.43% for this design. The comparison of modified designs is shown in Table 6-15 and 6-16 (in the appendices). From the above particle swarm optimisation plan, the maximum efficiency achieved is 88% at 680Nm torque and depicted below in 2nd PSO optimisation for 12/8 SRM design (in the appendices).

To improve the efficiency, a further test of 60 samples plan carried out as show. In this optimisation plan, the stator inner diameter was kept constant at 300mm, whereas stator pole, stator yoke thickness, airgap thickness, rotor pole arc, rotor yoke thickness, shaft diameter are considered as a design variable. As soon as the samples points are achieved their FEM simulation is carried out to get the results which are shown in Table 6-17 (in the appendices) and their efficiency and torque graph is shown in Fig. 3.18. In this optimisation plan, 6 Variables global optimisation Latin Hypercube Sampling Points of 12/8 SRM are taken and 60 samples are generated. In this optimisation, the sample number 40 gives the best results at 87% efficiency and 656Nm torque at 200mm actual length of the machine which has been considered for the design of 12/8 SRM and LHS samples are shown in Fig. 6.5 in the (appendices), and their efficiency and torque graph are shown in Fig. 3.19. The FEM simulation results of sample 40 have been described in detail in simulation section chapter 4.

Table 3-24 initial parameters for 12/8 SRM design at 170mm length

Stator			
Item	Design value	Minimum value	Maximum value
outer dia of the stator	500mm	Fixed	
Inner dia of the stator	335mm	Fixed	
Pole arc	15 deg	14	16
Pole width	43.7mm	40.8	46.6
Yoke length	30mm	27	37
Pole length	52.5mm	45.5	55.5
airgap	0.6mm	Fixed	
Rotor			
Rotor outer diameter	333.8mm	Fixed	
Pole arc	15.7 deg	15	17
Pole width	45.7mm	43.5	49.3
Yoke length	33.5mm	28	38
Pole length	73.4mm	68.9	78.9
Shaft diameter	120mm	Fixed	
Winding			
Number of turns	94	85	100
Wire diameter	1.8mm		

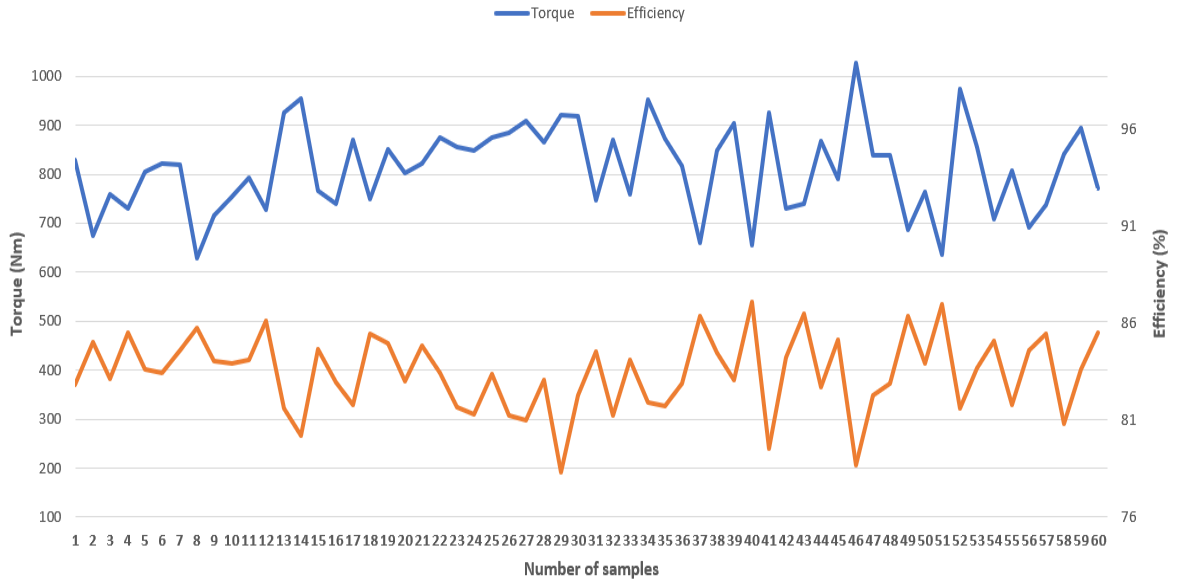


Fig. 3.18 efficiency and torque graph os 60 samples with 3rd optimisation

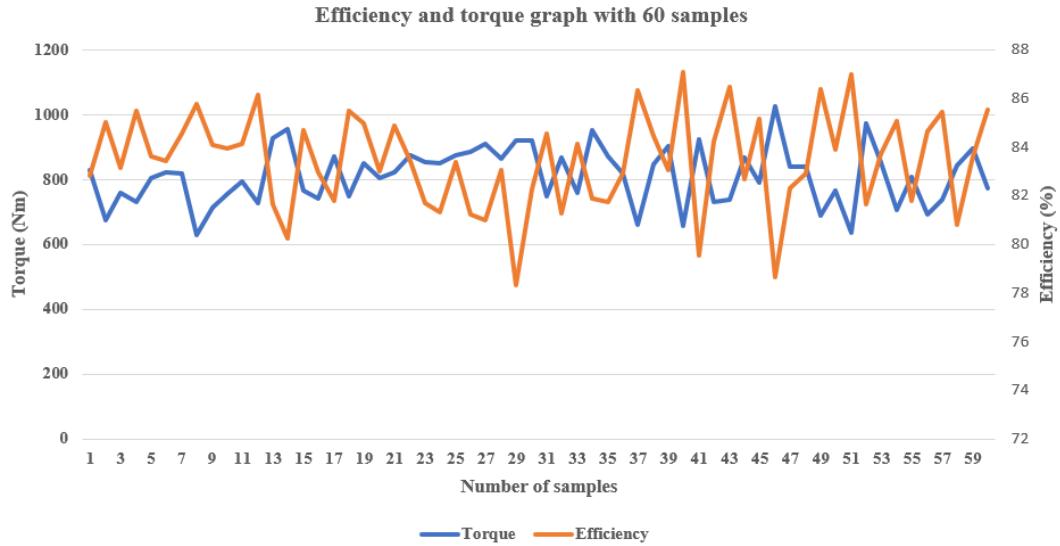


Fig. 3.19 Efficiency and torque graph for final 60 samples

3.16 12/8 SRM optimisation through constant speed and constant power

To analyse the constant speed and constant power, 40 more samples are generating while adding the slot filling factor and number of turns as shown in Fig. 6.6 (in the appendices). The air gap is kept constant 0.6mm. In this test two length of the machine have been tested at 170mm and 200mm. The initial 40 LHS samples for constant speed at 105rpm are shown in Table 6-18 (in the appendices). In the next plan, the same samples have been tested while keeping the power constant. The results of torque, efficiency is shown in Table 6-19 (in the appendices). Similarly, LHS samples are tested at 200mm stack length while keeping the speed and power constant and their results of efficiency and torque are shown in Table 6-20 and Table 6-21 (in the appendices) respectively. The efficiency profile at constant and constant power is shown in Fig. 3.21 and Fig. 3.22 respectively.

3.17 Constant speed analysis at 170mm and 105rpm

8 Variable Global Optimisation Latin Hypercube Sampling Points of 12/8 SRM

Air gap = 0.6 mm; Length= 170 mm *constant speed 105 rpm

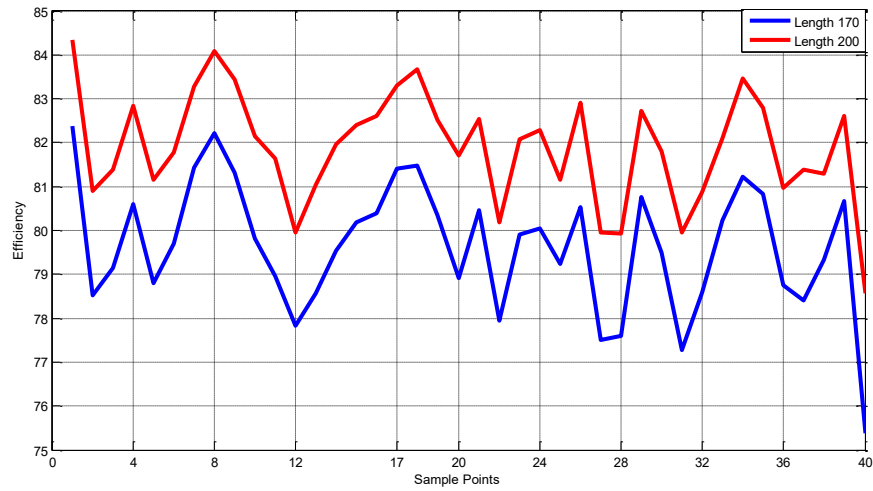


Fig. 3.20 efficiency at a constant speed

3.17.1 Efficiency at a constant Power

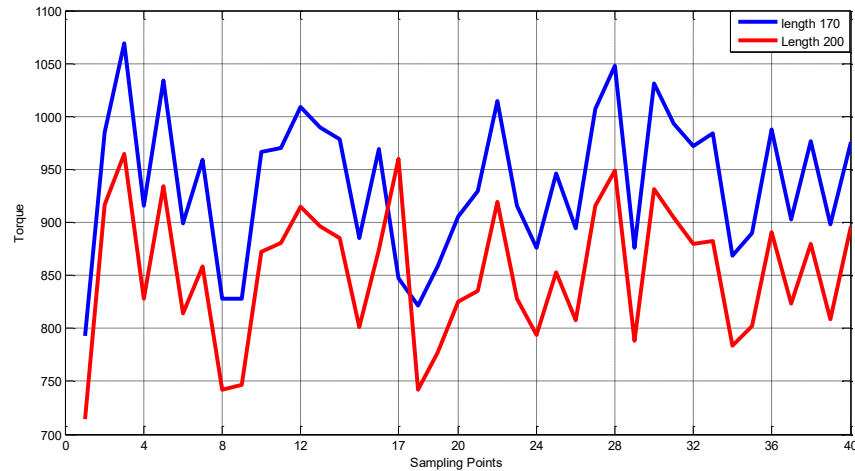


Fig. 3.21 Efficiency at constant power

3.18 Summary

In this chapter 3 optimisation has been carried of synchronous reluctance and switched reluctance machines. Two designs of synchronous reluctance rotor have been tested and analysed to improve the efficiency and to reduce the torque ripple. Keeping the size of the machine fixed for both SynRM and SRM at 500mm and a surrogate-based analysis and optimisation are applied to the machine.

The detailed process of optimisation has been examined here, and three steps are applied in the final optimisation process. Design of experiment technique is taken to consider the Latin Hypercube sampling. The plan is to choose randomly distributed and allocated sampling points which are not identical. In the

subsequent part, methods of construction of the surrogate model are inspected and compared. Due to the high precision, Kriging model is preferred to construct the surrogate model. The established surrogate model, an optimisation algorithm is used to discover the finest location, and in this thesis particle swarm optimisation algorithm is used.

For this novel methodology for surrogate optimisation, the optimisation of two design shapes for both square or round have been studied, assuming that two reluctance machines SynRM and SRM have the same dimensions in terms of stator out diameter and stack length. Only the other internal variables need to be varied and optimised in terms of efficiency and torque ripple analysis. In addition, based on this optimisation experience, the 3 flux barrier rotor for four variable problems such as flux barrier width, flux carrier width, edge angle, and shaft diameter has been extensively optimised for synchronous reluctance motor rotor, assuming the stator of the machine is similar to the 3-phase induction motor.

Chapter 4 Numerical design and simulation of Synchronous Reluctance Stator and Rotor

4.1 FEM Simulation

The most regularly used technique for magnetic field calculation is the finite element method FEM [221, 222]. The key advantage of FEM as compared to the other methods and procedures is the following: the prospect to define the object of any type; the ability to influence the discretization for diverse areas to reach the greater accuracy of designs with enhanced mesh refinement, and the optimal choice to clarify the limitations.

The calculation of magnetic field by means of finite element method permits to determine the major parameters of the machine-electromagnetic torque calculation, magnetic flux, and magnetic induction at various parts within the magnetic circuit as well as other parameters.

4.2 Synchronous Reluctance Rotor Design

As per the existing rotor design of SynRM, a novel rotor should be designed with the features to have low torque ripple with high efficiency and should be thermally stable. The main focus of this chapter is to design and simulation of SynRM rotor. Different flux barriers and flux carriers' shapes have been implemented to increase the performance of SynRM such as with and without rotor ribs, square and round shape design, symmetrical and asymmetrical design. The rotor of synchronous reluctance motor consists of two main electromagnetic components as per rotor pole (1) The flux carrier and (2) the flux barrier. A flux carrier comprised a ferromagnetic material leading to a high permeable path, while the flux barrier has a non-ferromagnetic material having a high reluctance path. In order to improve the saliency ratio, multiple flux carriers and flux barriers are created [61]. Initially, 20 Latin Hypercube samples have been generated from the rotor to test the efficiency and torque through the surrogate optimisation method which is shown in Table 4-1. To optimise the entire rotor study, the particle swarm optimisation method has been used to get best parameters. The *Infolytica Magnet* software has been used for FEM analysis. Therefore, the stator parameters remain unchanged for individual rotor analysis so as to keep constancy across each simulation. The rotor length and diameter are also retained constant excluding barrier size and width.

Table 4-1 Latin Hypercube samples for SynRM rotor design.

Barrier 1 width in mm	Barrier 2 width in mm	Barrier 3 width in mm	Barrier 4 width in mm	Torque in Nm	Efficiency in %	Power in kW
6.2	7.4	5.8	2.2	548.2	77.3	7.79
7.8	6.6	4.6	5.8	591.8	78.6	8.27
1.8	0.6	4.2	3.4	423	79.9	5.823
5.8	5	2.2	3	496.4	81.7	6.67
4.6	7	0.2	5.4	546	78.7	7.626
1	6.2	5.4	2.6	514	82.1	6.87
3	3.4	3	5	511.6	79.16	7.10
5.4	3	6.6	1.8	507.88	77.8	7.17
3.8	7.8	3.4	1.4	482	78.1	6.78
5	0.2	5	6.6	542	80.1	7.44
2.6	5.8	1.8	7	561.8	80.6	7.66
7	4.6	0.6	0.2	331.5	74.8	4.87
0.6	2.2	7.4	4.6	537	82.8	7.13
0.2	5.4	3.8	6.2	552	81.8	7.424
2.2	4.2	6.2	0.6	461.14	80.5	6.297
4.2	1.8	1.4	7.8	523.9	81	6.708
6.6	1.4	7	4.2	549.7	78	6.97
7.4	1	2.6	3.8	462.85	79	6.44
3.4	3.8	7.8	7.4	597.7	80.4	7.561
1.4	2.6	1	1	256.5	70.8	3.984

With the plan to tolerate the centrifugal forces and to provide the mechanical strength, iron ribs need to be added inside the flux barriers but this causes to reduce L_d/L_q due to stray flux path in q-axis [71, 103]. In these design studies, the iron rib width also depends upon the number of barriers as well as electromagnetic design. To reduce the simulation efforts, an investigation into the rotor design of the machine is carried out using radial ribs of 2mm. In this study, tangential ribs have not been taken into account.

To optimise the process, a coupling between *Matlab* coder, *Infolytica Magnet* and the *Motor Solve* has been used. In order to increase the machine's performance. All 20 solutions are computed in FE *Infolytica Magnet* software and the results are obtained. Throughout in these solutions, the author has chosen the one that suits the best-considered application. Latin hypercube samples of the 20 variables are shown in Fig. 4.1. Based on the author's expertise [223] the most important geometry parameters that actually influence the torque ripple of the synchronous reluctance motor are the width of flux barriers and the radius of curving edges. It should be noted that only the parameters of flux barriers have been optimised by the proposed surrogate optimisation using particle swarm optimisation method. The next phase of the research is the optimisation of the curving edges.

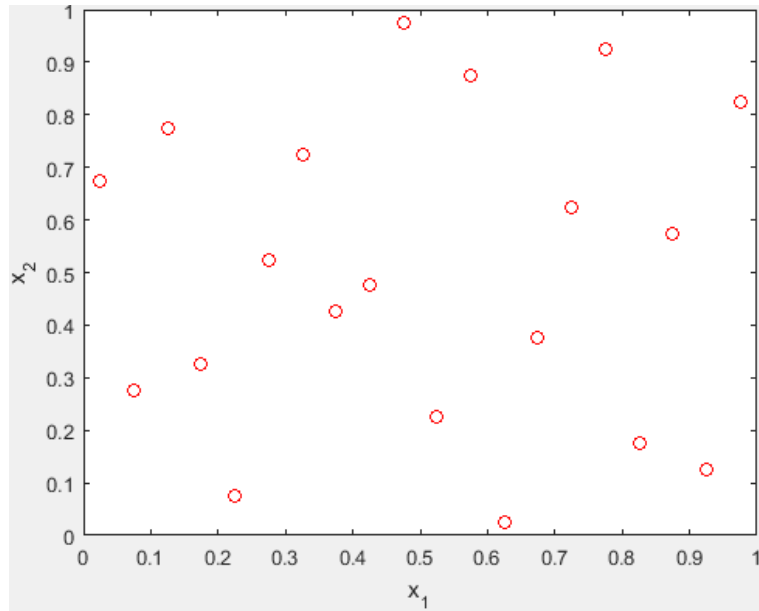


Fig. 4.1 20 Latin Hypercube samples of flux barriers for rotor Optimisation

2D FEM based design has been computed and its dimensions are shown in Table 4-2 and different rotor design steps are shown in Fig. 4.2. However, the author intends to carry out more investigation on the rotor to improve the efficiency and torque with curvature design optimisation.

Table 4-2 SynRM rotor flux barrier optimisation steps with and without ribs

Flux barrier 1 width in mm	Flux barrier 2 width in mm	Flux barrier 3 width in mm	Flux barrier 4 width in mm	Torque in Nm	Efficiency in %	Power in kW
7.5	7.5	7.5	7.5	591	80	8.11
8.5 rib 4mm	8.5	8.5	8.5	641.8	83.9	8.40
9.5 rib 3mm	9.5	9.5	9.5	629.7	82.3	8.40
7.5 no rib	7.5	7.5	7.5	651.5	80.9	8.85
7.5	7.5	7.5	7.5	635.2	83.8	8.33
5.02	6.70	12.32	4.83	782	85.6	10
5.02	6.70	12.32	6.11	792.4	85.82	10.15

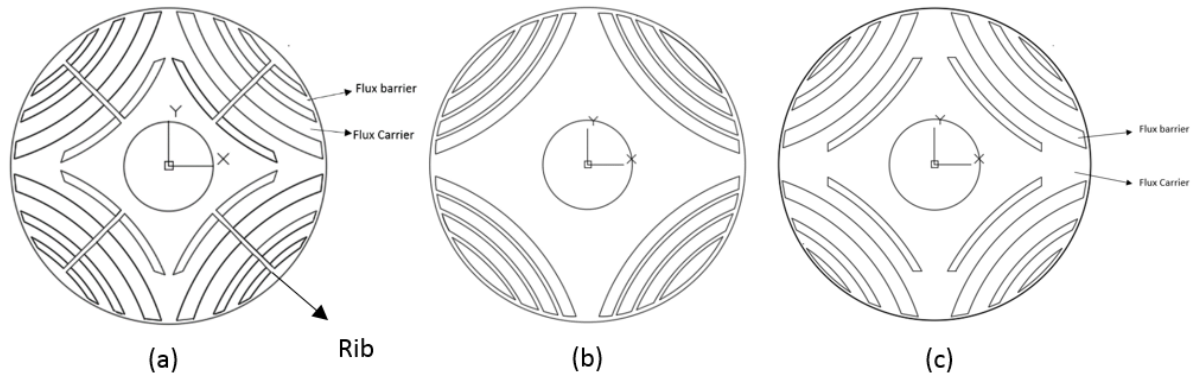


Fig. 4.2 Different rotor design steps for rotor optimisation. (a) Different flux barrier width with ribs (b) without ribs but equal flux barrier widths (c) different flux barrier width without ribs.

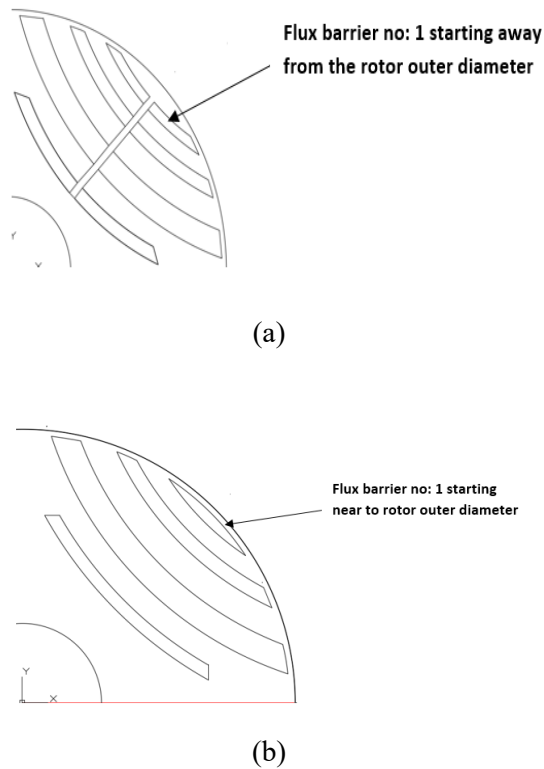


Fig. 4.3 design of Rotor flux barrier No: 1 (a) starting away from rotor outer diameter (b) starting near to rotor diameter.

Initially, the rotor is designed with random dimensions of variable flux barriers. The rib of 3.5mm with dimension is used as shown in Fig. 4.2 (a-b), the same rotor shape and barrier width are used in all the results of torque and efficiency which is depicted in Table 4-2. The first aim is to optimise the stator and to get the best stator among all those 20 samples. Then for rotor optimisation, all the barriers width are kept at the

same width 7.5mm as shown in the second row of Table 4-2, and 591Nm torque with 80% of efficiency is achieved. In the next step, the rib is tested to in between 4mm to 3mm along with 8.5 to 7.5mm flux barrier width this improves the flux and corresponding torque (641.8Nm & efficiency 83.9 for 4mm) and (629.7Nm & 82.3% for 3mm). For further testing, the barrier ribs are removed and the dimensions of all the ribs are kept the same which slightly improves the efficiency 80.9% and higher torque of 651.5 is achieved. It should be noted that up to this design, the starting flux barrier number 1 is kept away from the rotor outer diameter then in step 3 the first flux barrier rib is brought near to the rotor outer diameter, this reduces the torque but efficiency increased to 83.3 as depicted in Table 4-2 fifth row and shown in Fig. 4.3. It is tested to increase the continuous flux barrier width to check the effect on torque and efficiency up to 9.5mm width. The torque is reduced to 629.7Nm which affects the power rating of the overall machine. So, it is reflected that increasing the flux barrier width to a certain limit, causes a reduction in torque and efficiency in the design of SynRM. In the next step, different flux barriers width is tested, and simulation is carried out. This shows the improved results of 792Nm torque and 85.8% efficiency. The position of first flux barrier near to rotor outer diameter, improves the results as compared to those achieved away from the outer diameter. Thus, the machine is still under investigation as in the next step for the higher accuracy, more samples are generated to optimise the performance of Synchronous Reluctance motor.

In this thesis magnetic performance and other calculations have been carried out for the synchronous reluctance motor (SynRM) with the intention to validate the results with experimental data. Different rotors have been designed to achieve high torque with low ripples.

4.3 Standard Design and Simulations of the SynRM

In order to choose the best rotor design, seven different geometries of three and four flux barrier have been examined and a finite element analysis carried out. All the tests are conducted at 1500RPM as in Fig. 4.4 shows the different flux barrier designs of the rotor. (a) four flux barriers with V-shaped design. In this design, the flux barrier edge angle is kept 49 degrees and the torque ripple is 27%, which is good, but machine efficiency is very low. Therefore, the total average torque produced by the machine is 134Nm. One additional factor which is the flux density is higher up to 2.29T. In the design (b), more angle is provided to sharp edges, but the efficiency reduces to 37% and torque ripple is still higher to 70% and overall average torque is also reduced to 93Nm with flux density 2.2T. In this design (c), 132Nm torque is produced with 2.38T flux density and the torque ripple is 42%. In Fig. 4.5 (a) circular shape with four flux barrier design is tested which gives the efficiency 47% and 118Nm torque at 2.18T whereas torque ripple is slightly higher 44%. In design (b) three V-shaped flux barrier design is tested which produce the highest torque 158Nm with 70% and low torque ripple 30% but flux density is higher 2.7T. The design (c) gives 134Nm torque

and 2.5T density and torque ripple are higher up to 46% with 63% efficiency. In (d) three square-shaped flux barrier is used which produces 134Nm torque and 47% torque ripple at 2.17T flux density.

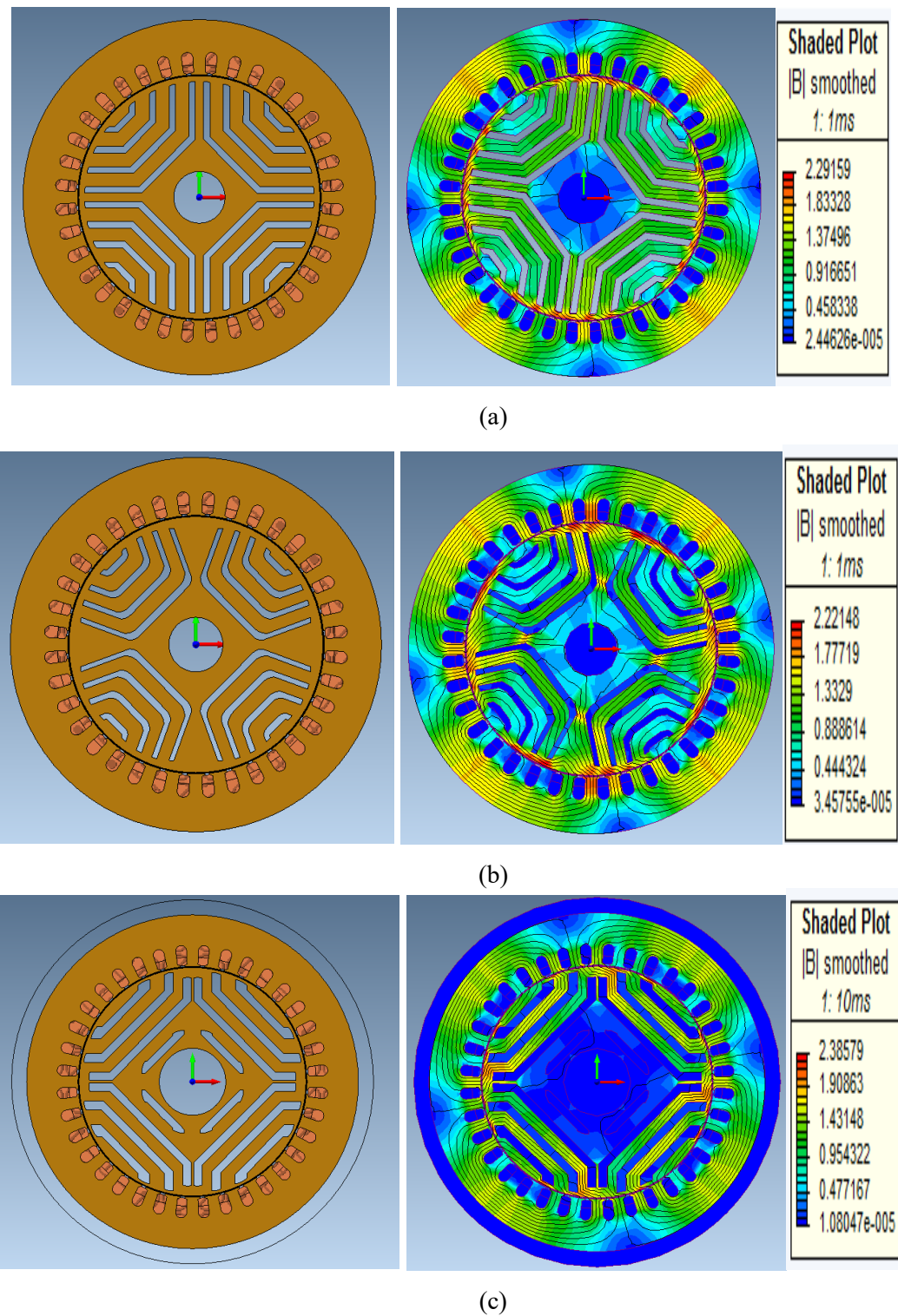
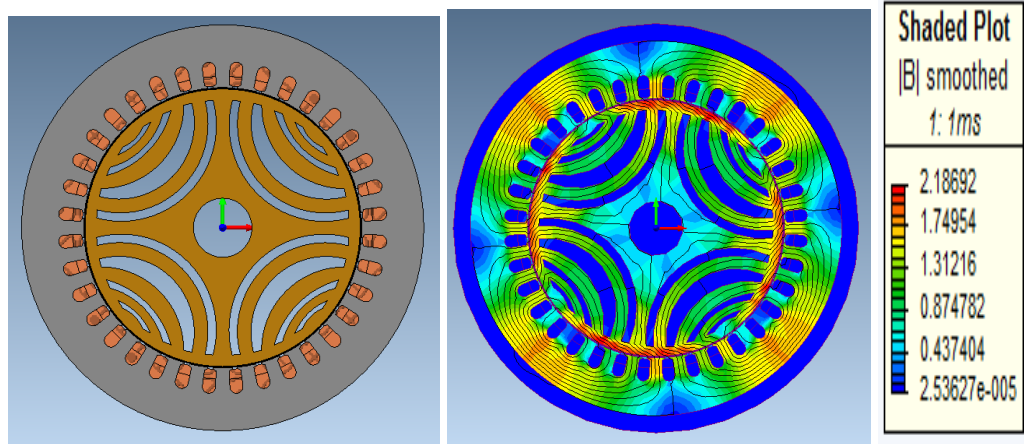
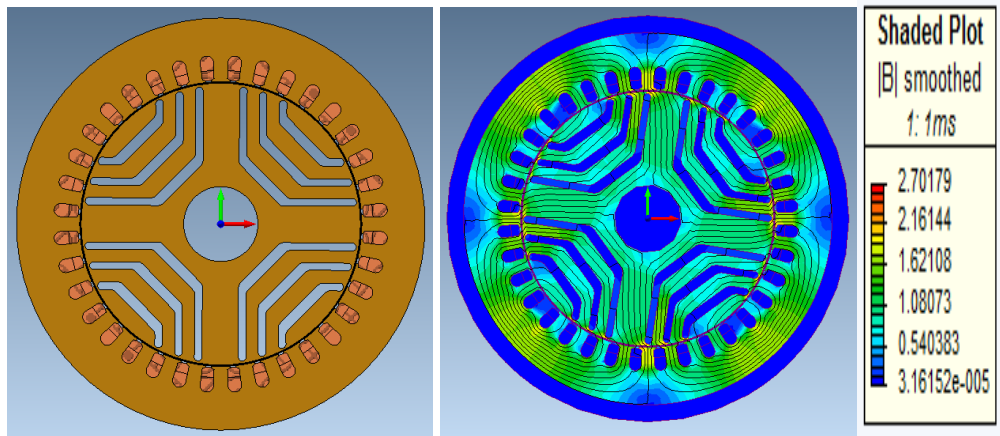


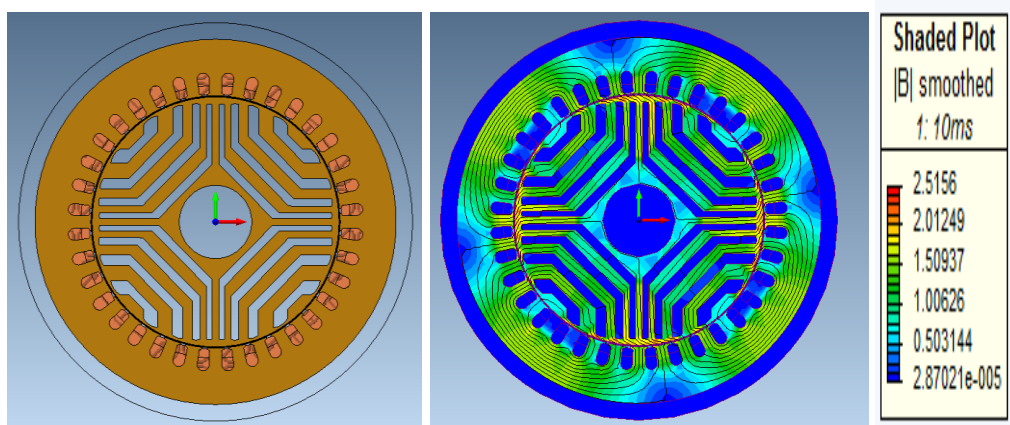
Fig. 4.4 different four flux barrier rotor designs for SynRM (a) 4 V-shaped flux barrier rotor (b) 4 square shaped rotor (c) 4 straight flux barriers with a slight angle at the edges.



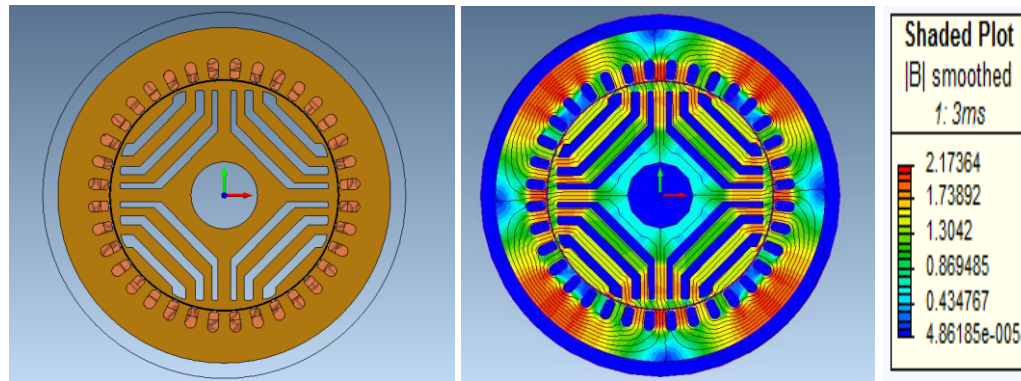
(a)



(b)



(c)

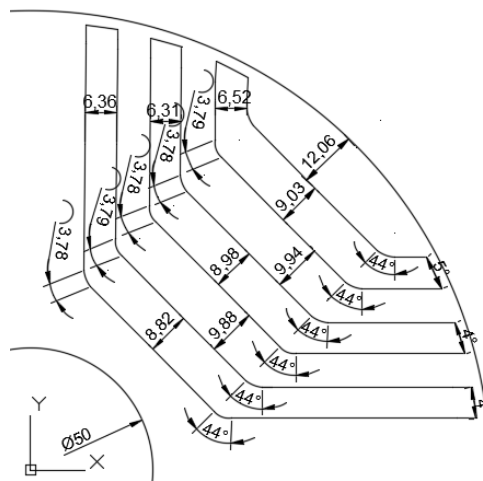


(d)

Fig. 4.5 Three and four flux barrier rotor designs for SynRM (a) 4 square shaped flux barrier rotor (b) 3V-shaped rotor (c) 4 square shaped flux barriers with a slight angle at the end and (d) 3 square shaped flux barriers.

4.4 The final design of the proposed SynRM rotor

Keeping above data analysis, in terms of torque, efficiency, torque ripple and flux density in the section of optimise rotor design, the author decided to take three V-shaped design as the main investigation point, because of higher torque production and high efficiency. The flux barrier width, flux carrier width and barrier edge with shaft diameter is modified in the design and finally, 3-Phase 24kW synchronous reluctance with 3 flux barriers motor is simulated with all specifications depicted in Table 6-22, Table 6-23, Table 6-24 and Table 6-25 (in the appendices). Initially, the same design of SynRM motor, 4 and 5 flux barrier square shaped is designed. However, the simulation outcomes are not up to the mark, and the motor is producing high flux density more than 2.7T and low torque in between (100 to 120Nm) which is not desirable for the high-efficiency output power application because the speed was fixed 1500rpm for the application of closed couple centrifugal pump.



(a)

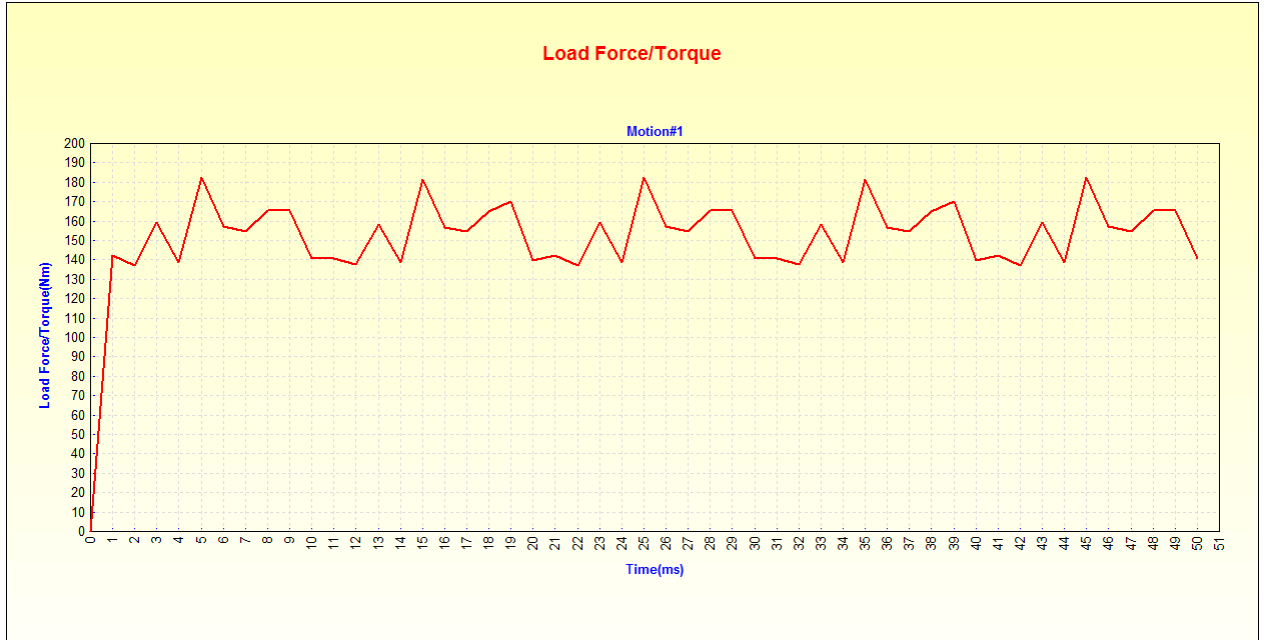


Fig. 4.7 Torque waveform of the proposed rotor

Further, the author decided to simulate another 3-flux barrier configuration, because flux barriers and carriers can be easily adjusted to a certain limit of saturation and to avoid higher flux density. In this regard, the square design with V-shaped scheme has been used to design the proposed rotor geometry, it has 3 flux barriers and 4 flux carriers on each 4th quadrant as their dimensions are shown in Fig. 4.6 (a-c) and torque waveform is shown in Fig. 4.7. The main advantages are due to increased flux carrier width to pass the maximum magnetic lines and minimum magnetic flux density is possible. However, no compromise is made in between saliency ratio. The 3-phase 24kW SynRM used in this thesis is shown in Fig. 4.8 (a-b) proposed design of SynRM and the mesh view analysis is shown in Fig. 4.8(c). For current magnitude control, the voltage driven sinusoidal supply as an input source for winding is provided. The 2.1T flux density and rated current with electromagnetic torque established are shown in Fig. 4.9 (a to c). Also, the simulated copper, eddy current with hysteresis losses are 358watts and the stator hysteresis and eddy current losses are 379watts.

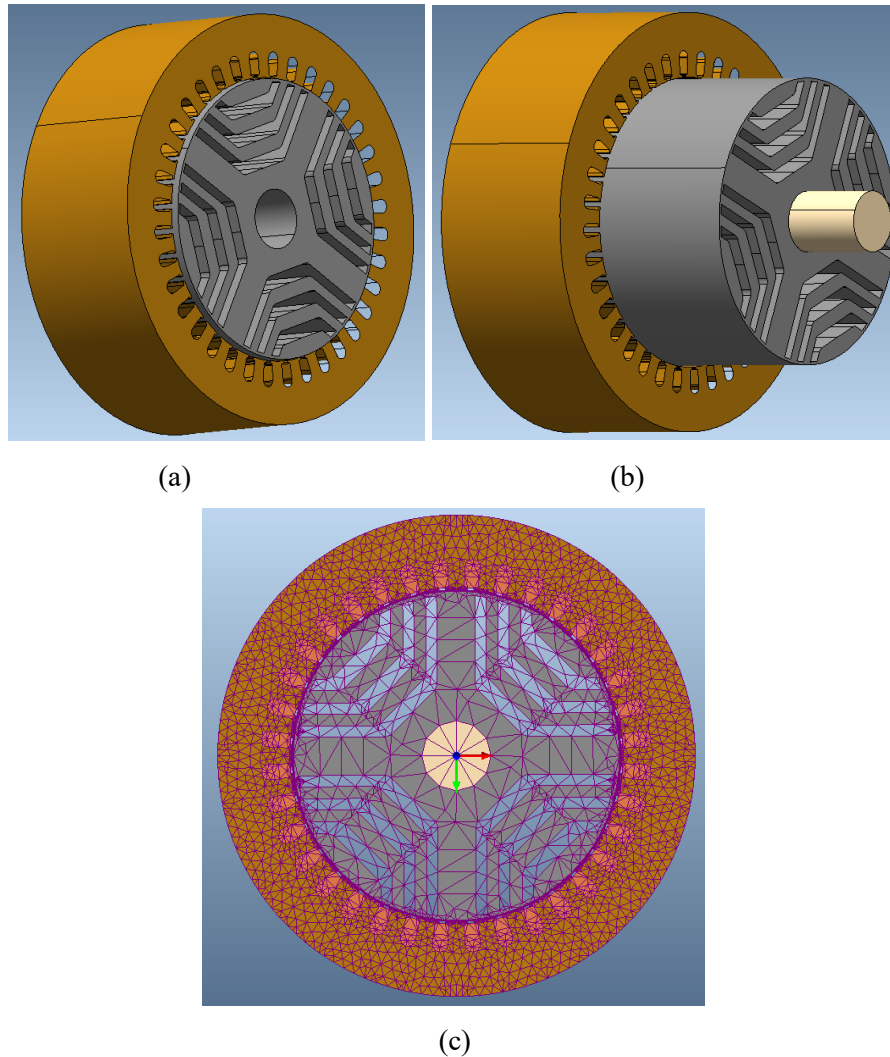
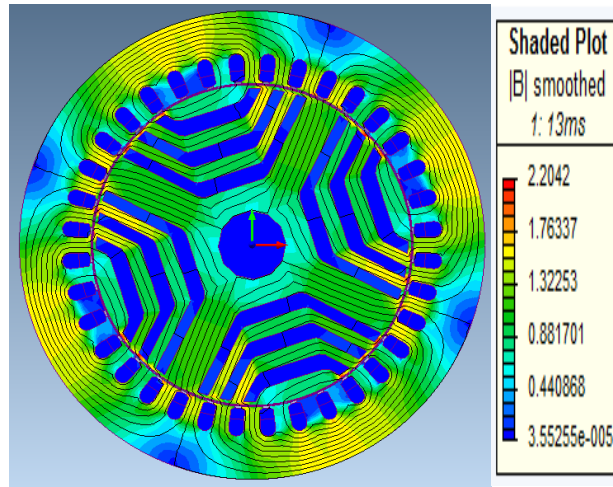


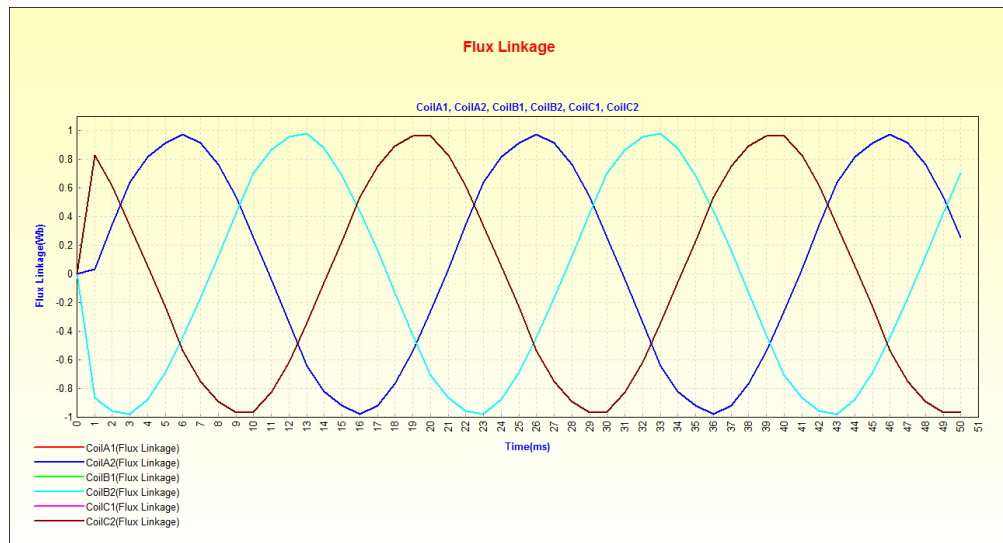
Fig. 4.8 2D SynRM model (a) side view only stator and rotor (b) side view with shaft (c) Mesh view

As per availability issues in manufacturing, a duplicate stator has been used in these simulations is similar to IM made by Cummins (BCI-184) machine which has 36 slots double layer winding which is shown in Fig. 4.10. The rotor geometry is very important to achieve high peak and average torque having a smaller amount of torque ripples. The saliency ratio is affected due to rotor geometry which defines the number of flux barriers, pole numbers, edge effect its shape and dimensions. As the complete focus is on the flux barrier width of the rotor, thus the study of pole number and edge effects are also the subject of this work, therefore a rotor having 4 poles is studied and has been considered for the SynRM design. The shape and dimensions of the flux barrier is already depicted in Fig. 4.6, so that is why their positioning and width (dimensions) have been taken into account for the study in this research. The rotor hysteresis and eddy current losses are 56watts. The New core 1000/65 material with nonlinear lamination properly is selected for the design of stator and M350-50A used for rotor lamination material in the machine. The transient simulation at 500ms with the mode of velocity driven is done, it is noticed that starting torque of the

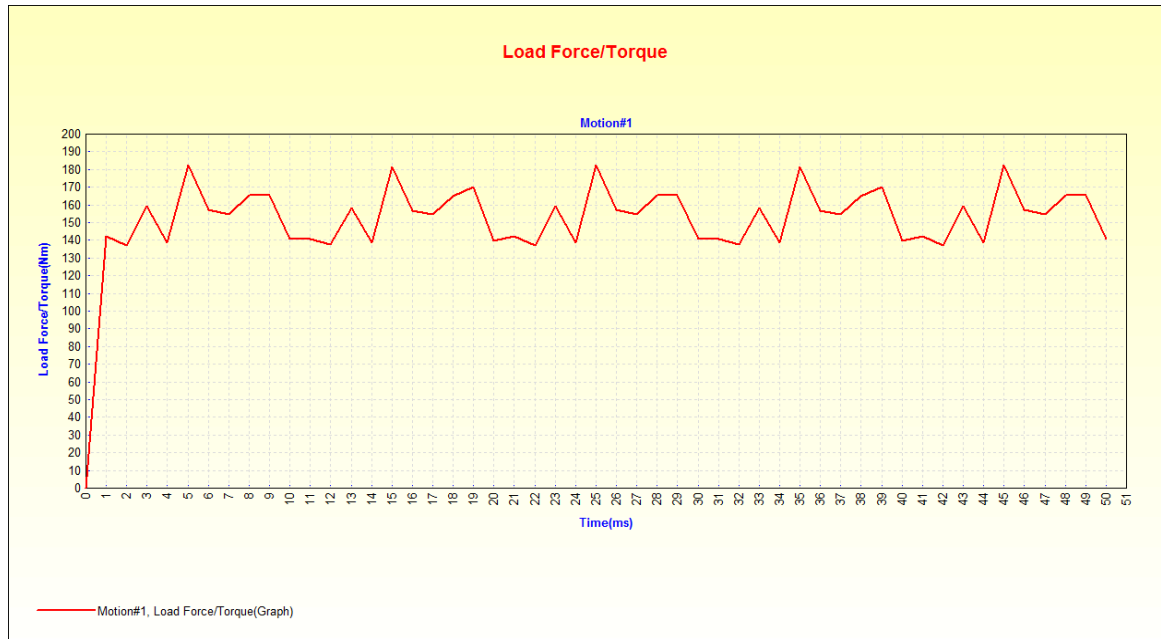
simulated machine is around 180Nm which is good, and the motor provides the nominal average torque of 154.30Nm with almost 90% efficiency.



(a)



(b)



(c)

Fig. 4.9 shows (a) the shaded plot view with 2.1 (Tesla) magnetic flux density (b) Flux linkage (c) shows the load force torque produced by the proposed machine

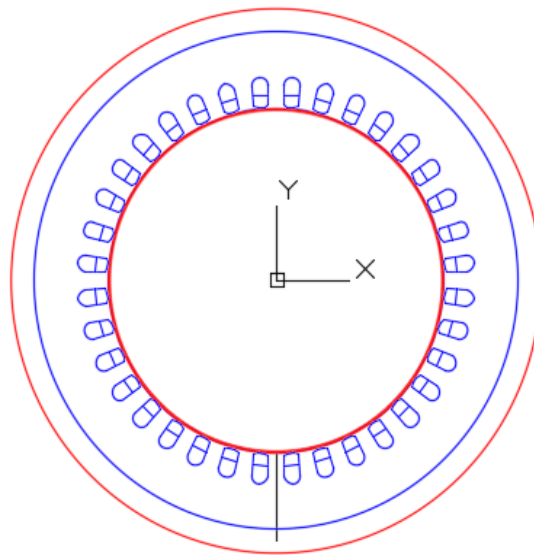


Fig. 4.10 4 poles 36 slots double layer stator

4.5 Design of 10kW SynRM for Direct- Drive Applications

2DFE model of 8.58kW is produced by *Infolytica Magnet* machine design software to assess the effectiveness of the design as a direct-drive for the application of Raymond Pulveriser. The rotor is featured by 4 square shaped flux barriers as shown in Fig. 4.11. The machine design specifications are shown in Table 4-3. The machine is driven from optimised 36 slots double layer winding stator. The same

optimisation procedure is adopted as described in chapter 3. The stator dimensions are shown in Table 6-26 (in the appendices). The rotor diameter is 300mm with 87mm shaft diameter and M-19-29 Ga material has been used for the machine design. The total optimised width of flux carrier is about 70.59mm whereas each width is 14.11mm. The overall flux barrier width is 49mm with 10.33mm each individual barrier is shown in Table 6-27 (in the appendices).

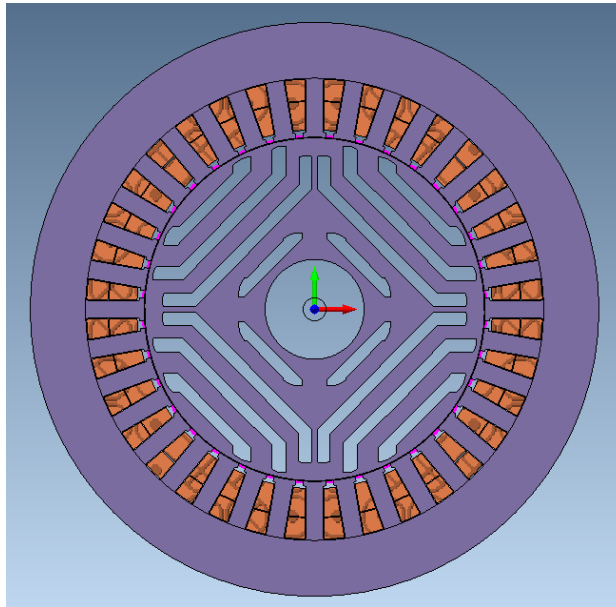
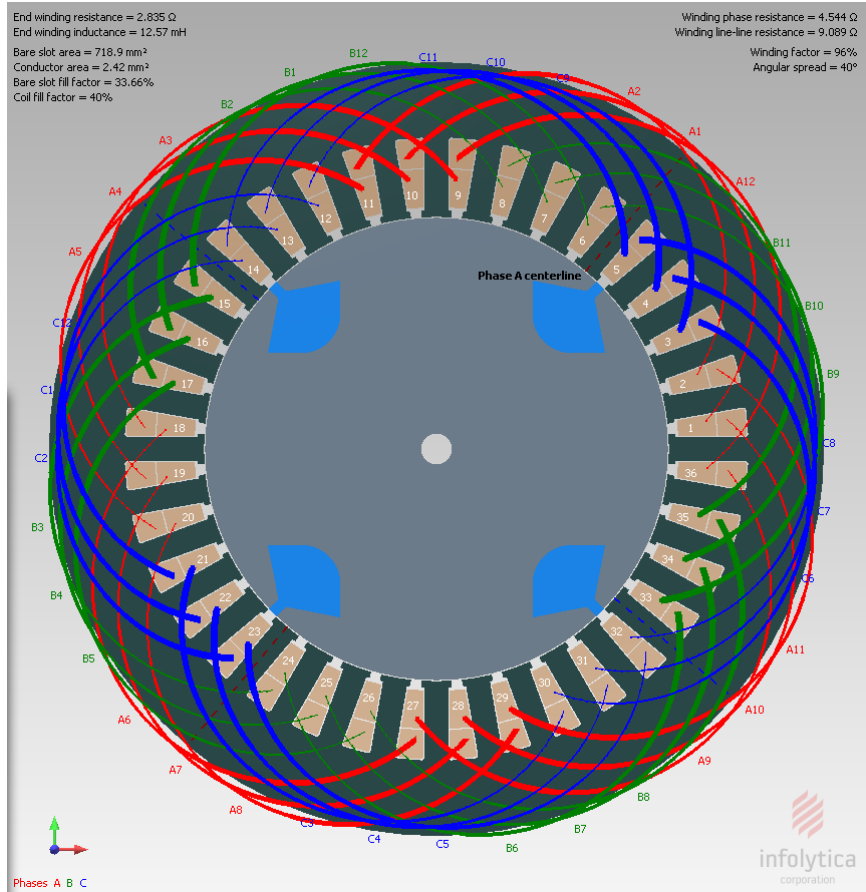


Fig. 4.11 Square shaped 4 flux barrier for Raymond Pulveriser

As per the optimisation process, 52% slot fill factor is used with 53 number of turns. The end winding resistance is 2.385Ω . The lap winding has been used with 9 coil spans, and Copper: 100% IACS (International Annealed Copper Standard). Total 7mm^2 stranded conductor area is used to pass 26Amp current. The complete standard winding design specifications are shown in Table 6-28 (in the appendices) and full three-phase winding arrangement is shown in Fig. 4.12. The stator slots and teeth dimensions are shown in Fig. 4.13.

Table 4-3 design specifications of the 8.58kW motor for direct drive application

Item	Value	Item	Value
Phase Voltage	380V AC supply	Frequency	50 Hz
Power	8.58kW	Synchronous Speed	105 rpm
Airgap thickness	0.67mm	Stator Winding Arrangement	Double-Layer
Rated Current	26 Amp	Rated torque	780Nm
Waveform	AC Sinusoidal	Stator Winding Arrangement	Double-Layer
Efficiency	91.217%	Shaft Diameter	87mm
Shaft Diameter	87mm	Stack Length	200 mm
Pole Numbers	4	Number of phases	3
Number of slots	36	Flux density	2.3 Tesla



of

Fig. 4.12 Combined layoutwinding arrangement of all phases

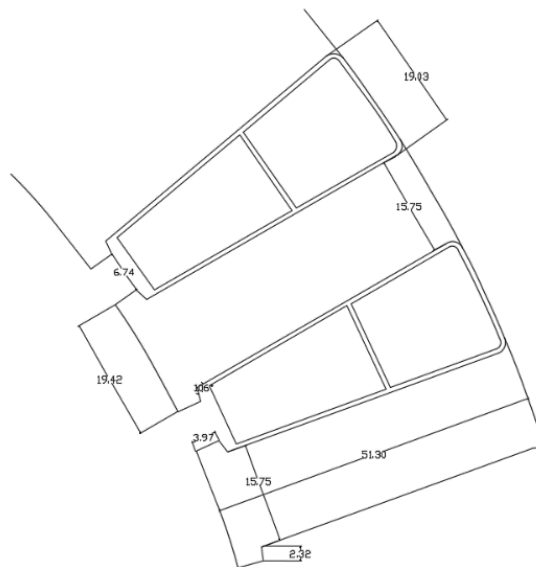


Fig. 4.13 stator slots and teeth dimensions in millimeters

The proposed 2D FEM synchronous reluctance motor model having 8.58kW is shown in Fig. 4.14 (a-b) showing the side view and shaft with designed flux barriers. The simulation tested at 105RPM and the machine has good starting torque around 2400Nm and 780Nm average torque. The current, voltage and torque waveforms are shown in Fig. 4.15. The flux density is very higher 2.5T which is shown in Fig. 4.16, and the shaded plot arc graph is shown in Fig. 4.17.

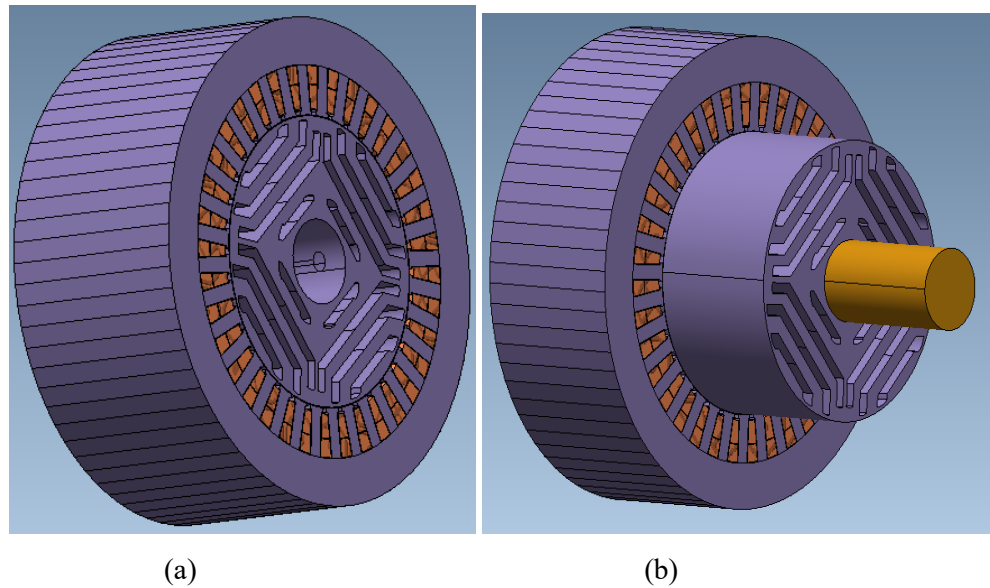
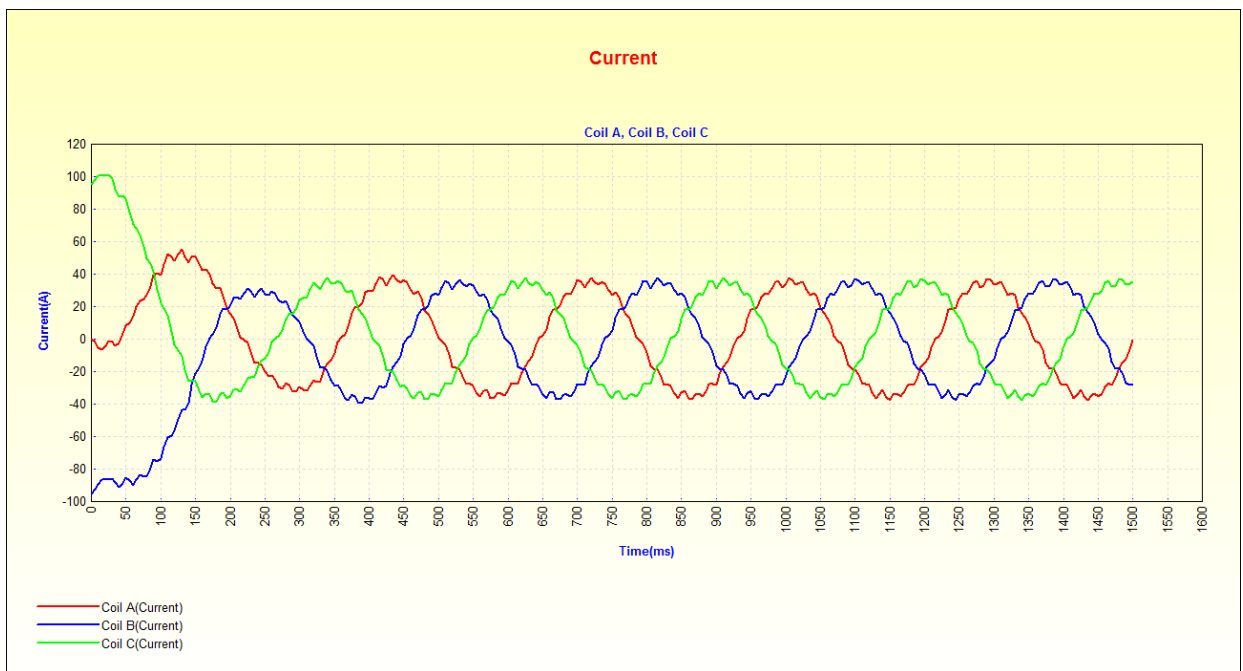
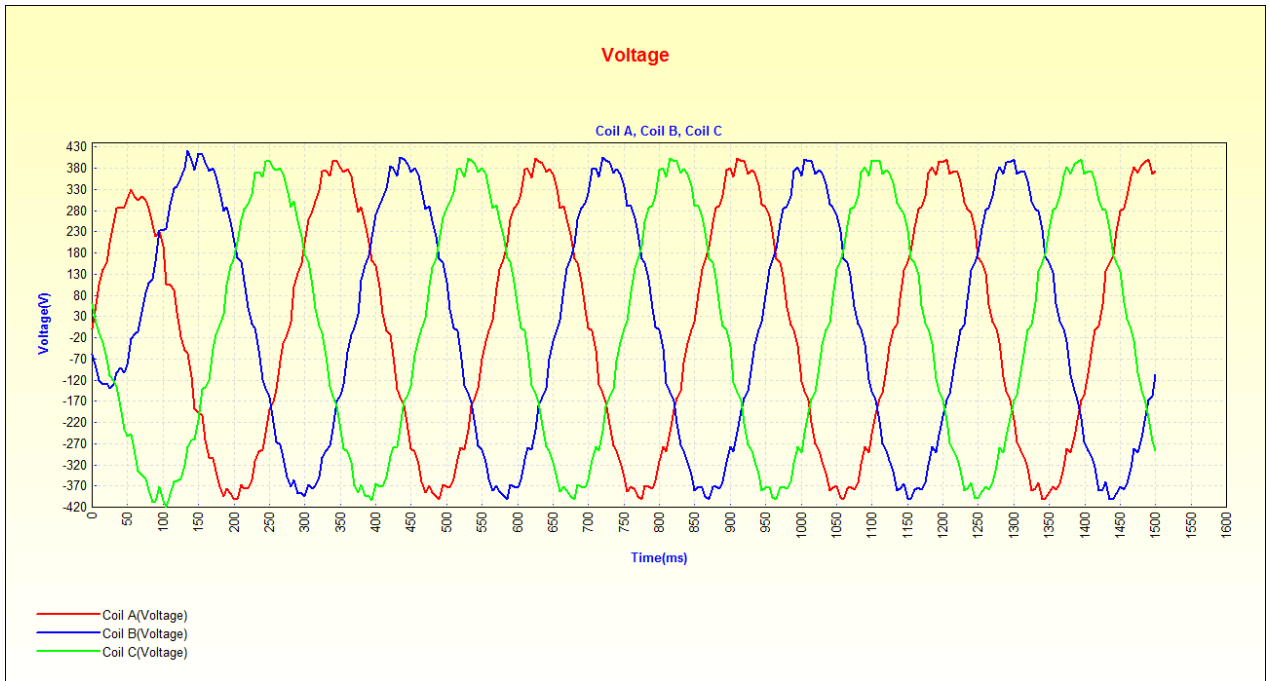


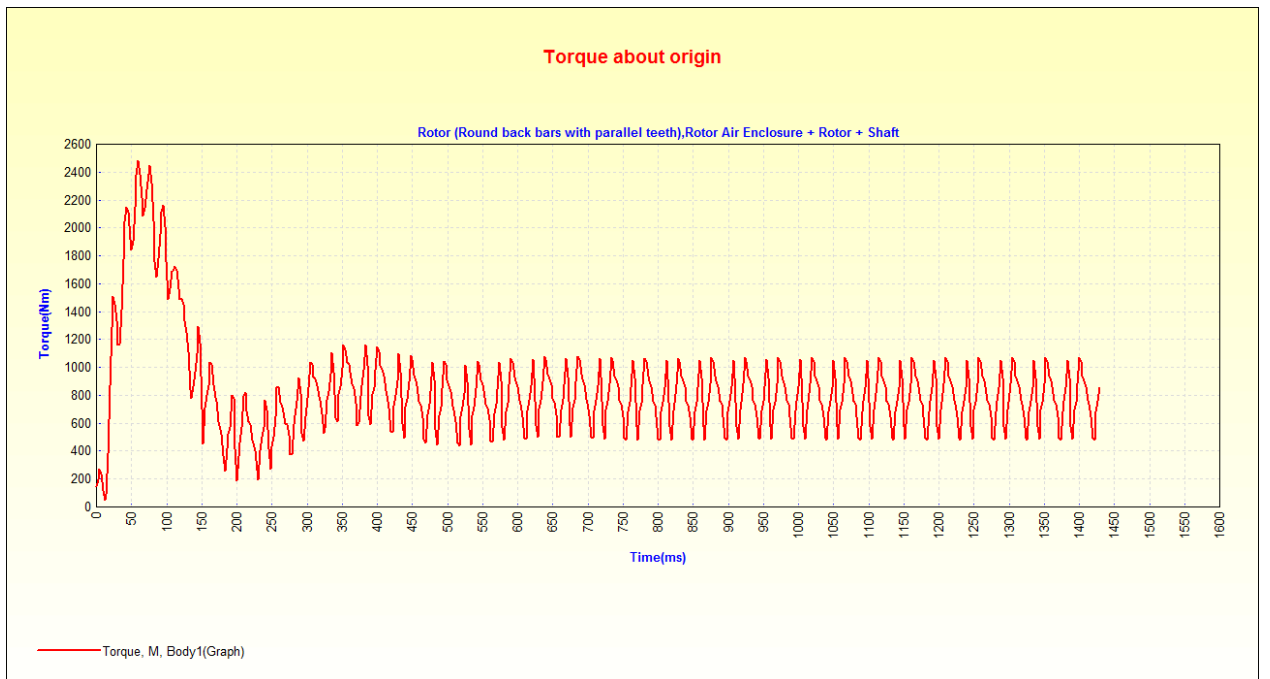
Fig. 4.14 8.58kW proposed SynRM (a) side view of motor thickness (c) side view of stator, rotor, and shaft



(a)



(b)



(c)

Fig. 4.15 shows 3.58kW SynRM design (a) current waveform (b) voltage waveform (c) Torque wave form

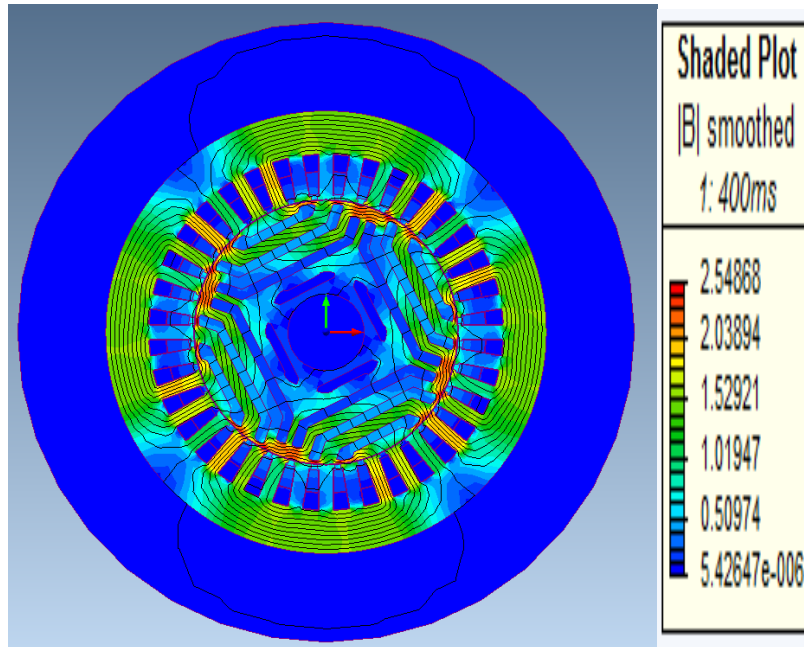


Fig. 4.16 shaded plot view of magnetic flux density 2.5T of 8.58kW motor

The performance characteristics of the 8.58kW motor with torque, efficiency, along with power are depicted in Table 4-4 (optimisation 1). Here torque ripple is higher around 57%, so that's why the author intended to increase the power up to 10kW. The core material is changed to M-15 26 GA of the main machine. This improved the efficiency of 93.34% and reduced the torque ripple 40.71% and the overall power is enhanced in (optimisation 2).

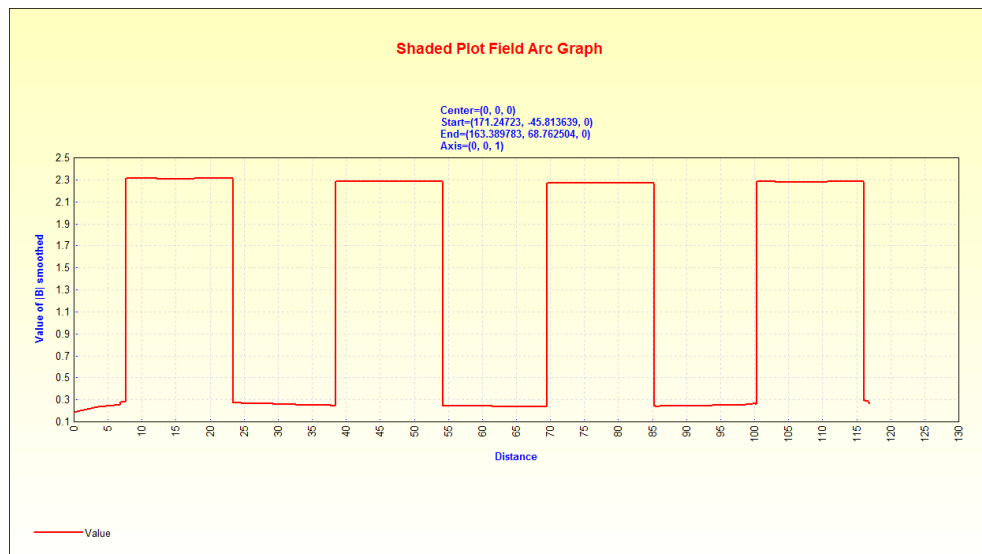
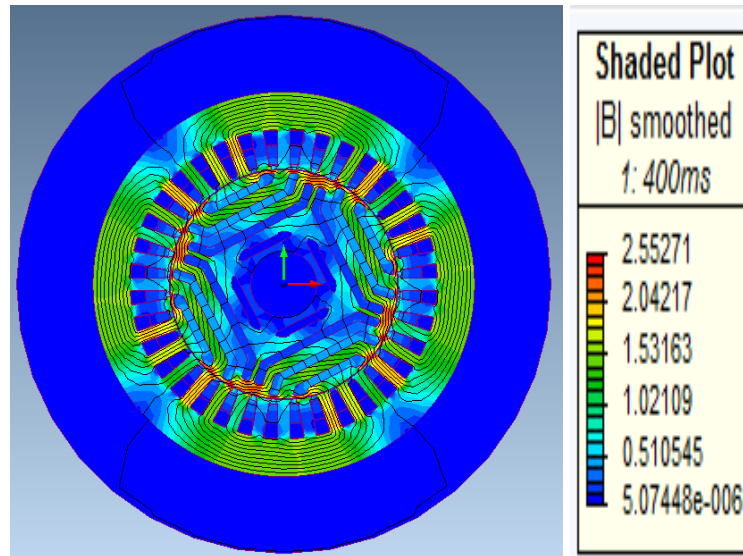


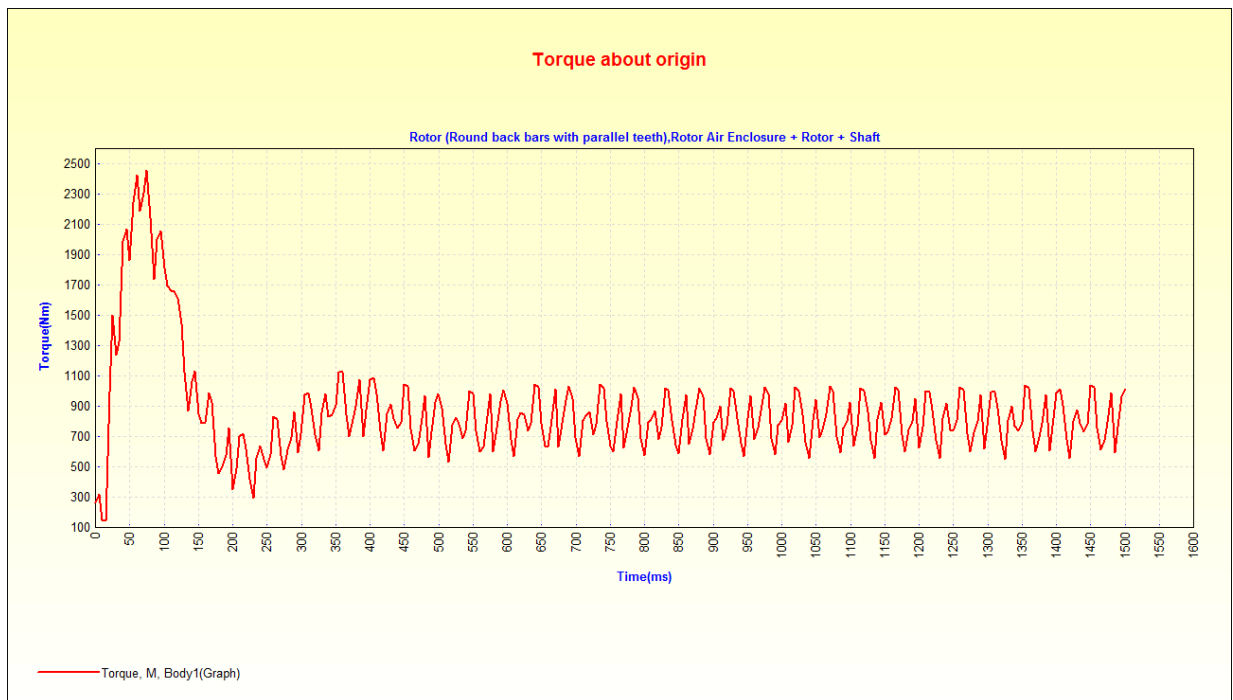
Fig. 4.17 shaded plot field arc graph

Table 4-4 performance of SynRM motor by different optimisations

Optimisation No	Torque in Nm	Efficiency in %	Power in kW	T-Ripple in %
1	802	91.01	8.58	57%
2	867	93.34	10.21	40.71%
3	756	91.31	9.10	216



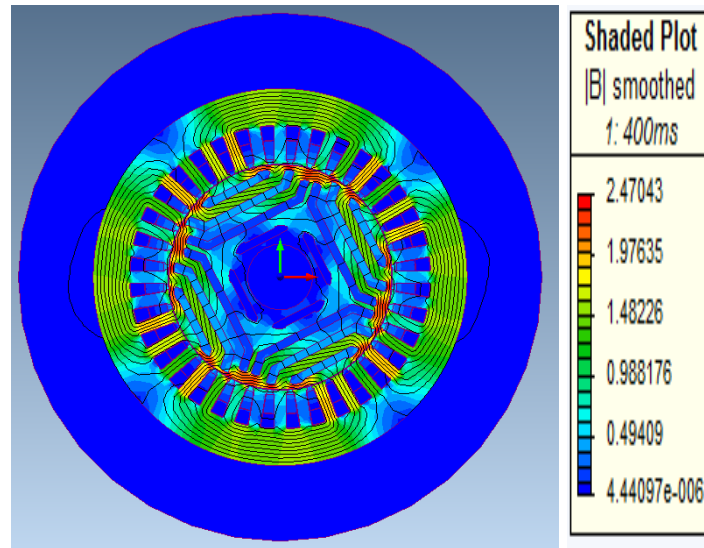
(a)



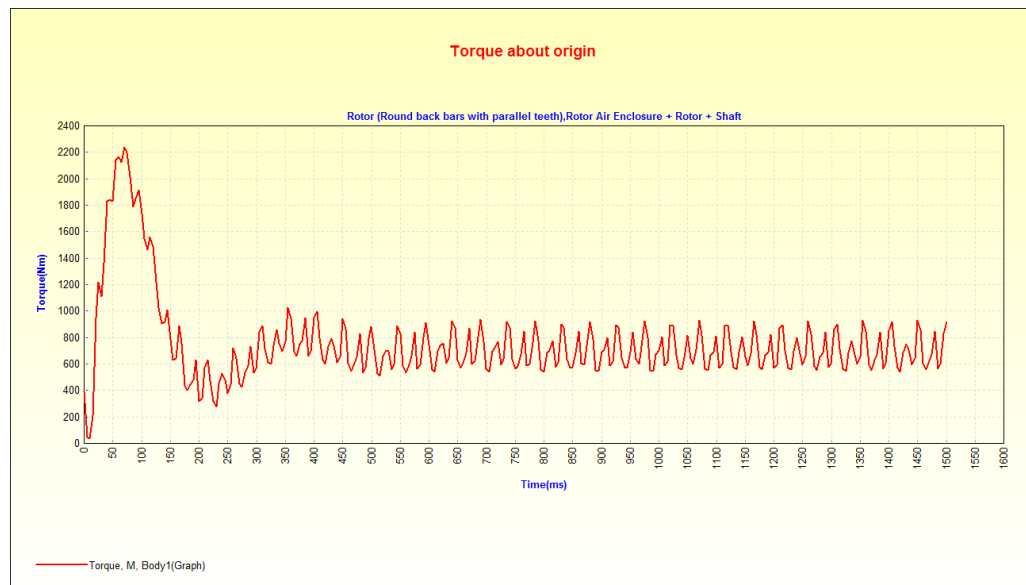
(b)

Fig. 4.18 shaded plot view of magnetic flux density 2.5T (b) Torque waveform of the 10.21kW motor

The shaded plot view and torque waveform at 10.21kW is shown in Fig. 4.18 (a-b). The material of the machine is the same. In the next test, 3mm length of the flux barrier decreased and simulated with the same design. This reduced the torque up to 756Nm with efficiency of 91.31%. Hence, the overall power also decreased 9.10kW which is shown in Table 4-4 (optimisation 3), and the shaded plot along with torque waveform at 9.10kW is shown in fig. 4.19.



(a)



(b)

Fig. 4.19 shaded plot view of magnetic flux density 2.47T (b) Torque waveform of the 9.10kW motor

4.6 Asymmetrical Rotor Geometry design

In this section, the asymmetrical rotor geometry of SynRM based on the proposed method are analysed and the 2D finite element design and the effect of torque ripple, efficiency and power are examined. Different asymmetrical rotor shapes are tested. i.e. initially the length of the flux barrier is decreased from the right-side and the angle is increased. The other side of the flux barrier remains the same as the original. The asymmetrical rotor is shown in Fig. 4.20. All the parameters of flux barriers with torque, efficiency, power, and torque ripples are shown in Table 6-29 (in the appendices).

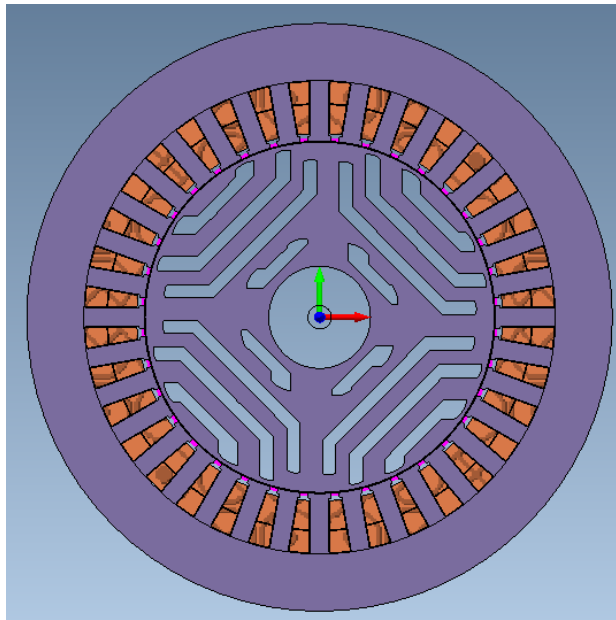


Fig. 4.20 Asymmetrical rotor design at 20mm length decreased final Model

The flux barrier length is reduced from the right side which results in an increase in efficiency. Fig. 4.21 shows the efficiency improvement profile. The maximum efficiency is achieved when 20mm flux barrier length is decreased and, in the result, 93.8% efficiency is achieved. The torque profile is shown in Fig 4.22 and the torque waveform is shown in Fig. 4.23.

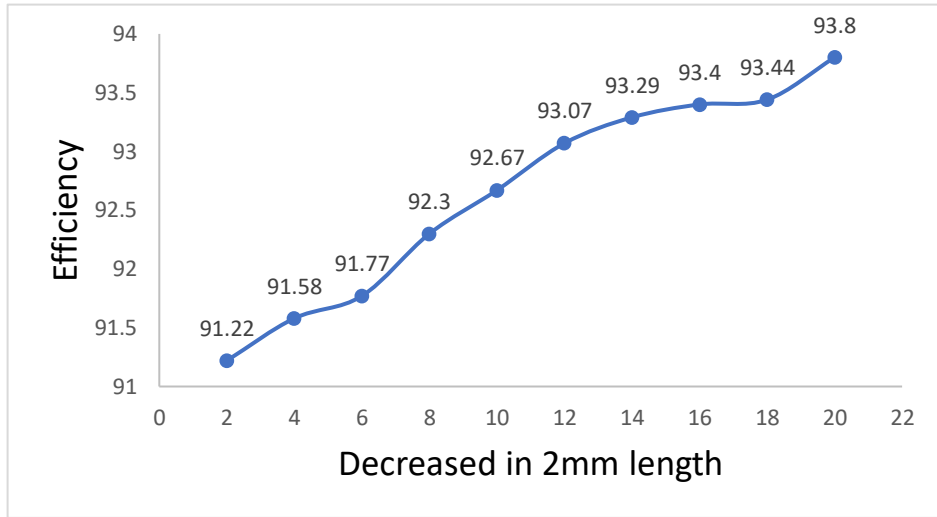


Fig. 4.21 efficiency improvement profile

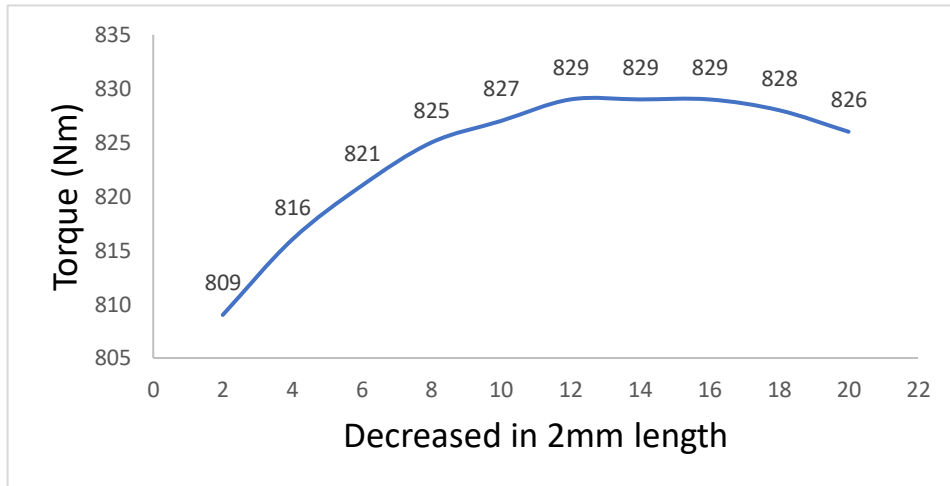


Fig. 4.22 torque improvement profile

The maximum torque 829Nm is produced when the 12mm flux barrier is decreased. It can be seen that the torque remains stable even 16mm flux barrier is decreased and starting torque reducing to 826Nm. After checking the asymmetrical geometry, the third flux barrier length is increased till the end of the outer boundary and a big change is seen in torque, and power as shown in Table 4-5 (optimisation 1). The torque increases to 973Nm. However, efficiency tends to reduce to 89.70%. Consequently, in the asymmetrical rotor of SynRM, the power is enhanced at 11.9kW.

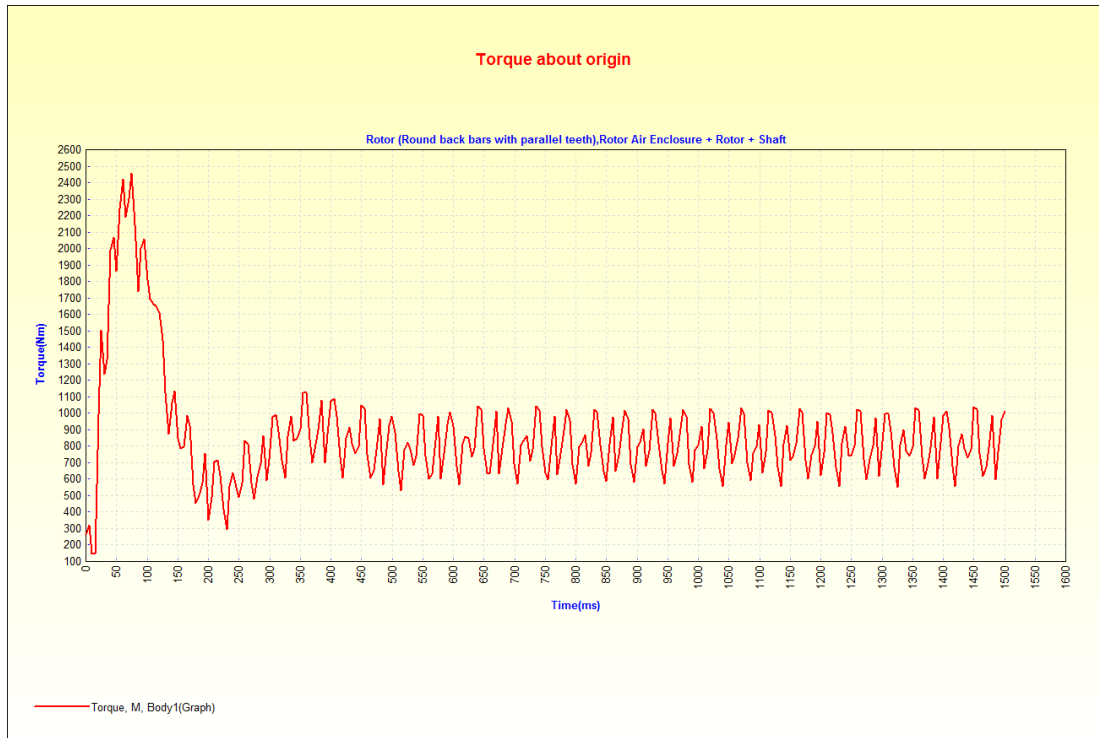


Fig. 4.23 Torque profile of best machine when 2mm length decreased

Table 4-5 performance of asymmetrical rotor when 3rd flux barrier end near the outer boundary

Optimisation No	Torque in Nm	Efficiency in %	Power in kW	Energy in Joules	T-Ripple in %
1	973	89.70	11.9	407	68
2	491	90.54	5.97	216	157
3	399	91.06	4.81	186	143
4	759	90.83	9.63	340	61

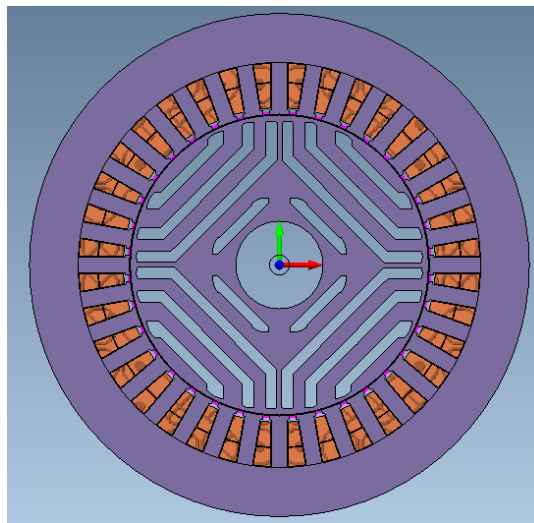


Fig. 4.24 Rotor with increase 3rd flux barrier end near the outer boundary

In order to create the asymmetry from the left side, the flux barrier edges were cut and are depicted in Table 4-5 (optimisation 2) and Fig. 4.25. The torque ripple is greatly higher 157% which is undesirable when the same edges were cut from the right side, as shown in Table 4-5 (optimisation 3) and Fig. 4.26, torque ripple is reduced to 143%.

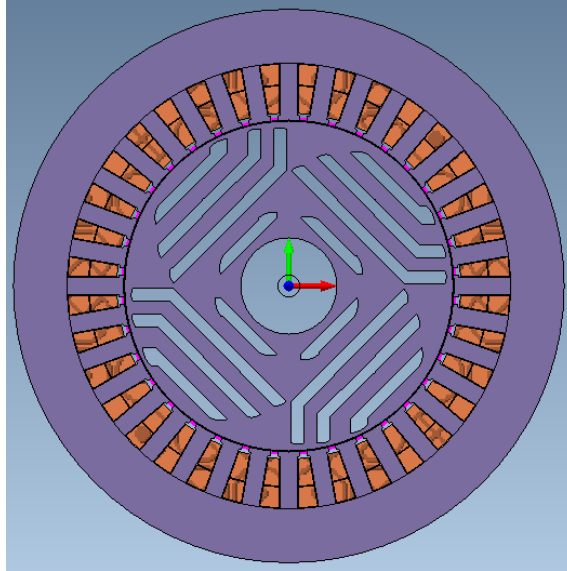


Fig. 4.25 Asymmetrical rotor while cutting one left side angle

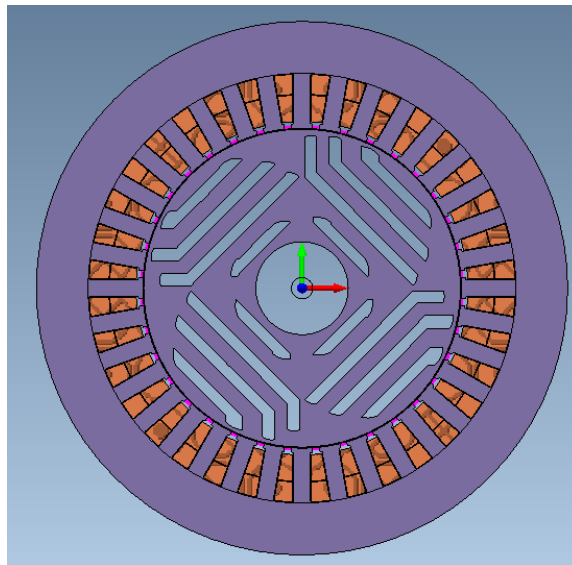


Fig. 4.26 asymmetrical rotor while cutting one right side angle

The two shapes of flux barrier shapes are used (square and round), so, to check the performance of asymmetry on right side of the flux barrier kept square shaped and left side was changed to round shape as shown in Fig. 4.27. In this design, the torque is lower 759Nm and torque ripple is high 61% with 90.83% as depicted in Table 4-5 (optimisation 4).

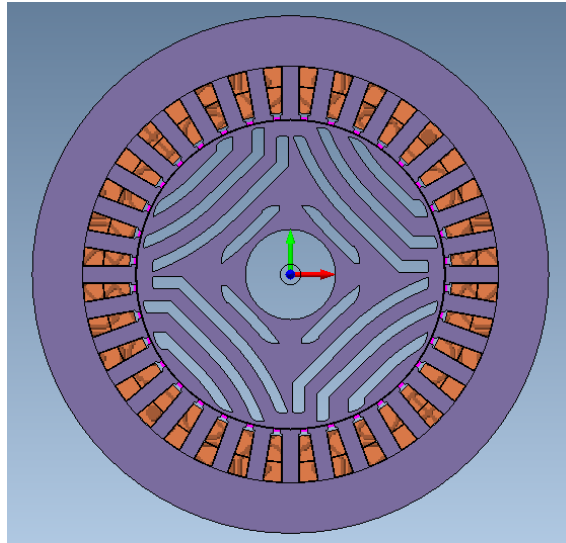


Fig. 4.27 Asymmetrical rotor with one side square one side round

Further 20 more parameters of LHS generated as depicted in Table 6-30 (in the appendices). This time the length is decreased, and the angle length kept same as shown in Fig 4.28. Now it has been observed that this increased the efficiency of 94.05% as shown in Fig. 4.29. Thus, it is observed that, the asymmetrical rotor contributes to increase in the torque ripple of the machine.

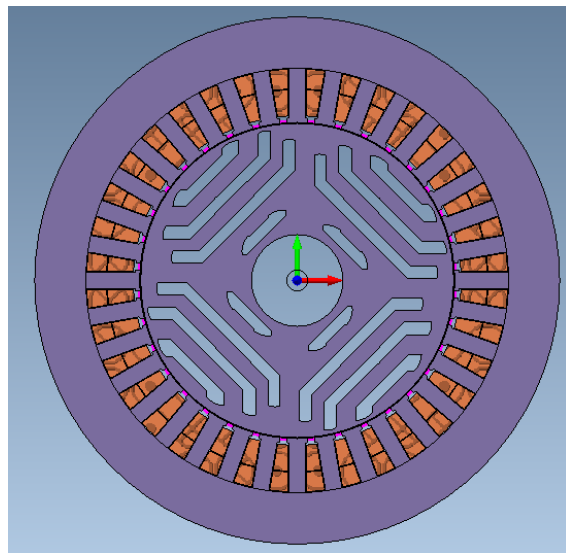


Fig. 4.28 Asymmetrical rotor with length decreased from left and angle length remains the same

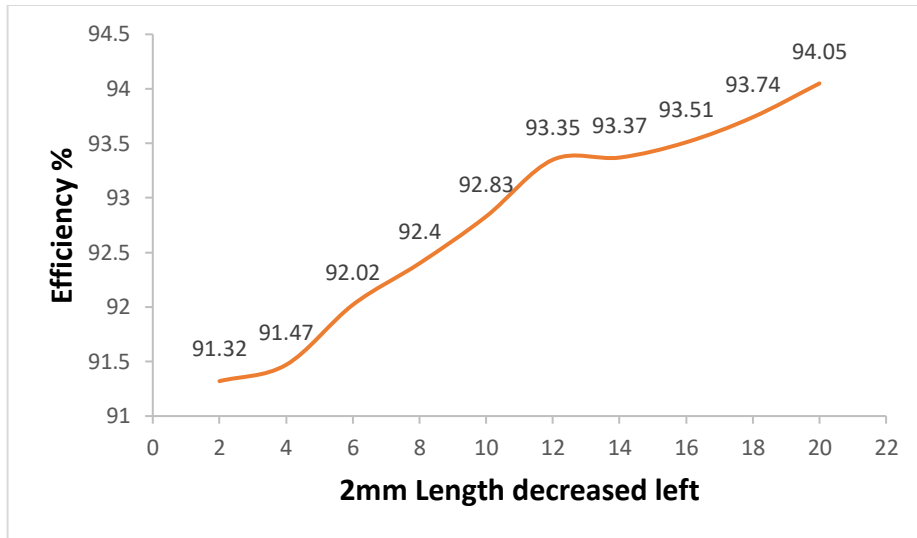


Fig. 4.29 Efficiency profile when length decreased and angle length remain the same

4.7 12/8 SRM FEM Simulation

This section describes the simulation of 12/8 switched reluctance motor which is shown in Fig. 4.30. In order to optimise the SRM, total of 440 samples have been tested as a trial and three optimisation carried out. A process of optimisation using static 2D finite element analysis *Motor solve* software is undertaken to analyse diverse design constraints. The conclusions are present with respect to torque and efficiency point of view. Different parameters have been optimised by surrogate and by considering the row number 15 and 29 from Table 6-14 (in the appendices), and their simulation results have been discussed in detail. Using FEM based optimisation, stator pole arc, stator yoke thickness, stator inner diameter, rotor pole arc, rotor yoke thickness, and shaft diameter have been thoroughly assessed, 1.91T of flux density of sample 15 and torque is shown in Fig. 4.31. The torque produced by LHS sample 15 is 671.95Nm at 90.2% efficiency, the 22.26A current, voltage graph is shown in Fig. 4.32. The copper losses are around 889W and the overall core losses are about 83.9W and are shown in Fig. 4.33.

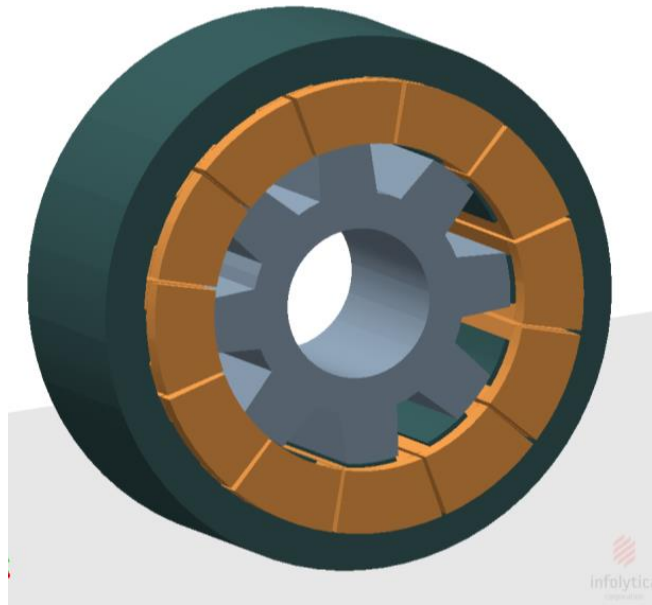


Fig. 4.30 12/8 switched reluctance model

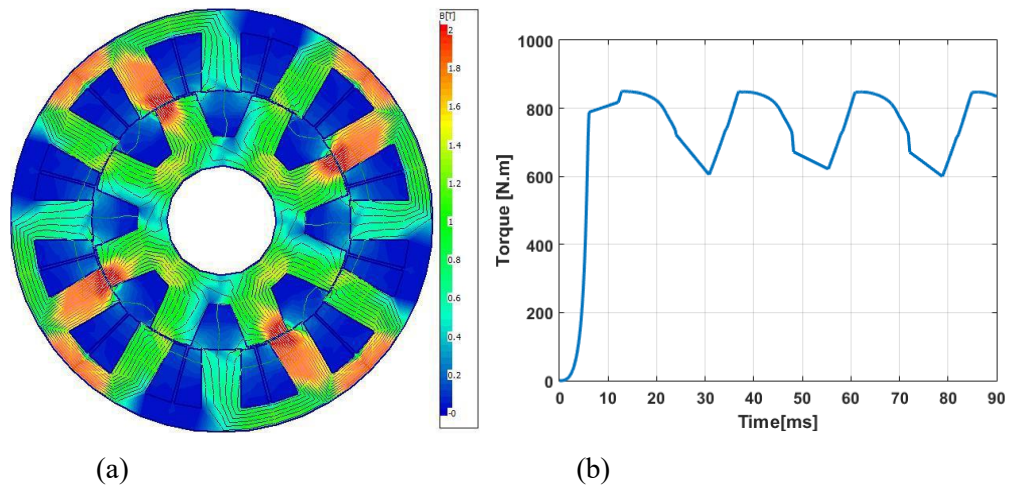
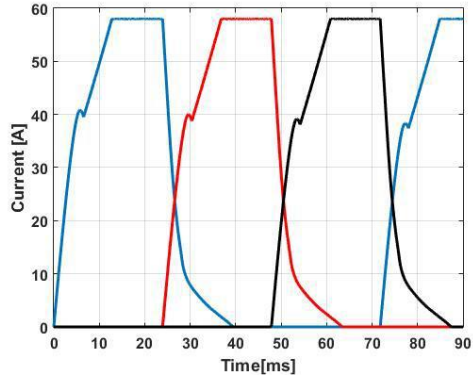
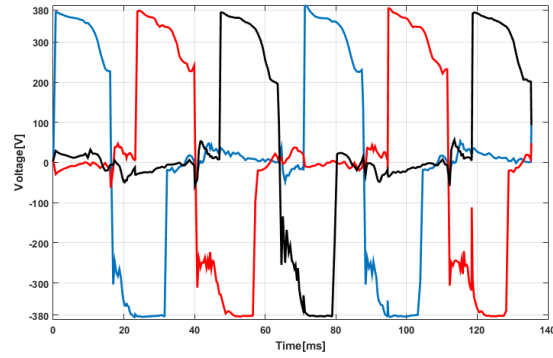


Fig. 4.31 12/8 SRM simulation results of sample 15

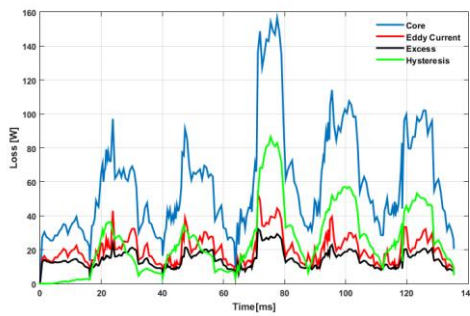


(a)

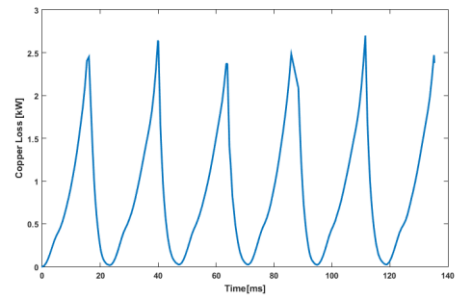


(b)

Fig. 4.32 Three phase current, and voltage graph of sample 15



(a)



(b)

Fig. 4.33 12/8 SRM copper and core losses of sample 15

Similarly, the simulation results of optimised LHS sample number 29 have been described, in this sample the efficiency is slightly higher than sample 15 around 90.66% whereas, the generated torque is reduced 630.15Nm. The magnetic flux density 1.91T and torque graph is depicted in Fig. 4.34. As per constant speed

and voltage operation, the current is reduced around 20.95A which is shown in Fig. 4.35. Due to the decrease of current the copper losses are also decreased to 798.7W and maximum core losses remain the same 85.57W as shown in Fig. 4.36.

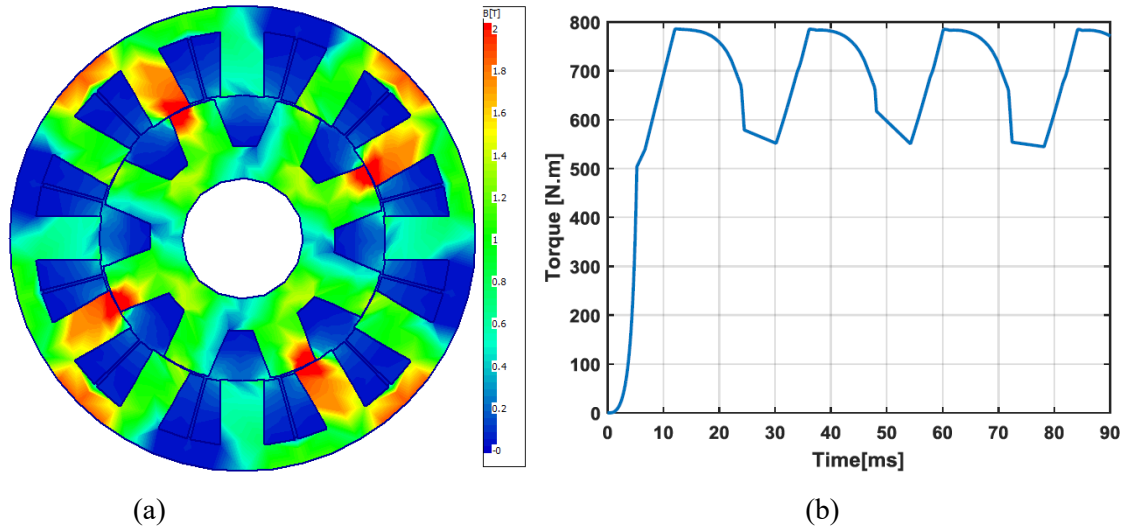
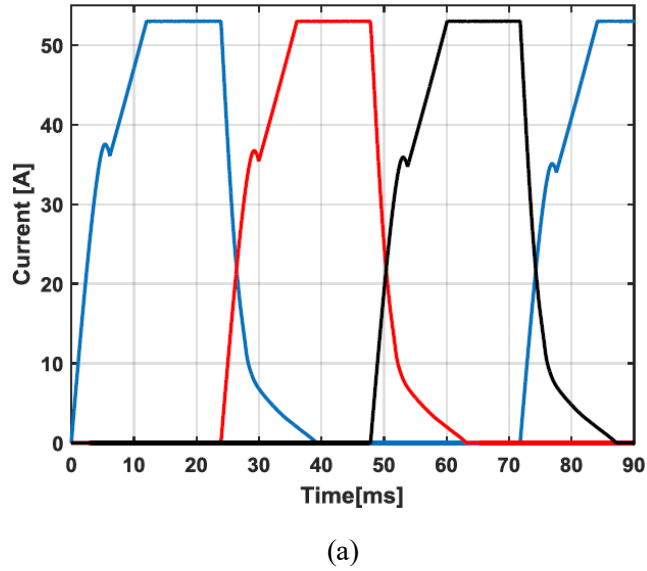
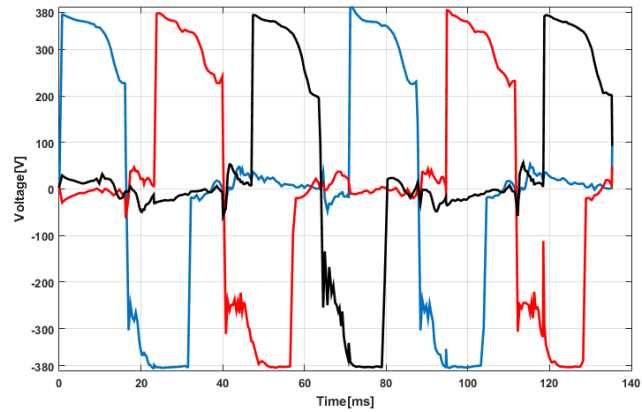


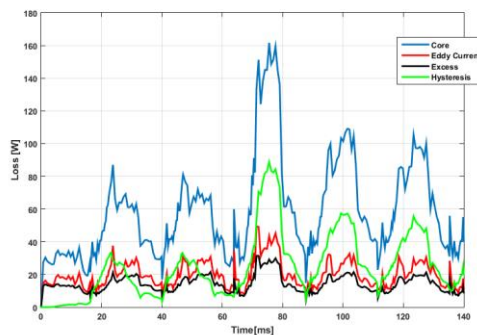
Fig. 4.34 12/8 SRM simulation results of sample 29



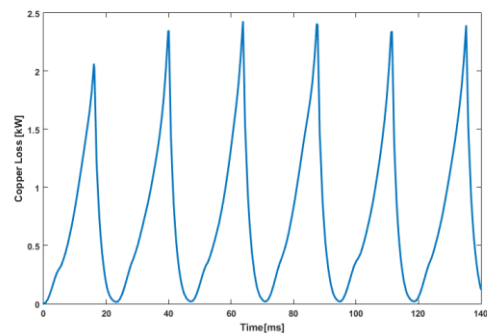


(b)

Fig. 4.35 Three phase current, and voltage graph of sample 29



(a)



(b)

Fig. 4.36 12/8 SRM copper and core losses of sample 29

In order to enhance the torque further, some slight modifications were made in the design and torque is enhanced in both the optimised design of sample 15 and 29. Based on the modified design of sample 15, the flux density 1.91 and torque 747Nm graph is shown in Fig. 4.37. The input current is about 25.71A and the three-phase supply voltage 380 is shown in Fig. 4.38. The copper losses are 1096watts and the iron losses are 82.96 watts as depicted in Fig. 4.39. Similarly, the slight modification is made in sample 29 but here we could not achieve the meaningful results, as the efficiency was slightly reduced to 90%. The torque is improved up to 728Nm. The flux density reduced to 1.897 with torque graph is shown Fig. 4.40. The current input is increased to 24.09A which is shown in Fig. 4.41 along with three-phase voltage and speed graph. Thus, the copper losses are higher due to high current 1007watts and the iron losses are reduced to 73.40 watts as shown in Fig. 4.42.

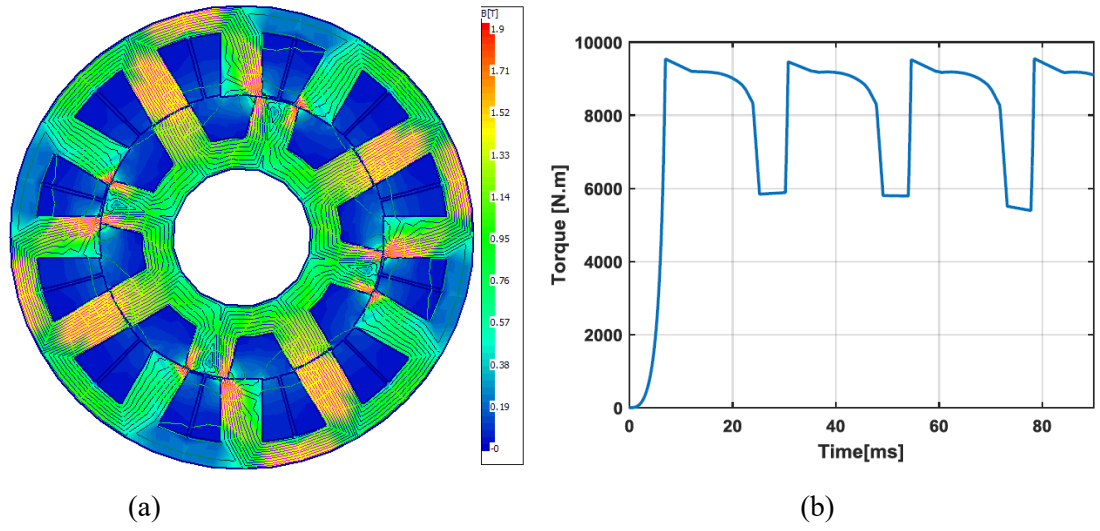


Fig. 4.37 12/8 SRM simulation results of modified sample 15

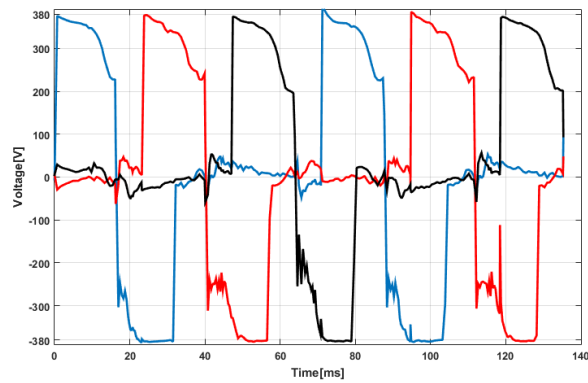
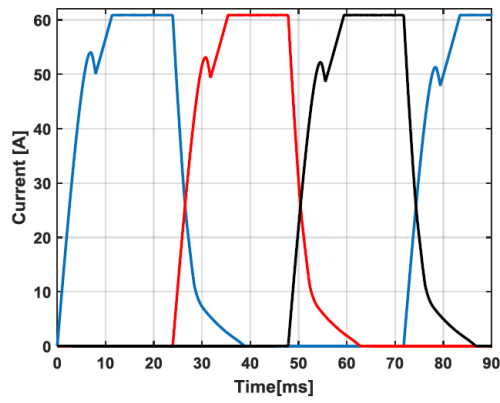
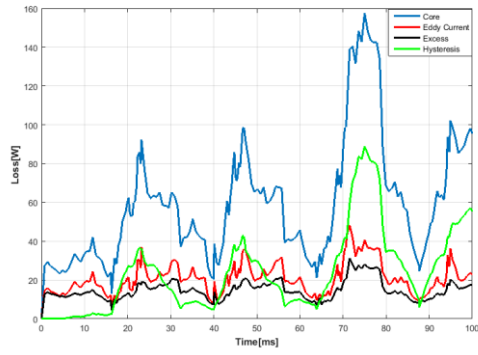
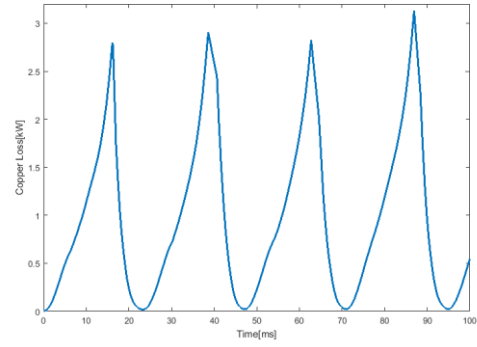


Fig. 4.38 Three phase current, and voltage graph of modified sample 15

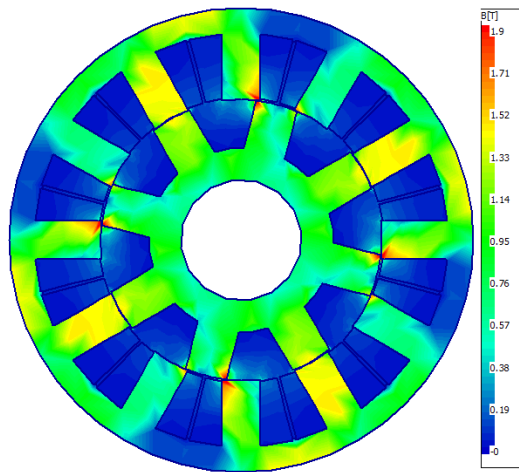


(a)

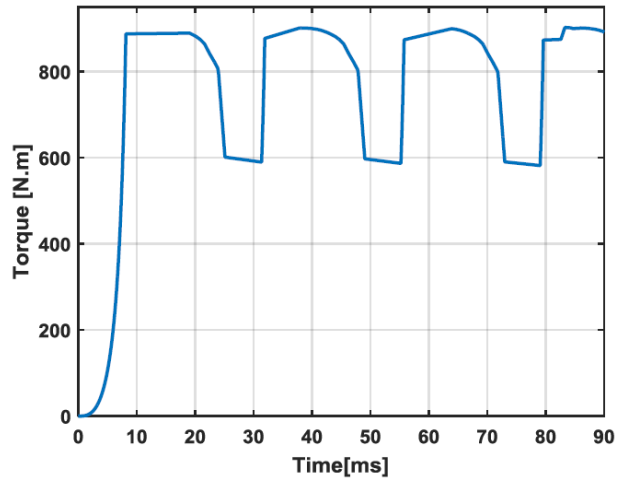


(b)

Fig. 4.39 12/8 SRM copper and core losses of modified sample 15

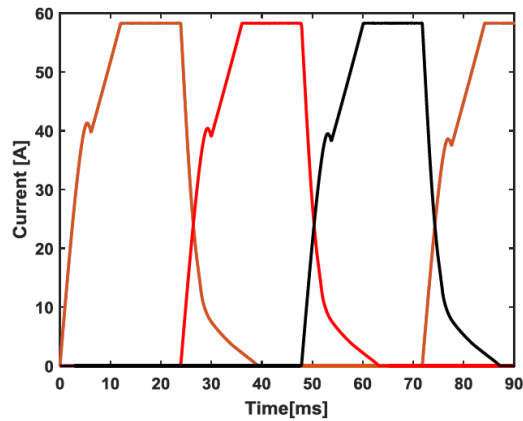


(a)

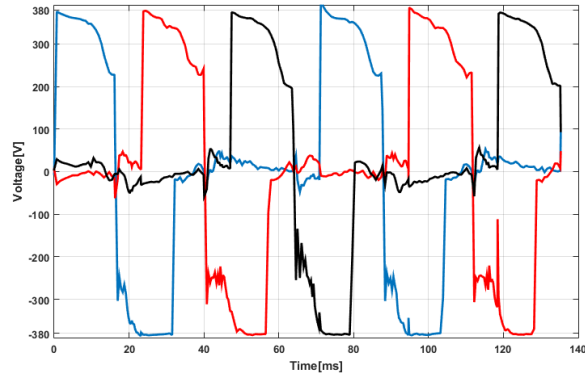


(b)

Fig. 4.40 12/8 SRM simulation results of modified sample 29

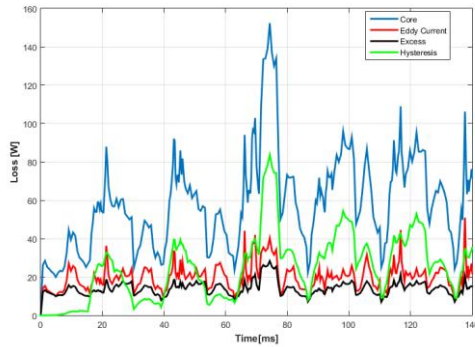


(a)

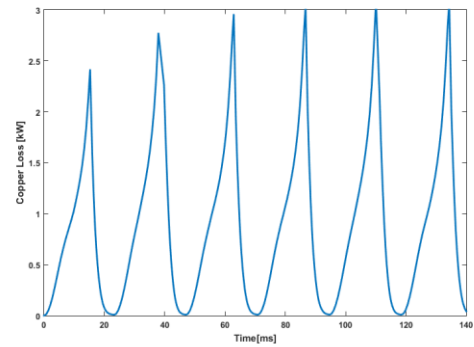


(b)

Fig. 4.41 Three phase current, speed and voltage graph of modified sample 29



(a)



(b)

Fig. 4.42 SRM copper and core losses of modified sample 29

The performance of the designed 12/8 SRM is analysed through finite element studies. The 2D finite element studies are carried out. By varying the design variables around starting values, the final optimised value is selected from the surrogate LHS sampling points. In the final design, the high-efficiency target for the machine size and parameters are chosen. The motor specifications are shown in Table 4-6. The FEM model is shown in Fig. 4.43. The optimal rotor diameter for the maximum efficiency is 300mm. The stator pole arc is 17.325 deg, the stator yoke thickness is 28.93mm. The stator inner diameter is 301mm. Rotor yoke thickness 33.91mm, rotor pole arc is 17.54 deg, and the shaft diameter is 140mm. At the rated operating speed 105rpm, 656.27Nm torque is produced at magnetic flux density 2T as shown in Fig. 4.44 and Fig. 4.45. The current and voltage waveform is shown in Fig. 4.46 and Fig. 4.47, equating to approximately 0.889kW copper losses and 0.091kW core losses.

Table 4-6 specifications for final model of SRM

No:	Item	Value
01	Input power	8.52kW
02	Output power	7.63kW
03	Torque	694Nm
04	Efficiency	89.6%
05	Voltage	257 V,RMS
06	Current	27.3 Amps RMS
07	Current density	2.73 (A/mm ²)
08	Total losses	0.98kW
09	Winding	0.889kW
10	Core losses	0.091kW
11	Torque per unit rotor volume	49.1 (kN.m/m ³)
12	Airgap stress	0.0245 (N/mm ²)

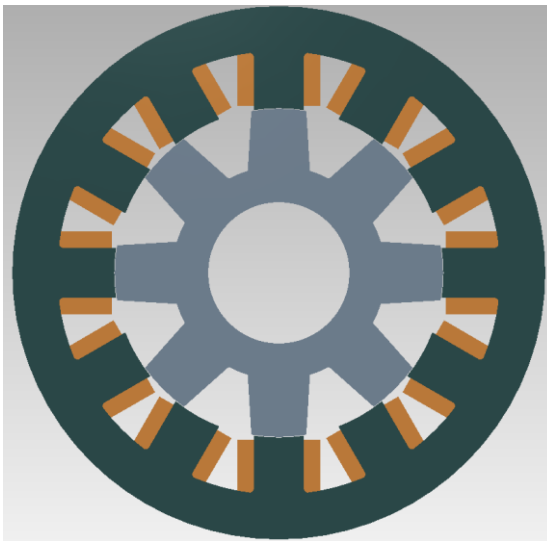


Fig. 4.43 final 12/8 Switched Reluctance Motor Design

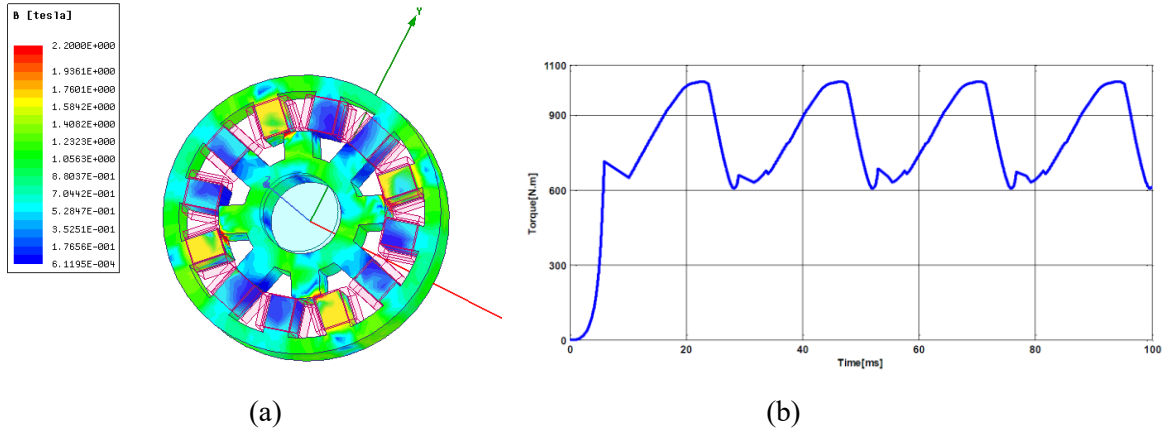


Fig. 4.44 final 12/8 SRM simulation results of flux density and torque

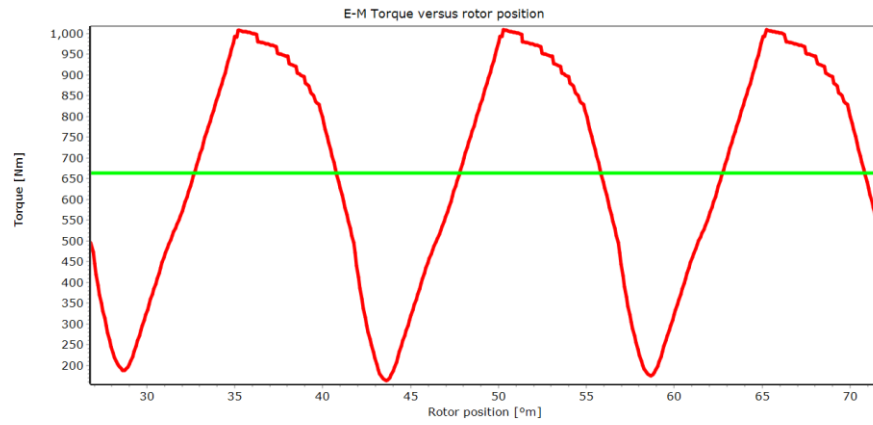


Fig. 4.45 average torque of final optimised design 12/8 SRM

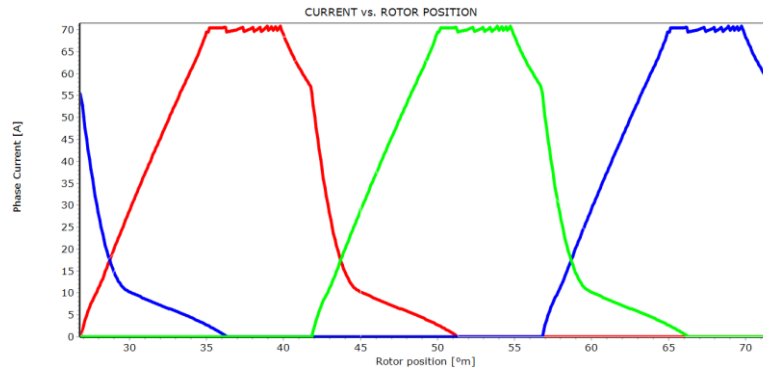


Fig. 4.46 Current Vs rotor position of final 12/8 SRM

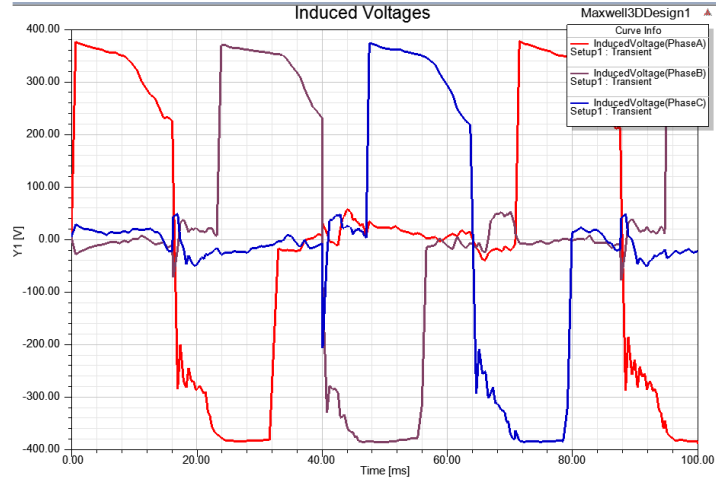


Fig. 4.47 3-Phase voltage of final 12/8 SRM

As per the results of both the reluctance machines. The higher efficiency and better performance characteristics are achieved in Synchronous reluctance machines. Therefore, the simulation results verify that 4 flux barrier synchronous reluctance machine would be the much better choice to select for the application of the Raymond Pulveriser.

4.8 72/48 SRM Design and Simulation

A three-phase 72/48 topology of SRM is projected in this work. This is based on a 6/4 SRM arrangement by the multiplying 12; the winding is placed on 24 stator poles. The detailed discussion and the existing machine used for the Raymond Pulveriser has already been discussed in the literature review current state of the art section and the complete system requirements are depicted in Fig. 2.4 and design parameters with the specification are shown in Table 2-1. The main benefit of the machines which has a greater number of poles is a small stroke angle. This leads to a very high average torque, a small torque ripple and shorter end-windings [92, 224]. Conversely, the iron losses are greater, at a higher frequency. In this design, more than 7 kNm torque is produced at 105 rated rpm. This arrangement has been placed in such a manner to minimize flux paths and reduce end windings effect which overall minimise losses and noise [20, 184, 225].

The main plan of this machine design is to improve the geometry for enhancing the maximum efficiency, average torque, and least torque ripple. Stator and rotor over-all size for 72/48 SRM is achieved, and the optimisation of the motor parameters (such as the arcs of the pole, back irons, and heights of the pole) is carried out.

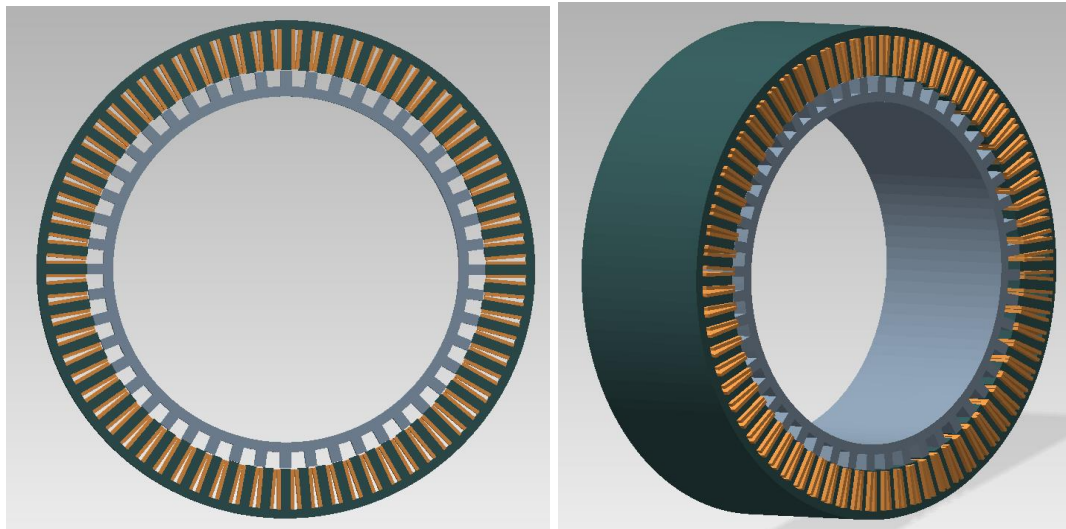
4.8.1 Step 1 Initial design

Depending on the geared system volume employed in Raymond Pulveriser, the stack length is 340mm and diameter is 1000mm, and other parameters are optimised. Generally, torque and power density is influenced by air gap length. This also depends on tolerance. The pole arcs β_s and β_r have some constraints as stated in

[92]. In this work, the stator pole arc is 2.95° and rotor pole arc is 3.05° . Therefore, the pole width of the rotor and stator along with most influential parameters are taken from [91, 92]. The preliminary parameters are described in Table 4-7, whereas FEM design is depicted in Fig. 4.48.

Table 4-7 The initial design parameters of the 72/48 SRM

Parameter	Value	Parameter	Value
Machine size in mm	1000	Outer dia of the rotor in mm	798
Slot depth Stator in mm	84.55	Slot depth rotor in mm	29
pole width of the stator in mm	20.59	pole width of the rotor in mm	21.23
Stator poles numbers	72	Stack length in mm	340
coils per slot	2	filling factor in %	56.3
Stator yoke in mm	15.45	Rotor yoke in mm	15.71
Rotor poles numbers	48	Air gap in mm	1
The angle of stator pole in degree	2.95	The angle of rotor pole in degrees	3.05
Winding Turns	12	Shaft dia in mm	708.58



(a)

(b)

Fig. 4.48 Initial 72/48 SRM design (a) front view (b) side view

4.8.2 Step 2 Optimisation of major parameters

Following main parameters such as β_s , β_r , b_{sy} , b_{ry} , N_p , D_{sh} are optimised whereas other parameters are fixed. The torque profile while changing the design parameters is depicted in Fig. 4.49. Input phase voltage are 510V and the supply current is controlled by hysteresis current control. The effect of the most essential parameters are taken from [20]. The influence on average torque and torque ripple by the stator pole arc angle on the average torque is shown in Fig. 4.50 (a-d). This reflects that the variations in the average torque, and torque ripple, in the rotor pole arc angle in the range (2.95° and 3.2°) and present effect of stator yoke

thickness (10 to 30 mm) and rotor yoke thickness (15 to 25 mm) on the average torque, and torque ripple. Simulations were run by changing the number of turns between 3-7. Fig. 4.49(e) shows that the highest average torque is obtained with 15 turns per coil configuration. Fig. 4.49(f) shows the shaft diameter, effect of torque ripple and torque. In practice, D_{sh} is a fixed parameter for a mechanical reason.

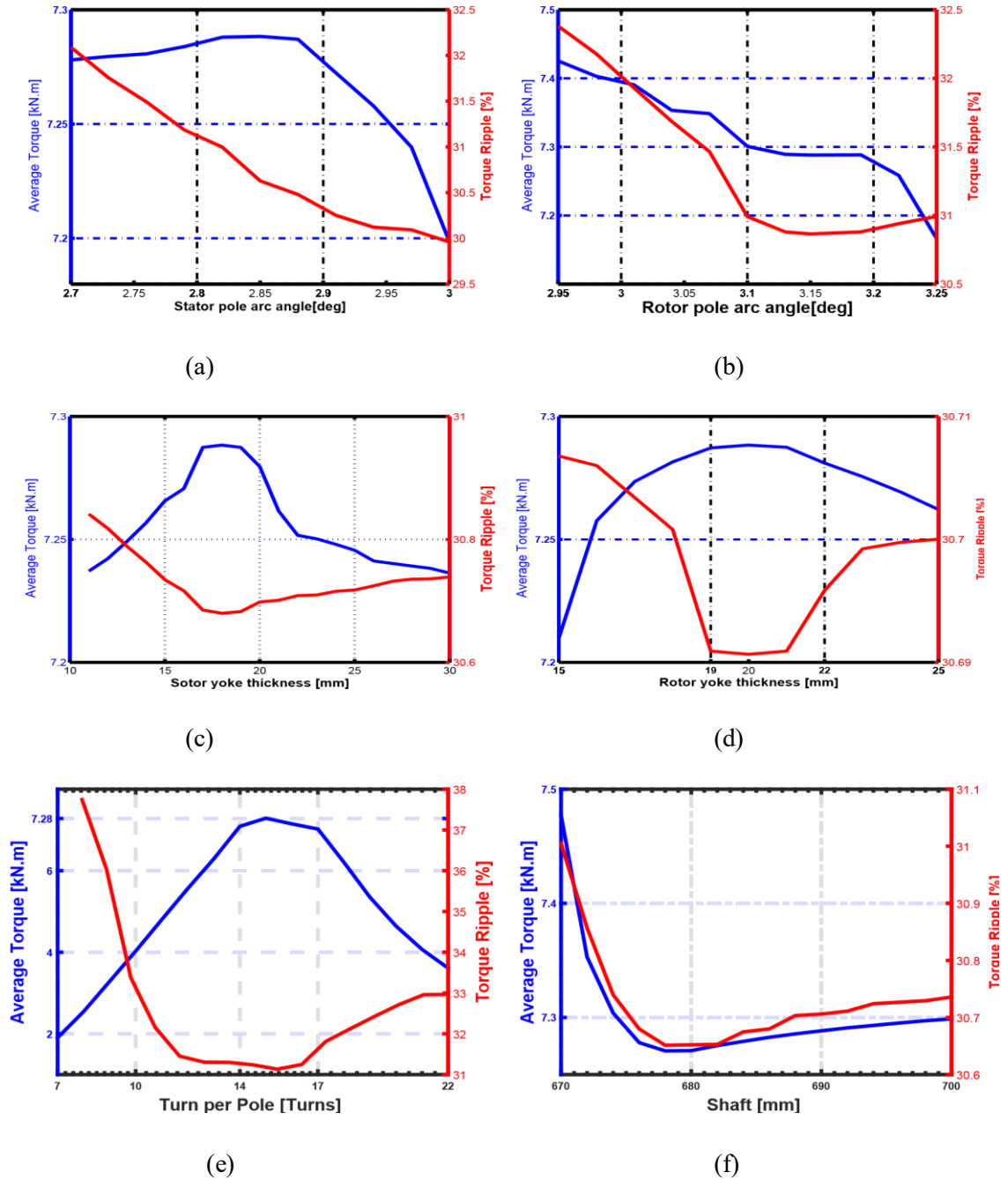


Fig. 4.49 variations of the torque and torque ripple as a function of major parameters (a) B_s (b) B_r (c) b_{sy} (d) b_{ry} (e) N_p (f) D_{sh} [43]

The conducted torque profiles and torque ripple by changing the parameters at the same time display in Fig. 4.50. The best parameters values are $\beta_s = 2.85^\circ$, $\beta_r = 3.15^\circ$, $b_{sy} = 215$ mm, $b_{ry} = 20$ mm, and $N_p = 15$ turns. The geometrical dimensions of the final design are shown in Table 4-8.

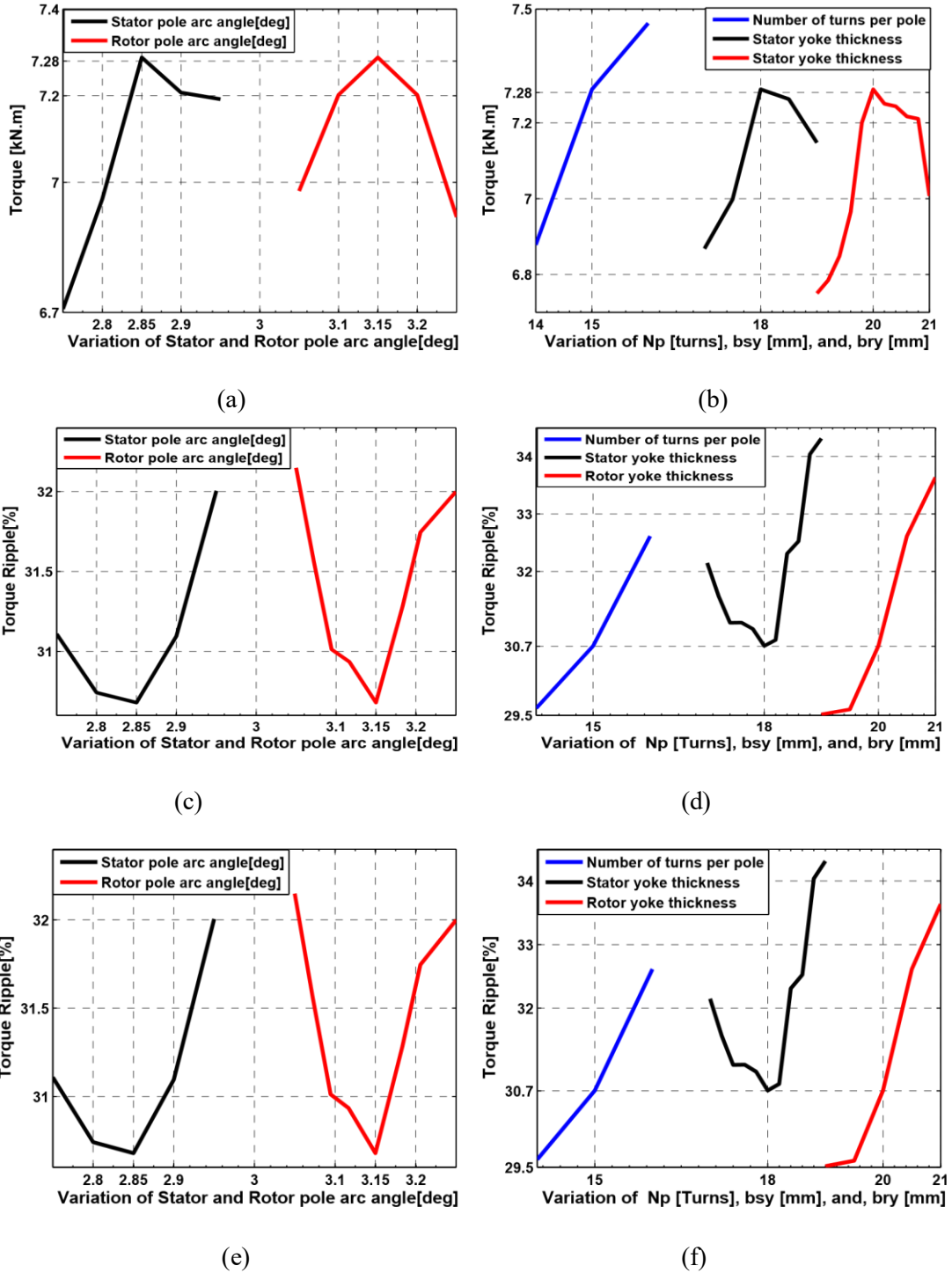


Fig. 4.50 torque ripple and average torque profile while parameters variations instantaneously. (a) B_s and B_r (b) B_{sy} , B_{ry} and N_p (c) B_s and B_r (d) B_{sy} , B_{ry} and N_p

Table 4-8 The final dimensions of the design

Parameter	Value	Parameter	Value
The thickness of yoke (stator) in mm	18	The thickness of yoke (rotor) in mm	20
Machine size	1000	Rotor dia (outside)	798
The angle of stator pole arc in degrees	2.85	The angle of rotor pole arc in degrees	3.15
Slot depth (stator) in mm	82	Slot depth (rotor) in mm	39
Turns	15	Dia of the shaft in mm	680
Pole width of the stator in mm	19.89	Pole width of the rotor in mm	21.93
coils on each slot	2	Filling factor in %	70.3
Rotor pole numbers	48	airgap	1
Stator pole numbers	72	Machine length in mm	340

It is clear from Table 4-8, the angle of the stator pole is shorter than the initial design but it is quite close. Therefore, the optimum design has a greater number of turns. This increases the filling factor and decreases power loss [226]. The change in the inductance for the optimised SRM is closed with the unaligned point as compare to the initial model. Therefore, the optimised machine torque is higher within its region. Consequently, the loop of energy conversion is better for the optimised machine, which gives a better torque up to 7 kNm which has low torque ripples. The initial and optimised design profile loop is shown in Fig. 4.51 and compares both the design characteristics. The diagram of optimised design for 72/48 SRM is shown in Fig. 4.52.

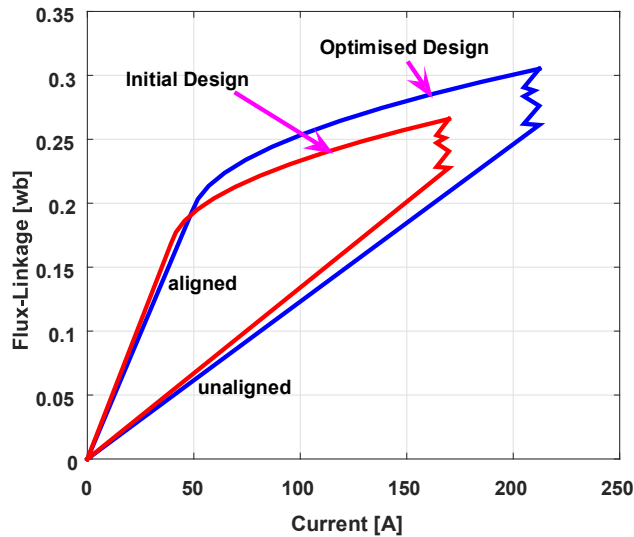


Fig. 4.51 Energy loop comparison in between flux linkage and current curves for initial and optimised design

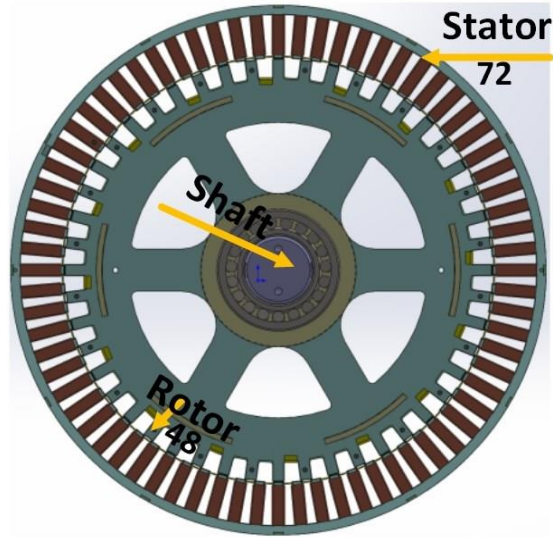


Fig. 4.52 The diagram of the optimised design 72/48 SRM

4.8.3 Characteristics of 72/48 SRM design.

In order to avoid the negative torque, the exciting phase winding near the unaligned position, the current is turned off quickly before the aligned position. The useful calculation has been made in [36] for the torque curve. The 3.75-degree angle represents the fully unaligned position and 7.5 refers aligned position. Fig. 4.53 shows the torque against rotor position. The point range between 4.8° to 7° degrees have the peak torque, hence it is verified.

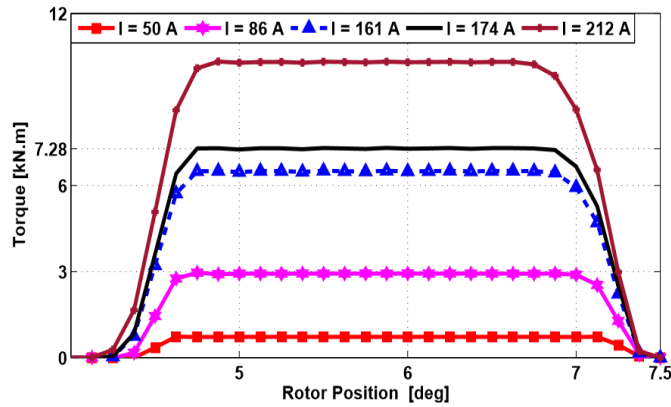


Fig. 4.53 static torque versus rotor position of optimised SRM design at the variable current

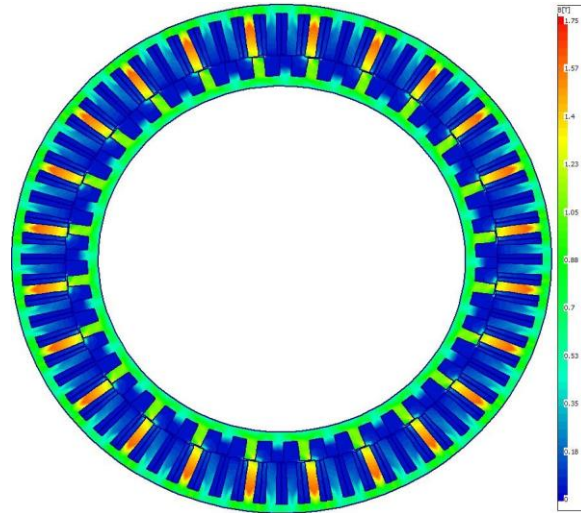


Fig. 4.54 The flux density of the proposed machine

The asymmetrical half-bridge converter is used to obtain the performance. The switching sequence at turn-on angle 3.87 degrees and a turn-off angle of 6.37 degrees is selected and the current chopper control at A phase is applied. Fig. 4.54 shows the magnet flux arrangement at 105 rpm rated speed with 7.28 kNm torque of the two-dimensional FEM model which is developed for 72/48 SRM. When phase winding is energised, and then again it is turned ON after every 7.5°. In Fig. 4.55 and Fig. 4.56, the torque and phase currents are specified as functions of the rotor position, 7.28 kN.m average torque, and 174A dc current is obtained.

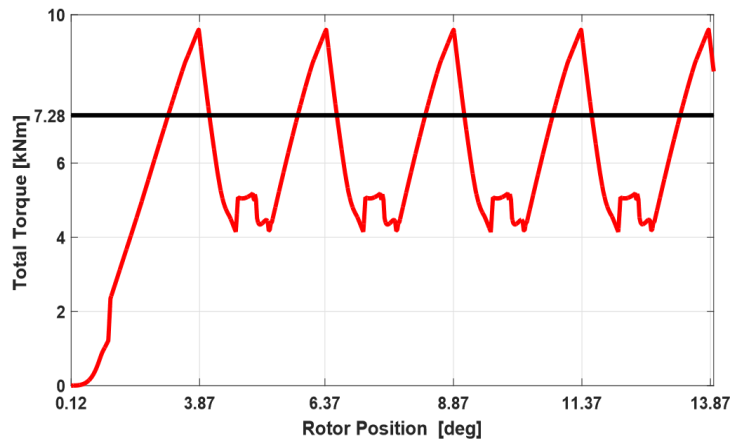


Fig. 4.55 Position of the rotor and developed Torque

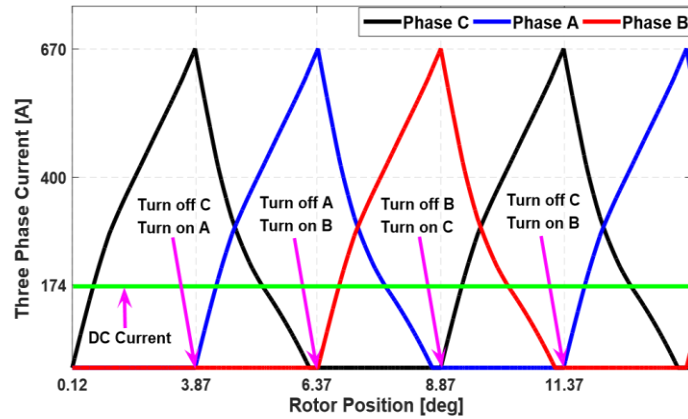


Fig. 4.56 position of rotor against current supplied

4.9 Summary

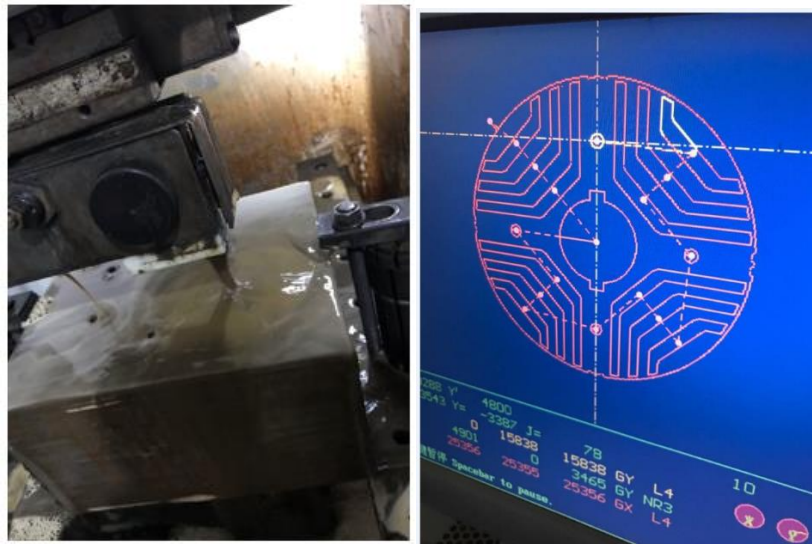
In this chapter, the design and FEM simulation of three machines is carried out. First of all, a 10kW synchronous reluctance motor is designed and optimised. 24 and 36 number of stator slots are tested. Different number of flux barriers are designed with square and round shaped. Finally, 4 flux barriers rotor with square shape is chosen as a best machine in terms of low high torque production and efficiency for direct-drive mining application. The FEM simulation of 12/8 SRM is done while varying different stator and rotor variables. Additionally, the simulation of asymmetrical rotor geometry is done with improved efficiency and power ratings, but this contributed to high torque ripples.

Then different designs of synchronous reluctance motor for closed coupled centrifugal pump is carried out and a 3 V-shaped flux barrier rotor is selected as best choice for the prototype. Further FEM simulation testing of 72/48 SRM is done with optimised variables. This machine has higher 1000mm diameter and high-power ratings 75kW. The final optimised design is chosen for manufacturing. The simulation results show the effective performances of all the machines and their experimental results are analysed in the next chapter.

Chapter 5 Experimental Validation

Subsequently, the machine performance was examined in order to test the optimised rotor design scheme and the 3-flux barrier rotor design is chosen. For further refinement and Surrogate-based optimisation technique is applied with four main variables of rotor design which were flux barrier width, flux carrier width, shaft diameter, and barrier edge angle. Total 300 Latin hypercube samples are generated to check the torque, efficiency, torque ripples and magnetic flux density. Finally, the best design is selected for prototype development.

Synchronous reluctance rotor is finalised and prototyped. The photographs of rotor manufacturing at the factory are shown in Fig. 5.1. The machine's stator is taken from standard Cummins BCI-184F as a duplicate machine. The details of the rotor design and shape as per dimensions are shown in Table 6-22 and 6-23 (in the appendices). The Cummins stator has double-layer star connected distributed winding machine and each layer having 144mm^2 surface area which is shown in Fig. 5.2. It is adequate to operate as a main AC power supply for various applications such as commercial applications, household appliances, small scale residential use and electrical lighting.



(a)

(b)



(c)

Fig. 5.1 photographs during the manufacturing (a) initial rotor manufacturing stage laminations of the prototyped rotor (b) dimensions of rotor design settings on CNC machine (c) cutting of laminations as per the proposed shape of the rotor.

The details of rotor specifications and dimensions are shown in Table 6-25 (in the appendices). The symmetrical rotor with three V-shaped flux barriers manufactured by the factory is shown in Fig. 5.3 and the filling of PVC material inside of the flux barriers are shown in Fig. 5-4 and Fig. 5.5, filling of PVC material inside with cover plate and assembled rotor with the shaft is shown in Fig. 5.6.



Fig. 5.2 Cummins BCI-184F machine



Fig. 5.3 photograph of the manufactured rotor from the factory



Fig. 5.4 photograph of the PVC filling inside of the rotor flux barriers



Fig. 5.5 photograph of the PVC filling inside of the rotor with cover plate

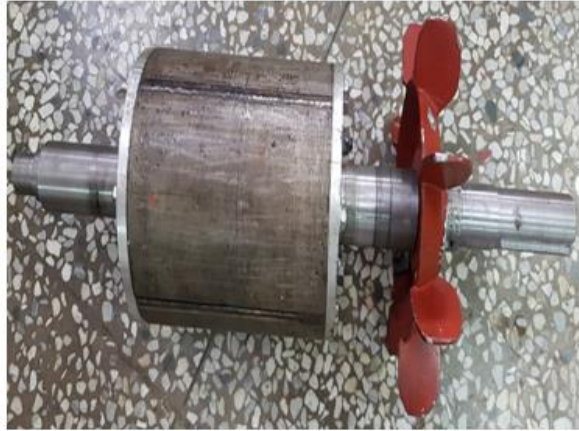


Fig. 5.6 photograph is assembled rotor with shaft

The rotor is assembled and polished through the machining process, which is shown in Fig. 5.7. In order to improve the rotor's mechanical integrity in the manufacturing process, polyvinyl chloride material is inserted inside of the flux barrier. The complete rotor manufacturing stages from manufacturing in the factory to the assembled rotor in the machining process are shown in Fig. 5.8. As it has already been described, the stator for the proposed motor used is identical of standard Cummins BCI-184F machine, and the complete specifications are described in [207, 208]. There is a short-pitched 2/3 winding arrangement with double layer star connection. Each slot area is 144mm^2 for individual layer. The experimental test rig of the whole work is built and tested as depicted in Fig. 5.9.



Fig. 5.7 photograph of the assembled rotor after machining

5.1.1 Rotor Fabrication

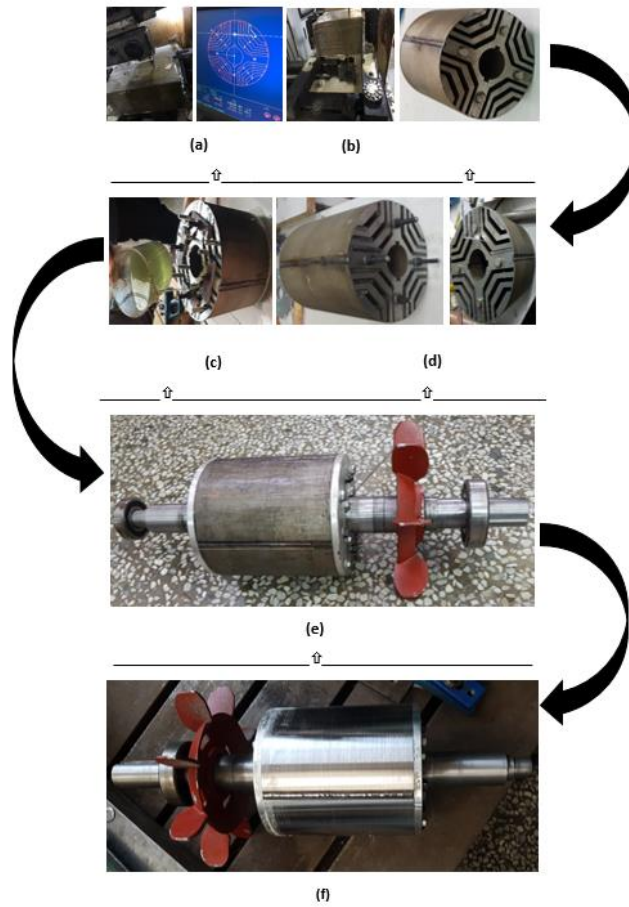


Fig. 5.8 prototype development stages of the proposed rotor (a) early manufacturing from the factory (b) manufactured design rotor (c) flux barrier filling with magic (d) flux barrier insertion with magic and PVC filling with magic and PVC (e) assembled rotor with shaft (f) final assembled rotor after machining

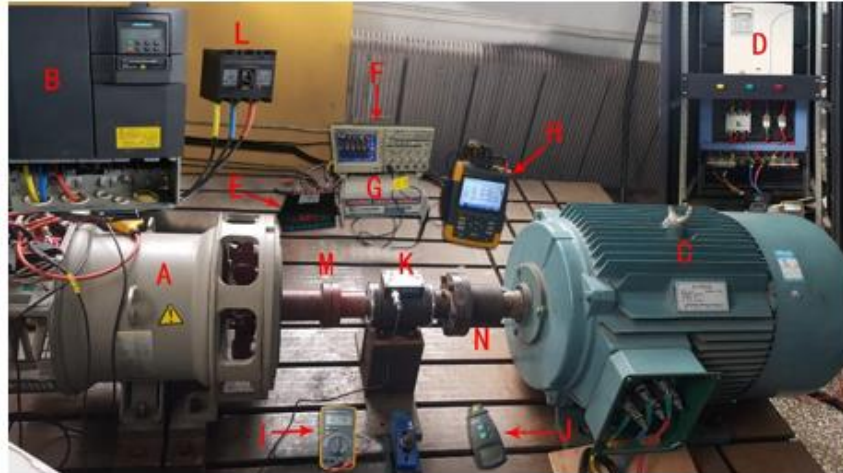


Fig. 5.9 Experimental test rig

- A. The SynRM B. Siemens Drive C. 55kW load motor
 D. ABB Drive E. Temperature meter F. Oscilloscope Tektronix TDS 2024B
 G. Torque meter JN-338 H. Fluke power meter
 I. Multimeter J. Speed meter K. Torque transducer
 L. Siemens circuit breaker CDM10-100/3300 Delixi
 M. Motor side coupling N. Load side coupling

5.2 Specifications of the Original Machine

Table 5-1 provides essential stator specifications. This is a duplicate machine made by Cummins PI-144F. The photograph and the detailed specifications are taken from the supplier as depicted in Fig. 6.1 (in the appendix) and full details are available in Table 5-1.

Table 5-1 Specification of Cummins stator PI-144F

Item	Value	Item	Value
Rated Frequency (Hz)	50	Stack Length (mm)	200
Winding Arrangement	Double-layer Star	Power ratings in kVA	27.5
Stator OD (mm)	310	Rated Speed (rpm)	1500
Stator Slot Number	36	Numbers of poles	4
Rotor OD (mm)	188	Rated Power Factor	0.8
Stator ID (mm)	192	Rated Line Voltage (V)	380

5.3 Test proceedings

The following equipment BS EN 60034-4:2008 and BS EN 60034-2-1:2007 has been selected as per British standards.

5.3.1 Voltage

Three-phase AC Synchronous motor should be appropriate for balanced and sinusoidal voltages, during rated load conditions limits of distortion and inequality occur, therefore temperature should not reach to a hazardous level.

5.3.2 Frequency

Throughout the testing, 0.3% of the overall frequency should be maintained.

5.3.3 Resistance

Generally, in the stator winding, line-to-line resistance is considered for AC machine is a polyphase system. The test resistance should be find out within the quickest time interval to avoid any thermal interference.

5.4 Direct measurement

5.4.1 Winding resistance and inductance measurements

The measurements of resistance and inductance are taken at the winding connections while keeping the rotor at a stationary position at ambient temperature (14°C). The measurement of stator winding resistances and inductances are taken separately for each phase. Three readings are taken from the outer winding terminals, as shown in Table 5-2. The three-phase winding terminals have been presented in Fig. 5.10 and photographs of 3 winding-resistance reading are shown in Fig. 5.11.

Table 5-2 Resistance and Inductance measurement results

Phase	The line to line resistance of the winding in Ω	the line to line winding Inductance in henry
Phase-1	0.247	0.839
Phase-2	0.268	0.839
Phase-3	0.245	0.837
Average	0.253	0.850

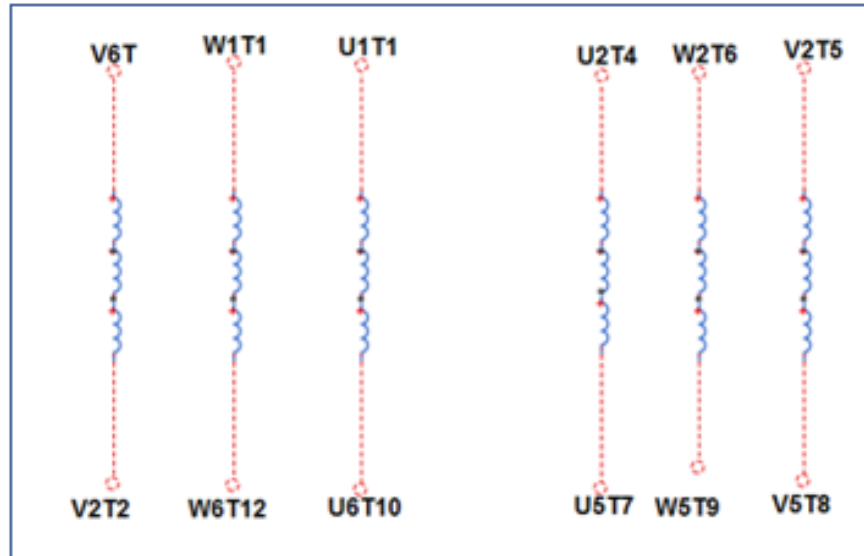


Fig. 5.10 Three-phase double layer winding terminals

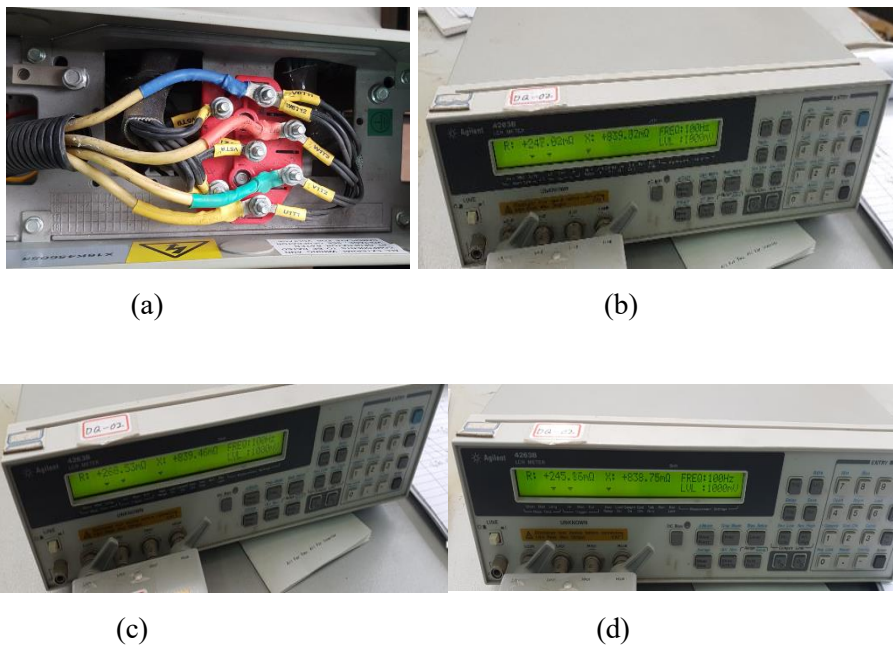


Fig. 5.11 3 resistance taken from winding Photographs of (a) 3-phase terminals (b) winding 1 resistance (c) winding 2 resistance (d) winding 3 resistance

5.4.2 Torque measurement

The JN-338 Series torque measuring instrument used in this experiment is from SanJing United Technology Corporation, Beijing as presented in Fig. 5.12. Fig. 5.13 shows the torque transducer used for measuring

the torque. $\pm 0.2\%$ precision is available to measure 100N-m. Generally, the square-wave signal is produced by transducer which refers as an input signal at a certain frequency, as depicted in Fig. 5.14.



Fig. 5.12 Torque measuring instrument JN-338 series



Fig. 5.13 Torque transducer coupled with the shaft

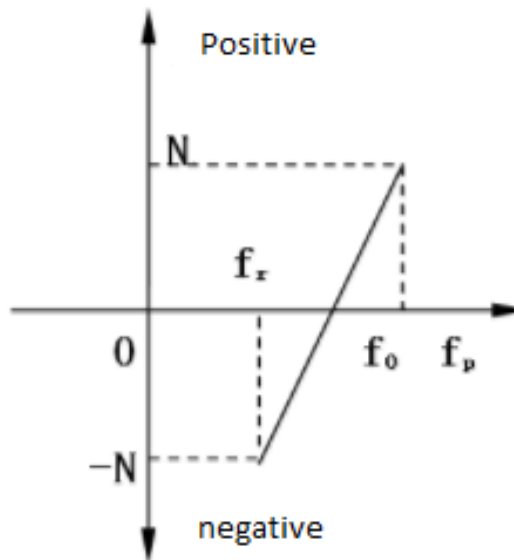


Fig. 5.14 Torque signal

The following equations are used for torque amplitude calculation:

$$\begin{cases} M_p = N \frac{f - f_p}{f_p - f_0} \\ M_r = N \frac{f_r - f}{f_0 - f_r} \end{cases}$$

where torque signal represents the frequency f , positive frequency is represented by f_p at 15 kilo Hertz, zero-point frequency is denoted by f_0 at 10 kilo Hertz, The negative frequency of torque is denoted by f_r at 5 kilo Hertz, and N shows maximum amplitude of torque with full scale here 100 N-m torque is considered.

5.4.3 Speed measurement

The speed signal is similar like a torque signal as a square wave. The square-wave frequency signal indicates the machine speed established on the equation as follows:

$$N_s = 60 * f / Z$$

Here frequency signal is represented by f and Z is overall tech numbers of teeth. For the current device 60 number is calculated. The torque and speed signals example are depicted in Fig. 5.15.

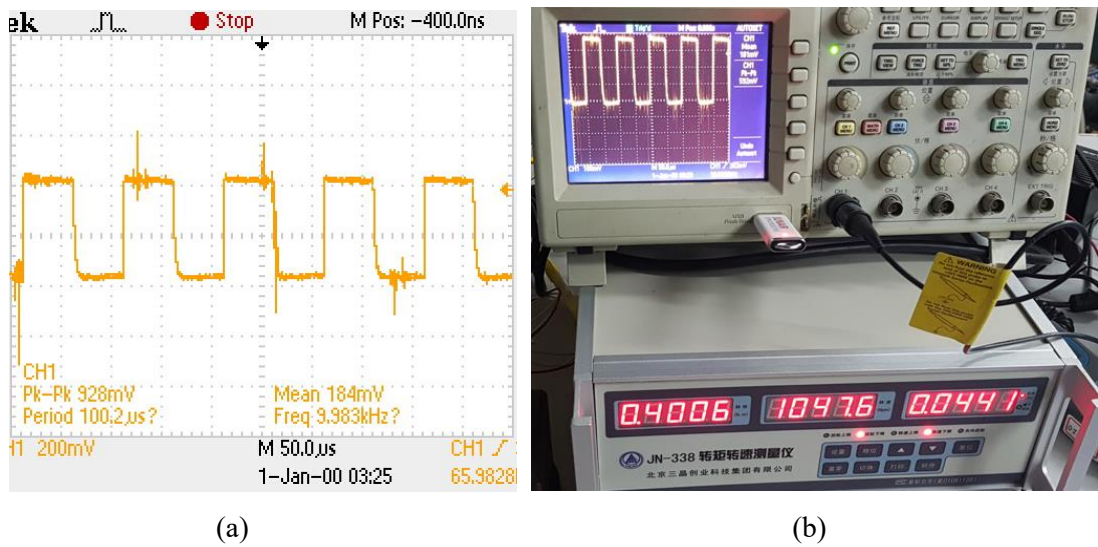


Fig. 5.15 photographs of (a) torque and (b) oscilloscope signals of speed measurement

5.4.4 Megger Testing. (Winding short circuit test).

The megger testing is carried out on each of the winding to avoid the short circuit with the stator. The meter reading is very high more than mega-ohms (MΩ) and through this test, it is confirmed that winding

insulation is proper and high temperature will not damage the insulation. Fig. 5.16, is the photograph of megger testing.



Fig. 5.16 photograph of 3-phase stator winding megger testing

5.5 Indirect Measurement

The following subsections explain the indirect measurements and calculations.

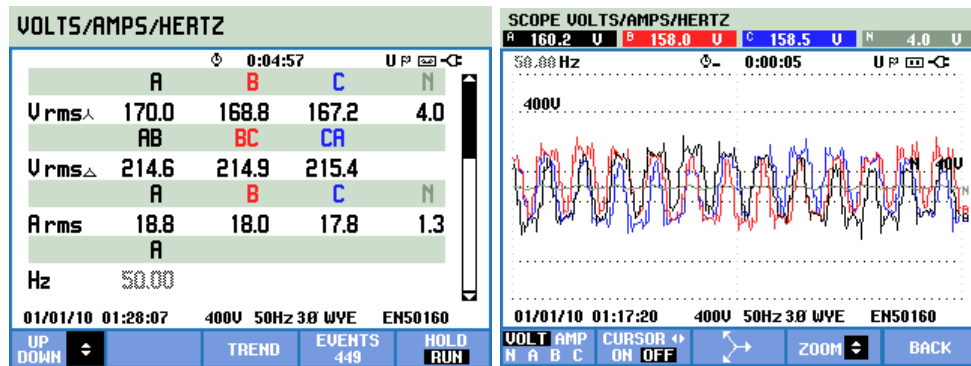
5.5.1 No-Load test

This test is carried out while running the SynRM without coupling shaft with other machines, at rated current and voltage (by adjusting the supply frequency from 0 to 50Hz). The test is conducted at ambient Temperature=16.5° C. Initially the machine is run for 30 minutes to know the stability as well as temperature rise. During the no-load test, supply frequency is changed with gradual steps and different points with the help of 22kW Siemens micro master 440 variable frequency drive as shown in Fig. 5.17. Its parameter setting is also described in the next section.

The testing is done at fifteen different driven speed and at ten different frequencies. The frequency is varied at steps: 5 up to 32Hz. Thus, the machine speed is changing according to synchronous speed from 150 to 1500 RPM.

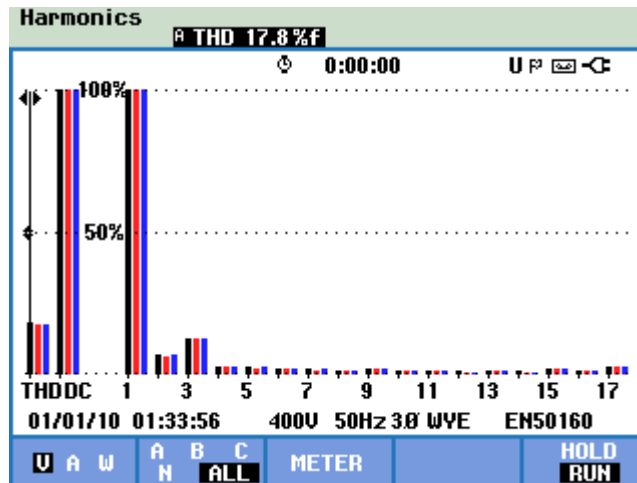


Fig. 5.17 Siemens Micromaster 440 of 22kW variable frequency drive



(a)

(b)



(c)

Fig. 5.18 No-load test results (a) RMS current and voltage and current value (b) voltage waveform (c) total harmonic distortion

The following readings are recorded simultaneously.

--Supply frequency;

--Temperature;

--Speed;

--Current

--Voltage;

--Harmonics;

The no-load test results are shown in Table 6-32 in the appendix and test results are shown in Fig. 5.18. It has been observed that as the machine is running continuously, it is more stable in terms of current and total harmonics distortion.

5.5.2 No Load Test while coupling the shaft with 55kW load motor

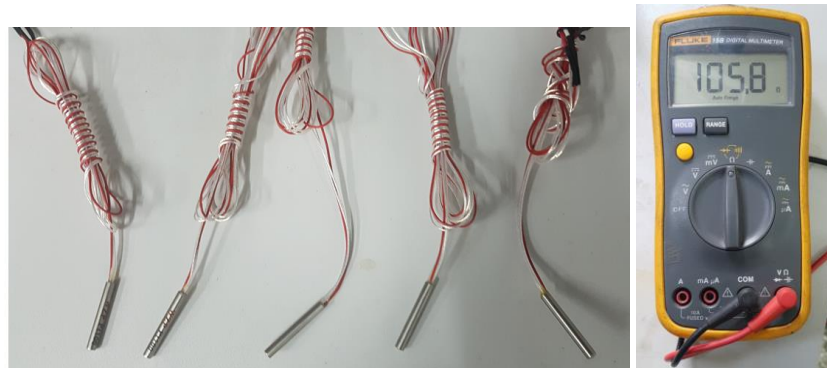
The test is conducted at ambient temperature=13.3⁰C. A 55kW PMSM is coupled with the tested machine as shown in Fig. 5.19. The load motor specifications are depicted in Table 5-3, and overall data results are shown in Table 6-33 (in the appendices). In the test below, intervals of 5 Hz frequency is varied and the results are taken after each step. For temperature measurement, 5 PT100 type thermocouples are used, 3 of them are used to measure the winding temperature at 120 mechanical degree apart and remaining thermocouples measure stator core temperature. The photographs of thermocouples, their ohmic reading as well as their various locations on the stator are shown in Fig. 5.20.



Fig. 5.19 load machine of 55kW coupled with during no load

Table 5-3 specifications of 55kW load motor

Item	Value
rated power	55kW
speed	3000rpm
torque	352Nm
No: of phases	3
P.f	0.88
Drive system	ABB-ACS800



(a)

(b)



(c)

Fig. 5.20 Photographs of (a) thermocouples PT100 (b) Ohmic reading on multimeter (c) location of 5 thermocouples on the stator.

Fig. 5.21 shows the temperature readings at 5 to 50Hz and frequency versus speed chart is shown in Fig. 5.22, while gradually increasing the frequency, the speed varies in a linear trend way from 150 to 1500rpm.

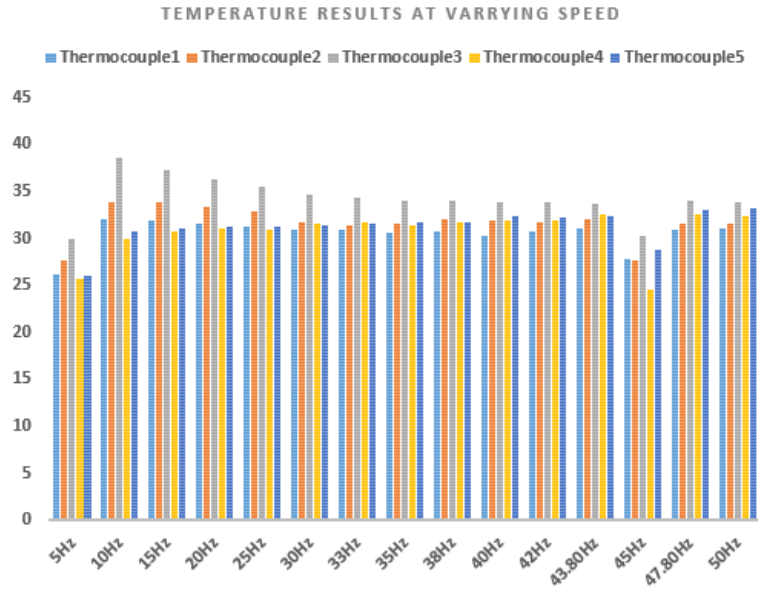


Fig. 5.21 Temperature graph as different input frequency and speed

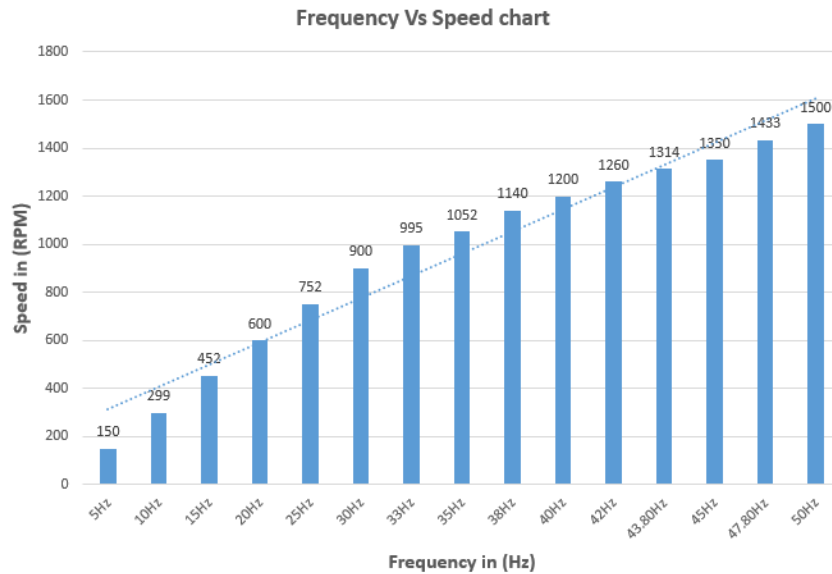


Fig. 5.22 frequency Vs speed chart and linearly trend line

Fig. 5.23 shows the vibration reading measured from 0 to 50Hz. Also, the total harmonic distortion has three data measurement which is written separately in Table 6-34 (in the appendices). The line to neutral and line to line voltages and harmonics are measured at 50Hz which are shown in Fig. 5.24. After 30Hz data collection, the interval is reduced to 2 and 3Hz for safety so that the temperature and current should not exceed the higher rated value.

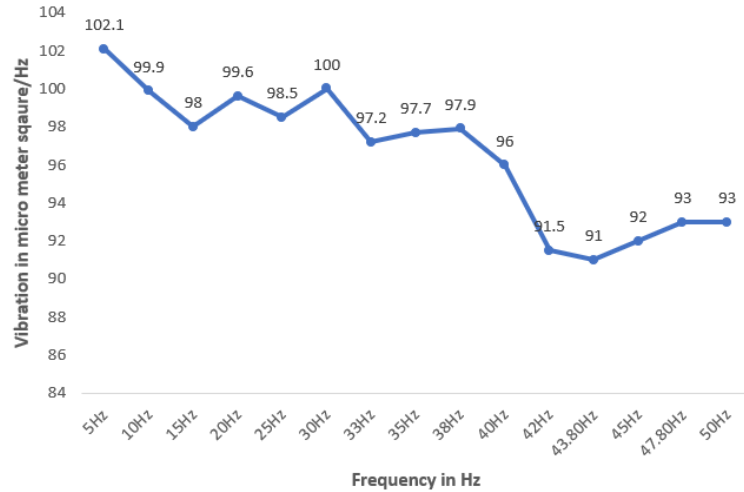
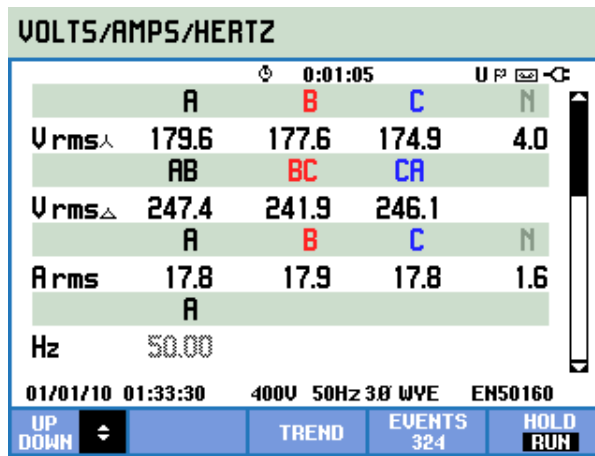
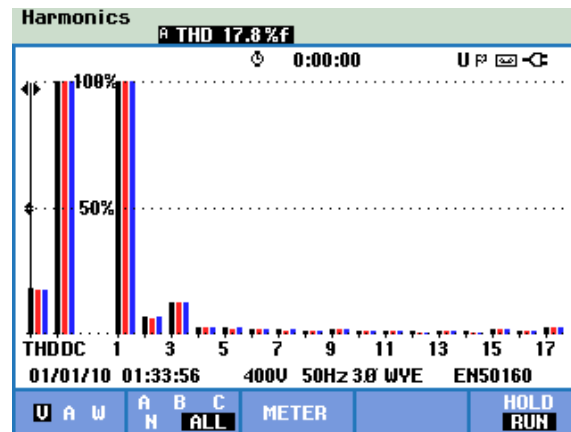


Fig. 5.23 vibration measurement at variable frequency



(a)



(b)

Fig. 5.24 shows (a) 3-phase current and voltage reading (b) total harmonic distortion measurement at 50Hz

Additionally, it can be noted that the from no-load test results, the number of harmonics and vibration is decreasing as the machine is getting higher speed mainly due to this fact the machine's performance becomes more stable. The reduction of harmonics and vibration content is, therefore, an important achievement in the results.

5.5.3 LOW-Speed test

To verify the performance of the test machine, the low-speed test is performed. In the low-speed test, different performances of synchronous reluctance motor are assessed. The speed is varied from 150 to 1500rpm by Siemens micro master 440 variable speed drive. The load motor of 55kW is driven by ABB ACS800 anti-clockwise direction at a different speed and torque settings and all the parameters are noted such as current, voltage, power, power factor and harmonics. The load motor of 55kW specifications are depicted in Table 5-3 and the related machine data calculation is as follows:

Calculation of Torque in the motor which is under test:

Test machine power rating is 24KW and RPM are known then we can calculate the torque as follows:

$$T = \frac{9.55 * 24}{1500 \text{ speed in RPM}} = 0.1528 \text{ kNm which is equal to } 152 \text{ Nm}$$

Similarly, the equation below can also be used as follows.

$$T = \frac{30 * \text{Power}}{\pi * 1500} = \frac{30 * 24}{3.14 * 1500} = 0.152 \text{ kNm} = 152 \text{ Nm}$$

55kW motor as a load torque calculation

$$T = \frac{9.55 * 55}{1491 \text{ speed in RPM}} = 0.352 \text{ kNm which is equal to } 352 \text{ Nm}$$

Similarly, the equation below can also be used as under:

$$T = \frac{30 * \text{Power}}{\pi * 1491} = \frac{30 * 55}{3.14 * 1491} = 0.352 \text{ kNm} = 352 \text{ Nm}$$

The loading machine is operated by ABB ACS800 drive. Both the drive parameters settings are described as follows.

First of all, we need to know the design parameters means specifications of the machine (test machine and load machine) which are as shown in Table 6-22 (in the appendices) and Table 5-3 and then all the parameters are inserted into the drive step by step.

5.5.4 Steps of parameter settings of Siemens Micromaster 440

The Siemens Micromaster 440 used in the experiment is shown in Table 6-31(in the appendices) equipment (2) and the drive parameter are shown in Table 5-4. The following steps are taken to drive the synchronous reluctance motor.

Step-1= First of all, turned ON the power supply of the Siemens drive and then pressed “P”, then all the things are turned into zero-zero, from the up-arrow key pressed to 10, and used FN (function) key and Enter. The screen turned to zero and then again pushed arrow key and then selected as 1 and then pressed “P”, from above all the steps screen showed as P0010 which means that the drive has reached quick commissioning mode. Now as per the given manual, number 304 is the voltage which is required to be inserted in the drive. In this way, voltage, 380 are inserted, we can change any voltage as per given specifications of the machine while pressing “P” and scrolling the arrow key and then press enter. For the next variable enter “P” and chose 305 for current and insert the current 26A and press “P” to get the next value 307 which is rated power in kilowatt. As our machine’s rated power is 24kW. For the next value which is 308 actually means to enter the power factor 0.88. The next value is 310 which means the frequency at 50Hz. The next value is 311 means speed in RPM and then press “P”. It is noted that whatever the parameters we want to select we can give the input to the machine as per requirement.

Step-2= The number 1 means to locally control the machine locally from the red button, for remotely control option 2 was for PLC type control. As per our preferences, we run the machine from locally throughout, so we just kept the mode at digit 1 and then pressed “P”.

Step-3= Now we need to set the Ramp-up and Ramp downtime which means that within how many times the machine should be started and get the maximum start-up time like in 5 or 10 seconds or 4 seconds etc. The digit 21 means within how many seconds the machine should be stopped, this may be 10 seconds and then press enter P. and with the arrow key select digit 2 which means that all the values will be automatically calculated and will be recorded and then again press P. Now busy signal will come on screen which is calculating and synchronizing with motor. Now P3900 will be appeared and then press FN key and it will come r0.000, so now press ‘P’ and the machine is ready for start-up. Now from the red button top left to give the command to start. As we select the low frequency ‘0’ then it will remain minimum at 5Hz which will also be displayed on the screen and now from up-arrow key increase the frequency which will increase the speed as per our desired value. Now increase the frequency up to 50Hz and now can be stopped with push button, if we want to run the reverse direction then press the reverse arrow key and machine will run in the reverse direction. It should also be noted that the –ve sign on the screen will also appear which reflect the reverse rotation of the machine.

Table 5-4 Siemens micro master drive parameters selected for Synchronous Reluctance Machine settings

P0003	1
P0004	0
P0010	0
P0100	0
P0304 (VOLTAGE)	380
P0305 (CURRENT)	26Amp
P0307 (Power)	22kW
P0308 (Power Factor)	0.8
P0310 (Frequency)	50Hz
P0311 (Speed)	1500RPM
P0700	1
P0970	0
P1000	1
P1080 (Minimum frequency)	0
P1082 (Maximum frequency)	50
P1120	21.10
P1121	10
P3900	0

5.6 Steps of parameter settings of ABB Drive ACC800

The ABB drive ACC800 is shown in Table 6-31 (in the appendices) equipment 8 and the drive parameters are shown in Table 5-5. First of all, we need to find the data of the machine for the start-up like kilowatt, frequency, voltage, current and motor speed.

Step-01. Turn the power supply and press PAR key and now this will take us into the parameters headings as we need to find the group 99 which need to be selected for our operation.

Step-02. Now press scroll key which is on the second row left first (double arrow bottom dark black). Now press the button until it comes 99 and from this language, the option will appear.

Step-03. Now press 3rd row which is at the 1st right button (single arrow). As we go down, we find the values which need to be changed so we need to reach towards the speed option.

Step-04. Press enter, now bracket will appear on the current value and to change the value use single arrow key Up and Down, once we have the correct value of speed the press Enter and now bracket will be removed, we follow this process right way to group 99 with all the data available on the motor nameplate.

Step-05. Once we have provided all the input settings, now we need to get back to the home page. This is done by simply pressing the ACT button, which means the actual key. As we have entered all the data in group 99 ready to start the drive.

Step-06. Now we need to check the drive is being controlled by locally or not, so on the top left-hand corner, as it can be seen that, there is no L written on the screen which is what we are looking for.

Step-07. Now press LOC. Left 1st Row on the 4th number and now alphabet L will appear. Now we have full control over the drive on the motor from our key part.

Step-08. Now press REF Key and bracket will appear on the top, and Hz signal, now we can then enter the drive reference frequency.

Step-09. As all the required setting is done now the machine is ready to start then press the start key. The overall low speed test data results are shown in Table 5-6 and Table 6-34 (in the appendices).

Table 5-5 ABB Drive parameters selected for couples machine ACC800 start-up settings

Language	English
Motor ID run mode	IDMAGN
Motor Nom power	55kW
Motor Nom Speed	1491
Motor Nom Frequency	50Hz
Motor Nom Current	100Amp
Motor Nom Voltage	380
Motor Control Mode	SCALAR✓/DTC
Application Restore	No
Application Macro	Y-CTRL

Table 5-6 Low-speed Test Temperature readings of the test machine from 0-50 frequency and 0 to 1500RPM rated speed.

Frequency	T1	T2	T3	T4	T5	RPM
5Hz	29.3	30	31.9	32	27.6	150
17Hz	32.3	34.1	37.2	30	31.4	513
25Hz	32.3	34	36.6	31.3	31.8	750
0.9Nm Torque applied by ABB at 50Hz						

25Hz	32.8	34.5	36.8	33	32.7	750
30Hz	32.8	34.2	36.7	33.2	33.2	899
1.4Nm Now Torque Applied on the machine						
30Hz	32.7	34.1	36.7	33.4	33.6	900
35Hz	33	34.5	37.1	33.6	34.1	1050
1.7 Nm Torque Applied on the machine						
35Hz	33.5	34.9	37.5	34.3	34.6	1050
40Hz	34.1	35.2	37.9	34.8	35.7	1200
2.3Nm Now Torque Applied on the machine						
40Hz	34.2	35.2	37.9	34.4	35.9	1200
45Hz	35.4	36.2	39.5	36.2	36.8	1356
3.4 Nm Torque Applied on the machine						
45Hz	36.1	37	40.2	37.1	37.8	1350
50Hz	36.6	37.7	41.1	37.6	38.3	1500

Table 5-7 low speed test current, voltage, power and power factor

Frequency	RPM	Current in Amps	Voltage in V	Power in kW	P.f
5Hz	150	18	139	0.22	0.09
17Hz	513	18.2	163	0.36	0.12
25Hz	750	17.8	181	41	0.14
Now Torque applied by ABB at 50Hz					
25Hz	750	18	181	0.51	0.16
30Hz	899	18	192	0.54	0.17
Now Torque Applied on the machine					

30Hz	900	18.2	191	0.68/0.76	0.21
35Hz	1050	19	200	0.85	0.224
Now Torque Applied on the machine					
35Hz	1050	18.8	200	0.94	0.25
40Hz	1200	18.9	211	1.10	0.26
Now Torque Applied on the machine					
Same all	1200	18.9	211	1.10	0.27
45Hz	1356	20.7	227	1.17	0.28
Now Torque Applied on the machine					
45Hz	1350	20.7	226	1.76	0.37
50Hz	1500	23.8	239	2.29	0.41

Table 5-8 Harmonics produces by the SynRM and parameter settings of load motor.

Harmonics	Torque Nm	ABB drive reference settings Hz/Rpm	ABB Drive current
512%	0.2	0.1Hz/	
44.7%	0.42	0.6/-9.8	2.4
	0.5	0.6/-9.8	2.9
Not Torque applied by ABB at 50Hz			
14.5/4.9/0.4		0.8/-11.7/-52%	45/6.3
8.3/3.0/0.5	0.9	0.8/-11.7	45/6.3
Now Torque Applied on the machine			
8.5/3.3/0.2	1.4	1/68%	68/10.1
7.5/4.8/0.3	1.7	1.1/-77%	67/11.4
Now Torque Applied on the machine			
7.4/4.2/0.2	1.7	1.2/-16rpm/-84%	72/15

12/8.2/2	2.3	1.2/-16rpm/-84%	72/15
Now Torque Applied on the machine			
12/8.1/0.3	2.3	1.4/-19/99	86/19
7.2/6.3/0.2	2.9	1.4/19.6	84/11.8
Now Torque Applied on the machine			
7.2/6.2/0.3	3.4	1.7/- 23.8/117.74T	102.84/12
5.9/6.1/0.3	3.9	1.7/-24.7rpm/- 113T	99.74/18

5.6.1 Low-speed test operation

Initially, the tested machine is started while giving three input frequency steps. The frequency is increased at 5, 17 and 25 hertz and speed are increased up to 750rpm, then gradually 0.9Nm torque is applied on the machine by 55kW load machine. The loading machine has 0.8Hz frequency and (-ve) 11.7rpm at 6.3A current. It has been observed that when the main motor frequency is increased then there is a change in ABB drive speed, torque as well as drive current. The temperature readings are shown in Table 5-6 whereas current, voltage, power, power factor and harmonics are shown in Table 5-7 and the harmonics reading and parameter setting of the load drive motor is shown in Table 5-8. The photographs of ABB drive penal setting are shown in table 6-31 and reading details are shown in Table 5-9 (A), first ABB drive penal reading - 9.8rpm anticlockwise applied at 0.6Hz and the -35% torque and 30.54A current draw by the load motor (B) second ABB drive penal reading 0.8Hz frequency, -11.7rpm at -52.75% torque applied which draws 46.65A (C) third ABB drive penal reading 1.1Hz -14.9rpm at -77.64% torque and 67.76A (D) fourth ABB drive penal reading 1.4Hz, -19.6rpm, -96.49% torque and 83.76A current.

Table 5-9 Torque applied by load machine ABB drive penal

Steps	Torque (Nm)	Frequency (Hz)	Speed (rpm)	Current (A)
A	35.19%	0.6	9.8	30.54
B	52.75	0.8	11.7	45.65
C	77	1.1	14.9	67.25
D	96.49	1.4	19.6	83.76

5.6.2 Over speed test

To verify the stability of the machine at high speed, the over speed test is performed. Firstly, the machine normal speed at 1500rpm and then gradually speed is increased while varying the frequency from 51-55Hz.

It is observed the machine is running well with thermally stable characteristics. The experimental results of over speed test are shown Table 5-10 and

Table 5-11. The photographs of over speed test result up to 55Hz are shown in Fig. 5.25 and Fig. 5.26 (a) voltage and current reading (b) waveform of voltage and current (c) Power and power factor results and (d) harmonics reading.

Table 5-10 Overspeed test results while varying frequency 50 to 55Hz

Speed Rpm	Frequency in hz	Voltage in V	Current in Amps	Power in kW	P.f	Harmonics in %
1530	51Hz	245	18.6	0.68	0.44	6.6%
1560	52Hz	246	22.5	0.67	0.63	6.3%
1590	53Hz	249	18.0	0.65	0.59	6.3%
1620	54Hz	251.9	18.1	0.65	0.65	6.9%
1635	54.5Hz	250	17.3	0.64	0.64	6.3%
1650	55Hz	251	17.2	0.64	0.64	6.4%

Table 5-11 Overspeed Test Temperature readings of the test machine from 0-50 frequency and 0 to 1500RPM rated speed.

Speed Rpm	Frequency	T1	T2	T3	T4	T5
1530	51Hz	29.5	29.6	32.1	23.4	31
1560	52Hz	29.8	30	32.4	27.4	31.7
1590	53Hz	30.2	30.2	32.7	29.2	31.9
1620	54Hz	30.3	30.3	33	31.7	32.2
1635	54.5Hz	30.6	30.8	33	31.3	22.6
1650	55Hz	30.9	30.8	33.1	32.3	32.8

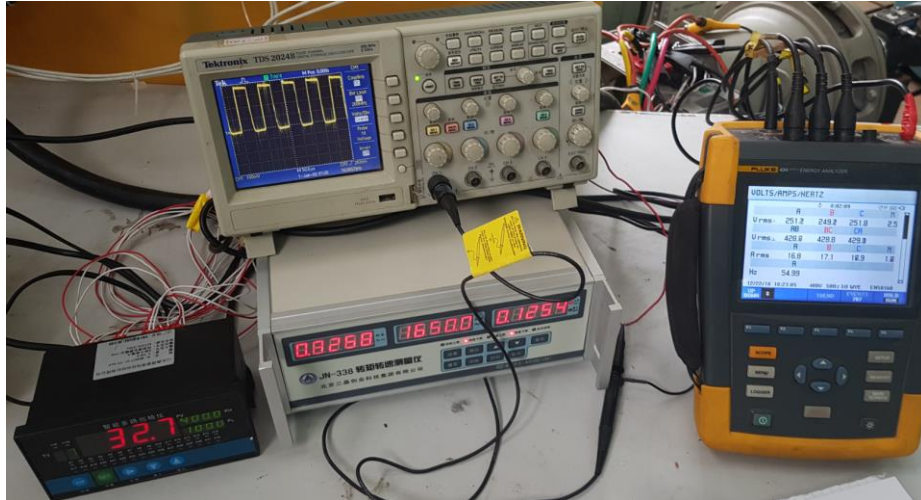
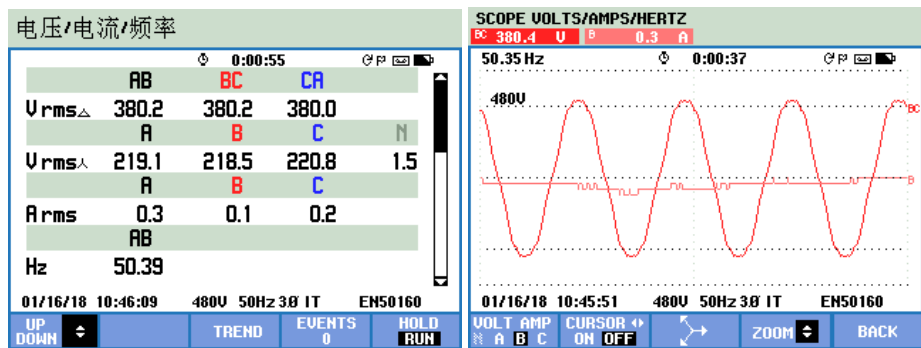
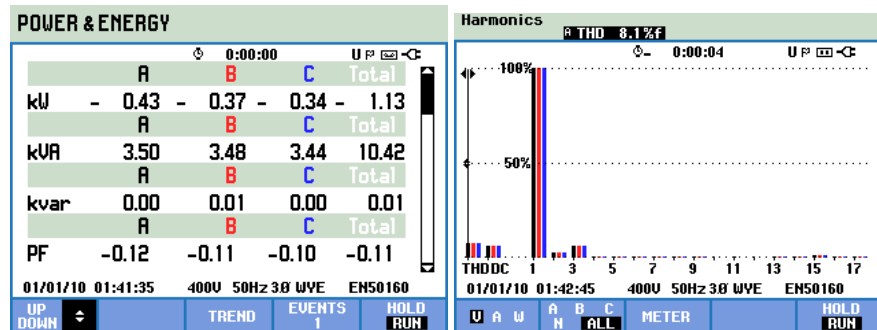


Fig. 5.25 equipment used and test results of over speed



(a)

(b)



(c)

(d)

Fig. 5.26 over speed test results up to 55hz maximum

After testing the 51Hz frequency the input frequency is increased at 52Hz through Siemens drive and motor reached 1560rpm with 0.124 harmonics. In the next step, the input frequency is incrementally increased by the step of 1 and now the frequency reaches at 53Hz with 1590rpm. Similarly, the input frequency is

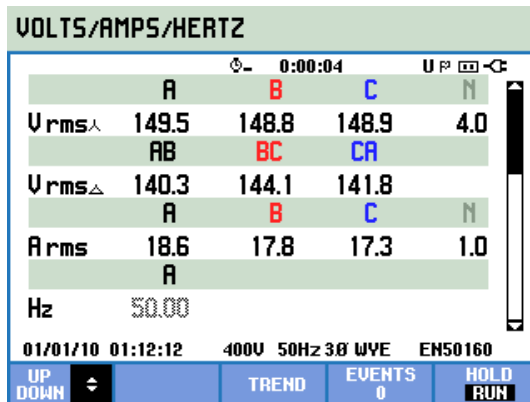
enhanced by Siemens drive up to 55Hz at 1650rpm. The maximum current is produced at 55hz is 17.2 along with 249.3 rms voltage at 0.65kW power. The test results and parameters are shown in Table 5-12.

Table 5-12 over speed test results data at 55hz

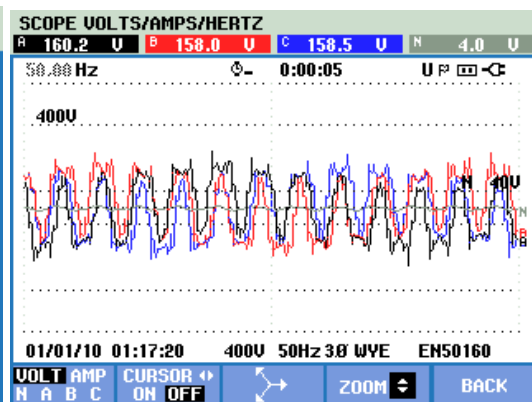
Item	Value
Current	17.2
Voltage (r.m.s)	249.3
frequency	55hz
Speed in rpm	1650
Torque in Nm	0.7512
Temperature in °C	22°C
Harmonics in %	6.5%
Power in kW	0.65
KVA	4.25
KVAR	3.78
P.f	0.15

5.6.3 Retardation Test

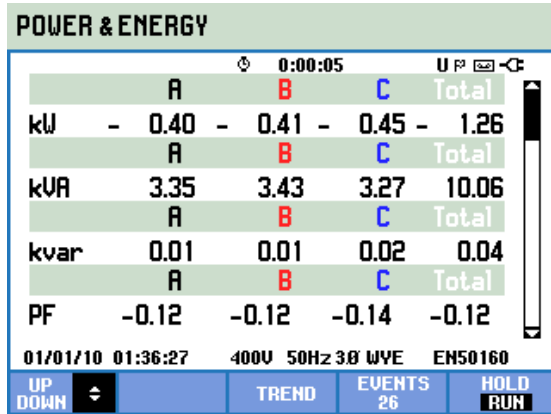
The retardation test is carried out at 16.3°C ambient temperature. In this test, the test machine (synchronous reluctance) is started and its speed is increased up to rated 1500rpm and then the machine is suddenly stopped while cutting the supply off from the Siemens drive and the time of retardation is calculated. During startup, the total time taken is 3 minutes and 36 seconds to reach the maximum speed 1500RPM. The current is reached 18.1A and 240 voltage at the 50Hz input frequency. The photographs of retardation test results are shown in Fig. 5.27 (a) voltage and current reading (b) waveform of voltage and current (c) Power and power factor results and (d) torque and speed measurement. The readings are depicted in Table 5-13.



(a)



(b)



(c)



(d)

Fig. 5.27 retardation test results

Table 5-13 retardation test results

Item	Value
Total Speed up time	3 minutes and 36 seconds
Current	18.6Amp
Voltage	149V
Frequency	50Hz
Harmonics	7.4%
Power	0.4kW
Active Power	3.35kVA
Power Factor	0.12
Speed	1500RPM
Torque	0.5 Nm
Retardation time	1 minute 2 seconds
Machine running temperature	24 deg C

5.6.4 Analysis of Experiment Results

The main objective of the experiment work is to validate the simulation models during no-load, low speed and over speed tests. In addition, the accuracy of each method to predict the temperature at different speed of the machine is determined. In the over speed test as per Siemens drive default settings machine is started at a 5Hz frequency which runs at 150RPM at ambient temperature 16.2-degree centigrade. 5 thermocouple temperature sensors have been located at different positions in the test machine. Three sensors are used for winding and their location is 120 mechanical degree apart and two sensors are located at stator outer body. The results of over speed test of all the parameters and temperature parameters are shown in Table 5-10 and

Table 5-11 respectively. The readings T1, T2, and T3 show the winding temperature whereas T4 and T5 is the stator outer body temperature. The speed is controlled from the input supply frequency from Siemens drive. It can be observed from the data reading that the T3 has the highest reading 33.1⁰C at the 15Hz frequency with 1650RPM. The remaining temperature readings are below maximum which reflects that the

machine the thermally stable. The graph of the bar chart also depicts the temperature reading under various frequency changes as shown in Fig. 5.21. The no-load experimental data of speed, current, voltage, power, power factor, harmonics, and vibration are shown in Table. 6-32. The corresponding photos of 3-phase current waveform, amperes, voltage and frequency values with total harmonics distortion and generated torque waveform are shown in Fig. 5.18. It is observed that initially, the machine has high vibration at low speed but, as the speed is increased, the machine is also stable which is very good in terms of mechanical point of view.

5.6.5 Electromagnetic Comparison Between FEM and Experimental Results.

The main electromagnetic design aspects of 24kW Synchronous Reluctance Motor are presented in the section. The type of rotor having 3-V shaped flux barriers is considered for numerical and experimental work is shown in Fig. 5.28. The rotor configuration is well suited for the in terms of electromagnetic performance. The thermal design aspects are already presented in the chapter 5. However additional electromagnetic performance in terms of speed, magnetic flux density, current and voltage properties are discussed in the section.

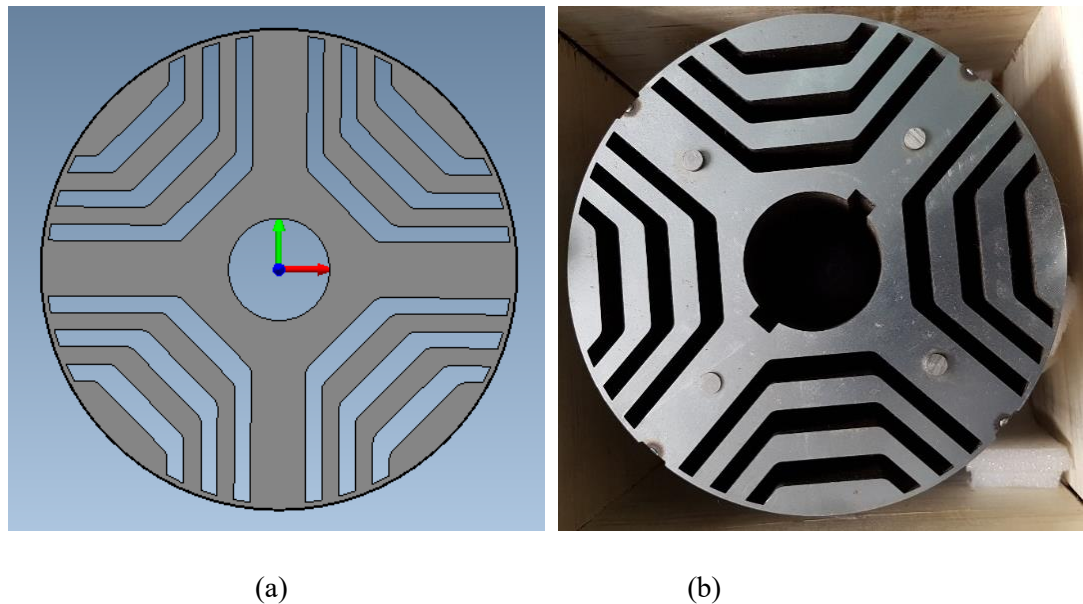


Fig. 5.28 V- Shape rotor of (a) numerically and (b) experimentally design

Generally, the performance of an electrical motor with electromagnetic design aspects is considered to be an independent phenomenon with respect to machine speed, and mostly the mechanical and thermal properties are dominated in the design. However, there is an increasing trend in matching both numerical and experimental electromagnetic performance to improve the accuracy of the design challenges.

The rotor of SynRM is traditionally manufactured by ALA (axially laminated anisotropy) and TLA (transverse laminated anisotropy). It has already been mentioned that the kind of ALA construction produces extra weight on the rotor and causes excessive flux leakages. Consequently, TLA type construction is the preference in most of the rotor construction while its capability to have good balancing, no vibration. As the main objective of this section is to illustrate the electromagnetic performances, so a time-stepping 2D FEM is chosen for discussion. In other words, speed, flux density, current and voltage results are taken into account in the analysis. The graph of FEM and Experiment results of speed is shown in Fig. 5.29. In the FEM model speed graph is taken after transient analysis and the date is taken from the speed results window from the *Infolytica Magnet* software. Usually the output speed results are in degree per second which are converted into RPM. In the experimental results, the speed is gradually varied by varying the input frequency of the Siemens drive. The speed signal is varied from 0 to 50Hz input frequency. The complete steps are already described in section 5.5.2. The discrepancy in the test results between simulation and experimental confirms the finite element simulation which shows the rotor comprised of 3-V shaped flux barrier design and 4 flux carriers works effectively. From the data analysis, there is a little bit difference between two results due to effect of end winding of two-dimensional finite element analysis. Fig. 5.30 shows the magnetic flux density in Tesla, and the complete data is shown in Table 6.36 (in the appendices).

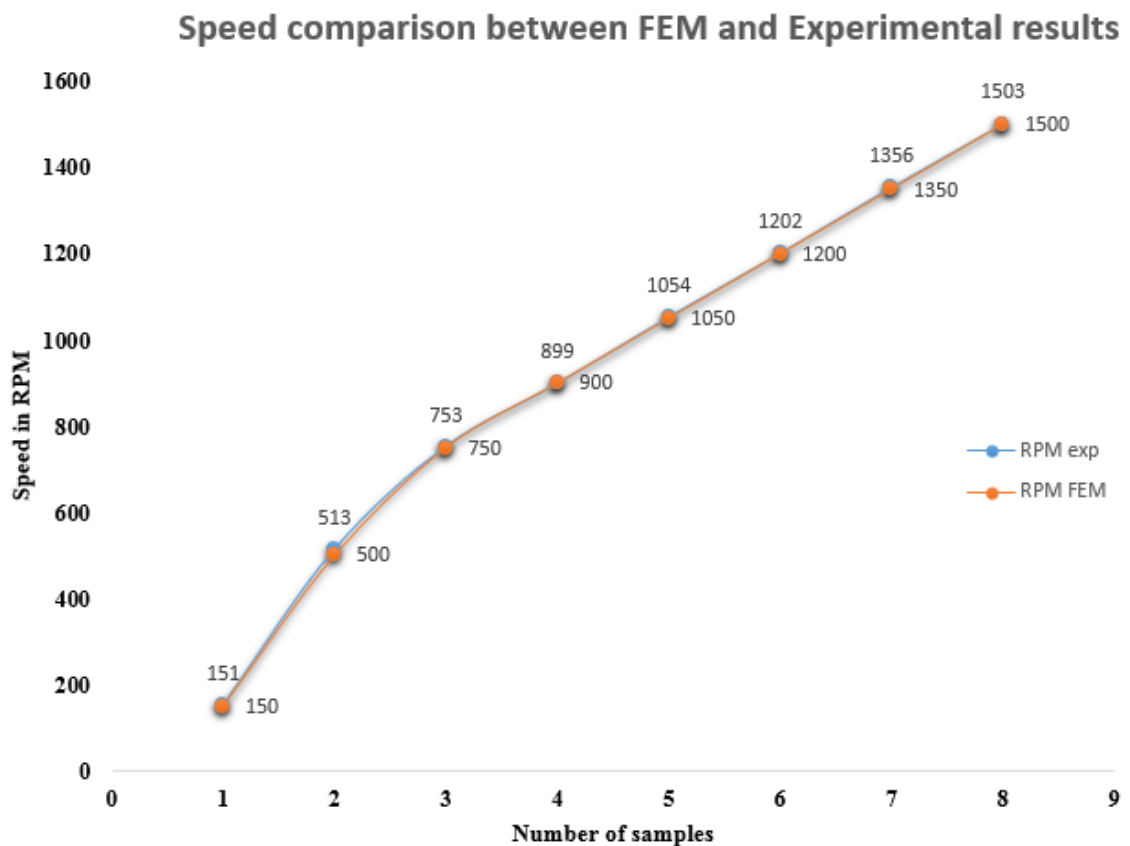


Fig. 5.29 Numerical and experiment speed results

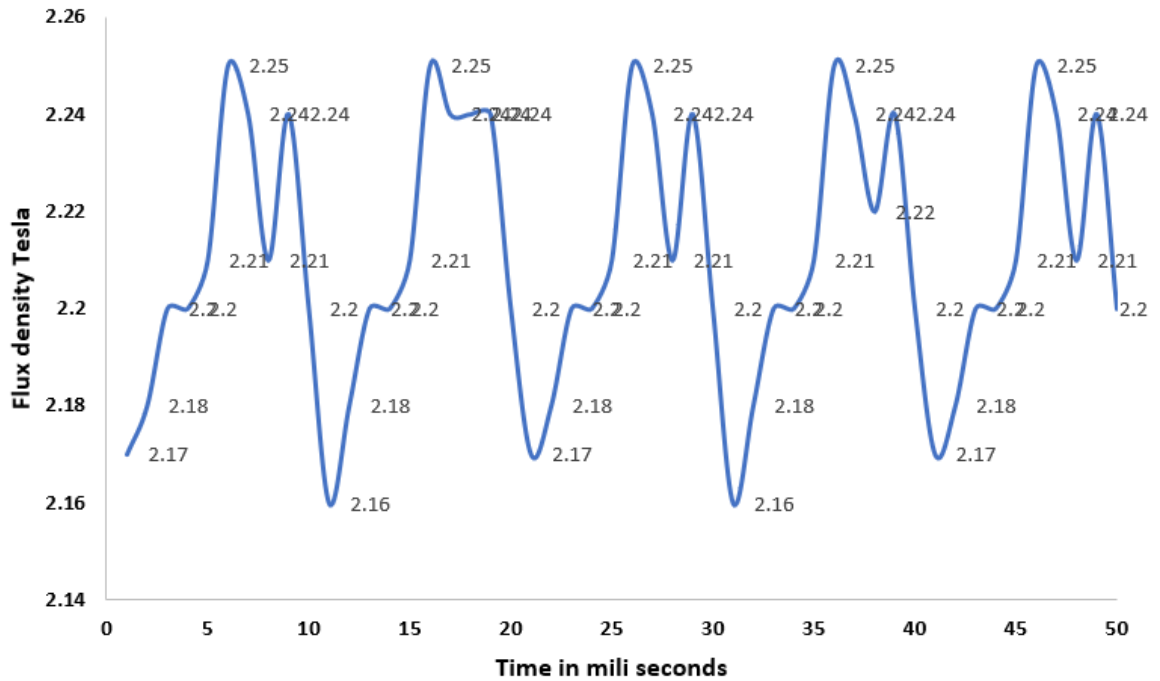


Fig. 5.30 Magnetic flux density vs time graph

A further test is carried out to measure the current and voltage of simulation and experimental results under several rotating speeds. The procedure for changing the speed in both simulation and experimental work is similar as described above. The RMS voltage and current of simulation and experimental results are plotted against speed as shown in Fig. 5.31 and Fig. 5.32 respectively.

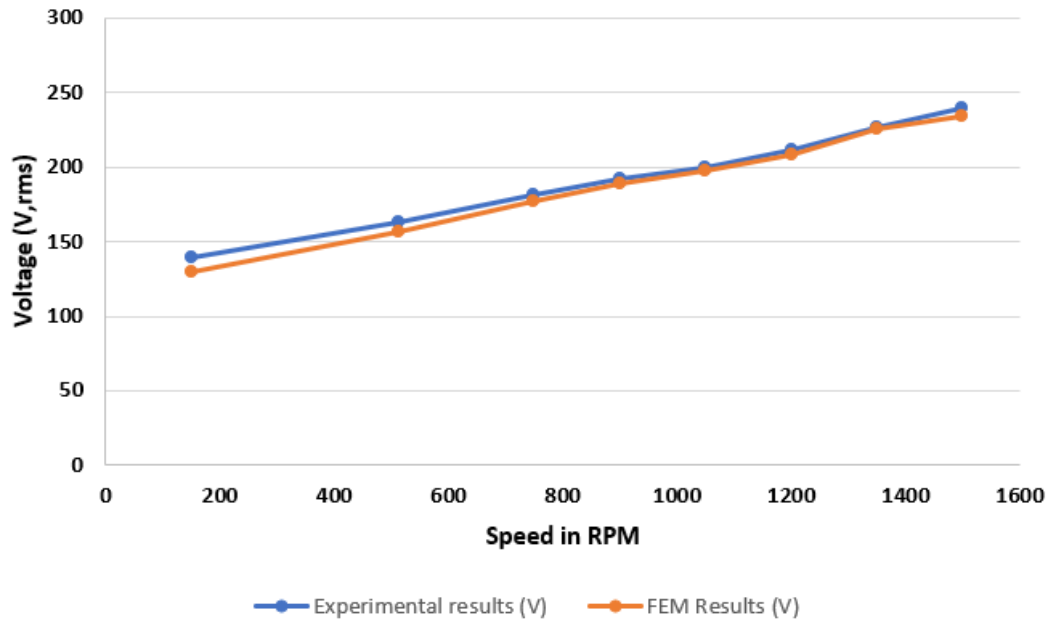


Fig. 5.31 Comparison of Numerical and experimental results of voltage vs speed

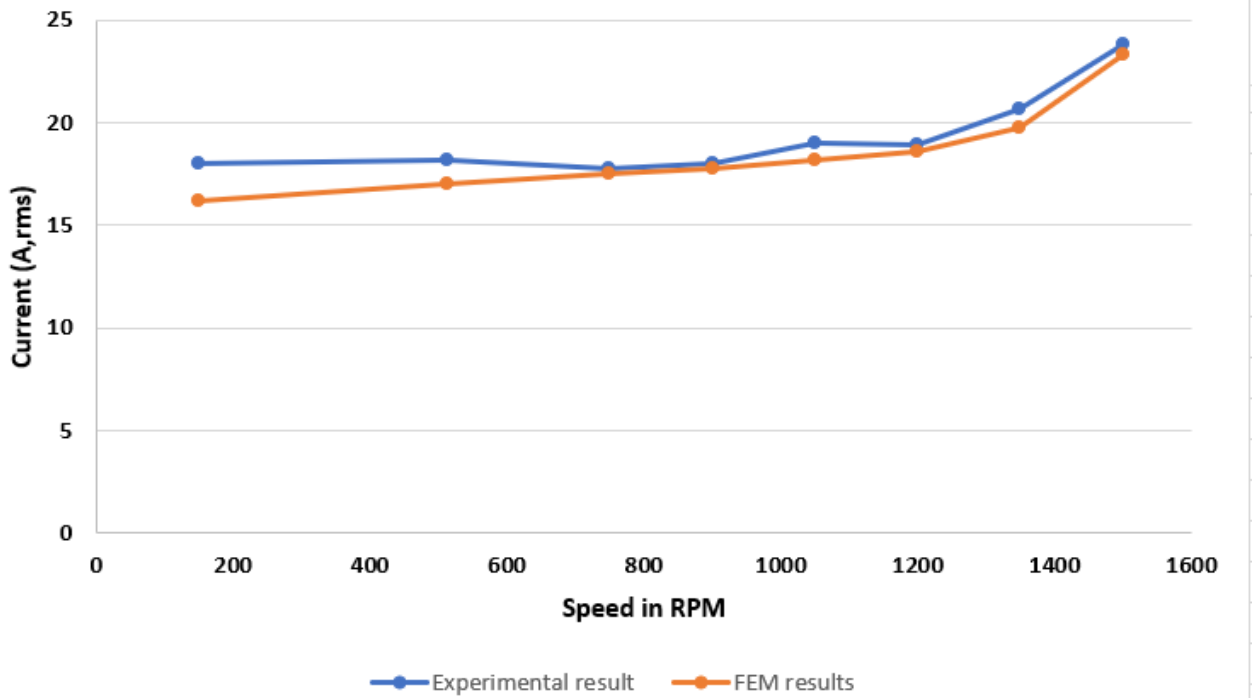


Fig. 5.32 Comparison of Numerical and experimental results of RMS current vs speed

In the experimental setup, the operation of variable speed is varied through the interval of 5Hz frequency with the control knob of the Siemens 440 drive. Each time the speed is measured through speed meter as depicted in Table- 6-31 row 4 (in the appendices). The maximum speed 1500rpm is achieved at 275 volts and the maximum speed is accomplished through experimental results and at 240 volts the 1500RPM is achieved by simulation results. The combined speed, voltage and current graph obtained by the experimental results are shown in Fig. 5.33, and the combined simulation results are shown in Fig. 5.34. It can be seen that due to end winding resistance the experimental voltage is slower than the simulation results. Additionally, the material characteristics incorporated into the simulation are not similar as compare to those of the actual material used in the manufactured rotor for experiment. Whereas the speed graph is almost the same in both simulation and experimental results. Since the speed, current and voltage results are influenced by the rotor design, so the optimisation gives effective results.

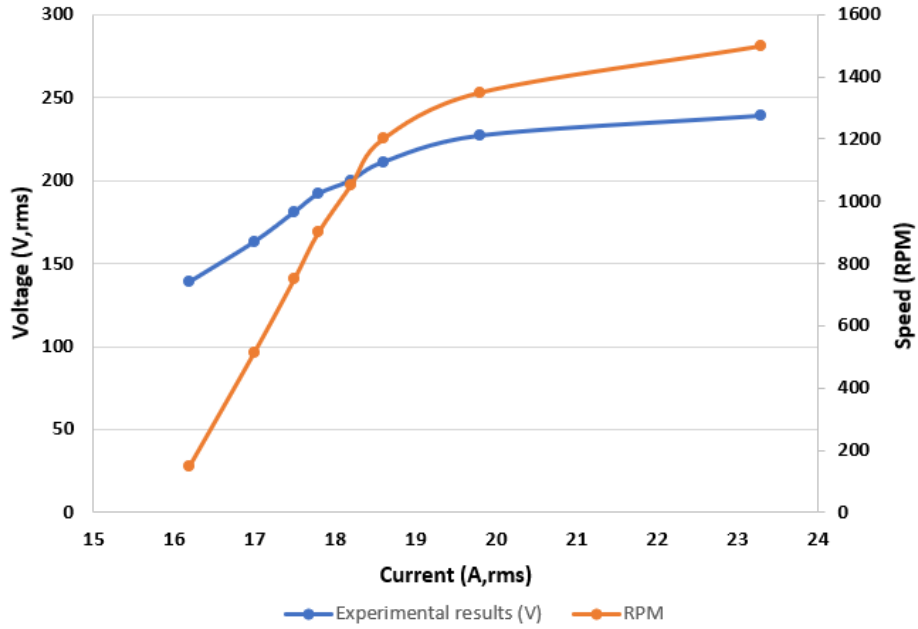


Fig. 5.33 Combined current, voltage and RPM graph of experimental results

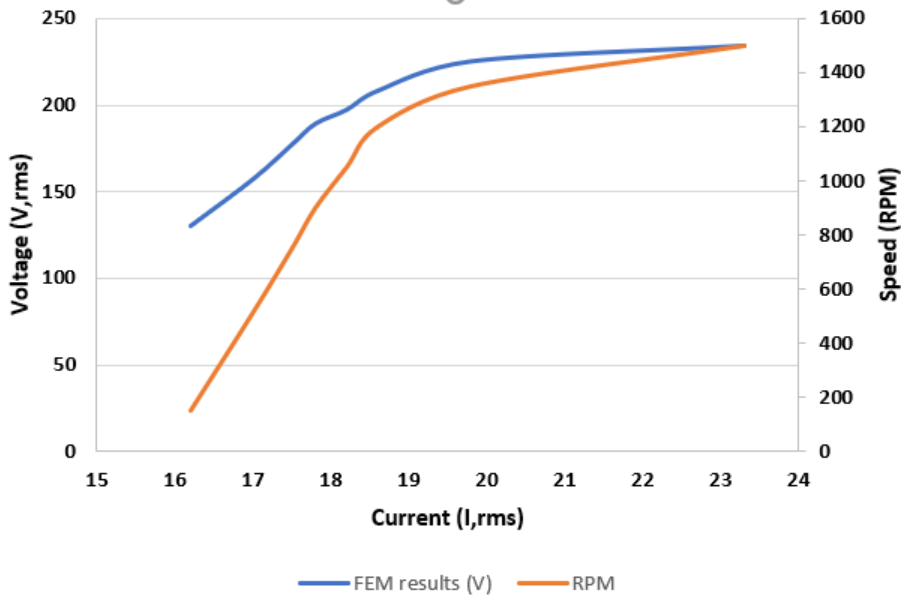


Fig. 5.34 Combined current, voltage and RPM graph of numerical results

5.7 Experimental verification of 72/48 Switched reluctance motor

The experiment test has been done to validate the developed design optimisation of 72/48 SRM. The fabricated machine is shown in Fig. 5.35. The design statements, which are described by the suggested optimisation, are listed in Fig. 4.48 and Table 4-7. The SRM is running at the loaded condition at the rated

105 rpm speed. The DC output phase current rating is 174 A, and bus voltage of 510V DC are used to excite the 72/48 SRM. The experimental test rig of 72/48 SRM is established as shown in Fig. 5.36.

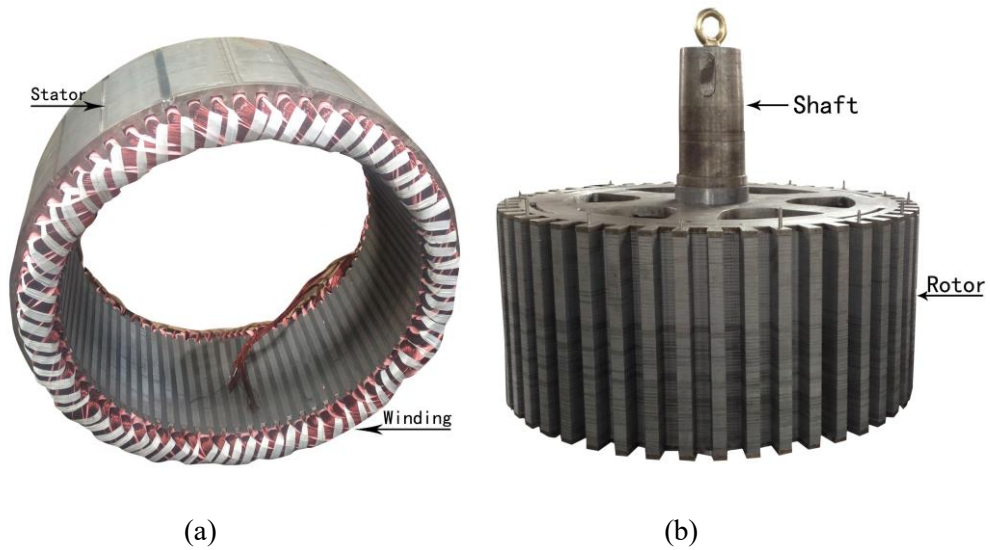


Fig. 5.35 fabrication of SRM (a) The stator (b) The rotor

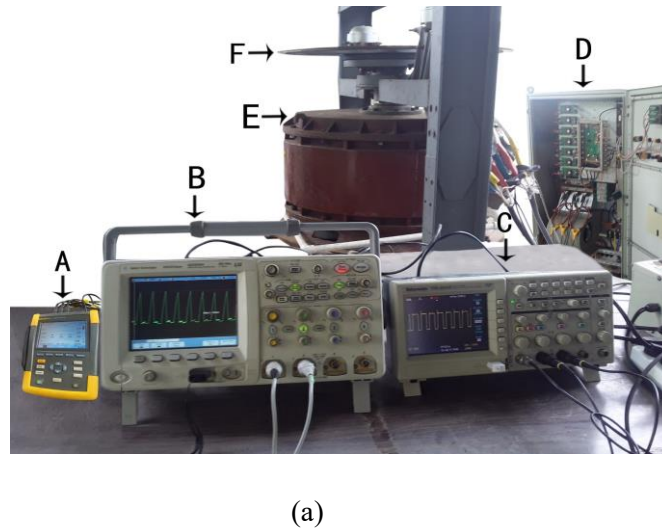


Fig. 5.36 The complete diagram of the experimental test bench

Different types of equipment are used to perform these experiments, which are an oscilloscope with a Hall sensor, three-phase power quality analyser (Fluke 434) is used to record the input and output. Optical digital tachometer (DT2234A) to measure the speed. The wave-forms of pulse-width from the testing are shown in Fig. 5.36. The no-load and load tests data results of 3 current waveforms are depicted in Fig. 5.37 and Fig. 5.38. There is a good balance, as the current waveform models are similar. The simulation and hardware results validate the performance. Table 5-14 shows the experimental results at 105rpm and 510 DC voltage

when loading conditions are varied. A Fluke power analyser (434) with three phases is used for determining the harmonics (THD) at the current supply is shown in Fig. 5.39. Table 5-15 shows an evaluation of the proposed SRM along with the existing IM drive. This shows that the projected design model provides enhanced performance and greater torque for the application of Raymond Pulveriser.

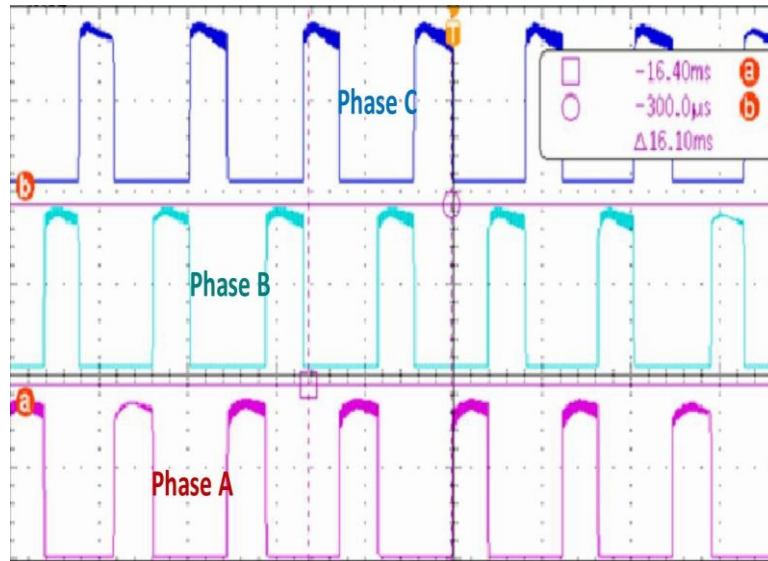


Fig. 5.37 Pulse width modulation waveform

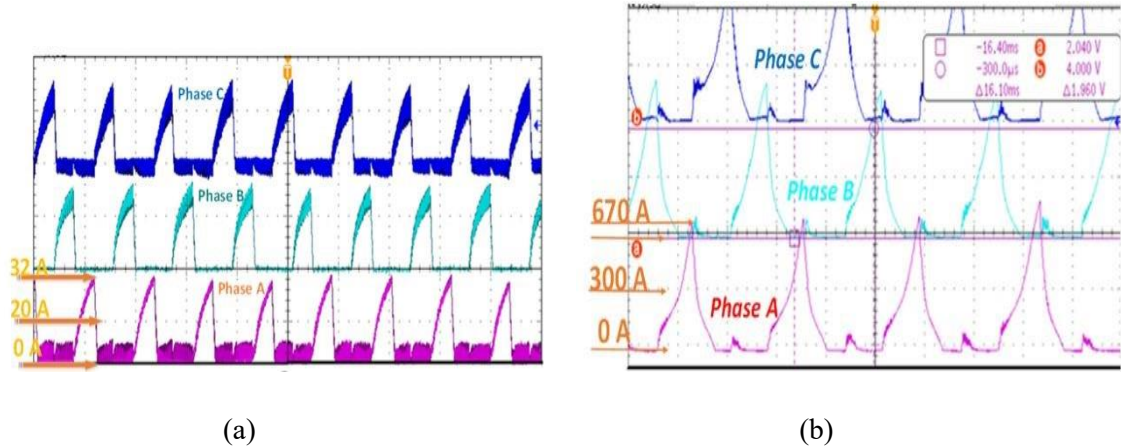


Fig. 5.38 Current waveform of a prototype of 72/48 SRM (a) No-load (b) Load

Table 5-14 Experimental results for loading test [43]

Parameters	DC Current in Amps	Losses in kW	Torque in kNm	Efficiency in (%)
Test No-1	5.01	2.5	0.005	2.3
Test No-2	11.15	2.8	0.262	50.7
Test No-3	12.88	2.94	0.330	55.2
Test No-4	57.1	3.95	2.32	86.4
Test No-5	85.7	4.813	3.56	88.9
Test No-6	114.3	5.95	4.78	89.7
Test No-7	171.5	8.59	7.20	90.19

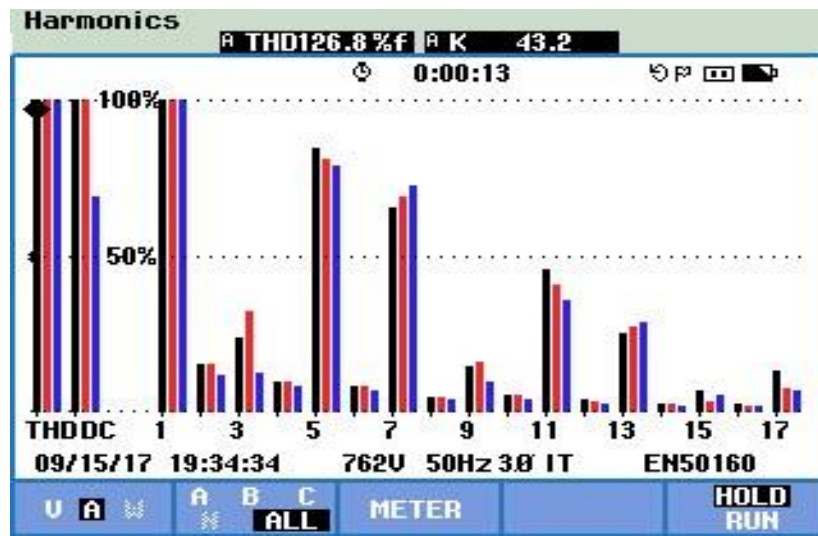


Fig. 5.39 The THD of the supply current [43]

Table 5-15 comparisons with the cost proposed the design of SRM and IM (2SIE 280 S4) for mining application

Parameters	System of Gear-Drive	Induction Motor (2SIE 280 S4)	Switched Reluctance Motor (Proposed)
Full load efficiency in %	59.32	94.2	90.19
Torque in kNm	7	0.481	7.28
Weight [kg]	1050	678	1180
Rate speed in rpm	105	1488	105
Motor Price in USD	1350	9000	12000
Power in kW	75	75	75

5.7.1 Electromagnetic Comparison of 72/48 SRM

In order to verify both simulation and experimental results of the proposed machine comprised of 72/48 SRM, an electromagnetic performance comparison is done in between current, torque, efficiency and power losses. Fig. 5.40 shows the graph of output current of the machine.

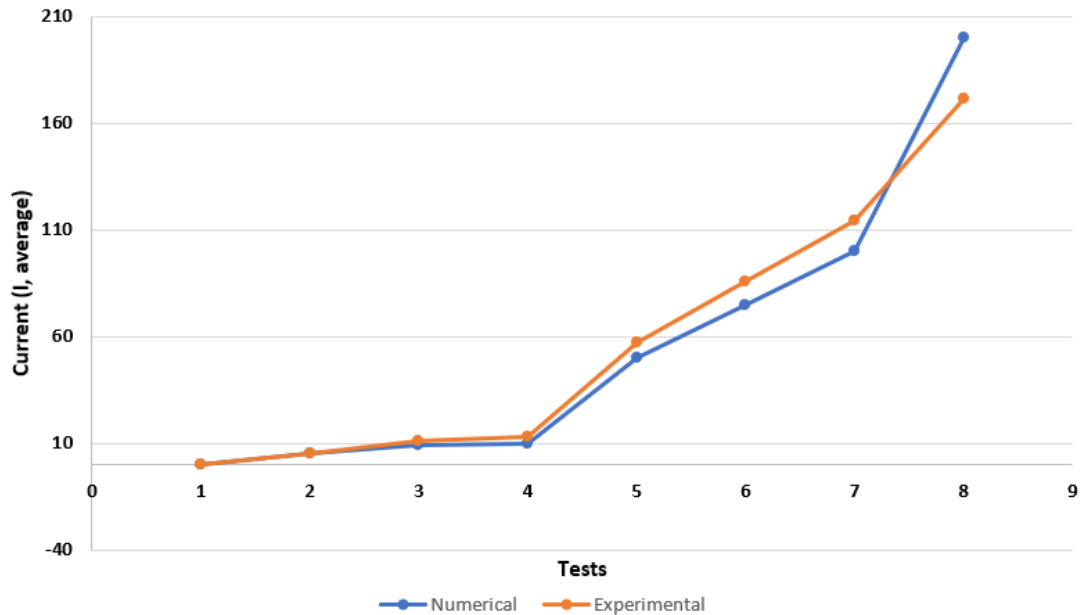


Fig. 5.40 Numerical and experimental results of the output current of 72/48 SRM

The load current is gradually increased from 0 to 200 Amps. The current drop is less sensitive by the variation of load in both simulation and experimental results. Therefore, in this case, current droopage is not significant. Hence, the proposed machine performs better under variable load. It should be noted that the current in simulation result is slightly higher than experiment due to absence of end winding. When a switched reluctance motor works at low speed having low load, a lower DC-link voltage is required to be used for reducing switching frequency, switching noise and switching losses. And for optimising chopping current waveform, at high speed, a higher DC-link voltage is used to reduce demagnetisation issues. It can be obtained from Fig. 5.41, total torque produced is more than 7kNm at full load. The operation under full load and both experimental results and FEA simulation provide similar pull-up torque. The amplitude of both simulation and experimental results verified the design. Fig. 5.42 shows a comparison between simulation and experimental efficiency. There is symmetry between simulation and experimental data. It can be seen that initially the efficiency is 50% up to test 3, whereas it is increased and reached 90% when the maximum load is applied. The outcome of the proposed machine confirms the excellent performance and diverse load conditions.

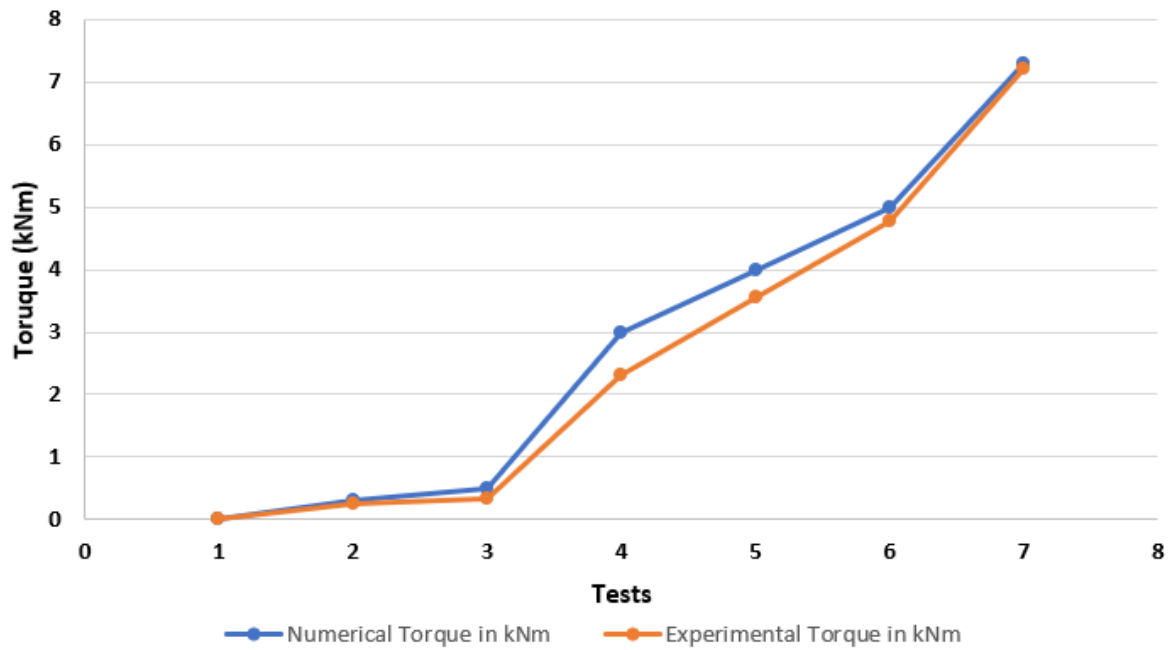


Fig. 5.41 Numerical and experimental results of the output torque of 72/48 SRM

Fig. 5.43 shows the simulation and experimental graph of power losses and the current graph. The overall power losses in experimental results are higher due to copper losses (I^2R losses). As the load current increases, the power losses become more. Thus, their possibility that the entire losses in the machine can be reduced by reducing the excessive I^2R losses. From the given analysis and experimental results, it can be proved that the proposed topology is feasible. However, the proposed topology has two disadvantages which need to have a particular consideration. One is the higher number of stator poles needs higher number of switches so the switching pattern. The solution is to have quick sequence of operations through converter such as asymmetrical bridge converter topology. The other is that the machine size is very heavy and bulky which contributes to high space and requirement which must be minimised. This thesis has also reduced the size of 1000mm machine to 500mm machine and verified both (SynRM and SRM). Whereas the compromised is made in torque produced and power ratings.

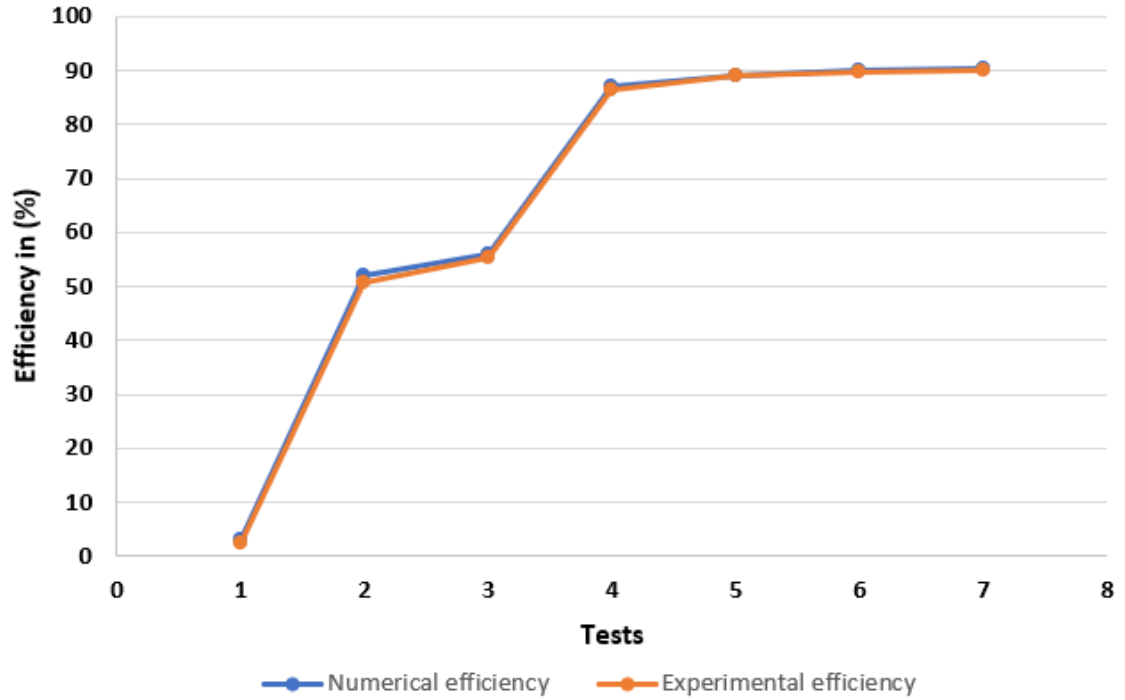


Fig. 5.42 Numerical and experimental results of efficiency of 72/48 SRM

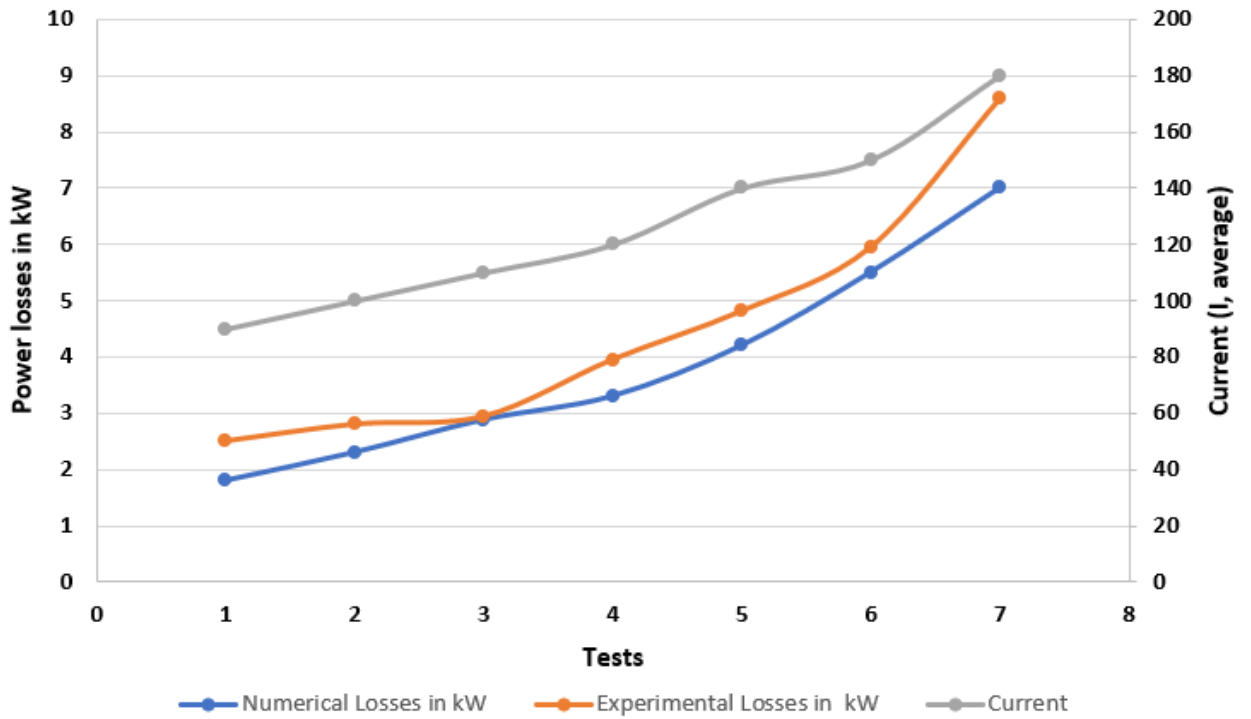


Fig. 5.43 Numerical and experimental results of power losses with respect to current of 72/48 SRM

5.8 Summary

In this chapter, the results obtained from both experiments and simulation tests are analysed. There is an agreement between both simulation and experimental results. The new rotor having 3 V-shaped is manufactured which is validated by the finite element predictions.

The SynRM rotor manufacturing process is thoroughly discussed along with the insertion of thermocouple inside of the Cummins stator. Additionally, filling of polyvinyl chloride material is thoroughly described which provides strong mechanical integrity and contribute to a better mechanical and thermal performance throughout the experiment. As it is also observed in the previous chapter 4 that, asymmetrical rotor geometry can also enhance the output torque, power, and efficiency which needs to be tested in rotor manufacturing. Apart from that, a no-load test, low-speed test, Overspeed test, and retardation test is conducted and analysed under different loading conditions. Furthermore, experimental testing of 72/48 SRM is carried out with effective current, torque, efficiency and power loss comparison. The data results show good performance of the machine.

Chapter 6 Conclusion and Future Work

The findings of this work are summarised in this chapter followed by an indication of the future work. Studies on SynRM design with different geometrical designs of the flux barriers, carriers together with the application of surrogate optimisation method have been carried out. The rotor designs are tested out in simulation and experiment for centrifugal pumps. A Surrogate-based particle swarm optimisation technique has been used for refining the machine design and providing a suitable geometrical setting of flux barriers and carriers. Different designs of the proposed machines have been analysed by varying the barrier shape, edge angle, and shaft diameter in order to reduce the power losses and torque ripples. The experimental results have validated the proposed approach and rotor designs in terms of effective thermal and mechanical performances of the machines.

6.1 Conclusions

This work has led to several research findings.

First of all, the related literature review has been presented in Chapter 2, and this has shown the type of electrical machine used for different industrial applications. Especially reluctance motors have huge potential for energy-efficient, magnet-free, and environmentally friendly machines. Additionally, the comparison between switched reluctance and synchronous reluctance machines for different industrial applications have been carried out. The stator design of SynRMs is similar to induction motors whereas the rotor design of SynRMs is related to the number of flux barrier shapes. A lot of research work has already been conducted on the design topologies of the SynRMs design. Nowadays, induction motors are used for the Raymond Pulveriser and Centrifugal pump applications, which have geared drive systems. They are designed to operate for a wide range of speed, so the problem of IMs is that they have excessive rotor losses and are not designed and run efficiently at the best operating points. As the Synchronous reluctance motor has the stator similar to IMs and the solid rotor is used, there are no rotor power losses. In this thesis, new rotor designs for the Raymond Pulveriser and centrifugal pump are proposed.

In terms of the manufacturing of rotor, the Computerised Numerical Control (CNC) router was selected as the cutting technology method. The technique of transversally laminated rotor was successful and this reduced the manufacturing efforts in low dimensions. The main advantages of using this technology were ease of use for the manufacturer and the ability to achieve very high tolerance. However, there was a disadvantage, which was only one lamination property (M350-steel) material was available to use. Additionally, there was an option to manufacture the rotor from laser cutting but, considerations by three electrical steel supplied (JFE Steel, Japan; L&H Components, UK; Tata Steel UK) have warned that laser

cutting can generate more local heating in a material which may lead to bigger edge effect in the lamination stacks, possibly reducing permeability and increasing iron losses in the material. In addition to this, the balancing of the rotor using washers bolted into the rotor end caps/discs was also a successful method and will be used in future motor design and manufacturing.

Further, the study of direct-drive carried out. The key advantages of direct-drive have reduced the cost of installation. This correspondingly enhances the system response due to the elimination of gear and repair and lubrication costs. It has been observed experimentally that the symmetrical rotor can improve the effective thermal and mechanical performance of the machine and can be beneficial for some applications which are uni-directional in machine operations, as this work is targeted.

In chapter 3, three direct-drive synchronous reluctance motors are designed and optimised for Raymond Pulveriser. Their performance is analysed in terms of power losses, efficiency, torque and torque ripple. Initially, stator and rotor designs are conducted for a 10kW motor with 24 and 36 slots square and round flux barriers. Also, the ends of flux barriers have been examined. Overall, 420 samples have been tested for the final design for a symmetrical rotor design. A Surrogate-based particle swarm optimisation technique is developed to aid in the design of the motor and its optimisation on the width of flux barrier and carriers. Different designs of the proposed machines have been studied by varying the barrier shape, edge angle, and the shaft diameter in order to reduce the losses and torque ripple. In the following design, a 12/8 SRM has been thoroughly investigated as per the suitability of the application requirements. The most influencing parameters considered for the design are stator pole arc, stator yoke width, stator inner diameter, rotor pole arc, rotor yoke width, air gap, rotor outer diameter, and shaft diameter. Similarly, the technique was applied to get the best parameters of the 12/8 SRM. The main consideration in the design of a synchronous reluctance machine is potentially high torque ripple, causing unwanted noise and vibration. The SBO provided a number of stepping stones to the development of more complex optimisation process such as 5 to 7 flux barriers rotor design. The design which offered the best objective function in the optimisation was found to be magnetically saturated. Therefore, a new design is carried out in FEM by changing these parameters by trial-and-error around the previous optimised range. While selecting the optimised 3 flux barriers and 4 flux carriers, the proposed rotor design technique from the surrogate models has the best performance to meet the design requirements. The SBO has proven to be of value and so should be applied to the other machines. However, the FEM based on velocity driven analysis has been discussed in this thesis which is limited to the certain rated speed and cannot be considered for dynamic effects. For example, the load driven analysis at higher electrical frequencies-based process is required for the optimisation. In addition to distributed winding, it is beneficial to adopt fractional slots concentrated windings in the proposed SynRM.

- The synchronous reluctance motor (SynRM) and switched reluctance motor (SRM) are optimised based on surrogate models in an aim to achieve high efficiency under the maximum torque for low-speed direct-drive mining applications and for closed coupled centrifugal pumps. Designs of experiment (DOE) techniques were presented, whilst one of these the Latin hypercube sampling (LHS) was selected to generate the random and uniform sampling distributions. Sensitivity analysis (SA) was carried out to identify important independent design variables (IDV). The SMs of the reluctance machines' performance is constructed using LHS and Kriging modeling. The Particle Swarm Optimisation (PSO) based SMs techniques are adopted to optimise the machines. The optimisation results have been successfully validated using the finite element analysis (FEA). The computational cost of the proposed technique of optimisations based on SMs is lower than the conventional optimal design techniques based on an FEA, without sacrificing the precision of the SRM design. The 3 V-shape SynRM is evaluated in 2D FEA software and validated by experiments. A 2D FEA and experimental outcomes show that the SynRM direct-drive has better characteristics to replacement the conventional motor option in close-coupled centrifugal pumps.
- Two design shapes (Square and Round) have been tested for the flux barriers in synchronous reluctance rotor. Under the same design constraints, the square shape gives 2%, 7% higher efficiency and torque respectively.
- It has been observed that besides the design parameters, the slot filling factor has a great influence on machine performance in terms of efficiency, out torque and power. In the first optimisation process, the filling factor is kept 65% which gives 83.9% efficiency and 788.6Nm torque at 10.32kW of power. If the slot filling factor is reduced by 52.9% then efficiency is reduced by 2.2% and approximately 13% of the machine torque is reduced. This should be noted that the above optimisation process is done on distributed winding, however fractional slot concentrated winding can be compared with distributed winding and efficiency analysis can be further explored.
- For 10kW SynRM with 3 square shape flux barriers, under the same design parameters has 0.076% higher efficiency as compared to 4 flux barriers. Additionally, the torque is also improved by 3.37% with 4.22% higher power. In addition to this, synchronous reluctance motor comparison between single layer and double winding for Raymond Pulveriser should be done. If the number of poles is also considered into account, then this would be more effective design process.

In chapter 4, the FEM simulation of all the three machines with symmetrical and asymmetrical rotor designs and their effects on energy efficiency and torque ripple has been analysed. In the asymmetrical rotor, as the flux barrier length is decreased then energy, torque, power, efficiency and torque ripple is varied. The different round and square stator slot shapes have been refined and numerically analysed.

- The rotor design method which is based on asymmetrical pole structure is presented in this study. As all the flux barriers have equal lines of symmetry and identical and allow a quarter section of this machine to be modeled on Infolytica magnet software. This effectively reduces the calculation and computational time and optimisation process as compare to complete the model design. Although the design strategy has proven to be effective in reducing torque ripple, but two different rotor geometries of flux barriers and carriers having different numbers can be optimised and then manufactured separately, which actually leads to an increase the calculation efforts and manufacturing expense, but also can increase the reliability of the design and characteristics of the machine. Thus, as per the requirement of this work, 2D FEM analysis is an effective tool for the optimisation of the rotor, care should be taken at a higher speed to make some allowance for a 3D effect.
- It is should be noted that the increase in flux barrier width beyond limit reduces the efficiency and torque in the rotor design. An increase of 1.5mm flux barrier width may reduce 3.96% efficiency and 3.45% torque in the machine. The value of magnetic flux density is different during simulation running from 0 to 500 milliseconds. At the end of simulation the tesla value is lower than the starting value, this can be analysed more precisely in further research.
- In asymmetrical rotor design, the 10.29% torque ripple can be minimised if the flux barrier length is reduced to 20mm. Additionally, 2.75% of efficiency is enhanced, In this way, 2.058% average torque is also enhanced whereas if the objective function is to increase the torque then decreased flux barrier at 12mm, can improve the torque at 0.36% more.

In Chapter 5, a 24kW synchronous reluctance motor is prototyped and experimental results validate the numerical designs for a centrifugal pump. The manufacturing and assembling process has been described as step by step. The variable frequency drive and its setup of Siemens and ABB drives for the test machine are also described. Overall, the 3-phase synchronous reluctance motor design with three flux barriers design may offer low torque ripple, thermally stable and efficiency benefits. The Surrogate-based particle swarm optimisation technique is an efficient tool for the machine design and providing a suitable width of flux barriers, the barriers shapes, edge angle and shaft diameter for efficiency and torque improvement.

- The proposed rotor has been tested on a distributed winding stator which relatively contains a high number of slots (36 slots in Cummins stator). Which achieved a fairly low value of torque ripple without skewing. This leads to additional savings in manufacturing costs and improves machine

performance. Whereas, additional rotor skewing, for concentrated winding machine torque ripple below 5% are obtainable. For improving the mechanical strength, flux barriers are filled with magic epoxy and polyvinylchloride was also successful, this overall increased the mechanical integrity of the rotor.

- In the 72/48 SRM for mining applications, the proposed motor design could increase 7.28kNm torque and 90.19% efficiency, which is much higher than the existing IM drives (59.32%). Therefore, switched reluctance motor has a capability to be used as an alternative of induction motors in mining (Raymond Pulverising) direct-drive applications. The surrogate-based particle swarm optimisation technique is applied to a 10kW 12/8 SRM and SynRM, which can output 694Nm Torque and 89.6% efficiency at 8052kW power output optimised with the same technique, the synchronous reluctance motor design has power output rating 9.6kW with 802Nm torque and 91.01% efficiency. It may be concluded that the synchronous reluctance motor has better output than an equivalent switched reluctance motor, presumably due to the full-wave generating a field of three-phase in SynRM. Additionally, a comparison between 12/8 and 18/12 machine can be further explored and optimised under same machine dimensions and efficiency and torque can be enhanced for the application of Raymond Pulveriser.
- The construction of the 3V-shaped flux barriers and 4 flux carriers synchronous reluctance rotor provided the validation of the FEM results. The electromagnetic performance of the assembled motor matches specifications. However, over this diameter of the constructed rotor's performance was reduced due to the effect of machining. The machining process was essential to maintain the accurate outer diameter of the rotor but give rise to some power losses.

6.2 Future Work

Based on this work, a few areas can be further explored.

- Although some FEM design investigation has been carried out in the symmetrical rotor design can be improved by a combination of conventional FEM and the proposed surrogate-optimization technique.
- Hybrid rotor design may be developed to insert a small permanent magnet into 3 flux barriers. This will increase the flux density.
- Comparison between SRM and SynRM using Magnet, Motor solver and Maxwell is useful for Raymond Pulveriser machine in terms of torque and efficiency.

- In the place of the 55kW motor, the synchronous generator can be used to test the load torque of the machine.
- In this thesis, the Reluctance machine (both SynRM and SrM) is compared for Raymond Pulveriser but for closed coupled centrifugal pump only the SynRM has been compared whereas, SRM needs to be compared as well.
- Synchronous reluctance motor comparison between single layer and double layer winding for Raymond Pulveriser.
- Synchronous reluctance motor comparison between different numbers of poles such as 4 poles, 6 poles, and 8 poles through design in motor solver and imported into a magnet for Raymond Pulveriser.

REFERENCES

- [1] A. Salisu, L. Akanni, and A. Ogbonna, "Forecasting CO2 emissions: Does the choice of estimator matter?," 2018.
- [2] E. L. Owusu, "The relationship between energy consumption, CO2 emission, population growth and economic growth: An empirical multivariate causal linkage from Ethiopia," *ECONOMICS AND POLICY OF ENERGY AND THE ENVIRONMENT*, 2018.
- [3] A. Anbarzadeh and R. Tahavvori, "Sustainable Development by Green Engineering Materials," *Journal of Environmental Friendly Materials*, vol. 3, pp. 49-53, 2019.
- [4] A. Abdulai, "Simon Brand Memorial Address: The challenges and adaptation to climate change by farmers in Sub-Saharan Africa," *Agrekon*, vol. 57, pp. 28-39, 2018.
- [5] S. Cooper-Searle, F. Livesey, and J. M. Allwood, "Why are Material Efficiency Solutions a Limited Part of the Climate Policy Agenda? An application of the Multiple Streams Framework to UK policy on CO2 emissions from cars," *Environmental Policy and Governance*, vol. 28, pp. 51-64, 2018.
- [6] Y. Li, Y. Lin, J. Zhao, B. Liu, T. Wang, P. Wang, *et al.*, "Control of NO x emissions by air staging in small-and medium-scale biomass pellet boilers," *Environmental Science and Pollution Research*, pp. 1-13, 2019.
- [7] E. Beagle and E. Belmont, "Comparative life cycle assessment of biomass utilization for electricity generation in the European Union and the United States," *Energy Policy*, vol. 128, pp. 267-275, 2019.
- [8] M. Ehsani, Y. Gao, S. Longo, and K. Ebrahimi, *Modern electric, hybrid electric, and fuel cell vehicles*: CRC press, 2018.
- [9] M. Höök, "Mapping Chinese supply," *Nature Energy*, vol. 3, p. 166, 2018.
- [10] S. Singer, J.-P. Denruyter, and D. Yener, "The energy report: 100% renewable energy by 2050," in *Towards 100% Renewable Energy*, ed: Springer, 2017, pp. 379-383.
- [11] I. Energy and C. Change, "World Energy Outlook Special Report (2015)," *C) OECD/IEA*, p. 37, 2017.
- [12] C. J. Dalhammar and J. L. Richter, "Interdisciplinary Research on Energy Efficiency Standards and Climate Change Mitigation: Methods, Results, and Communication," in *University Initiatives in Climate Change Mitigation and Adaptation*, ed: Springer, 2019, pp. 333-350.
- [13] V. Prakht, V. Dmitrievskii, and V. Kazakbaev, "Developing and experimental study a 1.5 kW synchronous reluctance motor of ultra premium efficiency (IE5 class)," in *Power and Electrical Engineering of Riga Technical University (RTUCON), 2017 IEEE 58th International Scientific Conference on, 2017*, pp. 1-5.
- [14] F. Bua, L. Martirano, L. Cristaldi, L. Mongiovì, C. Lavecchia, and M. Liziero, "Standardization framework on energy efficiency measuring and monitoring," in *Environment and Electrical Engineering and 2017 IEEE Industrial and Commercial Power Systems Europe (EEEIC/I&CPS Europe), 2017 IEEE International Conference on, 2017*, pp. 1-5.
- [15] R. K. Dixon, E. McGowan, G. Onysko, and R. M. Scheer, "US energy conservation and efficiency policies: Challenges and opportunities," *Energy Policy*, vol. 38, pp. 6398-6408, 2010.
- [16] E. Union, "Directive 2009/28/EC of the European Parliament and of the Council of 23 April 2009 on the promotion of the use of energy from renewable sources and amending and subsequently repealing Directives 2001/77/EC and 2003/30/EC," *Official Journal of the European Union*, vol. 5, p. 2009, 2009.
- [17] J. D. Widmer, R. Martin, and M. Kimiabeigi, "Electric vehicle traction motors without rare earth magnets," *Sustainable Materials and Technologies*, vol. 3, pp. 7-13, 2015.

- [18] S. Parry and E. Douglas, "In China, the true cost of Britain's clean, green wind power experiment: Pollution on a disastrous scale| Mail Online," *MailOnline*. <http://www.dailymail.co.uk/home/moslive/article-1350811/In-China-true-cost-Britains-clean-green-wind-power-experiment-Pollution-disastrous-scale.html> (accessed March 5, 2012), 2011.
- [19] J. Pyrhonen, T. Jokinen, and V. Hrabovcova, *Design of rotating electrical machines*: John Wiley & Sons, 2009.
- [20] T. J. E. Miller, *Electronic control of switched reluctance machines*: Newnes, 2001.
- [21] J. Gao, H. Sun, L. He, Y. Dong, and Y. Zheng, "Optimization design of switched reluctance motor based on particle swarm optimization," in *Electrical Machines and Systems (ICEMS), 2011 International Conference on*, 2011, pp. 1-5.
- [22] X. Xue, K. W. E. Cheng, T. W. Ng, and N. C. Cheung, "Multi-objective optimization design of in-wheel switched reluctance motors in electric vehicles," *IEEE Transactions on industrial electronics*, vol. 57, pp. 2980-2987, 2010.
- [23] Syed Abid ali Shah Bukhari, WenPing Cao, Tiejiang Yuan, and Kamran Ahmed Samo, "Design and Comparative Investigation of a 12/8 and A 6/4 Switched Reluctance Machines for Electric Vehicles," *INTERNATIONAL JOURNAL OF ENGINEERING SCIENCES & RESEARCH TECHNOLOGY*, vol. 6, p. 13, 25-8-2017 2017.
- [24] M. Gamba, G. Pellegrino, and A. Vagati, "Design of non conventional Synchronous Reluctance machine," 2018.
- [25] M. Palmieri, M. Perta, F. Cupertino, and G. Pellegrino, "Effect of the numbers of slots and barriers on the optimal design of synchronous reluctance machines," in *Optimization of Electrical and Electronic Equipment (OPTIM), 2014 International Conference on*, 2014, pp. 260-267.
- [26] M. Degano, M. Carraro, and N. Bianchi, "Selection criteria and robust optimization of a traction PM-assisted synchronous reluctance motor," *IEEE Transactions on Industry Applications*, vol. 51, pp. 4383-4391, 2015.
- [27] F. N. Jurca and C. Martis, "Analysis of outer rotor synchronous reluctance motor for low-speed applications," in *Electrical Drives and Power Electronics (EDPE), 2017 19th International Conference on*, 2017, pp. 242-247.
- [28] N. Bianchi, E. Fornasiero, E. Carraro, S. Bolognani, and M. Castiello, "Electric vehicle traction based on a PM assisted synchronous reluctance motor," in *Electric Vehicle Conference (IEVC), 2014 IEEE International*, 2014, pp. 1-6.
- [29] S. Taghavi and P. Pillay, "A mechanically robust rotor with transverse-laminations for a synchronous reluctance machine for traction applications," in *Energy Conversion Congress and Exposition (ECCE), 2014 IEEE*, 2014, pp. 5131-5137.
- [30] M. Muteba, B. Twala, and D.-V. Nicolae, "Torque ripple minimization in synchronous reluctance motor using a sinusoidal rotor lamination shape," in *Electrical Machines (ICEM), 2016 XXII International Conference on*, 2016, pp. 606-611.
- [31] M. Sanada, K. Hiramoto, S. Morimoto, and Y. Takeda, "Torque ripple improvement for synchronous reluctance motor using an asymmetric flux barrier arrangement," *IEEE Transactions on Industry Applications*, vol. 40, pp. 1076-1082, 2004.
- [32] R. Saidur, "A review on electrical motors energy use and energy savings," *Renewable and sustainable energy reviews*, vol. 14, pp. 877-898, 2010.
- [33] R. Saidur, S. Mekhilef, M. B. Ali, A. Safari, and H. Mohammed, "Applications of variable speed drive (VSD) in electrical motors energy savings," *Renewable and sustainable energy reviews*, vol. 16, pp. 543-550, 2012.
- [34] N. Schachter, "Energy efficient speed control using modern variable frequency drives," *Publication CIMENTEC Engineering Ltd*, pp. 1-8.

- [35] M. Hannan, J. A. Ali, A. Mohamed, and A. Hussain, "Optimization techniques to enhance the performance of induction motor drives: A review," *Renewable and Sustainable Energy Reviews*, vol. 81, pp. 1611-1626, 2018.
- [36] A. Joseph and T. R. Chelliah, "A review of power electronic converters for variable speed pumped storage plants: Configurations, operational challenges, and future scopes," *IEEE Journal of Emerging and Selected Topics in Power Electronics*, vol. 6, pp. 103-119, 2018.
- [37] C. M. Franchi, *Electrical Machine Drives: Fundamental Basics and Practice*: CRC Press, 2019.
- [38] M. Barnes, *Practical variable speed drives and power electronics*: Newnes, 2003.
- [39] M. P. Kazmierkowski and H. Tunia, "Automatic control of converter-fed drives," *ELECTRONIC ENGINEERING*, vol. 4, p. 6, 1994.
- [40] H. Tanaka and H. Machida, "Half-toroidal traction-drive continuously variable power transmission," *Proceedings of the Institution of Mechanical Engineers, Part J: Journal of Engineering Tribology*, vol. 210, pp. 205-212, 1996.
- [41] W. Tong, *Mechanical design of electric motors*: CRC press, 2014.
- [42] N. Okaeme, "Automated robust control system design for variable speed drives," University of Nottingham, 2008.
- [43] E. Elhomdy, G. Li, J. Liu, A. A. S. Bukhari, and W.-P. Cao, "Design and Experimental Verification of a 72/48 Switched Reluctance Motor for Low-Speed Direct-Drive Mining Applications," *Energies*, vol. 11, p. 192, 2018.
- [44] M. A. Raj and A. Kavitha, "Effect of Rotor Geometry on Peak and Average Torque of External Rotor Synchronous Reluctance Motor (Ex-R SynRM) in comparison with Switched Reluctance Motor for Low Speed Direct Drive Domestic Application," *IEEE Trans. Ind. Appl.*, vol. 53, 2015.
- [45] M. Suzuki, "Direct drive technology and its impact on gearmotor business," *Power Transmission Engineering*, 2009.
- [46] N. Matsui, T. Makino, and H. Satoh, "Autocompensation of torque ripple of direct drive motor by torque observer," *IEEE Transactions on Industry Applications*, vol. 29, pp. 187-194, 1993.
- [47] M. Sanada, S. Morimoto, and Y. Takeda, "Interior permanent magnet linear synchronous motor for high-performance drives," *IEEE transactions on industry applications*, vol. 33, pp. 966-972, 1997.
- [48] T. M. Jahns and W. L. Soong, "Pulsating torque minimization techniques for permanent magnet AC motor drives-a review," *IEEE transactions on industrial electronics*, vol. 43, pp. 321-330, 1996.
- [49] F. Meier, "Permanent-magnet synchronous machines with non-overlapping concentrated windings for low-speed direct-drive applications," KTH, 2008.
- [50] T. A. Lipo, "Synchronous reluctance machines-a viable alternative for AC drives?," *Electric Machines and Power Systems*, vol. 19, pp. 659-671, 1991.
- [51] T. Miller, A. Hutton, C. Cossar, and D. A. Staton, "Design of a synchronous reluctance motor drive," *IEEE Transactions on industry applications*, vol. 27, pp. 741-749, 1991.
- [52] A. Vagati, A. Fratta, G. Franceschini, and P. Rosso, "AC motors for high-performance drives: a design-based comparison," *IEEE Transactions on Industry Applications*, vol. 32, pp. 1211-1219, 1996.
- [53] A. Boglietti, A. Cavagnino, M. Pastorelli, and A. Vagati, "Experimental comparison of induction and synchronous reluctance motors performance," in *Industry Applications Conference, 2005. Fourtieth IAS Annual Meeting. Conference Record of the 2005*, 2005, pp. 474-479.
- [54] T. Finken, M. Felden, and K. Hameyer, "Comparison and design of different electrical machine types regarding their applicability in hybrid electrical vehicles," in *2008 18th International Conference on Electrical Machines*, 2008, pp. 1-5.

- [55] S. Yammine, C. Henaux, M. Fadel, S. Desharnais, and L. Calégari, "Synchronous reluctance machine flux barrier design based on the flux line patterns in a solid rotor," in *Electrical Machines (ICEM), 2014 International Conference on*, 2014, pp. 297-302.
- [56] P. S. Ghahfarokhi, A. Belahcen, A. Kallaste, T. Vaimann, L. Gerokov, and A. Rassolkin, "Thermal Analysis of a SynRM Using a Thermal Network and a Hybrid Model," in *2018 XIII International Conference on Electrical Machines (ICEM)*, 2018, pp. 2682-2688.
- [57] E. Howard, M. J. Kamper, and S. Gerber, "Asymmetric flux barrier and skew design optimization of reluctance synchronous machines," *IEEE Transactions on Industry Applications*, vol. 51, pp. 3751-3760, 2015.
- [58] S. Taghavi and P. Pillay, "A sizing methodology of the synchronous reluctance motor for traction applications," *IEEE Journal of Emerging and Selected Topics in Power Electronics*, vol. 2, pp. 329-340, 2014.
- [59] R.-R. Moghaddam, F. Magnussen, and C. Sadarangani, "Novel rotor design optimization of synchronous reluctance machine for low torque ripple," in *2012 XXth International Conference on Electrical Machines*, 2012, pp. 720-724.
- [60] N. Bianchi, S. Bolognani, D. Bon, and M. Dai PrÉ, "Torque harmonic compensation in a synchronous reluctance motor," *IEEE Transactions on energy conversion*, vol. 23, pp. 466-473, 2008.
- [61] D. Staton, T. Miller, and S. Wood, "Maximising the saliency ratio of the synchronous reluctance motor," in *IEE Proceedings B (Electric Power Applications)*, 1993, pp. 249-259.
- [62] M. Kamper and A. Volsdhenk, "Effect of rotor dimensions and cross magnetisation on Ld and Lq inductances of reluctance synchronous machine with cageless flux barrier rotor," *IEE Proceedings-Electric Power Applications*, vol. 141, pp. 213-220, 1994.
- [63] J. Ikaheimo, J. Kolehmainen, T. Kansakangas, V. Kivela, and R. R. Moghaddam, "Synchronous high-speed reluctance machine with novel rotor construction," *IEEE Transactions on Industrial Electronics*, vol. 61, pp. 2969-2975, 2014.
- [64] M. E. H. Zaim, "High-speed solid rotor synchronous reluctance machine design and optimization," *IEEE Transactions on Magnetics*, vol. 45, pp. 1796-1799, 2009.
- [65] H. Hofmann and S. R. Sanders, "High-speed synchronous reluctance machine with minimized rotor losses," *IEEE Transactions on Industry Applications*, vol. 36, pp. 531-539, 2000.
- [66] Y. Gessese and A. Binder, "Axially slitted, high-speed solid-rotor induction motor technology with copper end-rings," in *Electrical Machines and Systems, 2009. ICEMS 2009. International Conference on*, 2009, pp. 1-6.
- [67] I. Boldea, Z. Fu, and S. Nasar, "Performance evaluation of axially-laminated anisotropic (ALA) rotor reluctance synchronous motors," *IEEE transactions on industry applications*, vol. 30, pp. 977-985, 1994.
- [68] D. Platt, "Reluctance motor with strong rotor anisotropy," in *Industry Applications Society Annual Meeting, 1990., Conference Record of the 1990 IEEE*, 1990, pp. 224-229.
- [69] D. Platt, "Reluctance motor with strong rotor anisotropy," *IEEE transactions on industry applications*, vol. 28, pp. 652-658, 1992.
- [70] M. J. Kamper, F. Van der Merwe, and S. Williamson, "Direct finite element design optimisation of the cageless reluctance synchronous machine," *IEEE Transactions on Energy Conversion*, vol. 11, pp. 547-555, 1996.
- [71] S. M. Taghavi and P. Pillay, "A mechanically robust rotor with transverse laminations for a wide-speed-range synchronous reluctance traction motor," *IEEE Transactions on Industry Applications*, vol. 51, pp. 4404-4414, 2015.
- [72] J. Kostko, "Polyphase reaction synchronous motors," *Journal of the American Institute of Electrical Engineers*, vol. 42, pp. 1162-1168, 1923.

- [73] L. Pan, P. Liu, L. Ma, and Z. Li, "A supply chain based assessment of water issues in the coal industry in China," *Energy Policy*, vol. 48, pp. 93-102, 2012.
- [74] M. S. Roni, S. D. Eksioğlu, E. Searcy, and K. Jha, "A supply chain network design model for biomass co-firing in coal-fired power plants," *Transportation Research Part E: Logistics and Transportation Review*, vol. 61, pp. 115-134, 2014.
- [75] J. Carvalho Jr, M. Wang, N. Miller, B. Daniel, and B. Zinn, "Controlling mechanisms and performance of coal burning Rijke type pulsating combustors," in *Symposium (International) on Combustion*, 1985, pp. 2011-2017.
- [76] G. Lodhi, "Operation and Maintenance of Crusher House for Coal Handling in Thermal Power Plant.," *International Journal Of Mechanical Engineering And Robotics Research*, vol. 2, pp. 449-455, 2013.
- [77] A. Williams, M. Pourkashanian, and J. Jones, "Combustion of pulverised coal and biomass," *Progress in energy and combustion science*, vol. 27, pp. 587-610, 2001.
- [78] T. Uslu, E. Sahinoglu, and M. Yavuz, "Desulphurization and deashing of oxidized fine coal by Knelson concentrator," *Fuel Processing Technology*, vol. 101, pp. 94-100, 2012.
- [79] M. G. Valix, D. J. Harris, I. W. Smith, and D. L. Trimm, "The intrinsic combustion reactivity of pulverised coal chars: The use of experimental pore diffusion coefficients," in *Symposium (International) on Combustion*, 1992, pp. 1217-1223.
- [80] [Http://www.arvos-group.com](http://www.arvos-group.com). (accessed on 1 September 2017). *Raymond Mills. On-line available*.
- [81] J. Jung, S. Ulbrich, and W. Hofmann, "Design process of a high torque density direct drive involving a transverse flux machine," in *Electrical Machines (ICEM), 2014 International Conference on*, 2014, pp. 1096-1102.
- [82] M. Ilic, R. Marino, S. Peresada, and D. Taylor, "Feedback linearizing control of switched reluctance motors," *IEEE Transactions on Automatic Control*, vol. 32, pp. 371-379, 1987.
- [83] R. S. Wallace and D. G. Taylor, "Low-torque-ripple switched reluctance motors for direct-drive robotics," *IEEE transactions on robotics and automation*, vol. 7, pp. 733-742, 1991.
- [84] A. Ray, "Design and Performance Evaluation of Switched Reluctance Machines with Higher Number of Rotor Poles for Low Power Propulsion Applications," 2013.
- [85] H. Mahdavian, "A smart motor drive system for domestic and industrial applications," Victoria University of Technology, 2001.
- [86] N. Hashemnia and B. Asaei, "Comparative study of using different electric motors in the electric vehicles," in *Electrical Machines, 2008. ICEM 2008. 18th International Conference on*, 2008, pp. 1-5.
- [87] M. Yildirim, M. Polat, and H. Kürüm, "A survey on comparison of electric motor types and drives used for electric vehicles," in *Power Electronics and Motion Control Conference and Exposition (PEMC), 2014 16th International*, 2014, pp. 218-223.
- [88] H. Chen and D. Zhang, "The switched reluctance motor drive for the direct-drive joint of the robot," in *Robotics and Automation, 2001. Proceedings 2001 ICRA. IEEE International Conference on*, 2001, pp. 1439-1443.
- [89] R. Krishnan, *Switched reluctance motor drives: modeling, simulation, analysis, design, and applications*: CRC press, 2001.
- [90] M. Harris and T. E. Miller, "Comparison of design and performance parameters in switched reluctance and induction motors," in *Electrical Machines and Drives, 1989. Fourth International Conference on*, 1989, pp. 303-307.
- [91] S. Shoujun, L. Weiguo, D. Peitsch, and U. Schaefer, "Detailed design of a high speed switched reluctance starter/generator for more/all electric aircraft," *Chinese Journal of Aeronautics*, vol. 23, pp. 216-226, 2010.

- [92] G.-I. Jeong, Z. Xu, and J.-W. Ahn, "Design of SRM considering dual drive modes," in *Industrial Technology (ICIT), 2014 IEEE International Conference on*, 2014, pp. 872-876.
- [93] R. Krishnan, R. Arumugan, and J. F. Lindsay, "Design procedure for switched-reluctance motors," *IEEE Transactions on Industry Applications*, vol. 24, pp. 456-461, 1988.
- [94] C. M. Donaghy-Spargo, "Synchronous reluctance motors with fractional slot-concentrated windings," Newcastle University, 2016.
- [95] M. Gamba, G. Pellegrino, A. Cavagnino, Z. Gmyrek, and M. Lefik, "Rotor end effects on FEM-based flux mapping of synchronous reluctance motors," in *Electric Machines and Drives Conference (IEMDC), 2017 IEEE International*, 2017, pp. 1-7.
- [96] M. Mohammadi, T. Rahman, R. Silva, M. Li, and D. Lowther, "A computationally efficient algorithm for rotor design optimization of synchronous reluctance machines," *IEEE Transactions on Magnetics*, vol. 52, pp. 1-4, 2016.
- [97] T. Matsuo and T. A. Lipo, "Rotor design optimization of synchronous reluctance machine," *IEEE Transactions on Energy Conversion*, vol. 9, pp. 359-365, 1994.
- [98] C. Donaghy-Spargo, "Synchronous reluctance motor technology: opportunities, challenges and future direction," *Engineering & technology reference.*, pp. 1-15, 2016.
- [99] S. Neusüs and A. Binder, "Design of a synchronous reluctance rotor for the stator of an 11 kW induction machine," *e & i Elektrotechnik und Informationstechnik*, vol. 135, pp. 177-186, 2018.
- [100] S. Neusüs and A. Binder, "Shaping and dimensioning of the flux barriers in synchronous reluctance machines," in *Optimization of Electrical and Electronic Equipment (OPTIM) & 2017 Intl Aegean Conference on Electrical Machines and Power Electronics (ACEMP), 2017 International Conference on*, 2017, pp. 509-516.
- [101] R. Rajabi Moghaddam, "Synchronous reluctance machine (SynRM) in variable speed drives (VSD) applications," KTH Royal Institute of Technology, 2011.
- [102] A. Vagati, M. Pastorelli, G. Franceschini, and C. Petrace, "Design of low-torque-ripple synchronous reluctance motors," in *Industry Applications Conference, 1997. Thirty-Second IAS Annual Meeting, IAS'97., Conference Record of the 1997 IEEE*, 1997, pp. 286-293.
- [103] A. Vagati, G. Franceschini, I. Marongiu, and G. Troglia, "Design criteria of high performance synchronous reluctance motors," in *Industry Applications Society Annual Meeting, 1992., Conference Record of the 1992 IEEE*, 1992, pp. 66-73.
- [104] K. Cheng, Y. Yeung, C. Tang, X. Xue, and D. Sutanto, "Topology analysis of switched reluctance drives for electric vehicles," in *Power Electronics and Variable Speed Drives, 2000. Eighth International Conference on (IEE Conf. Publ. No. 475)*, 2000, pp. 512-517.
- [105] A. Emadi, *Energy-Efficient Electric Motors, Revised and Expanded*: CRC Press, 2018.
- [106] P. Cochran, *Polyphase induction motors, analysis: design, and application*: CRC Press, 2018.
- [107] S. Aryza, M. Irwanto, Z. Lubis, A. P. U. Siahaan, R. Rahim, and M. Furqan, "A Novelty Design of Minimization of Electrical Losses in A Vector Controlled Induction Machine Drive," in *IOP Conference Series: Materials Science and Engineering*, 2018, p. 012067.
- [108] J. Yuan, D. Meng, G. Lian, J. Zhang, H. Li, and F. Ban, "The Stator Slot-Type Optimization of Electrical Excitation Flux-Switching Motor and Its Maximum Torque/Copper Loss Control," *IEEE Transactions on Applied Superconductivity*, vol. 29, pp. 1-5, 2019.
- [109] E. A. Klingshirn and H. E. Jordan, "Polyphase induction motor performance and losses on nonsinusoidal voltage sources," *IEEE Transactions on Power Apparatus and Systems*, pp. 624-631, 1968.
- [110] J. G. Zhu, S. Hui, and V. Ramsden, "A generalized dynamic circuit model of magnetic cores for low- and high-frequency applications. I. Theoretical calculation of the equivalent core loss resistance," *IEEE Transactions on Power Electronics*, vol. 11, pp. 246-250, 1996.

- [111] E. Cardelli, L. Fiorucci, and E. Della Torre, "Estimation of MnZn ferrite core losses in magnetic components at high frequency," *IEEE transactions on magnetics*, vol. 37, pp. 2366-2368, 2001.
- [112] Y. Zhang, P. Pillay, M. Ibrahim, and M.-C. Cheng, "Magnetic characteristics and core losses in machine laminations: High-frequency loss prediction from low-frequency measurements," *IEEE transactions on industry applications*, vol. 48, pp. 623-629, 2011.
- [113] K. Anderson, J. Lin, and A. Wong, "Experimental and Numerical Study of Windage Losses in the Narrow Gap Region of a High-Speed Electric Motor," *Fluids*, vol. 3, p. 22, 2018.
- [114] Y. Gai, M. Kimiabeigi, Y. C. Chong, J. D. Widmer, X. Deng, M. Popescu, *et al.*, "Cooling of Automotive Traction Motors: Schemes, Examples, and Computation Methods," *IEEE Transactions on Industrial Electronics*, vol. 66, pp. 1681-1692, 2018.
- [115] L. Chang, "Comparison of ac drives for electric vehicles-A report on experts' opinion survey," *IEEE Aerospace and Electronic Systems Magazine*, vol. 9, pp. 7-11, 1994.
- [116] H. Akimoto, "Overview of Policy Actions and Observational Data for PM2. 5 and O3 in Japan: A Study of Urban Air Quality Improvement in Asia," 2017.
- [117] A. K. Amegah and S. Agyei-Mensah, "Urban air pollution in Sub-Saharan Africa: Time for action," *Environmental Pollution*, vol. 220, pp. 738-743, 2017/01/01/ 2017.
- [118] D. Hagstedt, F. Marquez, and M. Alakula, "A comparison between PMSM, EMSM and SMSM in a BAS application," in *Electrical Machines, 2008. ICEM 2008. 18th International Conference on*, 2008, pp. 1-5.
- [119] W. Cao, A. A. S. Bukhari, and L. Aarniovuori, "Review of Electrical Motor Drives for Electric Vehicle Applications," *Mehran University Research Journal of Engineering and Technology*, vol. 38, pp. 525-540, 2019.
- [120] T. M. Jahns and V. Blasko, "Recent advances in power electronics technology for industrial and traction machine drives," *Proceedings of the IEEE*, vol. 89, pp. 963-975, 2001.
- [121] A. G. Jack, B. C. Mecrow, and J. A. Haylock, "A comparative study of permanent magnet and switched reluctance motors for high-performance fault-tolerant applications," *IEEE transactions on industry applications*, vol. 32, pp. 889-895, 1996.
- [122] D. Diallo, M. E. H. Benbouzid, and A. Makouf, "A fault-tolerant control architecture for induction motor drives in automotive applications," *IEEE transactions on vehicular technology*, vol. 53, pp. 1847-1855, 2004.
- [123] E. Cornell, R. Guess, and F. Turnbull, "Advanced motor developments for electric vehicles," *IEEE Transactions on Vehicular Technology*, vol. 26, pp. 128-134, 1977.
- [124] T. Jahns, "Getting Rare-Earth Magnets Out of EV Traction Machines: A review of the many approaches being pursued to minimize or eliminate rare-earth magnets from future EV drivetrains," *IEEE Electrification Magazine*, vol. 5, pp. 6-18, 2017.
- [125] Y. Guan, Z. Q. Zhu, I. A. A. Afinowi, J. C. Mipo, and P. Farah, "Difference in maximum torque-speed characteristics of induction machine between motor and generator operation modes for electric vehicle application," *Electric Power Systems Research*, vol. 136, pp. 406-414, 2016/07/01/ 2016.
- [126] M. Zeraoulia, M. E. H. Benbouzid, and D. Diallo, "Electric motor drive selection issues for HEV propulsion systems: A comparative study," *IEEE Transactions on Vehicular technology*, vol. 55, pp. 1756-1764, 2006.
- [127] M. Guarnieri, "When cars went electric, part one [historical]," *IEEE Industrial Electronics Magazine*, vol. 5, pp. 61-62, 2011.
- [128] G. Dancygier and J.-C. Dolhagaray, "Motor control law and comfort law in the Peugeot and Citroen electric vehicles driven by a dc commutator motor," in *Power Electronics and Variable Speed Drives, 1998. Seventh International Conference on (Conf. Publ. No. 456)*, 1998, pp. 370-374.

- [129] S. Williamson, M. Lukic, and A. Emadi, "Comprehensive drive train efficiency analysis of hybrid electric and fuel cell vehicles based on motor-controller efficiency modeling," *IEEE Transactions on Power Electronics*, vol. 21, pp. 730-740, 2006.
- [130] D.-H. Cho, H.-K. Jung, and C.-G. Lee, "Induction motor design for electric vehicle using a niching genetic algorithm," *IEEE transactions on industry applications*, vol. 37, pp. 994-999, 2001.
- [131] W. Tiecheng, Z. Ping, Z. Qianfan, and C. Shukang, "Design characteristics of the induction motor used for hybrid electric vehicle," in *Electromagnetic Launch Technology, 2004. 2004 12th Symposium on*, 2005, pp. 523-527.
- [132] Z. Zhu and D. Howe, "Electrical machines and drives for electric, hybrid, and fuel cell vehicles," *Proceedings of the IEEE*, vol. 95, pp. 746-765, 2007.
- [133] M. A. Rahman and P. Zhou, "Analysis of brushless permanent magnet synchronous motors," *IEEE Transactions on Industrial Electronics*, vol. 43, pp. 256-267, 1996.
- [134] C. Chan, J. Jiang, G. Chen, X. Wang, and K. Chau, "A novel polyphase multipole square-wave permanent magnet motor drive for electric vehicles," *IEEE Transactions on Industry Applications*, vol. 30, pp. 1258-1266, 1994.
- [135] H. Weh, H. Mosebach, and H. May, "Design concepts and force generation in inverter-fed synchronous machines with permanent magnet excitation," *IEEE Transactions on Magnetics*, vol. 20, pp. 1756-1761, 1984.
- [136] J. G. West, "DC, induction, reluctance and PM motors for electric vehicles," *Power Engineering Journal*, vol. 8, pp. 77-88, 1994.
- [137] C. Chan, J. Jiang, G. Chen, X. Wang, and K. Chau, "A novel polyphase multipole square-wave permanent magnet motor drive for electric vehicles," in *Applied Power Electronics Conference and Exposition, 1993. APEC'93. Conference Proceedings 1993., Eighth Annual, 1993*, pp. 315-321.
- [138] L. Tang and G.-J. Su, "High-Performance Control of Two Three Phase Permanent Magnet Synchronous Machines in an Integrated Inverter for Automotive Applications," in *Power Electronics Specialists Conference, 2007. PESC 2007. IEEE, 2007*, pp. 2001-2007.
- [139] Y.-P. Yang and D.-S. Chuang, "Optimal design and control of a wheel motor for electric passenger cars," SAE Technical Paper 0148-7191, 2005.
- [140] N. Rahim, W. Hew, and A. Mahmoudi, "Axial-flux permanent-magnet brushless dc traction motor for direct drive of electric vehicle," *International Review of Electrical Engineering*, vol. 6, pp. 760-769, 2011.
- [141] C. Ma, Q. Li, L. Deng, C. Chen, Q. Liu, and H. Gao, "A Novel Sound Quality Evaluation Method of the Diagnosis of Abnormal Noise in Interior Permanent-Magnet Synchronous Motors for Electric Vehicles," *IEEE Transactions on Industrial Electronics*, vol. 64, pp. 3883-3891, 2017.
- [142] P. Dai, W. Sun, N. Xu, Y. Lv, and X. Zhu, "Research on energy management system of hybrid electric vehicle based on permanent magnet synchronous motor," in *Industrial Electronics and Applications (ICIEA), 2016 IEEE 11th Conference on*, 2016, pp. 2345-2349.
- [143] T. Takahashi, M. Takemoto, S. Ogasawara, W. Hino, and K. Takezaki, "Size and Weight Reduction of an In-Wheel Axial-Gap Motor Using Ferrite Permanent Magnets for Electric Commuter Cars," *IEEE Transactions on Industry Applications*, 2017.
- [144] A. Athavale, K. Sasaki, B. S. Gagas, T. Kato, and R. Lorenz, "Variable Flux Permanent Magnet Synchronous Machine (VF-PMSM) Design Methodologies to Meet Electric Vehicle Traction Requirements with Reduced Losses," *IEEE Transactions on Industry Applications*, 2017.
- [145] C. Espanet, J. Kauffmann, and R. Bernard, "Comparison of two in-wheel permanent magnet motors for military applications," in *Vehicle Power and Propulsion Conference, 2006. VPPC'06. IEEE, 2006*, pp. 1-6.

- [146] O. Ustun, M. Yilmaz, C. Gokce, U. Karakaya, and R. Tuncay, "Energy management method for solar race car design and application," in *Electric Machines and Drives Conference, 2009. IEMDC'09. IEEE International*, 2009, pp. 804-811.
- [147] M. Terashima, T. Ashikaga, T. Mizuno, K. Natori, N. Fujiwara, and M. Yada, "Novel motors and controllers for high-performance electric vehicle with four in-wheel motors," *IEEE Transactions on Industrial electronics*, vol. 44, pp. 28-38, 1997.
- [148] A. Lidozzi, L. Solero, F. Crescimbeni, and A. Di Napoli, "SVM PMSM drive with low resolution hall-effect sensors," *IEEE Transactions on Power Electronics*, vol. 22, pp. 282-290, 2007.
- [149] Q. Guo, C. Zhang, L. Li, D. Gerada, J. Zhang, and M. Wang, "Design and implementation of a loss optimization control for electric vehicle in-wheel permanent-magnet synchronous motor direct drive system," *Applied Energy*, 2017.
- [150] Z. Zhu and C. Chan, "Electrical machine topologies and technologies for electric, hybrid, and fuel cell vehicles," in *Vehicle Power and Propulsion Conference, 2008. VPPC'08. IEEE*, 2008, pp. 1-6.
- [151] P. P. Acarnley, R. J. Hill, and C. W. Hooper, "Detection of rotor position in stepping and switched motors by monitoring of current waveforms," *IEEE Transactions on Industrial Electronics*, pp. 215-222, 1985.
- [152] M. Ehsani, I. Husain, and A. B. Kulkarni, "Elimination of discrete position sensor and current sensor in switched reluctance motor drives," *IEEE Transactions on Industry Applications*, vol. 28, pp. 128-135, 1992.
- [153] S. R. MacMinn, W. J. Rzesos, P. M. Szczesny, and T. M. Jahns, "Application of sensor integration techniques to switched reluctance motor drives," *IEEE Transactions on Industry Applications*, vol. 28, pp. 1339-1344, 1992.
- [154] M. Ehsani, I. Husain, S. Mahajan, and K. Ramani, "New modulation encoding techniques for indirect rotor position sensing in switched reluctance motors," *IEEE Transactions on Industry Applications*, vol. 30, pp. 85-91, 1994.
- [155] I. Husain and M. Ehsani, "Rotor position sensing in switched reluctance motor drives by measuring mutually induced voltages," *IEEE Transactions on Industry Applications*, vol. 30, pp. 665-672, 1994.
- [156] J. Zhu, K. W. E. Cheng, X. Xue, and Y. Zou, "Design of a New High-Torque-Density In-Wheel Switched Reluctance Motor for Electric Vehicles," *IEEE Transactions on Magnetics*, 2017.
- [157] S. Abid Ali Shah Bukhari, Wenping Cao, Kamran Ahmed Samo, Zheng Liu and Shahzeb Ansari, "Electrical Motor Drive Technologies for Green Electric Vehicle: A Review," *Engineering Science and Technology International Research Journal*, vol. 1, pp. 1-10, 2017.
- [158] Z. Zhou, X. Sun, L. Chen, Z. Yang, S. Han, K. Li, *et al.*, "A segmented rotor type switched reluctance machine for BSGs of hybrid electric vehicles: Concept, design and analysis," in *Electrical Machines and Systems (ICEMS), 2017 20th International Conference on*, 2017, pp. 1-4.
- [159] N. Zabihi and R. Gouws, "A review on switched reluctance machines for electric vehicles," in *Industrial Electronics (ISIE), 2016 IEEE 25th International Symposium on*, 2016, pp. 799-804.
- [160] M. Ruba and D. Fodorean, "Motor-drive solution for light electric vehicles based on a switched reluctance machine," in *Automation, Quality and Testing, Robotics (AQTR), 2016 IEEE International Conference on*, 2016, pp. 1-6.
- [161] K. M. Rahman, B. Fahimi, G. Suresh, A. V. Rajarathnam, and M. Ehsani, "Advantages of switched reluctance motor applications to EV and HEV: Design and control issues," *IEEE transactions on industry applications*, vol. 36, pp. 111-121, 2000.
- [162] D. E. Cameron, J. H. Lang, and S. D. Umans, "The origin and reduction of acoustic noise in doubly salient variable-reluctance motors," *IEEE Transactions on Industry Applications*, vol. 28, pp. 1250-1255, 1992.

- [163] J. Lyu, K. Zhou, H. Rong, and F. Mao, "Design methodology of a multiplicity switched reluctance motor for a high performance direct-drive rotary table," *International Journal of Applied Electromagnetics and Mechanics*, pp. 1-17.
- [164] C. D. Gilmore, "Direct drive actuator with switched reluctance motor," ed: Google Patents, 2018.
- [165] W. A. Dorsett, J. B. Dillinger, M. J. Lyten, M. N. Barr, B. M. Neilson, and D. F. Owings, "Systems, methods, and apparatuses for storing energy in a mining machine," ed: Google Patents, 2018.
- [166] E. Bostanci, M. Moallem, A. Parsapour, and B. Fahimi, "Opportunities and Challenges of Switched Reluctance Motor Drives for Electric Propulsion: A Comparative Study," *IEEE Transactions on Transportation Electrification*, vol. 3, pp. 58-75, 2017.
- [167] A. Walker, M. Galea, D. Gerada, C. Gerada, A. Mebarki, and N. Brown, "Development and design of a high performance traction machine for the FreedomCar 2020 traction machine targets," in *Electrical Machines (ICEM), 2016 XXII International Conference on*, 2016, pp. 1611-1617.
- [168] A. Athavale, K. Sasaki, B. S. Gagas, T. Kato, and R. D. Lorenz, "Variable flux permanent magnet synchronous machine (VF-PMSM) design to meet electric vehicle traction requirements with reduced losses," in *2016 IEEE Energy Conversion Congress and Exposition (ECCE)*, 2016, pp. 1-8.
- [169] H. Li and K. W. Klontz, "Rotor design to reduce secondary winding harmonic loss for induction motor in hybrid electric vehicle application," in *Energy Conversion Congress and Exposition (ECCE), 2016 IEEE*, 2016, pp. 1-6.
- [170] N. Kunihiro, K. Nishihama, M. Iizuka, K. Sugimoto, and M. Sawahata, "Investigation into Loss Reduced Rotor Slot Structure by Analyzing Local Behaviors of Harmonic Magnetic Fluxes in Inverter-fed Induction Motor," *IEEE Transactions on Industry Applications*, 2016.
- [171] W. Li, J. Cao, and X. Zhang, "Electrothermal analysis of induction motor with compound cage rotor used for PHEV," *IEEE Transactions on industrial electronics*, vol. 57, pp. 660-668, 2010.
- [172] B. Burkhart, A. Klein-Hessling, I. Ralev, C. P. Weiss, and R. W. De Doncker, "Technology, research and applications of switched reluctance drives," *CPSS Transactions on Power Electronics and Applications*, vol. 2, pp. 12-27, 2017.
- [173] O. Argiolas, E. Nazeraj, O. Hegazy, J. De Backer, A. Mohammadi, and J. Van Mierlo, "Design optimization of a 12/8 Switched Reluctance Motor for electric and hybrid vehicles," in *Ecological Vehicles and Renewable Energies (EVER), 2017 Twelfth International Conference on*, 2017, pp. 1-10.
- [174] W. Uddin, T. Husain, Y. Sozer, and I. Husain, "Design Methodology of a Switched Reluctance Machine for Off-Road Vehicle Applications," *IEEE Transactions on Industry Applications*, vol. 52, pp. 2138-2147, 2016.
- [175] K. Koibuchi, T. Ohno, and K. Sawa, "A basic study for optimal design of switched reluctance motor by finite element method," *IEEE Transactions on Magnetics*, vol. 33, pp. 2077-2080, 1997.
- [176] A. Chiba, Y. Takano, M. Takeno, T. Imakawa, N. Hoshi, M. Takemoto, *et al.*, "Torque Density and Efficiency Improvements of a Switched Reluctance Motor Without Rare-Earth Material for Hybrid Vehicles," *IEEE Transactions on Industry Applications*, vol. 47, pp. 1240-1246, 2011.
- [177] Y. Hori, "Looking at cars 100 years in the future," in *Mechatronics (ICM), 2013 IEEE International Conference on*, 2013, pp. 31-35.
- [178] Y. Takano, M. Takeno, N. Hoshi, A. Chiba, M. Takemoto, S. Ogasawara, *et al.*, "Design and analysis of a switched reluctance motor for next generation hybrid vehicle without PM materials," in *Power Electronics Conference (IPEC), 2010 International*, 2010, pp. 1801-1806.
- [179] H.-C. Chiu, J.-H. Jang, W.-M. Yan, and R.-B. Shiao, "Thermal performance analysis of a 30 kW switched reluctance motor," *International Journal of Heat and Mass Transfer*, vol. 114, pp. 145-154, 2017.

- [180] K. Kiyota and A. Chiba, "Design of switched reluctance motor competitive to 60-kW IPMSM in third-generation hybrid electric vehicle," *IEEE Transactions on Industry Applications*, vol. 48, pp. 2303-2309, 2012.
- [181] M. Kawa, K. Kiyota, J. Furqani, and A. Chiba, "Acoustic noise reduction of a high efficiency switched reluctance motor for hybrid electric vehicles with novel current waveform," in *Electric Machines and Drives Conference (IEMDC), 2017 IEEE International*, 2017, pp. 1-6.
- [182] J. Furqani, M. Kawa, K. Kiyota, and A. Chiba, "Comparison of current waveforms for noise reduction in switched reluctance motors," in *Energy Conversion Congress and Exposition (ECCE), 2017 IEEE*, 2017, pp. 752-759.
- [183] Z. Omac, M. Polat, E. Öksüztepe, M. Yıldırım, O. Yakut, H. Eren, *et al.*, "Design, analysis, and control of in-wheel switched reluctance motor for electric vehicles," *Electrical Engineering*, pp. 1-12, 2017.
- [184] T. Miller, *Permanent Magnet and Reluctance Motor Drives*: Oxford, UK: Oxford Science Publications, 1989.
- [185] N. Rahim, H. W. Ping, and M. Tadjuddin, "Design of axial flux permanent magnet brushless DC motor for direct drive of electric vehicle," in *Power Engineering Society General Meeting, 2007. IEEE*, 2007, pp. 1-6.
- [186] Y.-P. Yang and D. S. Chuang, "Optimal design and control of a wheel motor for electric passenger cars," *IEEE Transactions on Magnetics*, vol. 43, pp. 51-61, 2007.
- [187] F. Profumo, Z. Zhang, and A. Tenconi, "Axial flux machines drives: A new viable solution for electric cars," *IEEE Transactions on Industrial Electronics*, vol. 44, pp. 39-45, 1997.
- [188] J. H. Kim, Y. Li, and B. Sarlioglu, "Novel six-slot four-pole axial flux-switching permanent magnet machine for electric vehicle," *IEEE Transactions on Transportation Electrification*, vol. 3, pp. 108-117, 2017.
- [189] Z. Jia, H. Lin, H. Yang, and C. Mi, "Transverse flux permanent magnet motor with double-C stator hoops and flux-concentrated rotor for in-wheel drive electric vehicle," in *Energy Conversion Congress and Exposition (ECCE), 2014 IEEE*, 2014, pp. 4804-4808.
- [190] Z. Wan, A. Ahmed, I. Husain, and E. Muljadi, "A novel transverse flux machine for vehicle traction applications," in *Power & Energy Society General Meeting, 2015 IEEE*, 2015, pp. 1-5.
- [191] K. M. Rahman, N. R. Patel, T. G. Ward, J. M. Nagashima, F. Caricchi, and F. Crescimbeni, "Application of direct-drive wheel motor for fuel cell electric and hybrid electric vehicle propulsion system," *IEEE Transactions on Industry Applications*, vol. 42, pp. 1185-1192, 2006.
- [192] Z. Yu and C. Jianyun, "Power factor analysis of transverse flux permanent machines," in *Electrical Machines and Systems, 2005. ICEMS 2005. Proceedings of the Eighth International Conference on*, 2005, pp. 450-459.
- [193] D.-c. Popa, V. Iancu, I.-a. Viorel, and L. Szabó, "ON THE DESIGN OF THE MODULAR LINEAR TRANSVERSE FLUX RELUCTANCE MOTORS," in *Proc. 6TH International Conference on Electromechanical and Power Systems*, 2007.
- [194] J. Gan, K. Chau, C. Chan, and J. Jiang, "A new surface-inset, permanent-magnet, brushless DC motor drive for electric vehicles," *IEEE Transactions on Magnetics*, vol. 36, pp. 3810-3818, 2000.
- [195] Z. Han, L. Guangyou, and S. Yuping, "Design and simulation of FRM as a vehicle-wheel motor," in *Electronics, Communications and Control (ICECC), 2011 International Conference on*, 2011, pp. 1992-1995.
- [196] C. Riley, N. Sawant, D. Ilea, A. Venskus, A. Bedford, A. Michaelides, *et al.*, "Simulation based design of reluctance motors for traction applications in hybrid and electric vehicles," in *Power Electronics, Machines and Drives (PEMD 2014), 7th IET International Conference on*, 2014, pp. 1-6.
- [197] I. Boldea, C. I. Pitic, C. Lascu, G.-D. Andreescu, L. Tutelea, F. Blaabjerg, *et al.*, "DTFC-SVM motion-sensorless control of a PM-assisted reluctance synchronous machine as starter-alternator for hybrid electric vehicles," *IEEE Transactions on Power Electronics*, vol. 21, pp. 711-719, 2006.

- [198] B. He, O. Ghattas, and J. F. Antaki, "Computational strategies for shape optimization of time-dependent Navier–Stokes flows," *Engineering Design Research Center, TR-CMU-CML-97-102, Carnegie Mellon Univ*, 1997.
- [199] D. L. Rodriguez, "Multidisciplinary optimization method for designing boundary-layer-ingesting inlets," *Journal of Aircraft*, vol. 46, pp. 883-894, 2009.
- [200] S. Kim, K. Leoviriyakit, and A. Jameson, "Aerodynamic shape and planform optimization of wings using a viscous reduced adjoint gradient formula," in *Second MIT Conference on Computational Fluid and Solid Mechanics at MIT, Cambridge, MA*, 2003.
- [201] S. Nadarajah, A. Jameson, and J. Alonso, "Sonic boom reduction using an adjoint method for wing-body configurations in supersonic flow," in *9th AIAA/ISSMO symposium on multidisciplinary analysis and optimization*, 2002, p. 5547.
- [202] S. K. Nadarajah, S. Kim, A. Jameson, and J. J. Alonso, "Sonic boom reduction using an adjoint method for supersonic transport aircraft configurations," in *IUTAM Symposium Transsonicum IV*, 2003, pp. 355-362.
- [203] T. J. Robinson, C. M. Borrer, and R. H. Myers, "Robust parameter design: a review," *Quality and Reliability Engineering International*, vol. 20, pp. 81-101, 2004.
- [204] L. Ilzarbe, M. J. Álvarez, E. Viles, and M. Tanco, "Practical applications of design of experiments in the field of engineering: a bibliographical review," *Quality and Reliability Engineering International*, vol. 24, pp. 417-428, 2008.
- [205] L. M. Kasankala, Y. Xue, Y. Weilong, S. D. Hong, and Q. He, "Optimization of gelatine extraction from grass carp (*Catenopharyngodon idella*) fish skin by response surface methodology," *Bioresource Technology*, vol. 98, pp. 3338-3343, 2007.
- [206] A. I. Khuri and S. Mukhopadhyay, "Response surface methodology," *Wiley Interdisciplinary Reviews: Computational Statistics*, vol. 2, pp. 128-149, 2010.
- [207] T. Yuan, N. Yang, W. Zhang, W. Cao, N. Xing, Z. Tan, *et al.*, "Improved Synchronous Machine Rotor Design for the Easy Assembly of Excitation Coils Based on Surrogate Optimization," *Energies*, vol. 11, p. 1311, 2018.
- [208] N. Yang, W. Cao, Z. Liu, Z. Tan, Y. Zhang, S. Yu, *et al.*, "Novel asymmetrical rotor design for easy assembly and repair of rotor windings in synchronous generators," in *Magnetics Conference (INTERMAG), 2015 IEEE*, 2015, pp. 1-1.
- [209] C. Kontoravdi, S. P. Asprey, E. N. Pistikopoulos, and A. Mantalaris, "Application of Global Sensitivity Analysis to Determine Goals for Design of Experiments: An Example Study on Antibody-Producing Cell Cultures," *Biotechnology progress*, vol. 21, pp. 1128-1135, 2005.
- [210] N. V. Queipo, R. T. Haftka, W. Shyy, T. Goel, R. Vaidyanathan, and P. K. Tucker, "Surrogate-based analysis and optimization," *Progress in aerospace sciences*, vol. 41, pp. 1-28, 2005.
- [211] Y. Mack, T. Goel, W. Shyy, and R. Haftka, "Surrogate model-based optimization framework: a case study in aerospace design," in *Evolutionary computation in dynamic and uncertain environments*, ed: Springer, 2007, pp. 323-342.
- [212] J.-P. Costa, L. Pronzato, and E. Thierry, "A comparison between Kriging and radial basis function networks for nonlinear prediction," in *NSIP*, 1999, pp. 726-730.
- [213] C. Ma, L. Qu, Z. Tan, X. Song, W. Cao, Z. Liu, *et al.*, "Multiobjective optimization of switched reluctance motors based on design of experiments and particle swarm optimization," *IEEE Transaction on Energy Conversion*, pp. 1144-1153, 2015.
- [214] G. G. Wang, "Adaptive response surface method using inherited latin hypercube design points," *Journal of Mechanical Design*, vol. 125, pp. 210-220, 2003.
- [215] Y. Duan and D. M. Ionel, "A review of recent developments in electrical machine design optimization methods with a permanent-magnet synchronous motor benchmark study," *IEEE Transactions on Industry Applications*, vol. 49, pp. 1268-1275, 2013.

- [216] X. Song, L. Lv, J. Li, W. Sun, and J. Zhang, "An advanced and robust ensemble surrogate model: extended adaptive hybrid functions," *Journal of Mechanical Design*, vol. 140, p. 041402, 2018.
- [217] X. Song, J. Zhang, S. Kang, M. Ma, B. Ji, W. Cao, *et al.*, "Surrogate-based analysis and optimization for the design of heat sinks with jet impingement," *IEEE Transactions on Components, Packaging and Manufacturing Technology*, vol. 4, pp. 429-437, 2014.
- [218] M. Juneja and S. Nagar, "Particle swarm optimization algorithm and its parameters: A review," in *2016 International Conference on Control, Computing, Communication and Materials (ICCCCM)*, 2016, pp. 1-5.
- [219] M. Ibrahim, P. Sergeant, and E. Rashad, "Simple design approach for low torque ripple and high output torque synchronous reluctance motors," *Energies*, vol. 9, p. 942, 2016.
- [220] A. Vagati, M. Pastorelli, G. Francheschini, and S. C. Petrache, "Design of low-torque-ripple synchronous reluctance motors," *IEEE Transactions on Industry Applications*, vol. 34, pp. 758-765, 1998.
- [221] R. Dobriyan, S. Vitolina, L. Lavrinovicha, and J. Dirba, "Theoretical and Experimental Research of Synchronous Reluctance Motor," *Latvian Journal of Physics and Technical Sciences*, vol. 54, pp. 38-47, 2017.
- [222] J. R. Claycomb, *Applied electromagnetics using QuickField and Matlab*: Laxmi Publications, Ltd., 2010.
- [223] M. Ruba, F. Jurca, L. Czumbil, D. D. Micu, C. Martis, A. Polycarpou, *et al.*, "Synchronous reluctance machine geometry optimisation through a genetic algorithm based technique," *IET Electric Power Applications*, pp. 431-438, 2017.
- [224] S. Nakano, K. Kiyota, and A. Chiba, "Design consideration of high torque-density switched reluctance motor for hybrid electrical vehicle," in *2016 19th International Conference on Electrical Machines and Systems (ICEMS)*, 2016, pp. 1-6.
- [225] T. Miller, "Switched Reluctance Motors and Their Control." Oxford: Magna Physics Publishing and Clarendon Press, 1993.
- [226] H. Hayashi, K. Nakamura, A. Chiba, T. Fukao, K. Tungpimolrut, and D. G. Dorrell, "Efficiency improvements of switched reluctance motors with high-quality iron steel and enhanced conductor slot fill," *IEEE Transactions on Energy Conversion*, vol. 24, pp. 819-825, 2009.

Appendices

Table 6-1 Initial 40 Latin Hypercube Samples with round slot shape for SynRM design

S, No	Air gap in mm	Slot depth in mm	Tooth width in mm	Shaft diameter	Flux Barrier width in mm	Barrier edge angle in °	Flux carrier width in mm	Slot openings in mm	Torq: in Nm	Eff: in %	Power in kW	Fill factor in %
1	0.93	50.3	15.4	111	11.6	34.4	14.6	7.22	7.22	794	88.9	9.82
2	0.65	55.5	12.3	121	12.3	38.4	15.2	7.42	7.42	794	86.5	10.1
3	0.78	52.5	13.3	127	12.7	40.8	15.6	7.54	7.54	827	87	10.4
4	0.58	50.7	14.1	63	8.24	15.2	11.7	6.26	6.26	661	90	8.06
5	0.72	51.7	16.6	77	9.21	20.8	12.6	6.54	6.54	684	91	8.25
6	0.70	53.3	12.7	119	12.16	37.6	15.1	7.38	7.38	746	88	9.32
7	0.80	56.9	16.3	101	10.90	30.4	14.0	7.02	7.02	701	89	8.64
8	0.73	55.3	13.9	110	14.26	49.6	16.9	7.98	7.98	808	87	10.1
9	0.77	58.9	13.8	120	13.56	45.6	16.3	7.78	7.78	777	86	9.83
10	0.84	58.3	13.6	79	9.36	21.6	12.7	6.58	6.58	630	87	7.95
11	0.63	54.5	15.8	71	8.80	18.4	12.2	6.42	6.42	660	90	8.0
12	0.91	51.1	12.1	69	8.66	17.6	12.1	6.38	6.38	629	87	7.9
13	0.82	58.7	15.3	145	13.98	48	16	7.9	7.9	772	87	9.7
14	0.56	59.5	13.0	117	12.02	36.8	15.0	7.34	7.34	743	87	9.39
15	0.51	55.9	15.6	123	12.44	39.2	15.3	7.46	7.46	805	88	10.0
16	0.57	50.9	13.7	97	13.82	28.8	13.8	6.94	6.94	737	88.9	9.12
17	0.90	55.1	13.5	95	13.7	28	13.7	6.9	6.9	688	88.7	8.53
18	0.55	57.7	16.0	73	8.94	19.2	12.3	6.46	6.46	637	89	7.85
19	0.53	59.9	16.4	57	7.82	12.8	11.4	6.14	6.14	593	90	7.18
20	0.85	53.5	12.9	99	10.76	29.6	13.9	6.98	6.98	708	88	8.84
21	0.54	52.7	16.8	51	7.40	10.4	11.0	6.02	6.02	584	91	7.04
22	0.96	56.7	14.8	129	12.83	41.6	15.7	7.58	7.58	777	87	9.77
23	0.52	57.3	14.9	53	7.54	11.2	11.1	6.06	6.06	564	89	6.91
24	0.89	54.9	15.9	85	9.78	24	13.1	6.7	6.7	669	90.5	8.13
25	0.74	58.1	12.4	125	13.14	43.2	15.9	7.66	7.66	778	86	8.55
26	0.67	51.3	15.7	87	9.92	24.8	13.2	6.74	6.74	727	90.7	8.81
27	0.92	57.1	15.0	89	10.06	25.6	13.3	6.78	6.78	663	89.8	7.3
28	0.69	51.9	16.7	125	13.42	44.8	16.2	7.74	7.74	827	88	10.3
29	0.60	53.9	16.2	103	11.04	31.2	14.1	7.06	7.06	742	88.4	8.39
30	0.94	59.7	13.2	120	13.84	47.2	16.5	7.86	7.86	761	86.5	8.37
31	0.97	54.1	14.4	107	11.28	32.8	14.4	7.14	7.14	745	88	9.31
32	0.86	54.3	14.0	122	13	42.4	15.8	7.62	7.62	819	87	10.3
33	0.61	51.5	12.8	67	8.52	16.8	12.0	6.34	6.34	643	88	7.96
34	0.59	53.7	12.2	81	9.50	22.4	12.8	6.62	6.62	648	87	8.16
35	0.50	54.7	12.0	115	11.88	36	14.9	7.3	7.3	762	86.4	9.69
36	0.98	50.5	14.5	55	7.68	12	11.3	6.1	6.1	605	90.3	7.37
37	0.71	57.5	13.4	93	10.34	27.2	13.5	6.86	6.86	670	88.6	8.31
38	0.95	52.1	13.1	109	11.46	33.6	14.5	7.18	7.18	763	87	9.54
39	0.66	56.3	15.1	113	11.74	35.2	14.7	7.26	7.26	762	88	9.49
40	0.79	53.1	12.5	65	8.38	16	11.9	6.3	6.3	620	88	7.7

6.2.1 PSO optimised parameters by Surrogate

Swarming...

Reached limit of 200 iterations

Final best point: [0.50012 50 17 111.37]

xopt =

0.5001 50.0000 17.0000 111.3738

fval =

-89.3071

optscale =

0.5001 50.0000 17.0000 111.3738 -89.3071

Harmonic =

9.7104

Torque =

800.0002

Swarming...

Average cumulative change in value of the fitness function

Final best point: [22.001 50 15.882 8]

xopt =

22.0005 50.0000 15.8825 8.0000

fval =

-85.2383

optscale =

22.0005 50.0000 15.8825 8.0000 -85.2383

Harmonic =

9.4549

Torque =

800.0001

Table 6-2 rotor optimisation and turns with 3 flux barriers

S, No	Flux Barrier width in mm	Flux carrier width in mm	Flux barrier edge angle in °	No: of turns	Torque in Nm	Efficiency in %	Power in kW	Fill factor in %
01	39.79	63.00	45.79	61.26	715.7	92	8.5	67
02	35.37	70.74	50.00	39.37	1644	88.9	20.33	42
03	33.71	71.29	31.05	49.47	1004	92	11.97	54
04	41.45	68.53	18.42	56.21	900.7	91.9	10.77	61
05	33.16	66.87	20.53	52.84	835	93	9.18	57
06	34.82	66.32	35.26	57.89	736.9	93	8.67	62
07	32.05	67.97	33.16	37.68	1509	87	18.9	40
08	31.50	64.11	28.95	46.11	1049	92	12.43	50
09	40.89	63.55	24.74	51.16	1079	91.9	12.9	56
10	42.00	71.84	39.47	54.53	1031	91.2	12.4	59
11	35.92	69.63	26.84	64.63	638	92.6	7.5	70
12	37.03	65.21	10.00	36.00	1652	86	20.90	39
13	38.68	64.66	16.32	68.00	620	92.9	7.33	74
14	40.34	72.39	14.21	66.32	675	91	8.09	72
15	32.61	69.08	47.89	47.79	1074	92	12.79	51
16	36.47	70.18	22.63	42.74	1481	90	18	46
17	39.24	72.95	37.37	41.05	1695	89	20	45

18	34.26	65.76	12.11	62.95	619	92	7.35	68
19	38.13	67.42	43.68	44.42	1509	96	17.26	47
20	37.58	73.50	41.58	59.58	773	94.4	9	45

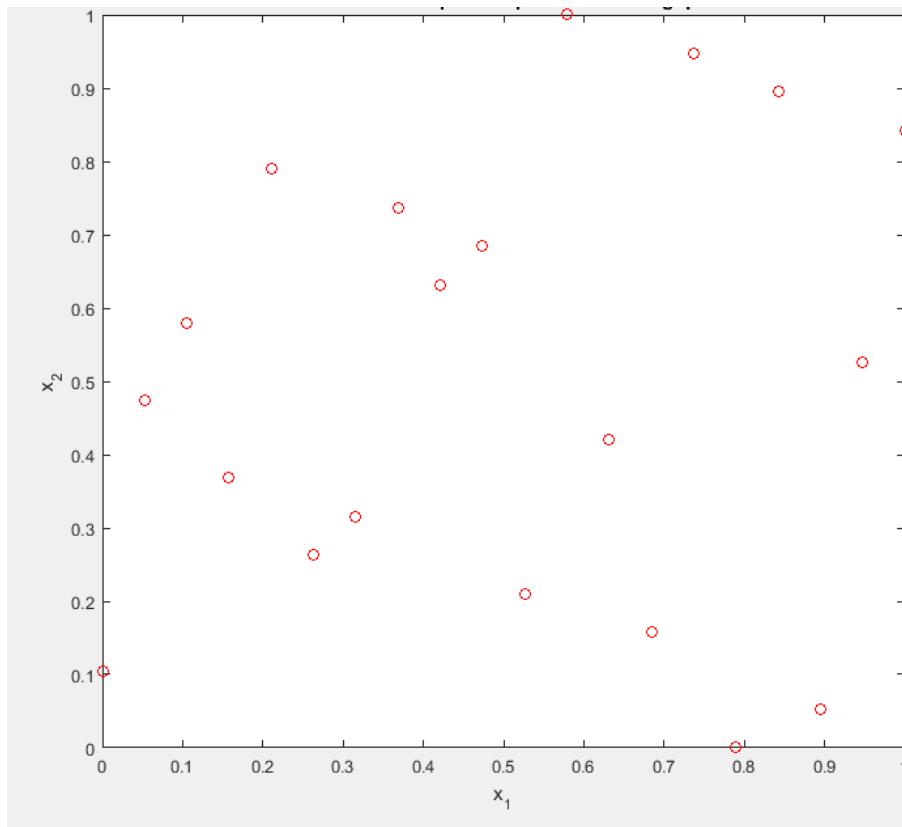


Fig. 6.1 Latin Hypercube samples for 2nd optimisation

6.2.2 PSO optimised values No 1*

Swarming...

Reached limit of 200 iterations

Final best point: [32.498 63.829 49.299 51.743]

xopt =

32.4980 63.8292 49.2990 51.7429

fval =

-93.9870

optscale =

32.4980 63.8292 49.2990 51.7429 -93.9870

Harmonic =

900.0001

Torque =

10.0000

6.2.3 PSO optimised values No 2*

```
Swarming...
Reached limit of 200 iterations
Final best point: [37.608 73.5 50 58.982]

xopt =
    37.6079    73.4998    49.9997    58.9824

fval =
   -94.7940

optscale =
    37.6079    73.4998    49.9997    58.9824   -94.7940

Harmonic =
     9.2941

Torque =
    800.0019
```

6.2.4 PSO optimised values No 3*

```
Swarming...
Average cumulative change in value of the fitness function over 50 generations less than
Final best point: [33.225 66.386 50 53.886]

xopt =
    33.2245    66.3856    50.0000    53.8862

fval =
   -94.3783

optscale =
    33.2245    66.3856    50.0000    53.8862   -94.3783

Harmonic =
     9.5333

Torque =
    850.0018
```

Table 6-3 shows the 3 flux barriers and 4 flux carriers while considering only stable torque

S, No	Flux Barrier width in mm	Flux carrier width in mm	Flux barrier edge angle in °	No: of turns	Torque in Nm	Efficiency in %	Power in kW	Fill factor in %
01	39.79	63.00	45.79	61.26	463.9	88.8	5.74	67
02	35.37	70.74	50.00	39.37	1636	88.8	20.24	42
03	33.71	71.29	31.05	49.47	766	90.03	9.35	54
04	41.45	68.53	18.42	56.21	900	91.9	10.76	61
05	33.16	66.87	20.53	52.84	599.77	90.8	7.26	57
06	34.82	66.32	35.26	57.89	543	91.4	6.53	62
07	32.05	67.97	33.16	37.68	1570	88.24	19.57	40
08	31.50	64.11	28.95	46.11	855	91.32	10.29	50
09	40.89	63.55	24.74	51.16	815	89.56	10.1	56
10	42.00	71.84	39.47	54.53	796.77	9.85	88.9	59
11	35.92	69.63	26.84	64.63	408.24	89	5.04	70
12	37.03	65.21	10.00	36.00	1726	87.4	21.71	39
13	38.68	64.66	16.32	68.00	381.53	89.03	4.71	74
14	40.34	72.39	14.21	66.32	431	87.7	5.41	72
15	32.61	69.08	47.89	47.79	860	90.61	10.44	51
16	36.47	70.18	22.63	42.74	1396	89.9	17.06	46
17	39.24	72.95	37.37	41.05	1665	89.01	20.57	45
18	34.26	65.76	12.11	62.95	390.69	87.40	4.91	68
19	38.13	67.42	43.68	44.42	1408	90.05	17.19	47
20	37.58	73.50	41.58	59.58	583	92.74	6.91	45

Table 6-4 shows the data of 4 flux barriers and 5 flux carriers

S, No	Flux Barrier width in mm	Flux carrier width in mm	Flux barrier edge angle in °	No: of turns	Torque in Nm	Efficiency in %	Power in kW	Fill factor in %
01	9.94	12.6	45.79	61.26	884	92.5	10.5	67
02	8.84	14.14	50.00	39.37	1844	86.4	23.45	42
03	8.427	(14.25	31.05	49.47	1173	92.2	13.98	54
04	10.36	13.70	18.42	56.21	958	91	11.57	61
05	8.29	13.37	20.53	52.84	1016	92.9	12.02	57
06	8.70	13.26	35.26	57.89	915.28	93.5	10.75	62
07	8.01	13.54	33.16	37.68	1748	88.25	21.77	40
08	7.875	12.82	28.95	46.11	1275	92.09	15.22	50
09	10.22	12.71	24.74	51.16	1255	92.04	14.99	56
10	10.5	14.368	39.47	54.53	908	91.9	9.1	59
11	8.98	13.926	26.84	64.63	761	92.8	9.01	70
12	9.25	13.04	10.00	36.00	1850	87.3	23.29	39
13	9.67	12.93	16.32	68.00	759	92.6	9.015	74
14	10.08	4.478	14.21	66.32	642	92.78	7.61	72
15	8.15	13.816	47.89	47.79	1279	92.36	15.23	51
16	9.11	14.03	22.63	42.74	1699	89.5	20.8	46
17	9.81	14.59	37.37	41.05	1628	89.3	20.03	45
18	8.56	13.152	12.11	62.95	805	93.35	9.48	68
19	9.53	13.484	43.68	44.42	1734	89.7	21.24	47
20	9.39	14.7	41.58	59.58	793	92.5	9.43	45

6.2.5 PSO optimised values for 4 flux barriers and 5 carriers and

Swarming...

Average cumulative change in value of the fitness function over 50 generations

Final best point: [41.309 70.599 49.999 53.328]

xopt =

41.3093 70.5995 49.9995 53.3282

fval =

-92.1989

optscale =

41.3093 70.5995 49.9995 53.3282 -92.1989

Harmonic =

985.6983

Torque =

10.0000

Table 6-5 square shape flux barrier design with stable torque data

S, No	Flux Barrier width in mm	Flux carrier width in mm	Flux barrier edge angle in °	No: of turns	Torque in Nm	Efficiency in %	Power in Kw	Fill factor in %
01	9.94	12.6	45.79	61.26	546	89.5	6.98	67
02	8.84	14.14	50.00	39.37	1931	86.98	24.42	42
03	8.427	(14.25	31.05	49.47	944	90.5	11.46	54
04	10.36	13.70	18.42	56.21	668	87.7	8.38	61
05	8.29	13.37	20.53	52.84	758	90.79	9.19	57
06	8.70	13.26	35.26	57.89	611	90.7	7.41	62
07	8.01	13.54	33.16	37.68	1829	88.7	22.67	40
08	7.875	12.82	28.95	46.11	1213	91.7	14.54	50
09	10.22	12.71	24.74	51.16	1034	90.5	12.56	56
10	10.5	14.368	39.47	54.53	643	90.6	7.80	59
11	8.98	13.926	26.84	64.63	548.91	90.32	6.68	70
12	9.25	13.04	10.00	36.00	1943	87.8	24.32	39
13	9.67	12.93	16.32	68.00	495	89.1	6.11	74
14	10.08	4.478	14.21	66.32	438	89.7	5.36	72
15	8.15	13.816	47.89	47.79	1111	91.3	13.38	51
16	9.11	14.03	22.63	42.74	1734	89.77	21.24	46
17	9.81	14.59	37.37	41.05	1634	89.4	20.09	45
18	8.56	13.152	12.11	62.95	550	90.56	6.68	68
19	9.53	13.484	43.68	44.42	1761	89.93	21.54	47
20	9.39	14.7	41.58	59.58	559	89.68	6.85	45

6.2.6 PSO Optimisation for 4 square shape flux barriers

Swarming...

Reached limit of 200 iterations

Final best point: [31.5 63 50 55.279]

xopt =

31.5000 63.0001 50.0000 55.2792

fval =

-91.2729

optscale =

31.5000 63.0001 50.0000 55.2792 -91.2729

Harmonic =

800.0000

Torque =

9.7318

Table 6-6 shows 3 square shape flux carrier and 4 flux carriers data

S, No	Flux Barrier width in mm	Flux carrier width in mm	Flux barrier edge angle in °	No: of turns	Torque in Nm (Stable)	Efficiency in %	Power in kW	Fill factor in %
01	13.26	15.75	45.79	61.26	474	75.83	6.87	67
02	11.79	17.685	50.00	39.37	1667	88.25	20.77	42
03	11.23	17.822	31.05	49.47	802	90.54	9.74	54
04	13.81	17.13	18.42	56.21	685	89.9	8.38	61
05	11.05	16.717	20.53	52.84	617	89.9	7.53	57
06	11.60	16.58)	35.26	57.89	521	90.73	6.31	62
07	10.68	16.99	33.16	37.68	1591	87.4	20.02	40
08	10.5	16.02	28.95	46.11	972	94.35	11.33	50
09	13.63	15.88	24.74	51.16	841	89.86	10.29	56
10	14	17.96	39.47	54.53	826	89.16	10.19	59
11	11.97	17.40	26.84	64.63	401	88.69	4.9	70
12	12.34	16.30	10.00	36.00	1739	86.85	22.01	39
13	12.66	16.16	16.32	68.00	352	87.86	4.40	74
14	13.44	18.09	14.21	66.32	425	93.38	5.00	72
15	10.87	17.27	47.89	47.79	927	91.05	11.19	51
16	12.15	17.54	22.63	42.74	1456	89.55	17.88	46
17	13.08	18.23	37.37	41.05	1679	88.68	20.81	45
18	11.42	16.44	12.11	62.95	392	90.03	4.78	68
19	12.71	16.85	43.68	44.42	1465	89.74	17.95	47
20	12.52	18.37	41.58	59.58	549	89.09	6.77	45

6.2.7 PSO Optimisation for square shape 3 flux barrier and 4 flux carrier design.

Swarming...

Average cumulative change in value of the fitness function over 50 generations less than 1e-06

Final best point: [31.5 64.55 28.489 48.631]

xopt =

31.5000 64.5501 28.4893 48.6308

fval =

-94.6200

optscale =

31.5000 64.5501 28.4893 48.6308 -94.6200

Harmonic =

9.5000

Torque =

810.1634

Table 6-7 shows round stator slots shape with 4 round flux carrier and 5 flux carriers data

S, No	Flux Barrier width in mm	Flux carrier width in mm	Flux barrier edge angle in °	No: of turns	Torque in Nm (Stable)	Efficiency in %	Power in kW	Fill factor in %
01	13.26	15.75	45.79	61.26	546	89.5	6.98	67
02	11.79	17.685	50.00	39.37	1931	86.98	24.42	42
03	11.23	17.822	31.05	49.47	944	90.5	11.46	54
04	13.81	17.13	18.42	56.21	668	87.7	8.38	61
05	11.05	16.717	20.53	52.84	758	90.79	9.19	57
06	11.60	16.58)	35.26	57.89	611	90.7	7.41	62
07	10.68	16.99	33.16	37.68	1829	88.7	22.67	40
08	10.5	16.02	28.95	46.11	1213	91.7	14.54	50
09	13.63	15.88	24.74	51.16	1034	90.5	12.56	56
10	14	17.96	39.47	54.53	643	90.6	7.80	59
11	11.97	17.40	26.84	64.63	548.91	90.32	6.68	70
12	12.34	16.30	10.00	36.00	1943	87.8	24.32	39
13	12.66	16.16	16.32	68.00	495	89.1	6.11	74
14	13.44	18.09	14.21	66.32	438	89.7	5.36	72
15	10.87	17.27	47.89	47.79	1111	91.3	13.38	51
16	12.15	17.54	22.63	42.74	1734	89.77	21.24	46
17	13.08	18.23	37.37	41.05	1634	89.4	20.09	45
18	11.42	16.44	12.11	62.95	550	90.56	6.68	68
19	12.71	16.85	43.68	44.42	1761	89.93	21.54	47
20	12.52	18.37	41.58	59.58	559	89.68	6.85	45

Table 6-8 square slot design with 24 slots LHS samplings points at 100 turns

S, No	Airgap in mm	Slot depth in mm	Tooth width in mm	Shaft diameter in mm	Flux Barrier width in mm	Barrier edge angle in °	Flux carrier width in mm	Slot openings in mm	Torque in Nm	Eff: in %	Power in kW	Fill factor in %
1	0.66	52.7	20.8	106.88	9.60	21.00	17.13	15.88	862.0	90.9	10.43	54.0
2	0.51	56.2	25.7	64.63	7.51	35.00	19.88	10.03	755.7	92.2	9.01	61.6
3	0.81	57.7	18.5	100.38	11.70	41.00	15.88	14.98	789.0	87.3	9.93	44.0
4	0.94	58.7	19.0	80.88	13.46	45.00	16.13	12.28	718.0	95.6	8.26	44.0
5	0.56	51.2	21.2	58.13	8.21	15.00	17.38	9.13	482.8	96.7	5.49	57.0
6	0.59	54.2	17.6	103.63	(8.558)	27.00	15.38	15.43	531.5	97.0	6.03	46.0
7	0.71	53.7	20.3	77.63	10.30	25.00	16.88	11.83	573.5	95.9	6.57	52.0
8	0.89	55.2	23.0	61.38	12.76	31.00	18.38	9.58	684.9	95.0	7.86	56.0
9	0.76	57.2	23.5	67.88	11.01	39.00	18.63	10.48	435.4	96.0	4.95	54.0
10	0.91	55.7	25.3	80.25	13.11	33.00	19.63	16.33	717.0	95.0	8.23	60.0
11	0.69	56.7	18.1	51.63	9.96	37.00	15.63	8.23	508.8	96.0	5.78	45.0
12	0.79	51.7	24.8	97.13	11.36	17.00	19.38	14.53	649.7	96.0	7.42	65.0

13	0.96	50.2	22.1	74.38	13.81	11.00	17.88	11.38	722.9	96.0	8.27	61.0
14	0.84	50.7	23.9	54.88	12.06	13.00	18.88	8.68	648.0	96.0	7.13	66.0
15	0.86	52.2	19.9	87.38	12.41	19.00	16.63	13.18	668.2	96.0	7.65	53.0
16	0.54	59.2	19.4	71.13	7.86	47.00	16.38	10.93	464.5	96.0	5.27	45.0
17	0.74	59.7	24.4	93.88	10.66	49.00	19.13	14.08	609.8	95.0	6.99	53.0
18	0.64	53.2	22.6	84.13	9.26	23.00	18.13	12.73	560.1	95.0	6.45	58.0
19	0.61	54.7	21.7	113.38	8.91	29.00	17.63	16.78	545.0	96.0	6.22	53.0
20	0.99	58.2	17.2	90.63	14.16	43.00	15.13	13.63	723.	94.0	8.40	42.0

Table 6-9 square slot design with 24 slots LHS samplings points at 50 turns

No	Airgap in mm	Slot depth in mm	Tooth width in mm	Shaft diameter in mm	Flux Barrier width in mm	Barrier edge angle in °	Flux carrier width in mm	Slot openings in mm	Torque in Nm	Eff: in %	Power in kW	Fill factor in %
1	0.66	52.7	20.8	106.88	9.60	21.00	17.13	15.88	862	90.9	10.4	54
2	0.51	56.2	25.7	64.63	7.51	35.00	19.88	10.03	755.7	92.2	9.01	61.6
3	0.81	57.7	18.5	100.38	11.70	41.00	15.88	14.98	789	87.3	9.933	44
4	0.94	58.7	19.0	80.88	13.46	45.00	16.13	12.28	998	89	12.34	44
5	0.56	51.2	21.2	58.13	8.21	15.00	17.38	9.13	775	90.2	9.45	57
6	0.59	54.2	17.6	103.63	(8.558)	27.00	15.38	15.43	770	85	9.953	46
7	0.71	53.7	20.3	77.63	10.30	25.00	16.88	11.83	875	89.9	10.70	52
8	0.89	55.2	23.0	61.38	12.76	31.00	18.38	9.58	960	90.9	11.62	56
9	0.76	57.2	23.5	67.88	11.01	39.00	18.63	10.48	918	91	11.00	54
10	0.91	55.7	25.3	80.25	13.11	33.00	19.63	16.33	885	90.1	10.80	60
11	0.69	56.7	18.1	51.63	9.96	37.00	15.63	8.23	793	86	10.03	45
12	0.79	51.7	24.8	97.13	11.36	17.00	19.38	14.53	892	91	10.75	65
13	0.96	50.2	22.1	74.38	13.81	11.00	17.88	11.38	962	89	11.8	61
14	0.84	50.7	23.9	54.88	12.06	13.00	18.88	8.68	932	91	11.22	66
15	0.86	52.2	19.9	87.38	12.41	19.00	16.63	13.18	951	89	11.73	53
16	0.54	59.2	19.4	71.13	7.86	47.00	16.38	10.93	711.9	87.2	8.97	45
17	0.74	59.7	24.4	93.88	10.66	49.00	19.13	14.08	883.6	91	10.66	53
18	0.64	53.2	22.6	84.13	9.26	23.00	18.13	12.73	876.5	92	10.4	58
19	0.61	54.7	21.7	113.38	8.91	29.00	17.63	16.78	841	91	10.16	53
20	0.99	58.2	17.2	90.63	14.16	43.00	15.13	13.63	990	86	12.53	42

6.2.8 PSO generated optimised variables for 24 square stator slots

Swarming...

Reached limit of 200 iterations

Final best point: [0.57383 51.401 26 50]

xopt =

0.5738 51.4010 26.0000 50.0001

fval =

-92.2537

optscale =

0.5738 51.4010 26.0000 50.0001 -92.2537

Harmonic =

800.0000

Torque =

9.4722

Swarming...

Reached limit of 200 iterations

Final best point: [27.923 50 20 10.817]

xopt =

27.9235 49.9999 20.0000 10.8171

fval =

-92.3969

optscale =

27.9235 49.9999 20.0000 10.8171 -92.3969

Harmonic =

850.0003

Torque =

9.8984

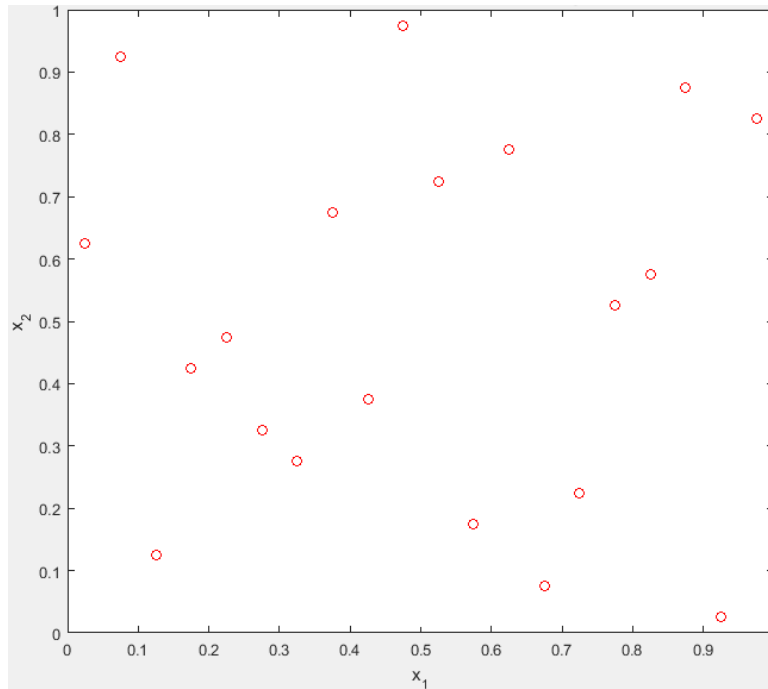


Fig. 6.2 Latin Hypercube Samples for 24 square shaped stator slots

Table 6-10 round slots design with 24 slots LHS samplings points

No	Airgap in mm	Slot depth in mm	Tooth width in mm	Shaft diameter in mm	Flux Barrier width in mm	Barrier edge angle in °	Flux carrier width in mm	Slot openings in mm	Torq: in Nm	Eff: in %	Power in kW	Fill factor in %
1	0.66	52.7	20.8	106.88	9.60	21.00	17.13	15.8	886	90	10.7	58
2	0.51	56.2	25.7	64.63	7.51	35.00	19.88	10.0	770	92	9.17	66
3	0.81	57.7	18.5	100.38	11.70	41.00	15.88	14.9	827	87	10.3	48
4	0.94	58.7	19.0	80.88	13.46	45.00	16.13	12.2	1019	88	12.6	47
5	0.56	51.2	21.2	58.13	8.21	15.00	17.38	9.13	806	90	8.87	62
6	0.59	54.2	17.6	103.63	8.55	27.00	15.38	15.4	799	85	10.2	50
7	0.71	53.7	20.3	77.63	10.30	25.00	16.88	11.8	902	90	11	56
8	0.89	55.2	23.0	61.38	12.76	31.00	18.38	9.58	840	80	10.2	60
9	0.76	57.2	23.5	67.88	11.01	39.00	18.63	10.4	940	91	11.3	58
10	0.91	55.7	25.3	80.25	13.11	33.00	19.63	16.3	904	90	11.0	64
11	0.69	56.7	18.1	51.63	9.96	37.00	15.63	8.23	844	87	10.5	48
12	0.79	51.7	24.8	97.13	11.36	17.00	19.38	14.5	913	91	10.9	71
13	0.96	50.2	22.1	74.38	13.81	11.00	17.88	11.3	984	89	12.0	66
14	0.84	50.7	23.9	54.88	12.06	13.00	18.88	8.68	948	91	11.4	70
15	0.86	52.2	19.9	87.38	12.41	19.00	16.63	13.1	972	89	10.6	57

16	0.54	59.2	19.4	71.13	7.86	47.00	16.38	10.9	758	87	9.56	48
17	0.74	59.7	24.4	93.88	10.66	49.00	19.13	14.0	907	90	10.9	57
18	0.64	53.2	22.6	84.13	9.26	23.00	18.13	12.7	892	91	10.6	62
19	0.61	54.7	21.7	113.38	8.91	29.00	17.63	16.7	867	91	10.4	57
20	0.99	58.2	17.2	90.63	14.16	43.00	15.13	13.6	1005	86	12.7	45

6.2.9 PSO generated optimised variables for 24 round stator slots

Swarming...

Reached limit of 200 iterations

Final best point: [0.57314 52.615 26 115]

xopt =

0.5731 52.6153 26.0000 114.9997

fval =

-93.2531

optscale =

0.5731 52.6153 26.0000 114.9997 -93.2531

Harmonic =

850.0002

Torque =

9.9013

Swarming...

Reached limit of 200 iterations

Final best point: [26.179 10 20 17]

xopt =

26.1789 10.0000 20.0000 17.0000

fval =

-93.4122

optscale =

26.1789 10.0000 20.0000 17.0000 -93.4122

Harmonic =

850.0001

Torque =

9.8068

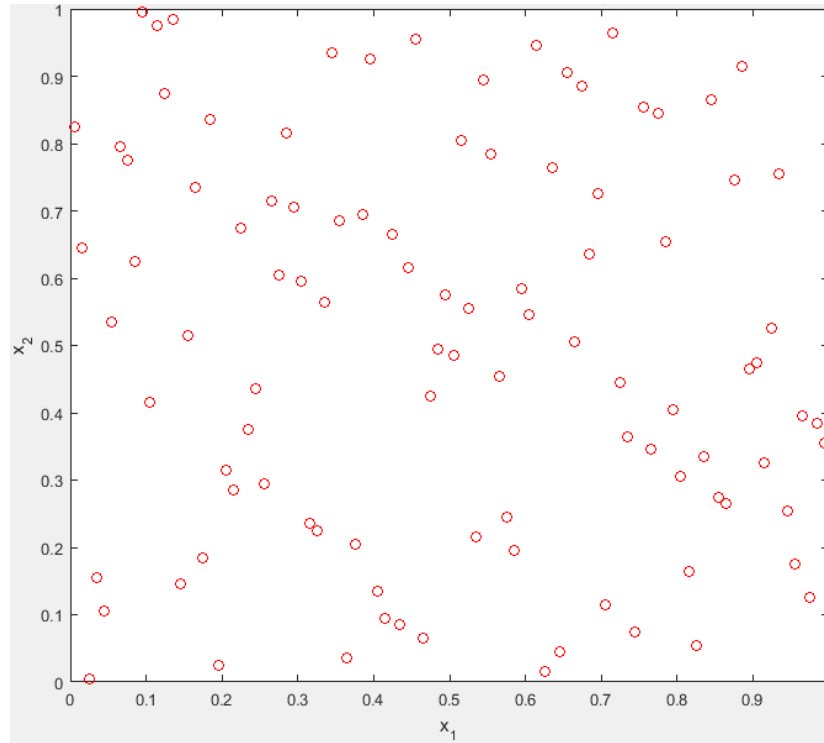


Fig. 6.3 Initial 100 Latin Hypercube samples for 12/8 SRM design

Table 6-11 12/8 Switched Reluctance Motor (10Kw; 105 rpm) achieved parameters of 12/8 SRM

Dimensions	Value	Range
Length of Motor [L_{stck}] (mm)	200	Fixed
Stator outer dia [D_{so}] (mm)	500	Fixed
Stator Inner Dia [D_{si}] (mm)	301.2	fixed
Pole arc of Stator [β_s] (deg)	16	15 to 18
Pole a width of Stator (mm)	41.918	39.31 to 47.11
Yoke Thickness of Stator (mm)	27.9	26.20 to 31.4
Pole length of Stator (mm)	71.5	68 to 73.2
Air gap (mm)	0.6	0.5 to 1
Outer Diameter of Rotor [D_{ro}] (mm)	300	299.2 to 300.2
Pole arc of Rotor [β_r] (deg)	16.8	15 to 20
Pole a width of Rotor (mm)	43.82	39.15 to 52.12
Yoke Thickness of Rotor (mm)	29.21	26.1 to 34.7
Pole length of Rotor (mm)	45.79	41 to 48
Shaft Diameter [D_{sh}] (mm)	150	fixed
Efficiency (%)	87.5	
Speed in rpm	105	
Torque in Nm	903.3	

Table 6-12 variable range selection for Latin Hypercube Samples for 12/8 SRM

Dimensions	The initial value of design 1	The initial value of design 2
Length of Motor (mm)	200	200
Stator outer dia in (mm)	500	500
Stator inner dia in (mm)	300.2 in range of (280 to 320)	361 in range of (340 to 380)
Yoke Thickness of Stator (mm)	29 (25 to 35)	32 (27 to 37)
Pole length of Stator (mm)	71 (65 to 75)	62.5 (60 to 65)
Pole arc of Stator (deg)	14.7 (14.25 to 15.6)	14.7 (14.25 to 15.6)
Pole a width of Stator (mm)	38.48 (37.23 to 40.74)	46.20 (43.5 to 49.5)
Air gap (mm)	0.6 (0.5 to 0.75)	0.6 (0.5 to 0.75)
Outer Diameter of Rotor (mm)	299 (279 to 318.5)	359.8 (338.8 to 378.8)
Yoke Thickness of Rotor (mm)	34.92 (28 to 36)	33 (27 to 37)
Pole length of Rotor (mm)	49.79 (49 to 53)	56.9 (53 to 60)
Pole arc of Rotor (deg)	16.04 (15.65 to 16.6)	15.75 (15.65 to 16.6)
Pole a width of Rotor (mm)	41.71 (40.7 to 43.2)	49.30 (45.5 to 51.5)
Shaft Diameter (mm)	130 (120 to 140)	180 (170 to 190)
Number of Turns per Pole	74 (68 to 76)	109 (105 to 110)
Slot Fill Factor (%)	73.08	71.82
Efficiency (%)	84.83	87.11
Rated Speed (rpm):	105	105
Rated Torque (N.m):	902.42	902.87

Table 6-13 12/8 SRM parameters for the 100 Latin Hypercube samples

S, No	Stator pole arc in °	Stator Yoke in mm	Stator inner diameter in mm	Air gap in mm	Rotor Yoke thickness in mm	Rotor pole arc in °	Shaft diameter in mm	Eff: in %	Torque in Nm
1.0	15.2	29.1	295.6	0.5	28.4	15.3	130.5	84.5	1010.0
2.0	17.7	31.0	294.6	0.8	33.9	19.4	142.1	88.3	631.4
3.0	15.8	29.5	309.6	0.7	29.8	16.4	137.1	86.3	926.2
4.0	17.4	28.5	295.9	0.8	33.3	19.0	143.5	87.8	658.9
5.0	16.8	31.1	299.1	1.0	32.1	18.1	148.9	86.4	736.0
6.0	17.8	29.1	303.6	0.7	34.2	19.6	138.3	89.7	630.7
7.0	15.3	29.6	308.4	0.6	28.6	15.4	135.9	84.8	1014.0
8.0	15.6	28.0	305.9	0.5	29.4	16.0	130.3	86.7	955.7
9.0	17.9	27.4	286.4	0.8	34.4	19.8	143.7	87.8	581.5
10.0	16.8	27.5	308.1	0.8	31.9	17.9	142.3	87.6	776.6

11.0	16.3	26.9	285.6	0.8	30.9	17.2	140.5	85.5	770.7
12.0	17.8	27.7	285.1	1.0	34.3	19.7	148.1	87.0	581.6
13.0	15.9	30.5	296.1	0.9	29.9	16.4	145.1	83.7	855.1
14.0	15.5	27.4	298.6	0.9	29.2	15.9	144.5	83.5	906.8
15.0	15.4	30.8	286.1	0.5	28.8	15.6	131.1	84.7	944.7
16.0	15.7	28.6	302.9	0.5	29.6	16.2	130.7	86.7	935.6
17.0	15.3	28.5	292.6	0.8	28.7	15.5	141.9	82.8	920.9
18.0	16.5	28.9	308.9	0.7	31.4	17.5	136.1	87.6	815.8
19.0	15.8	30.0	300.9	0.7	29.8	16.3	137.3	85.6	891.1
20.0	17.6	27.8	291.6	0.8	33.8	19.3	140.1	88.1	638.3
21.0	17.2	28.7	301.4	0.7	32.9	18.6	136.7	88.6	711.2
22.0	15.6	26.6	293.1	0.6	29.3	16.0	133.5	84.8	899.9
23.0	15.7	28.3	298.4	0.6	29.6	16.2	134.9	85.8	904.1
24.0	15.4	27.2	307.4	0.8	29.0	15.7	143.9	83.7	948.4
25.0	15.7	29.8	287.6	0.6	29.5	16.1	133.1	84.3	883.1
26.0	15.8	27.9	309.4	0.9	29.7	16.3	144.9	84.5	894.2
27.0	17.0	29.0	288.4	0.8	32.5	18.3	140.7	86.8	692.8
28.0	16.2	27.2	289.1	0.9	30.7	17.0	146.7	84.7	777.9
29.0	15.6	27.9	291.1	0.7	29.4	16.1	136.5	84.9	894.8
30.0	15.6	30.6	296.6	0.9	29.2	15.9	146.1	83.4	907.6
31.0	15.4	31.3	293.9	0.9	28.9	15.7	144.1	82.7	908.6
32.0	15.0	30.5	289.6	0.8	28.0	15.0	143.3	80.7	932.4
33.0	15.5	30.1	301.6	1.0	29.1	15.8	149.9	82.5	906.2
34.0	17.7	28.8	308.6	0.9	34.0	19.5	147.9	88.5	652.2
35.0	16.0	31.1	289.9	0.7	30.3	16.7	137.7	85.2	826.4
36.0	17.0	30.9	294.9	1.0	32.4	18.3	148.7	86.5	705.7
37.0	15.2	30.4	295.4	1.0	28.4	15.3	148.3	81.1	921.8
38.0	17.6	30.2	293.4	0.6	33.9	19.4	132.1	89.0	646.8
39.0	16.1	29.9	288.6	0.8	30.4	16.8	141.1	84.9	809.0
40.0	17.1	27.1	286.6	0.6	32.7	18.5	135.5	87.8	674.9
41.0	16.6	29.2	295.1	0.7	31.5	17.6	137.5	87.1	775.4
42.0	16.5	30.4	292.9	0.8	31.5	17.6	141.3	86.3	757.8
43.0	17.1	30.1	300.4	0.8	32.7	18.5	142.7	87.6	712.3
44.0	15.3	31.4	299.4	0.9	28.6	15.5	147.7	81.9	931.3
45.0	17.1	29.6	290.1	0.9	32.6	18.4	146.9	86.6	685.2
46.0	17.8	30.2	303.4	0.9	34.3	19.7	147.3	88.7	625.3
47.0	16.9	26.6	306.9	0.7	32.2	18.1	137.9	87.5	755.2
48.0	17.3	28.2	302.6	1.0	33.1	18.8	149.7	87.3	673.4

49.0	15.5	29.0	305.1	0.7	29.0	15.8	138.1	85.0	967.3
50.0	16.1	27.5	303.9	0.5	30.5	16.9	131.7	87.4	864.8
51.0	18.0	28.4	294.1	0.6	34.6	19.9	134.7	89.7	594.2
52.0	16.6	30.9	301.1	0.9	31.7	17.7	144.3	86.7	766.7
53.0	16.1	26.7	289.4	0.8	30.4	16.8	141.7	84.9	806.6
54.0	17.7	28.1	306.1	0.7	34.1	19.6	139.5	89.4	642.9
55.0	15.2	30.3	291.4	0.5	28.5	15.4	130.9	84.1	971.0
56.0	16.6	27.6	292.4	0.7	31.6	17.7	139.9	86.2	749.5
57.0	16.3	29.8	296.4	0.5	30.8	17.1	131.5	87.5	821.8
58.0	16.0	27.6	306.6	0.5	30.2	16.6	130.1	87.3	898.0
59.0	16.5	28.9	287.1	0.8	31.2	17.4	142.5	85.6	748.6
60.0	17.9	28.4	298.1	0.8	34.5	19.8	140.9	89.2	611.7
61.0	16.2	29.9	287.9	0.9	30.6	16.9	147.5	83.7	784.4
62.0	17.1	31.2	307.1	0.9	32.8	18.6	145.5	88.2	723.1
63.0	16.4	28.6	297.6	0.6	31.2	17.4	135.3	86.9	798.5
64.0	17.5	26.8	302.4	0.5	33.5	19.1	131.3	89.9	673.2
65.0	15.9	29.4	290.6	0.6	30.0	16.5	135.1	85.7	857.4
66.0	16.4	31.2	298.9	0.6	31.0	17.3	134.3	87.5	814.9
67.0	15.1	27.3	305.4	0.6	28.2	15.2	132.9	83.5	1010.0
68.0	16.2	27.0	303.1	0.7	30.8	17.1	138.5	86.4	826.4
69.0	17.3	30.6	297.4	1.0	33.2	18.9	149.5	87.1	670.0
70.0	15.1	27.0	299.6	0.8	28.3	15.2	143.1	82.3	960.2
71.0	16.9	26.7	307.6	0.9	32.3	18.2	147.1	87.1	741.1
72.0	17.9	27.1	285.9	0.9	34.5	19.9	146.5	87.4	576.6
73.0	16.2	31.0	290.9	0.7	30.6	17.0	139.3	85.6	813.4
74.0	16.0	29.3	297.9	0.6	30.2	16.7	133.7	86.6	872.0
75.0	15.1	26.5	304.1	0.7	28.2	15.1	136.3	83.4	1019.0
76.0	16.7	27.7	296.9	0.9	31.9	17.9	145.7	86.3	736.5
77.0	17.4	29.7	309.1	0.5	33.3	18.9	131.9	89.8	714.3
78.0	17.5	30.7	293.6	0.9	33.7	19.2	145.9	87.6	644.6
79.0	15.9	27.7	286.9	1.0	30.1	16.6	148.5	82.6	803.1
80.0	16.3	29.5	302.1	0.7	31.0	17.2	139.7	86.5	816.4
81.0	16.5	29.3	300.6	0.7	31.3	17.5	139.1	87.1	799.6
82.0	17.7	28.8	304.4	0.7	34.1	19.5	138.9	89.5	646.2
83.0	17.2	26.9	285.4	0.8	33.0	18.7	140.3	87.1	659.9
84.0	17.2	28.3	309.9	0.8	32.9	18.7	142.9	88.5	712.1
85.0	16.9	30.2	300.1	0.6	32.3	18.2	135.7	88.1	741.8
86.0	17.5	28.1	290.4	0.6	33.6	19.2	133.9	89.0	636.9

87.0	17.4	28.0	294.4	0.7	33.4	19.0	136.9	88.6	668.5
88.0	17.0	30.8	304.6	1.0	32.5	18.4	149.3	87.2	715.8
89.0	16.4	26.8	304.9	0.9	31.1	17.3	145.3	86.3	805.5
90.0	15.9	30.0	307.9	1.0	30.0	16.5	149.1	84.5	879.4
91.0	16.7	28.7	301.9	0.8	31.8	17.8	141.5	87.0	766.5
92.0	18.0	28.2	292.1	0.6	34.7	20.0	132.7	89.7	596.5
93.0	15.3	31.3	297.1	0.6	28.8	15.6	132.3	85.1	979.6
94.0	17.3	30.7	288.9	0.7	33.1	18.8	138.7	87.4	668.9
95.0	16.7	30.3	287.4	0.6	31.7	17.8	132.5	87.4	753.9
96.0	17.6	27.8	306.4	0.6	33.7	19.3	134.1	89.9	670.5
97.0	16.8	29.4	305.6	0.6	32.0	18.0	133.3	88.4	781.4
98.0	16.8	29.2	291.9	0.6	32.1	18.0	134.5	87.7	733.7
99.0	17.4	27.3	288.1	0.9	33.5	19.1	146.3	86.8	634.5
100.0	15.0	29.7	299.9	0.9	28.1	15.1	144.7	81.4	971.4

6.2.10 1st PSO optimisation variable for 12/8 SRM design with 100 samples

```

Swarming...
Reached limit of 200 iterations
Final best point: [17.472 26.778 302.9 0.5085]
Final best point: [29.931 19.448 135.83 0.503]
xopt =
29.9305 19.4476 135.8279 0.5030
17.4720 26.7776 302.8952 0.5085
fval =
-88.9906
-90.1274
optscale =
optscale =
17.4720 26.7776 302.8952 0.5085 -90.1274 29.9305 19.4476 135.8279 0.5030 -88.9906
Harmonic =
33.9999
Harmonic =
33.0617
Torque =
680.0008
Torque =
680.0000
>>

```

12/8 SRM 60 LHS Sample Points

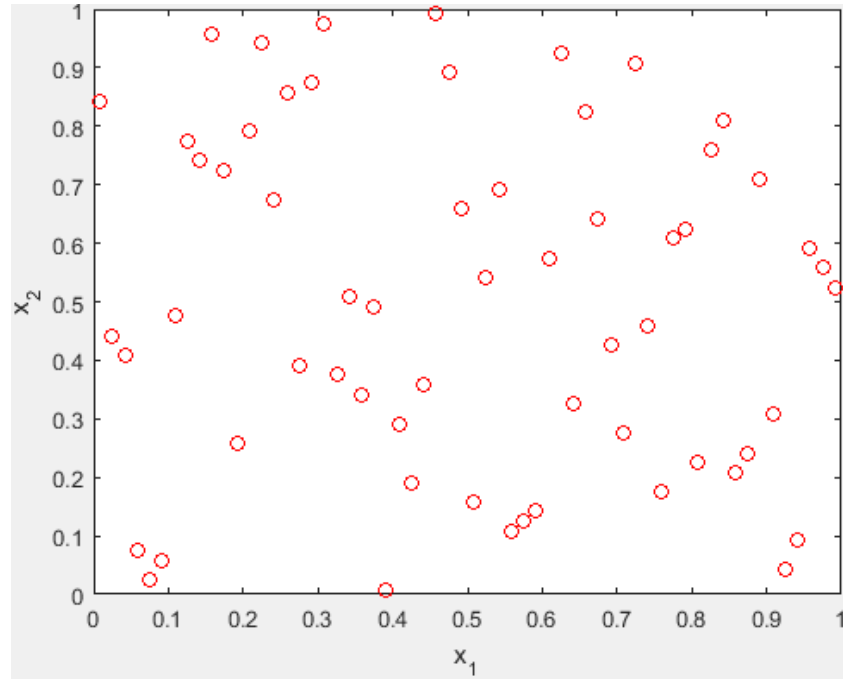


Fig. 6.4 Initial 60 Latin Hypercube samples for 12/8 SRM design

Table 6-14 12/8 SRM parameters for the 60 Latin Hypercube samples

S, No	Stator pole arc in °	Stator Yoke in mm	Stator inner diameter in mm	Air gap in mm	Rotor Yoke thickness in mm	Rotor pole arc in °	Shaft diameter in mm	Eff: in %	Torq: in Nm
1.00	15.72	29.80	301.87	0.69	29.62	16.21	137.50	85.49	916.60
2.00	16.07	28.17	285.20	0.85	30.40	16.79	143.83	83.50	795.67
3.00	15.87	30.78	287.29	0.59	29.95	16.46	133.50	85.37	848.22
4.00	16.57	29.15	309.79	0.70	31.52	17.63	138.16	87.91	814.94
5.00	17.42	27.60	299.79	0.73	33.42	19.04	139.16	88.72	673.55
6.00	16.97	30.54	297.29	0.80	32.41	18.29	141.83	88.57	734.06
7.00	17.87	29.39	300.20	0.95	34.42	19.79	148.16	88.32	614.87
8.00	16.72	27.11	289.37	0.78	31.85	17.88	141.16	88.69	737.52
9.00	17.62	27.68	292.70	0.61	33.86	19.38	134.50	89.05	635.53
10.00	17.32	29.48	286.87	0.64	33.19	18.88	135.50	88.18	665.05
11.00	16.37	31.35	304.79	0.55	31.07	17.29	132.16	88.27	843.79
12.00	16.02	28.99	291.04	0.76	30.29	16.71	140.50	85.33	829.56
13.00	16.27	27.43	308.54	0.63	30.85	17.13	135.16	87.58	845.56
14.00	15.32	28.82	298.95	0.51	28.73	15.54	130.50	85.11	984.68
15.00	17.57	27.52	308.95	0.56	33.75	19.29	132.50	90.26	671.95

16.00	16.52	27.27	299.37	0.80	31.41	17.54	142.16	85.99	769.48
17.00	17.17	30.95	293.95	0.67	32.86	18.63	136.83	88.14	697.27
18.00	17.52	30.46	290.62	0.71	33.64	19.21	138.50	88.54	646.14
19.00	17.47	30.21	304.37	0.90	33.53	19.13	145.83	88.35	667.88
20.00	17.27	27.35	309.37	0.83	33.08	18.79	143.16	88.25	702.74
21.00	15.22	26.62	307.29	0.84	28.50	15.38	143.50	83.00	972.94
22.00	17.07	28.58	288.54	0.65	32.63	18.46	136.16	87.48	693.71
23.00	15.17	26.86	301.45	0.60	28.39	15.29	133.83	84.23	1008.80
24.00	16.32	28.25	295.20	0.66	30.96	17.21	136.50	88.35	667.07
25.00	15.37	30.29	300.62	0.75	28.84	15.63	140.16	87.12	825.06
26.00	16.42	30.86	296.45	0.79	31.18	17.38	141.50	86.13	788.50
27.00	17.22	28.74	285.62	0.52	32.97	18.71	130.83	88.66	663.26
28.00	16.82	29.31	296.87	0.74	32.08	18.04	139.50	87.40	736.58
29.00	17.77	26.70	306.04	0.50	34.20	19.63	130.16	90.66	630.15
30.00	17.97	29.07	305.62	0.95	34.64	19.96	147.83	88.82	610.83
31.00	15.27	26.78	290.20	0.62	28.61	15.46	134.83	84.05	954.87
32.00	16.77	27.19	306.87	0.60	31.96	17.96	134.16	88.76	781.18
33.00	16.67	27.03	301.04	0.57	31.74	17.79	132.83	88.32	781.97
34.00	15.47	31.19	286.04	0.91	29.06	15.79	146.50	85.69	863.68
35.00	16.17	26.54	303.12	0.97	30.62	16.96	148.83	85.08	810.56
36.00	15.77	30.70	306.45	0.93	29.73	16.29	147.16	83.86	945.96
37.00	17.82	26.94	298.12	0.65	34.31	19.71	135.83	89.29	623.97
38.00	17.92	29.23	305.20	0.75	34.53	19.88	139.83	89.71	622.72
39.00	15.97	28.33	292.29	0.58	30.18	16.63	133.16	86.01	846.64
40.00	15.57	27.76	286.45	0.72	29.28	15.96	138.83	84.87	867.12
41.00	17.37	29.56	287.70	0.89	33.30	18.96	145.50	88.06	639.46
42.00	15.82	28.41	291.87	0.85	29.84	16.38	144.16	84.01	847.53
43.00	15.42	30.13	307.70	0.55	28.95	15.71	131.83	85.73	990.51
44.00	17.02	29.64	288.12	0.94	32.52	18.38	147.50	86.03	685.65
45.00	15.62	30.37	294.79	0.99	29.40	16.04	149.50	83.10	874.30
46.00	15.07	28.66	303.95	0.98	28.17	15.13	149.16	81.63	974.00
47.00	15.92	31.27	303.54	0.87	30.07	16.54	144.83	85.36	877.01
48.00	16.62	29.88	296.04	0.53	31.63	17.71	131.16	87.97	775.53
49.00	15.12	28.50	291.45	0.92	28.28	15.21	146.83	81.26	921.25
50.00	17.72	28.01	293.12	0.77	34.09	19.54	140.83	88.22	623.24
51.00	15.67	31.11	298.54	0.81	29.51	16.13	142.50	84.02	891.29
52.00	16.12	28.90	295.62	0.54	30.51	16.88	131.50	86.92	842.58
53.00	16.47	29.72	293.54	0.86	31.29	17.46	144.50	85.77	770.21

54.00	17.12	27.84	294.37	1.00	32.75	18.54	149.83	86.45	683.63
55.00	15.02	30.62	297.70	0.70	28.06	15.04	137.83	82.24	985.54
56.00	16.87	31.03	302.70	0.82	32.19	18.13	142.83	87.50	745.78
57.00	16.92	28.09	288.95	0.68	32.30	18.21	137.16	87.30	702.87
58.00	16.22	27.92	302.29	0.90	30.74	17.04	146.16	85.07	812.53
59.00	17.67	29.97	289.79	0.96	33.97	19.46	148.50	87.22	605.92
60.00	15.52	30.05	308.12	0.88	29.17	15.88	145.16	84.12	939.60

```

Swarming...

Reached limit of 200 iterations                               Final best point: [30.993 17.272 142.03 0.64339]
Final best point: [17.686 27.164 313.35 0.60066]

xopt =
xopt =
    17.6858  27.1639  313.3526  0.6007
    30.9932  17.2721  142.0323  0.6434

fval =
fval =
   -90.3992
   -86.2287

optscale =
optscale =
    17.6858  27.1639  313.3526  0.6007  -90.3992  30.9932  17.2721  142.0323  0.6434  -86.2287

Harmonic =
Harmonic =
    34.0000
    33.7024

Torque =
Torque =
    680.0001
    700.0000

```

Table 6-15 7 Variables Global Optimisation Latin Hypercube Sampling Points of 12/8 SRM

Models	Stator pole arc in °	Stator yoke in mm	Stator inner dia in mm	Airgap in mm	Rotor yoke thickness in mm	Rotor pole arc in °	Shaft Dia in mm	Eff: in %	Torq: in Nm
Sample row 15	17.5	27.5	308.958	0.5625	33.75	19.29	132.5	90	671.9
Modified sample row 15	17.1	27.5	306.958	0.5	33	18	150	89.3	747
Sample for row 29	17.775	26.704	306.04	0.504	34.19	19.62	130.1	90.6	630.1

Modified sample for row 29	15.9	27	303	0.5	34.19	17.325	130	90	728
-----------------------------------	------	----	-----	-----	-------	--------	-----	----	-----

Table 6-16 More variables Global Optimisation Latin Hypercube Sampling Points of 12/8 SRM

Models	Input current in Amps	Resistance (ohms)	Slot fill factor in %	Current density A/mm ²	Copper loss in w	Iron loss in w	Total loss (w)	flux density in T
Sample row 15	22.266	0.3306	75.52	2.640	889.34	83.9	1077	1.91
Modified sample row 15	25.71	0.3306	72.5	2.931	1096.94	82.9	1293	1.91
Sample for row 29	20.95	0.33	73.43	2.50	798.77	85.57	984	1.915
Modified sample for row 29	24.09	0.352	71.79	2.72	1007	73.40	1186	1.897

Table 6-17 (New) 6 Variables Global Optimisation Latin Hypercube Sampling Points of 12/8 SRM.

S, No	Stator pole arc in °	Stator Yoke thickness in mm	Air gap in mm	Rotor Yoke thickness in mm	Rotor pole arc in °	Shaft diameter in mm	Torque in Nm	Efficiency in %
1	16.13	26.24	0.85	30.47	17.54	100.83	829.00	82.83
2	16.43	29.19	0.87	34.63	19.96	149.17	674.86	85.02
3	15.83	26.68	0.99	32.91	18.96	129.17	759.72	83.13
4	17.38	29.54	0.61	31.33	18.04	110.83	729.35	85.49
5	17.63	28.32	0.72	28.61	16.46	79.17	804.14	83.63
6	17.98	28.84	0.79	27.75	15.96	69.17	822.73	83.44
7	17.28	29.71	0.55	28.90	16.63	82.50	819.08	84.57
8	17.88	27.28	0.80	33.77	19.46	139.17	629.18	85.76
9	16.33	29.02	0.98	33.48	19.29	135.83	714.68	84.07
10	16.53	28.06	0.92	32.05	18.46	119.17	755.06	83.95
11	16.88	28.50	0.65	30.04	17.29	95.83	793.10	84.14
12	16.93	28.41	0.60	32.62	18.79	125.83	727.53	86.13
13	17.03	31.36	0.69	26.17	15.04	50.83	926.16	81.63
14	15.38	29.80	0.88	27.89	16.04	70.83	953.92	80.24
15	16.08	28.15	0.75	32.77	18.88	127.50	766.84	84.68
16	17.18	27.46	0.93	30.76	17.71	104.17	740.27	82.96
17	16.03	31.18	0.81	29.18	16.79	85.83	870.89	81.80
18	17.23	27.02	0.51	31.05	17.88	107.50	749.04	85.46
19	16.28	30.06	0.54	30.33	17.46	99.17	850.43	84.99
20	17.53	27.11	0.85	28.47	16.38	77.50	803.27	83.03

21	15.88	29.10	0.58	31.62	18.21	114.17	820.89	84.87
22	15.33	29.36	0.71	30.90	17.79	105.83	874.37	83.45
23	15.68	27.80	0.96	30.19	17.38	97.50	855.22	81.69
24	17.13	27.98	0.83	27.61	15.88	67.50	848.57	81.30
25	15.28	31.01	0.82	31.19	17.96	109.17	874.57	83.37
26	16.78	28.67	0.97	27.32	15.71	64.17	883.95	81.24
27	16.98	29.45	0.94	26.46	15.21	54.17	908.13	80.99
28	17.68	30.84	0.70	26.89	15.46	59.17	864.84	83.04
29	15.53	27.20	0.89	27.03	15.54	60.83	920.20	78.33
30	15.18	27.72	0.74	29.76	17.13	92.50	919.38	82.28
31	17.93	30.92	0.70	29.90	17.21	94.17	746.79	84.55
32	16.48	28.24	0.86	28.18	16.21	74.17	869.20	81.27
33	16.73	29.28	0.78	31.76	18.29	115.83	759.81	84.13
34	15.48	29.62	0.57	28.32	16.29	75.83	951.82	81.89
35	17.48	26.94	0.77	26.60	15.29	55.83	872.26	81.72
36	16.58	26.85	0.76	29.61	17.04	90.83	817.62	82.92
37	17.78	26.42	0.56	33.05	19.04	130.83	659.11	86.35
38	15.08	27.63	0.55	32.19	18.54	120.83	847.51	84.47
39	16.63	26.76	0.60	27.46	15.79	65.83	903.21	83.07
40	17.33	28.93	0.53	33.91	19.54	140.83	656.28	87.07
41	15.93	31.10	0.95	27.18	15.63	62.50	925.25	79.52
42	15.63	28.58	0.75	34.49	19.88	147.50	730.13	84.24
43	15.78	27.89	0.50	34.20	19.71	144.17	738.98	86.46
44	16.18	29.88	0.68	29.33	16.88	87.50	867.39	82.70
45	15.98	30.58	0.64	32.34	18.63	122.50	790.61	85.16
46	15.03	30.40	0.73	26.32	15.13	52.50	1025.78	78.66
47	15.13	30.32	1.00	31.91	18.38	117.50	837.81	82.30
48	15.43	27.54	0.84	31.48	18.13	112.50	838.87	82.92
49	16.68	29.97	0.66	34.34	19.79	145.83	687.18	86.37
50	15.58	30.75	0.90	33.63	19.38	137.50	764.52	83.92
51	17.83	30.14	0.62	34.06	19.63	142.50	635.64	86.98
52	15.23	27.37	0.65	28.04	16.13	72.50	973.81	81.63
53	15.73	26.50	0.67	30.62	17.63	102.50	854.49	83.69
54	16.83	30.66	0.80	33.34	19.21	134.17	707.18	85.08
55	17.08	30.49	0.95	29.04	16.71	84.17	806.57	81.77
56	17.43	31.27	0.90	32.48	18.71	124.17	690.72	84.63
57	16.23	26.59	0.63	33.20	19.13	132.50	737.61	85.44
58	16.38	26.33	0.91	28.75	16.54	80.83	841.65	80.83

59	17.58	30.23	0.59	26.75	15.38	57.50	894.07	83.64
60	17.73	28.76	0.52	29.47	16.96	89.17	771.08	85.53

6.2.11 2nd PSO Optimisation from 60 samples while varying inner rotor

Swarming...

Reached limit of 200 iterations

Final best point: [17.956 28.459 0.51475 32.211]

xopt =

17.9561 28.4593 0.5148 32.2109

fval =

-86.8391

optscale =

17.9561 28.4593 0.5148 32.2109 -86.8391

Harmonic =

34.0000

Torque =

680.0001

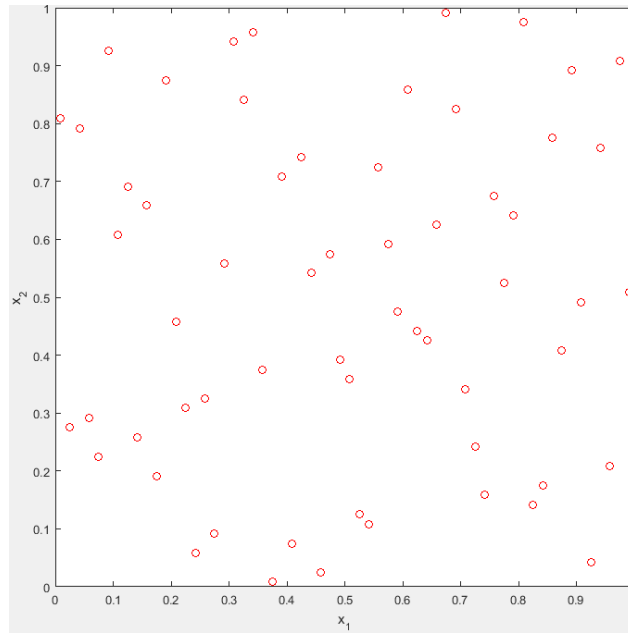


Fig. 6.5 60 samples of LHS samples

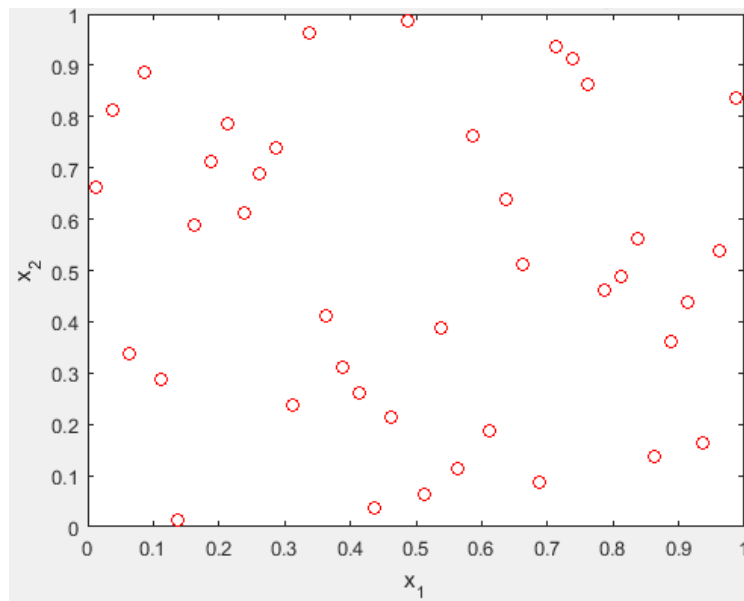


Fig. 6.6 40 LHS samples for constant speed and constant power analysis

Table 6-18 Global optimisation sample for 170mm at constant speed 105rpm

No	Stator Yoke	Rotor Yoke	Fill factor	No: of Turns	Stator pole arc	Stator pole length	Rotor pole arc	Rotor pole length	Eff:	Torq:	speed
01	35.6	29.4	51.8	98.3	15.7	46.9	16.2	77.8	82	793	105
02	29.9	35.4	47.3	90.1	14.6	52.9	15.7	72.3	79	985	105
03	31.6	30.1	50.8	86.7	14.9	47.6	16.1	70.0	79	1070	105
04	30.9	31.1	57.8	92.3	14.8	48.6	16.8	73.8	81	916	105
05	28.9	35.1	51.3	89.7	14.4	52.6	16.1	72.0	79	1034	105

06	32.1	28.6	45.3	96.8	15.0	46.1	15.5	76.8	80	899	105
07	28.4	28.1	56.8	95.7	14.3	45.6	16.7	76.0	81	959	105
08	29.1	35.9	59.8	99.1	14.4	53.4	17.0	78.3	82	828	105
09	33.6	33.1	50.3	97.9	15.3	50.6	16.0	77.5	81	828	105
10	29.4	34.1	58.8	90.4	14.5	51.6	16.9	72.5	80	966	105
11	35.9	31.6	52.3	85.6	15.8	49.1	16.2	69.3	79	971	105
12	27.1	34.6	42.8	94.2	14.0	52.1	15.3	75.0	78	1009	105
13	35.4	33.6	40.8	88.2	15.7	51.1	15.1	71.0	79	990	105
14	30.6	32.1	58.3	88.9	14.7	49.6	16.8	71.5	80	978	105
15	33.4	34.4	48.8	93.8	15.3	51.9	15.9	74.8	80	885	105
16	33.9	28.9	53.8	88.6	15.4	46.4	16.4	71.3	80	969	105
17	34.4	37.1	52.8	99.8	15.5	54.6	16.3	78.8	81	847	105
18	34.9	32.6	57.3	94.9	15.6	50.1	16.7	75.5	81	821	105
19	36.6	33.4	42.3	94.6	15.9	50.9	15.2	75.3	80	859	105
20	34.6	36.6	55.8	87.8	15.5	54.1	16.6	70.8	79	906	105
21	27.9	36.9	55.3	95.3	14.2	54.4	16.5	75.8	80	930	105
22	30.1	30.4	44.3	91.6	14.6	47.9	15.4	73.3	78	1014	105
23	36.4	29.6	40.3	93.1	15.9	47.1	15.0	74.3	80	915	105
24	36.1	32.4	43.3	93.4	15.8	49.9	15.3	74.5	80	876	105
25	28.6	33.9	49.8	98.7	14.3	51.4	16.0	78.0	79	946	105
26	31.9	37.9	59.3	90.8	15.0	55.4	16.9	72.8	81	895	105
27	33.1	29.9	41.3	89.3	15.2	47.4	15.1	71.8	78	1007	105
28	29.6	34.9	43.8	87.1	14.5	52.4	15.4	70.3	78	1048	105
29	27.4	36.1	54.8	99.4	14.1	53.6	16.5	78.5	81	876	105
30	32.6	29.1	53.3	86.3	15.1	46.6	16.3	69.8	79	1031	105
31	32.9	35.6	44.8	87.4	15.2	53.1	15.5	70.5	77	994	105
32	32.4	31.9	41.8	92.7	15.1	49.4	15.2	74.0	79	972	105
33	27.6	31.4	48.3	96.1	14.1	48.9	15.8	76.3	80	984	105
34	35.1	32.9	56.3	91.2	15.6	50.4	16.6	73.0	81	869	105
35	31.4	28.4	49.3	97.2	14.9	45.9	15.9	77.0	81	890	105
36	30.4	37.6	45.8	91.9	14.7	55.1	15.6	73.5	79	988	105
37	36.9	36.4	54.3	85.9	16.0	53.9	16.4	69.5	78	903	105
38	28.1	30.9	46.3	96.4	14.2	48.4	15.6	76.5	79	977	105
39	31.1	30.6	47.8	97.6	14.8	48.1	15.8	77.3	81	898	105
40	34.1	37.4	46.8	85.2	15.4	54.9	15.7	69.0	75	976	105

6.3 Constant power analysis at 170mm and 10kW

Air gap = 0.6 mm; Length= 170 mm *constant power 10kW

Table 6-19 Global optimisation sample for 170mm at constant power 10kW

No	Stator Yoke	Rotor Yoke	Fill factor	No: of Turns	Stator pole arc	Stator pole length	Rotor pole arc	Rotor pole length	Eff:	Torq:	speed
01	35.6	29.4	51.8	98.3	15.7	46.9	16.2	77.8	73	1223	78
02	29.9	35.4	47.3	90.1	14.6	52.9	15.7	72.3	83	745	128
03	31.6	30.1	50.8	86.7	14.9	47.6	16.1	70.0	85	687	139
04	30.9	31.1	57.8	92.3	14.8	48.6	16.8	73.8	81	894	107
05	28.9	35.1	51.3	89.7	14.4	52.6	16.1	72.0	84	726	132
06	32.1	28.6	45.3	96.8	15.0	46.1	15.5	76.8	79	930	103
07	28.4	28.1	56.8	95.7	14.3	45.6	16.7	76.0	83	831	115

08	29.1	35.9	59.8	99.1	14.4	53.4	17.0	78.3	77	1090	88
09	33.6	33.1	50.3	97.9	15.3	50.6	16.0	77.5	76	1111	86
10	29.4	34.1	58.8	90.4	14.5	51.6	16.9	72.5	83	812	117
11	35.9	31.6	52.3	85.6	15.8	49.1	16.2	69.3	82	799	119
12	27.1	34.6	42.8	94.2	14.0	52.1	15.3	75.0	82	748	127
13	35.4	33.6	40.8	88.2	15.7	51.1	15.1	71.0	82	773	123
14	30.6	32.1	58.3	88.9	14.7	49.6	16.8	71.5	82	792	121
15	33.4	34.4	48.8	93.8	15.3	51.9	15.9	74.8	79	959	99
16	33.9	28.9	53.8	88.6	15.4	46.4	16.4	71.3	83	809	118
17	34.4	37.1	52.8	99.8	15.5	54.6	16.3	78.8	78	1043	92
18	34.9	32.6	57.3	94.9	15.6	50.1	16.7	75.5	74	1144	84
19	36.6	33.4	42.3	94.6	15.9	50.9	15.2	75.3	77	1025	93
20	34.6	36.6	55.8	87.8	15.5	54.1	16.6	70.8	79	915	104
21	27.9	36.9	55.3	95.3	14.2	54.4	16.5	75.8	82	871	110
22	30.1	30.4	44.3	91.6	14.6	47.9	15.4	73.3	83	741	78
23	36.4	29.6	40.3	93.1	15.9	47.1	15.0	74.3	80	897	129
24	36.1	32.4	43.3	93.4	15.8	49.9	15.3	74.5	78	983	106
25	28.6	33.9	49.8	98.7	14.3	51.4	16.0	78.0	81	843	97
26	31.9	37.9	59.3	90.8	15.0	55.4	16.9	72.8	80	938	113
27	33.1	29.9	41.3	89.3	15.2	47.4	15.1	71.8	82	746	102
28	29.6	34.9	43.8	87.1	14.5	52.4	15.4	70.3	83	701	128
29	27.4	36.1	54.8	99.4	14.1	53.6	16.5	78.5	79	978	136
30	32.6	29.1	53.3	86.3	15.1	46.6	16.3	69.8	84	729	98
31	32.9	35.6	44.8	87.4	15.2	53.1	15.5	70.5	82	763	131
32	32.4	31.9	41.8	92.7	15.1	49.4	15.2	74.0	82	802	125
33	27.6	31.4	48.3	96.1	14.1	48.9	15.8	76.3	83	795	119
34	35.1	32.9	56.3	91.2	15.6	50.4	16.6	73.0	79	994	120
35	31.4	28.4	49.3	97.2	14.9	45.9	15.9	77.0	80	950	96
36	30.4	37.6	45.8	91.9	14.7	55.1	15.6	73.5	82	780	100
37	36.9	36.4	54.3	85.9	16.0	53.9	16.4	69.5	78	926	122
38	28.1	30.9	46.3	96.4	14.2	48.4	15.6	76.5	82	798	103
39	31.1	30.6	47.8	97.6	14.8	48.1	15.8	77.3	80	932	120
40	34.1	37.4	46.8	85.2	15.4	54.9	15.7	69.0	80	776	102

6.4 Constant speed analysis at 200mm and 105rpm

Air gap = 0.6 mm; Length= 200 mm *constant speed 105

Table 6-20 Global optimisation sample for 200mm at constant speed 105rpm

S, No	Stator Yoke thickness in mm	Rotor Yoke thickness in mm	Fill factor in %	No: of Turns	Stator pole arc in °	Stator pole length in mm	Rotor pole arc in °	Rotor pole length in mm	Eff: in %	Torq: in Nm	Speed in rpm
01	35.6	29.4	51.8	98.3	15.7	46.9	16.2	77.8	36	714	105
02	29.9	35.4	47.3	90.1	14.6	52.9	15.7	72.3	30	916	105
03	31.6	30.1	50.8	86.7	14.9	47.6	16.1	70.0	32	965	105
04	30.9	31.1	57.8	92.3	14.8	48.6	16.8	73.8	31	828	105
05	28.9	35.1	51.3	89.7	14.4	52.6	16.1	72.0	29	934	105
06	32.1	28.6	45.3	96.8	15.0	46.1	15.5	76.8	32	815	105
07	28.4	28.1	56.8	95.7	14.3	45.6	16.7	76.0	28	858	105

08	29.1	35.9	59.8	99.1	14.4	53.4	17.0	78.3	29	742	105
09	33.6	33.1	50.3	97.9	15.3	50.6	16.0	77.5	34	746	105
10	29.4	34.1	58.8	90.4	14.5	51.6	16.9	72.5	29	872	105
11	35.9	31.6	52.3	85.6	15.8	49.1	16.2	69.3	36	881	105
12	27.1	34.6	42.8	94.2	14.0	52.1	15.3	75.0	27	914	105
13	35.4	33.6	40.8	88.2	15.7	51.1	15.1	71.0	35	896	105
14	30.6	32.1	58.3	88.9	14.7	49.6	16.8	71.5	31	886	105
15	33.4	34.4	48.8	93.8	15.3	51.9	15.9	74.8	33	801	105
16	33.9	28.9	53.8	88.6	15.4	46.4	16.4	71.3	34	874	105
17	34.4	37.1	52.8	99.8	15.5	54.6	16.3	78.8	34	960	105
18	34.9	32.6	57.3	94.9	15.6	50.1	16.7	75.5	35	742	105
19	36.6	33.4	42.3	94.6	15.9	50.9	15.2	75.3	37	777	105
20	34.6	36.6	55.8	87.8	15.5	54.1	16.6	70.8	35	825	105
21	27.9	36.9	55.3	95.3	14.2	54.4	16.5	75.8	28	835	105
22	30.1	30.4	44.3	91.6	14.6	47.9	15.4	73.3	30	920	105
23	36.4	29.6	40.3	93.1	15.9	47.1	15.0	74.3	36	828	105
24	36.1	32.4	43.3	93.4	15.8	49.9	15.3	74.5	36	794	105
25	28.6	33.9	49.8	98.7	14.3	51.4	16.0	78.0	29	853	105
26	31.9	37.9	59.3	90.8	15.0	55.4	16.9	72.8	32	807	105
27	33.1	29.9	41.3	89.3	15.2	47.4	15.1	71.8	33	916	105
28	29.6	34.9	43.8	87.1	14.5	52.4	15.4	70.3	30	949	105
29	27.4	36.1	54.8	99.4	14.1	53.6	16.5	78.5	27	788	105
30	32.6	29.1	53.3	86.3	15.1	46.6	16.3	69.8	33	931	105
31	32.9	35.6	44.8	87.4	15.2	53.1	15.5	70.5	33	905	105
32	32.4	31.9	41.8	92.7	15.1	49.4	15.2	74.0	32	880	105
33	27.6	31.4	48.3	96.1	14.1	48.9	15.8	76.3	28	882	105
34	35.1	32.9	56.3	91.2	15.6	50.4	16.6	73.0	35	783	105
35	31.4	28.4	49.3	97.2	14.9	45.9	15.9	77.0	31	802	105
36	30.4	37.6	45.8	91.9	14.7	55.1	15.6	73.5	30	891	105
37	36.9	36.4	54.3	85.9	16.0	53.9	16.4	69.5	37	824	105
38	28.1	30.9	46.3	96.4	14.2	48.4	15.6	76.5	28	880	105
39	31.1	30.6	47.8	97.6	14.8	48.1	15.8	77.3	31	808	105
40	34.1	37.4	46.8	85.2	15.4	54.9	15.7	69.0	34	896	105

6.5 Constant speed analysis at 200mm and 10kW

Air gap = 0.6 mm; Length= 200 mm *constant power 10 kW

Table 6-21 Global optimisation sample for 200mm at constant power 10kW

S, No	Stator Yoke thickness in mm	Rotor Yoke thickness in mm	Fill factor in %	No. of Turns	Stator pole arc in °	Stator pole length in mm	Rotor pole arc in °	Rotor pole length in mm	Eff: in %	Torq: in Nm	Speed in rpm
01	35.6	29.4	51.8	98.3	15.7	46.9	16.2	77.8	36	714	105
02	29.9	35.4	47.3	90.1	14.6	52.9	15.7	72.3	69	1510	63
03	31.6	30.1	50.8	86.7	14.9	47.6	16.1	70.0	81	895	107
04	30.9	31.1	57.8	92.3	14.8	48.6	16.8	73.8	83	825	116
05	28.9	35.1	51.3	89.7	14.4	52.6	16.1	72.0	79	1081	88
06	32.1	28.6	45.3	96.8	15.0	46.1	15.5	76.8	82	868	110

07	28.4	28.1	56.8	95.7	14.3	45.6	16.7	76.0	76	1130	85
08	29.1	35.9	59.8	99.1	14.4	53.4	17.0	78.3	81	996	96
09	33.6	33.1	50.3	97.9	15.3	50.6	16.0	77.5	74	1334	72
10	29.4	34.1	58.8	90.4	14.5	51.6	16.9	72.5	72	1369	70
11	35.9	31.6	52.3	85.6	15.8	49.1	16.2	69.3	80	980	97
12	27.1	34.6	42.8	94.2	14.0	52.1	15.3	75.0	80	963	99
13	35.4	33.6	40.8	88.2	15.7	51.1	15.1	71.0	80	901	106
14	30.6	32.1	58.3	88.9	14.7	49.6	16.8	71.5	80	933	102
15	33.4	34.4	48.8	93.8	15.3	51.9	15.9	74.8	81	953	100
16	33.9	28.9	53.8	88.6	15.4	46.4	16.4	71.3	76	1166	82
17	34.4	37.1	52.8	99.8	15.5	54.6	16.3	78.8	81	973	98
18	34.9	32.6	57.3	94.9	15.6	50.1	16.7	75.5	75	1276	75
19	36.6	33.4	42.3	94.6	15.9	50.9	15.2	75.3	70	1411	68
20	34.6	36.6	55.8	87.8	15.5	54.1	16.6	70.8	73	1251	76
21	27.9	36.9	55.3	95.3	14.2	54.4	16.5	75.8	76	1112	86
22	30.1	30.4	44.3	91.6	14.6	47.9	15.4	73.3	79	1054	91
23	36.4	29.6	40.3	93.1	15.9	47.1	15.0	74.3	81	888	107
24	36.1	32.4	43.3	93.4	15.8	49.9	15.3	74.5	78	1087	88
25	28.6	33.9	49.8	98.7	14.3	51.4	16.0	78.0	75	1198	80
26	31.9	37.9	59.3	90.8	15.0	55.4	16.9	72.8	79	1019	94
27	33.1	29.9	41.3	89.3	15.2	47.4	15.1	71.8	77	1137	84
28	29.6	34.9	43.8	87.1	14.5	52.4	15.4	70.3	80	897	107
29	27.4	36.1	54.8	99.4	14.1	53.6	16.5	78.5	82	843	113
30	32.6	29.1	53.3	86.3	15.1	46.6	16.3	69.8	76	1190	119
31	32.9	35.6	44.8	87.4	15.2	53.1	15.5	70.5	83	870	110
32	32.4	31.9	41.8	92.7	15.1	49.4	15.2	74.0	80	918	104
33	27.6	31.4	48.3	96.1	14.1	48.9	15.8	76.3	79	967	99
34	35.1	32.9	56.3	91.2	15.6	50.4	16.6	73.0	81	955	100
35	31.4	28.4	49.3	97.2	14.9	45.9	15.9	77.0	76	1208	79
36	30.4	37.6	45.8	91.9	14.7	55.1	15.6	73.5	77	1148	83
37	36.9	36.4	54.3	85.9	16.0	53.9	16.4	69.5	80	939	101
38	28.1	30.9	46.3	96.4	14.2	48.4	15.6	76.5	75	1127	85
39	31.1	30.6	47.8	97.6	14.8	48.1	15.8	77.3	80	963	99
40	34.1	37.4	46.8	85.2	15.4	54.9	15.7	69.0	78	1130	84

Table 6-22 Design Specifications of the 24kW SynRM.

Parameter	Symbol	Value	Units
Rated power	P	24	kW
Phase Voltage	Vdc	380	V
Rated current	I	26	Amps
Shaft diameter	dsh	50	mm
Number of turns	Np	12	turns
Stator dia	ds	310	mm
Rotor dia	dr	188	mm
Air gap	g	1	mm
Stack length	l	200	mm

Stator poles	Ns	4	-
Rotor flux barriers		3	-
Rotor flux barrier edge angle	deg	4	o
Number of phases	m	3	-
Synchronous speed	nN	1500	rpm
Average torque	Tav	154	Nm
Saliency ratio		0.7	
frequency	f	50	Hz

Table 6-23 Design Specifications of the SynRM rotor

Item	Value	Item	Value
Rotor OD in mm	188 mm	Flux barrier edge angle	3 and 4 deg
Flux carrier total width in mm	42.17	Flux barrier total width	26.822
Each Flux carrier width in mm	12.06, 9.92, 9.97, 10.21	Each flux barrier width	9.02, 8.97, 8.81
Rotor Material	M350-50Amp		
1 st flux barrier length (start from Rotor outer diameter)			
Upper line	36mm	Lower line	35.9mm
2 nd flux barrier length			
Upper line	36mm	Lower line	36mm
3 rd flux barrier length			
Upper line	35.91mm	Lower line	35.63mm

Note: All the above dimension are clearly mentioned in the 4th quadrant view of the rotor.

Table 6-24 Design specifications

Item	Value	Item	Value
Phase Voltage	310V AC supply	Rated Frequency	50 Hz
Power	24.23kW	Rated Synchronous Speed	1500 rpm
Airgap thickness	1mm	Stator Winding Arrangement	Double-Layer
Rated Current	26.51 Amp	Rated torque	154.27Nm
Waveform	AC Sinusoidal	Stator Winding Arrangement	Double-Layer
Efficiency	89%	Flux density	2.1 Tesla
Shaft Diameter	50mm	Stack Length	200 mm
Pole Numbers	4	Number of phases	3
Number of slots	36		

Table 6-25 rotor dimensions

Item	Value	Item	Value
Rotor OD	188 mm	Flux barrier edge angle	3 and 4 deg
Flux carrier total width	42.17	Flux barrier total width	26.822
Each Flux carrier width	12.06, 9.92,9.97,10.21	Each flux barrier width	9.02, 8.97, 8.81
Rotor Material	M350-50Amp		
1 st flux barrier length (start from Rotor outer diameter)			
Upper line	36mm	Lower line	35.9mm
2 nd flux barrier length			
Upper line	36mm	Lower line	36mm
3 rd flux barrier length			
Upper line	35.91mm	Lower line	35.63mm

Please note: All the above dimension are clearly mentioned in the 4th quadrant view of the rotor below.

Table 6-26 stator dimensions of 8.58kW direct drive SynRM

Item	Value	Item	Value
Stator OD	500 mm	Stator ID	300 mm
Slot depth	51.3	Tooth width	15.75
Slot opening width	6.74	Tooth tang angle	10.8
Tooth tip thickness	3.97	Slot openings	6.74
Stator core thickness	49.76	Stator material	M-19 29 Ga

Table 6-27 rotor dimensions of the 8.85kW motor for direct drive

Item	Value	Item	Value
Rotor OD	299.33 mm	Flux barrier edge angle	49
Flux carrier total width	70.59	Flux barrier total width	41.30
Each Flux carrier width	14.11	Each flux barrier width	10.33
Rotor Material	M-19 29 Ga		
1 st flux barrier length (start from Rotor outer diameter)			
Upper line	65.6mm	Lower line	91.3mm
2 nd flux barrier length			
Upper line	114.42mm	Lower line	128.31mm
3 rd flux barrier length			
Upper line	133.49mm	Lower line	144.18mm
4 th flux barrier length			
Upper line	45.52mm	Lower line	72.59

Please note: All the above dimension are clearly mentioned in the 4th quadrant view of the rotor below.

Table 6-28 3-phase Winding specifications of 8.85kW rotor design

Item	Value	Item	Value
Bare slot area	718.9mm ²	Slot Fill factor	52%
Number of Turns	53	Stranded conductor area	7mm
End winding resistance	2.835Ω	End winding inductance	12.57mH
Number of parallel paths	1	Coil placement method	Over-under
Slot liner thickness	0.741	Coil separator thickness	0.741
Winding type	Lap	Number of coils per set	1
Coil span	9	Number of layers	2
Coil material	Copper: 100% IACS		

Table 6-29 asymmetrical rotor design parameters when length decreased (from the right side) and angle increased.

Decrease d mm	Barrier 1 in mm		Barrier 2 in mm		Barrier 3 in mm		Barrier 4 in mm		Torque Nm	Efficiency %	Power kW	Energy J	T-Ripple %
2	30.7	43.5	55.2	62.1	64.8	70.0	20.7	34.3	809	91.22	9.76	339	57
4	28.7	41.5	53.2	60.1	62.8	68.0	18.7	32.3	816	91.58	9.81	335	64
6	26.7	39.5	51.2	58.1	60.8	66.0	16.7	30.3	821	91.77	9.84	331	78
8	24.7	37.5	49.2	56.1	58.8	64.0	14.7	28.3	825	92.30	9.83	327	88
10	22.7	35.5	47.2	54.1	56.8	62.0	12.7	26.3	827	92.67	9.82	322	100
12	20.7	33.5	45.2	52.1	54.8	60.0	10.7	24.3	829	93.07	9.80	317	110
14	18.7	31.5	43.2	50.1	52.8	58.0	8.7	22.3	829	93.29	9.67	312	121
16	16.7	29.5	41.2	48.1	50.8	56.0	6.7	20.3	829	93.40	9.75	307	125
18	14.7	27.5	39.2	46.1	48.8	54.0	4.7	18.3	828	93.44	9.75	302	130
20	12.7	25.5	37.2	44.1	46.8	52.0	2.7	16.3	826	93.8	9.68	297	128

Note: torque ripple is increasing with decreasing length.

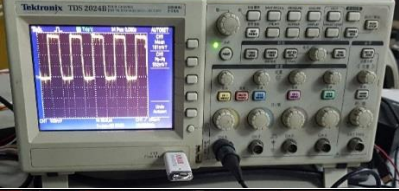
Table 6-30 parameters when length decreased and angle length remain the same

Decrease d mm	Barrier 1 in mm		Barrier 2 in mm		Barrier 3 in mm		Barrier 4 in mm		Torque Nm	Efficiency %	Power kW	Energy J	T-Ripple %
2	30.7	43.5	55.2	62.1	64.8	70.0	20.7	34.3	776	91.3	9.34	326	57
4	28.7	41.5	53.2	60.1	62.8	68.0	18.7	32.3	747	91.4	8.97	309	66
6	26.7	39.5	51.2	58.1	60.8	66.0	16.7	30.3	733	92.0	8.76	296	77
8	24.7	37.5	49.2	56.1	58.8	64.0	14.7	28.3	697	92.4	8.29	277	88
10	22.7	35.5	47.2	54.1	56.8	62.0	12.7	26.3	671	92.8	7.95	262	99
12	20.7	33.5	45.2	52.1	54.8	60.0	10.7	24.3	644	93.3	7.58	247	105
14	18.7	31.5	43.2	50.1	52.8	58.0	8.7	22.3	615	93.3	7.24	234	108
16	16.7	29.5	41.2	48.1	50.8	56.0	6.7	20.3	588	93.5	6.90	220	106
18	14.7	27.5	39.2	46.1	48.8	54.0	4.7	18.3	559	93.7	6.55	207	103
20	12.7	25.5	37.2	44.1	46.8	52.0	2.7	16.3	532	94.0	6.22	194	101

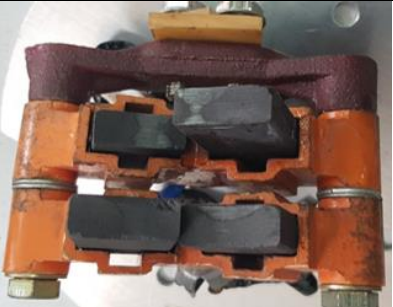
Note torque ripple is increasing with decreasing length.

Table 6-31 The equipment used in the experiment

Equipment	Items	PICs
(1) Multi-meters	V and I measurement (0.2% accuracy)	
(2) Siemens Drive	MICROMASTER 440. Frequency inverter range is covered 0.12- 22kW for constant torque.	
(3) Torque measurement	Torque measuring instrument ($\pm 0.2\%$ accuracy)	
(4) Frequency and speed measurement	1 rev/min accuracy	

<p>(5) Temperature measurement</p>	<p>5 thermocouple used for the temperature measurement and each thermocouple gives its own reading and temperature meter</p>	
<p>(6) Oscilloscope</p>	<p>Torque, and frequency measurement with Oscilloscope.</p>	
<p>(7) The 55kW motor used as a load machine</p>	<p>Permanent magnet machine with ABB drive speed control. 1480Rpm152Nm maximum torque.</p>	
<p>(8) ABB Drive</p>	<p>Frequency converter ABB EN_AC800 standard control</p>	
<p>(9) Vibration meter</p>	<p>To measure the vibration of the motor.</p>	
<p>(10) Proposed rotor design</p>	<p>Solid Synchronous reluctance rotor 3V-shaped flux barrier shape</p>	

	Material polyvinyl chloride inserted into the flux barriers. With both solid and liquid material.	
(11) Assembled rotor without shaft	After the insertion of polyvinyl chloride material, the rotor is mechanically fitted with nuts and bolts with an outer cover plate.	
(12) Symmetrical rotor for test	Rotor assembled with shaft and fan after machining.	
(13) Two rotors of Synchronous machine	First the symmetrical	
(14) Power Analyser (3- phase)	For measuring power and harmonics	
(15) Digital Tachometer	For contactless speed measurement	

<p>(16) Winding resistance measurement meter</p>	<p>Three phases winding insulation testing. To check the stator winding is not touching the body</p>	
<p>(17) Three phase winding connections</p>	<p>Red, yellow and blue phase terminal.</p>	
<p>(18) Carbon Brushes</p>	<p>Assembly of carbon brushes attached with the spring.</p>	



a



(b)



(c)



(d)

Fig. 6.7 Photographs of duplicate Cummins stator (PI-144F) (a-d)

Table 6-32 Results of No-load test

Hz	T1	T2	T3	T4	T5	Rpm	I	V	P	P.f	Harmonics
5Hz	31.9	33.8	39.0	29.3	28.9	140	19.9	134	0.24	0.09	87% THD
6Hz	35.7	38.0	44	31.3	32.6	154	22	136	0.34	0.10	87% THD
7Hz	41.9	44.2	51.8	35.2	36.2	210	20	138	0.34	0.13	86% THD
8.2Hz	47	50	55.3	45	43.7	242	17.6	141	0.31	0.11	86% THD
10Hz	47.2	49	55	44.8	44.1	300	18.0	145	0.28	0.10	86% THD
12Hz	45.5	47	53.4	42	41	362	18.5	149	0.28	0.10	84% THD
14.30Hz	44.5	46.1	51.2	41.8	40.1	429	17.6	155	0.29	0.12	84% THD
16.10Hz	43.5	45	50.4	39.7	38.8	482	16.8	159	0.36	0.13	82% THD
17Hz	42.1	44.2	49.2	38.8	37.3	508	18.5	164	0.49	0.11	72% THD
20Hz	40.1	42	48.3	37.1	36.2	602	18.7	169	0.48	0.11	47% THD
21.5Hz	39.5	41.4	47.3	36.7	35.3	647	18.2	174	0.48	0.11	43.3% THD
24Hz	39.2	41.3	46.9	36.1	34.8	719	17.6	179	0.39	0.12	17.8% THD
26Hz	38.8	40.7	45.7	35	33.3	786	18.5	183	0.39	0.13	16.8% THD
28Hz	38.2	40.1	45	33.8	32.1	840	19.1	188	0.39	0.12	15.5% THD
30.30	37.9	39.3	44.1	32.6	29.2	909	18.2	193	0.38	0.10	7.9% THD
32	33.6	35.4	31	31	27	961	18.9	198	0.42	0.11	13.6% THD

Table 6-33 No-load test data while coupling the shaft with 55kW load motor or No-load experimental data of temperature, speed, current, voltage, power, power factor, harmonics and vibration from 0-50Hz frequency.

Frequency	T1	T2	T3	T4	T5	Speed in rpm	Current in Amp	Voltage in volts	Power in kW	P.f	Harmonics in %	Vibration micro m ² /Hz
5Hz	26.1	27.7	29.9	25.7	26	150	17.8	155	0.28	0.08	36/2.4/1.2	102.1
10Hz	32	33.9	38.6	30	30.8	299	18.3	163.5	0.29	0.09	28.9/8.7/1.2	99.9

15Hz	31.9	33.8	37.3	30.8	31.1	452	18.2	172.9	0.36	0.10	21.2/0.8/4.3	98
20Hz	31.5	33.4	36.3	31.0	31.3	600	18	182	0.34	0.09	18.3/1.6/0.7	99.6
25Hz	31.3	32.9	35.5	30.9	31.3	752	18	190	0.36	0.10	16.7/0.4/5.3	98.5
30Hz	30.9	31.8	34.6	31.6	31.4	900	18.1	196.2	0.36	0.10	9.2/6.7/0.3	100
33Hz	30.9	31.4	34.4	31.7	31.6	995	19.7	199	0.38	0.11	13.6/2.4/14.7	97.2
35Hz	30.6	31.5	34	31.4	31.8	1052	18.2	202	0.40	0.11	8.5/7.5/0.4	97.7
38Hz	30.7	32.1	34	31.7	31.8	1140	18.4	208	0.42	0.11	14.5/12.4/7.1	97.9
40Hz	30.3	31.9	33.9	31.9	32.4	1200	18.4	213	0.45	0.12	14.3/11.2/6.5	96
42Hz	30.8	31.7	33.9	31.9	32.3	1260	18.8	217.4	0.52	0.13	8.26/12.1/6.9	91.5
43.80Hz	31.1	32	33.7	32.5	32.4	1314	21.7	221	0.53	0.13	8.3/13.7/0.9	91
45Hz	27.8	27.6	30.3	24.5	28.8	1350	18.4	229	0.52	0.13	6.7/4./0.8	92
47.80Hz	30.9	31.5	34.1	32.5	33.1	1433	18.0	236	0.55	0.13	8.3/13.7	93
50Hz	31	31.6	33.9	32.4	33.2	1500	18.4	249 L to N	0.56	0.14	6.4/5.1/0.6	93

Table 6-34 low slip test data while connecting 55kW motor as a load

Frequency	T1	T2	T3	T4	T5	RP M	Current in Amp	Voltage in volts	Power in kW	P.f	Harmonics in %	Torque Nm	ABB drive reference settings Hz/Rpm	ABB Drive current
5Hz	29.3	30	31.9	32	27.6	150	18	139	0.22	0.09	512%	0.2	0.1Hz/	
17Hz	32.3	34.1	37.2	30	31.4	513	18.2	163	0.36	0.12	44.7%	0.42	0.6/-9.8	2.4
25Hz	32.3	34	36.6	31.3	31.8	750	17.8	181				0.5	0.6/-9.8	2.9
Not Torque applied by ABB at 50Hz														
25Hz	32.8	34.5	36.8	33	32.7	750	18	181	0.51	0.16	14.5/4.9/0.4		0.8/-11.7/-52%	45/6.3
30Hz	32.8	34.2	36.7	33.2	33.2	899	18	192	0.54	0.17	8.3/3.0/0.5	0.9	0.8/-11.7	45/6.3
Now Torque Applied on the machine														
30Hz	32.7	34.1	36.7	33.4	33.6	900	18.2	191	0.68/0.76	0.21	8.5/3.3/0.2	1.4	1/68%	68/10.1
35Hz	33	34.5	37.1	33.6	34.1	1050	19	312	0.85	0.24	7.5/4.8/0.3	1.7	1.1/-77%	67/11.4
Now Torque Applied on the machine														

35Hz	33. 5	34 .9	37 .5	34 .3	34 .6	10 50	18.8	200			7.4/4.2/ 0.2	1.7		1.2/- 16rpm/- 84%	72/15
40Hz	34. 1	35 .2	37 .9	34 .8	35 .7	12 00	18.9	211	1.10	0.2 6	12/8.2/ 2	2.3		Same as above	
Now Torque Applied on the machine															
Same all														1.4/- 19/99	86/19
45Hz	35. 4	36 .2	39 .5	36 .2	36 .8	13 56	20.7	227	1.17	0.2 8	7.2/6.3/ 0.2	2.9		1.4/19.6	84/11. 8
Now Torque Applied on the machine															
45Hz	36. 1	37	40 .2	37 .1	37 .8	13 50	20.7	226	1.76	0.3 7	7.2/6.2/ 0.3	3.4		1.7/- 23.8/11 7.74T	102.8 4/12
50Hz	36. 6	37 .7	41 .1	37 .6	38 .3	15 00	23.8	239	2.29	0.4 1	5.9/6.1/ 0.3	3.9		1.7/- 24.7rpm /-113T	99.74/ 18

Table 6-35 List of Equipment used in the experimental setup

Proposed Rotor
Stamford stator
55kW motor
ABB Drive
ABB Load resistor
Siemens Drive
Siemens Resistor
Ammeter
Voltmeter
Fluke meter
Torque transducer
Torque measurement meter JN-338
5 PT100 Temperature sensor (Thermocouple)
Oscilloscope Tektronix TDS 2024B
Vibration meter EMT290 (Machin checker)
Siemens circuit breaker CDM10-100/3300 Delixi
12V Battery (Black)
Megger testing meter

Table 6-36 Magnetic Flux density of 3 flux barrier synchronous reluctance motor

S,No	Magnetic Flux density in Tesla
1	2.17
2	2.18
3	2.20
4	2.20
5	2.21
6	2.25
7	2.24
8	2.21
9	2.24
10	2.20
11	2.16
12	2.18
13	2.20
14	2.20
15	2.21
16	2.25
17	2.24
18	2.24
19	2.24
20	2.20
21	2.17
22	2.18
23	2.20
24	2.20
25	2.21
26	2.25
27	2.24
28	2.21
29	2.24
30	2.20
31	2.16
32	2.18
33	2.20
34	2.20
35	2.21
36	2.25
37	2.24
38	2.22
39	2.24
40	2.20
41	2.17
42	2.18
43	2.20
44	2.20
45	2.21
46	2.25
47	2.24
48	2.21
49	2.24
50	2.20